Objective evaluation of human manual control adaptation boundaries using a cybernetic approach

Lu, Tao

DOI
10.4233/uuid:a9409495-dcb4-43fb-bf2d-64341056654d

Publication date
2018

Document Version
Final published version

Citation (APA)
Lu, T. (2018). *Objective evaluation of human manual control adaptation boundaries using a cybernetic approach*. [Dissertation (TU Delft), Delft University of Technology]. https://doi.org/10.4233/uuid:a9409495-dcb4-43fb-bf2d-64341056654d

Important note
To cite this publication, please use the final published version (if applicable).
Please check the document version above.

ISBN: 978-94-028-0995-4

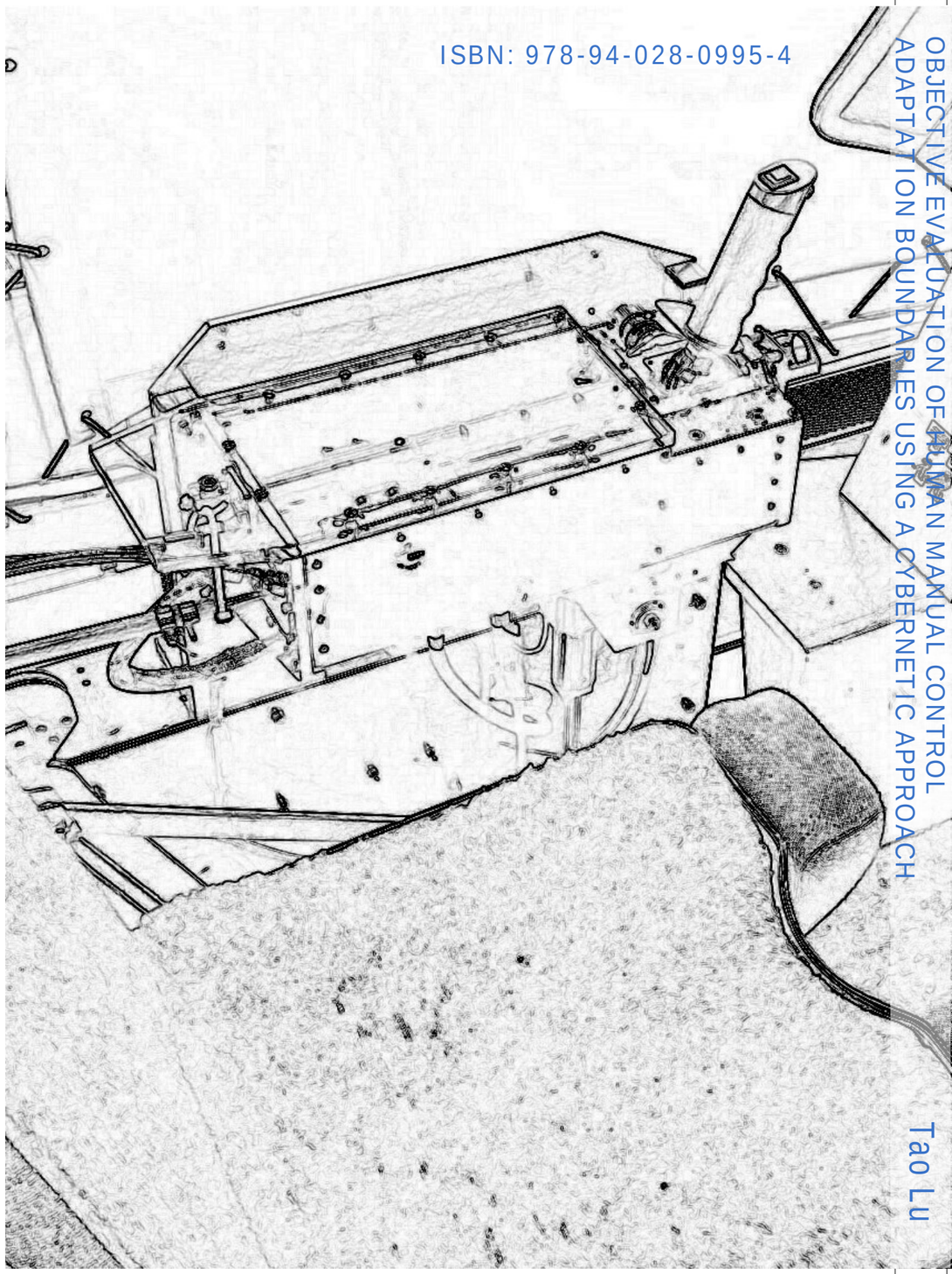

OBJECTIVE EVALUATION OF HUMAN MANUAL CONTROL ADAPTATION BOUNDARIES USING A CYBERNETIC APPROACH

Tao Lu

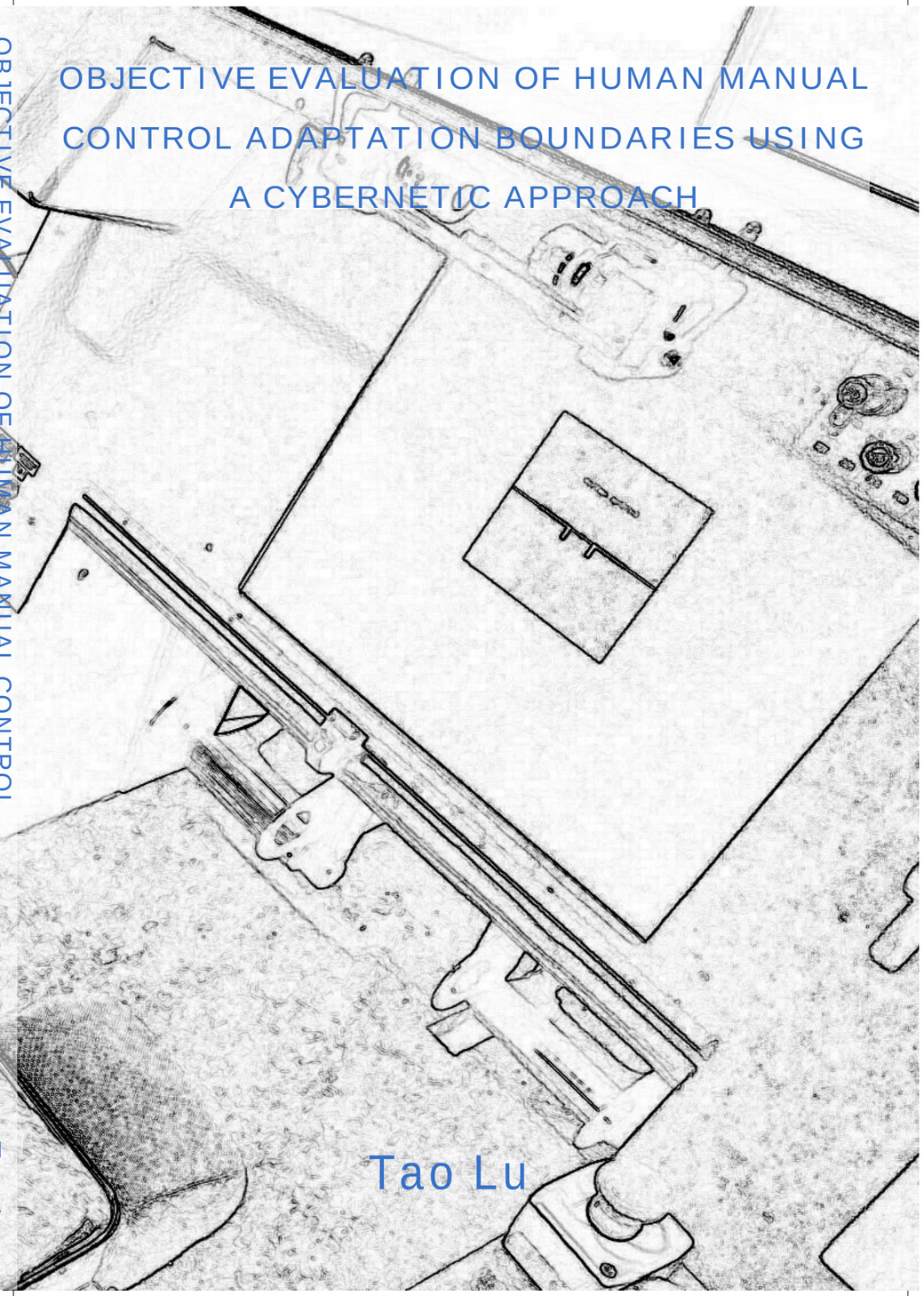

OBJECTIVE EVALUATION OF HUMAN MANUAL CONTROL ADAPTATION BOUNDARIES USING A CYBERNETIC APPROACH

Tao Lu

Invitation

to the public defense
of my thesis

OBJECTIVE EVALUATION OF
HUMAN MANUAL CONTROL
ADAPTATION BOUNDARIES USING
A CYBERNETIC APPROACH

in the Senaatszaal of the Aula of Delft University of Technology Mekelweg 5, Delft

Prior to the defense, at 09:30 there will be a short presentation about the thesis work

Tao Lu

Propositions

accompanying the dissertation

OBJECTIVE EVALUATION OF HUMAN MANUAL CONTROL ADAPTATION BOUNDARIES USING A CYBERNETIC APPROACH

by

Tao LU

1. The Integrated Manual Control Adaptation Boundaries (IMCAB) show that task performance, control activity and human control behavior are most sensitive to changes in controlled dynamics in the crossover frequency region. (This thesis)
2. The different shapes of the Manual Control Adaptation Boundaries (MCAB) for task performance, control activity and control behavior indicate that, various metrics need to be considered to describe human manual control adaptation. (This thesis)
3. With practical limitations on the duration of human-in-the-loop experiments, useful objective MCAB covering a wide frequency range cannot be developed without offline human operator simulation data. (This thesis)
4. When (I)MCAB are derived for pursuit or preview tracking tasks, the controlled dynamics would still be the most important element causing manual control adaptation. (This thesis)
5. Uncertainties, nonlinearities and noise in human manual control identification can be reduced by obtaining a more thorough understanding in our control behavior mechanisms.
6. As long as humans remain motivated to understand this world, models and model-based approaches can never be abandoned.
7. Though the variety in human behavior makes it difficult to model and predict that behavior, it contributes to make our world a better place.
8. Once an objective fact is given thought to or talked about, this fact is jeopardized to subjective interpretations and communications.
9. A research topic on “an economic way of constructing the walking and bike lanes with minimal maintenance in TU Delft” is necessary.
10. The most reliable way of identifying a non-Dutch person in the Netherlands is by observing whether and how she or he uses a raincoat or umbrella in heavy rain.

These propositions are regarded as opposable and defendable, and have been approved as such by the promotor dr. ir. M. M. van Paassen.

Objective Evaluation of Human Manual Control Adaptation Boundaries Using a Cybernetic Approach

OBJECTIVE EVALUATION OF HUMAN MANUAL CONTROL ADAPTATION BOUNDARIES USING A CYBERNETIC APPROACH

Proefschrift

ter verkrijging van de graad van doctor
aan de Technische Universiteit Delft,
op gezag van de Rector Magnificus prof. dr. ir. T.H.J.J. van der Hagen,
voorzitter van het College voor Promoties,
in het openbaar te verdedigen op dinsdag 10 april 2018 om 10:00 uur

door

Tao Lu

Master of Science, China
geboren te Chengdu, China.

Dit proefschrift is goedgekeurd door de promotoren:

dr. ir. M. M. van Paassen

Copromotor:

dr. ir. D. M. Pool

Samenstelling promotiecommissie:

Rector Magnificus,	voorzitter
Dr. ir. M. M. van Paassen,	Technische Universiteit Delft, promotor
Dr. ir. D. M. Pool,	Technische Universiteit Delft, copromotor
Overige leden:	
Prof. dr. A. R. Pritchett,	Pennsylvania State University
Prof. dr. J. van der Steen,	Erasmus Universiteit Rotterdam
Prof. dr. ir. H. Vallery,	Technische Universiteit Delft
Prof. dr. R. Curran,	Technische Universiteit Delft
Dr. ir. A. L. Schwab,	Technische Universiteit Delft
Prof. dr. ir. J. A. Mulder,	Technische Universiteit Delft, reservelid

Prof. dr. ir. M. Mulder heeft als begeleider in belangrijke mate aan de totstandkoming van het proefschrift bijgedragen.

Keywords: Manual Control; Human Adaptation; Human-Machine Interaction; Manual Control Adaptation Boundaries; Maximum Unnoticeable Added Dynamics; Cybernetic Approach; System Identification; Compensatory Tracking; Human Control Model Simulation and Optimization

Printed by: Ipskamp Printing

Front & Back: T. Lu

ISBN 978-94-028-0995-4

An electronic version of this dissertation is available at
`http://repository.tudelft.nl/`.

To my family

SUMMARY

OBJECTIVE EVALUATION OF HUMAN MANUAL CONTROL ADAPTATION BOUNDARIES USING A CYBERNETIC APPROACH

TAO LU

Manual control tasks can be found everywhere in our daily activities, and the human ability to adapt in controlling many different vehicles such as cars and airplanes make it possible for us to travel farther, faster and higher. The human adaptation ability to changes in the controlled element dynamics is indispensable for tasks requiring high performance and safety, and none of the state-of-the-art automatic control systems can compete. For example, in the racing industry, professional racing drivers are needed to adapt to different car configurations and consistently push the car to its performance limit in the driving simulator and on the track, which is important for designing and tuning the cars. In aviation, pilots are our "last line of defense" for flight safety, especially in emergency situations in which automatic flight systems fail.

It is also known, however, there are limitations in the human ability to adapt. Hence, in aviation, it is crucial to design airplanes that are both stable and easy to be controlled, the primary concerns for aircraft *handling qualities*. Traditionally, aircraft mode parameters such as short-period dynamics' damping and natural frequency are strictly limited to ensure good handling qualities. Augmented flight control systems, however, can add high-order responses to the original low-order aircraft dynamics, and if done without care, this can severely degrade aircraft handling qualities and thus flight safety. To enable the use of the vast database of handling qualities created for conventional aircraft, the Maximum Unnoticeable Added Dynamics (MUAD) envelopes were developed to describe pilots' (subjective) noticeability of the mismatch between the high-order (modified) and low-order (baseline) aircraft dynamics. In controlled experiments, such mismatch was typically induced with *added dynamics* representing the augmented flight control systems. In the frequency-domain, both the magnitude and the phase MUAD envelopes define boundaries within which any added dynamics are not perceived by pilots to noticeably change aircraft handling qualities. These MUAD envelopes are based on subjective ratings, and only qualitative information such as the noticeability of added dynamics are available. It is unknown whether and to what extent task performance, control activity or objective human operator control behavior would change for either unnoticeable or noticeable added dynamics. Moreover, these envelopes are difficult to re-evaluate and re-generate for different baseline aircraft and added dynamics. Recent research indicated that there are no universal MUAD envelopes for all controlled dynamics, since these envelopes are baseline bandwidth depen-

dent.

To overcome these drawbacks of the MUAD envelopes, the goal of this thesis is to develop a new metric, named the *Manual Control Adaptation Boundaries* (MCAB). This new metric should be able to objectively quantify the adaptation of human operator manual control behavior to different controlled dynamics. By comparing the frequency responses of added dynamics with the MCAB, the ranges of the relative changes in task performance, control activity, and human operator control behavior with respect to those of the baseline system can be known. Ideally, these boundaries are independent from any subjective rating, and can be re-generated and re-evaluated more easily, once the *task variables* are known, such as forcing functions, baseline and added dynamics.

In this thesis, the compensatory tracking task was selected for both predicting and measuring human control adaptation to different controlled dynamics. This task allows us to use a model-based, *cybernetic* approach, in which human operator control behavior is explicitly parameterized. Using both offline simulations to predict human adaptation, and human-in-the-loop experiments to measure real human adaptation, the MCAB can be formulated, modified and verified. In this thesis, most experiments used to develop the offline simulation and to verify the MCAB were conducted in the Human-Machine-Interaction (HMI) laboratory at the Aerospace Faculty of Delft University of Technology. For the experiments in which motion feedback was needed, the SIMONA Research Simulator (SRS) was used.

As a start of this thesis, a yaw tracking human-in-the-loop experiment was performed to show that the utilized cybernetic approach can be successfully applied to different types of controlled dynamics (gain, single integrator and double integrator) both without and with simulator motion feedback. For both gain and single integrator controlled dynamics, there were no significant differences in tracking performance and control activity between conditions without and with motion, and the utilization of motion feedback was very limited. For the double integrator, it was found that motion feedback was utilized to improve tracking performance, reduce lead time constant and increase visual time delay. These results indicated that for the double integrator and higher-order controlled dynamics (such as aircraft), motion feedback would be a key factor to study human control adaptation.

Since added dynamics were used as a key factor throughout this thesis to induce human control adaptation, it was crucial to know any potential effects of these dynamics on human control behavior. Moreover, it was necessary to investigate whether human control behavior would depend on the bandwidth of the baseline system, which could affect the formulation of the MCAB as well. To answer these questions, a human-in-the-loop aircraft-representative pitch attitude tracking task was performed, in which added up dipole dynamics with natural frequency at 3 rad/s were cascaded with both low and high-bandwidth baseline dynamics. The results show that, for both low and high-bandwidth systems, with increasing perturbations of the added dipoles, tracking performance worsened, control activity decreased and human operator visual gain decreased. Comparing the low and high-bandwidth systems, the trends of tracking performance, control activity and human operator control behavior with different added dynamics were very similar, indicating that the baseline dynamics' bandwidth had no direct effect on the relative changes in these variables with respect to those of the baseline dynamics. These results indicated that selecting only one set of baseline dynamics for developing the MCAB would be sufficient to achieve the thesis goals.

The remainder of this thesis focused on developing the MCAB, which were based on computer offline simulations and human-in-the-loop experiment verification. The offline simulations relied on the human control model, the general approach of using added dynamics to induce human control adaption and constrained nonlinear optimization techniques, to predict tracking performance, control activity and human operator control behavior. To tune and validate the offline simulation, a human-in-the loop aircraft pitch attitude tracking experiment was performed, in which the baseline dynamics were a Cessna Citation I's aircraft pitch dynamics, and the added dynamics were both up and down dipoles of their natural frequencies locating at 1, 3 and 7 rad/s, respectively. The same baseline dynamics and type of added dipole dynamics were also used for all later simulations and experiments in this thesis. By tuning the remnant-to-control variance ratio in the simulation, a high correlation between the simulation and experiment data was obtained for the tested baseline and added dynamics. This remnant-to-control variance ratio was then fixed for all the later simulations performed in this thesis. In the experiment, subjective ratings on the noticeability of the added dynamics were collected. However, the ratings were found to be inaccurate and inconsistent among subjects, and subjective ratings were not used in the remainder of this thesis, and no correlations were made between subjective data and objective measures.

This tuned offline simulation tool was directly used to generate the simulation-based MCAB. Simulation data of tracking performance, control activity and human operator control behavior for a number of 505 controlled dynamics were collected. Simulation results show that control activity was most sensitive to the added dynamics within the MUAD envelopes. Four dependent measures were selected to quantify the MCAB: the relative changes of tracking performance, control activity, ratio of the visual gain and lag time constant, and the lead time constant with respect to those of the baseline. The MCAB of each individual measure were both magnitude and phase boundaries defined in the frequency-domain, which were the "outermost" boundaries of all simulation added dipole dynamics, of which the corresponding dependent measure was below a certain amount of change. To tie in with the concept of the original MUAD envelopes, these four MCAB were then combined into one single set of boundaries, named the *Integrated Manual Control Adaptation Boundaries* (IMCAB). The IMCAB were calculated as the intersection of all the MCAB for magnitude and phase, respectively. The IMCAB are "hourglass-shaped", and are the narrowest at 3 rad/s, i.e., in the crossover frequency region, and much wider at other frequencies.

Before verifying these simulation-based MCAB with new experiment data, it was necessary to investigate to what extent motion feedback could affect the MCAB. For this, a human-in-the-loop aircraft pitch attitude tracking experiment perturbed by added dipole dynamics was performed in the SRS. Each dynamics configuration was tested both without and with simulator motion feedback. Discrepancies for the relative changes in tracking performance, control activity and human operator control behavior between the motion and no-motion cases were found to be very small, which indicated that the MCAB would not change very much even motion feedback was considered. Hence, the MCAB were further developed and verified without any motion feedback.

The human-in-the-loop experimental verification of the simulation-based MCAB focused on both up and down added dipoles, with gradually changing damping ratios, and with their natural frequencies at 1 rad/s. For the MCAB related dependent measures with

the tested up dipoles, the match between the simulation and experiment data was very good. For the tested down dipoles, clear discrepancies were observed for the relative changes in control activity and ratio of the visual gain and lag time constant. To account for these discrepancies at the tested down dipoles, two correction coefficients were calculated to match the simulation with the experiment data for the relative changes of the control activity and the ratio of the visual gain and lag time constant, respectively. All the simulation data of control activity and ratio of the visual gain and lag time constant (which formed the simulation-based (I)MCAB) were modified by multiplying these two correction coefficients, and the *modified* (I)MCAB were thus generated based on these modified simulation data. Due to the fact that the offline simulation prediction results were very close to the experiment data, these modifications were small, thus the modified (I)MCAB were very similar to the original simulation-based (I)MCAB. Finally, all the tested up and down dipoles were compared with the modified MCAB. In general, at 1 rad/s, the modified MCAB can accurately describe the relative changes in tracking performance, control activity and human operator control behavior with respect to those of the baseline.

Compared with the original MUAD envelopes, the MCAB developed based on the objective cybernetic approach are more quantitative, repeatable and also more easily verified. The MCAB are based on an explicit human control model and objective measures, which guarantees that the boundaries would not be affected by any subjective judgment. As long as the task variables for the control task are the same, these MCAB should be able to be re-generated. Moreover, following the same approach developed in this thesis, the MCAB can be applied to different controlled dynamics, added dynamics and forcing functions if necessary. Thus the (I)MCAB can be used as an alternative tool, for example, to evaluate (simulator) aircraft model fidelity and help assess the effects of augmented flight control systems on task performance, control activity and human operator control behavior. In the past, many of these investigations were conducted only using subjective methods.

In future work, it is necessary to investigate, whether and how the shape of (I)MCAB would change if different types baseline and added dynamics are used. Moreover, to generate the (I)MCAB by only modifying the parameters of the baseline aircraft dynamics would be of interest to investigate human sensitivity to the aircraft dynamics, which could be useful to gain insight into, for example, the relationship between objective control behavior and aircraft handling qualities. In the end, even though the (I)MCAB developed in this thesis are based on relatively simple compensatory tracking tasks, this does not stop the application of the (I)MCAB for more complicated manual control tasks such as pursuit or preview tracking tasks. The challenges that lie in front of us are mainly to more thoroughly understand and more precisely model human control behavior, which would facilitate the development of (I)MCAB for these more realistic and relevant control tasks in the near future.

SAMENVATTING

OBJECTIEVE BEPALING VAN DE LIMIETEN VAN MENSELIJKE STUURGEDRAGSAANPASSINGEN MET EEN CYBERNETISCHE AANPAK

TAO LU

Wij komen als mensen overal in onze dagelijkse activiteiten in aanraking met handmatige stuurtaken. Door het vermogen om ons naadloos aan te passen aan het besturen van veel verschillende voertuigen, zoals auto's en vliegtuigen, zijn we in staat om alsmaar verder, sneller en hoger te reizen. Het vermogen van menselijke bestuurders om zich aan te passen aan de dynamische karakteristieken van bestuurde voertuigen is essentieel voor veel taken waar hoge stuurprecisie en hoge mate van veiligheid vereist is. Op dit moment kan op dat vlak nog geen enkel geavanceerd automatisch besturingssysteem zich meten met de mens. Bijvoorbeeld, bij autoraces zijn de professionele coureurs essentiële factor om consequent het uiterste uit de raceauto's te halen, met mogelijk wijzigende ontwerpen en configuraties. Daarmee vervullen deze bestuurders ook meteen een belangrijke rol in het verder ontwerpen en finetunen van de auto's zelf. In de luchtvaart zijn menselijke piloten nog steeds onze "laatste verdedigingslinie" voor het verzekeren van de vliegveiligheid, vooral in noodsituaties waarin veel van de huidige automatische vluchtsystemen falen.

We weten echter ook dat er limieten zijn aan het vermogen van de mens om zich aan te passen. Om die reden wordt het bijvoorbeeld in de luchtvaart van cruciaal belang geacht om zorg te dragen voor de *besturingseigenschappen* van vliegtuigen en door goed ontwerp te zorgen dat die inherent stabiel zijn en dus gemakkelijk kunnen worden bestuurd. De traditionele aanpak om goede besturingseigenschappen te garanderen houdt in dat er gezorgd wordt dat de karakteristieken van de inherente eigenmodes van het vliegtuig, zoals de natuurlijke frequentie en demping van de snelle slingering ("short-period mode"), binnen gewenste marges vallen. In moderne vliegtuigen kunnen echter de beschikbare automatische stabiliserings- en besturingssystemen zorgen voor extra, mogelijk niet-lineaire en hoge orde, dynamica bovenop de inherente vliegdynamica, wat de besturingseigenschappen van het vliegtuig ernstig, mogelijk tot het gevaarlijke toe, kan verslechteren. Om ook de enorme database verzameld voor onderzoek naar de besturingseigenschappen van conventionele vliegtuigen te kunnen toepassen, zijn daarom "Maximum Unnoticeable Added Dynamics" (MUAD) criteria ontwikkeld, die de (subjectieve) merkbaarheid van dit soort verschillen met de originele (lage orde) vliegdynamica aangeven. In gecontroleerde wetenschappelijke experimenten worden de grenzen van de merkbaarheid van verschillen doorgaans bepaald door die te induceren met expliciete *toegevoegde dynamica* die bijvoorbeeld de effecten van extra hoge orde dynamica van geavanceerde besturingssystemen benade-

ren. De MUAD-criteria bestaan uit grenzen, gedefinieerd in het frequentiedomein, op de absolute waarde en faseverdraaiing die maximaal door toegevoegde dynamica mag worden geïnduceerd voordat die merkbaar worden voor piloten en dus de besturingseigenschappen van het vliegtuig zou veranderen. De beschikbare MUAD-criteria zijn afgeleid uit subjectieve beoordelingsdata van piloten, voornamelijk kwalitatieve informatie over bijvoorbeeld de merkbaarheid van toegevoegde dynamica. Tot op heden is het onbekend of, en in welke mate, de objectieve stuurprestaties, stuuractiviteit en het objectieve gemeten stuurgedrag van menselijke bestuurders zich aanpassen aan toegevoegde dynamica die volgens de MUAD-criteria merkbaar of niet merkbaar zouden moeten zijn. Ten tweede zijn, door de directe afhankelijkheid van subjectieve pilootgegevens, deze criteria moeilijk te verifiëren en opnieuw te genereren voor verschillende basisvliegtuigdynamica en toegevoegde dynamica. Recent onderzoek heeft aangetoond dat er geen universele MUAD-criteria zijn voor alle bestuurde dynamica, omdat de merkbaarheidsgrenzen afhankelijk zijn van de bandbreedte van de basisvliegtuigdynamica.

Om deze nadelen van de originele MUAD-criteria aan te pakken, wordt in dit proefschrift een nieuw criterium te ontwikkeld, wat de aanpassing van het menselijke stuurgedrag als gevolg van het toevoegen van verschillende gecontroleerde dynamica expliciet en objectief kwantificeert. Dit nieuw ontwikkelde criterium wordt in dit proefschrift de *Manual Control Adaptation Boundaries* (MCAB) genoemd. Door de frequentieresponsie van bepaalde toegevoegde dynamica te vergelijken met de MCAB, kan de grootte van de relatieve verandering in taakprestaties, stuuractiviteit en kritieke instellingen van het menselijke stuurgedrag worden bepaald. Aangezien de menselijke aanpassingslimieten hoogstwaarschijnlijk sterk afhankelijk zijn van de instellingen van verschillende kritieke *taakvariabelen* – zoals de basis vliegtuigdynamica, de toegevoegde dynamica en de bandbreedte van de taak ("forcing functions") – is het van belang dat de grenzen van de MCAB eenvoudig voor meerdere gevallen (en dus zonder experimenten en subjectieve beoordelingen) kunnen worden bepaald.

In dit proefschrift wordt een modelgebaseerde, *cybernetische*, aanpak gevolgd om de aanpassingen in het menselijke stuurgedrag zo expliciet mogelijk te kunnen kwantificeren. Door te werken met menselijk stuurgedrag in compenserende stuurtaken is het mogelijk om menselijke stuurgedragsaanpassingen als gevolg van veranderde vliegdynamica via beschikbare modellen van menselijk vaardigheids-gebaseerd stuurgedrag kwantitatief te analyseren. Op deze manier kunnen voorspellingen van menselijke stuurgedragsaanpassingen uit computer simulaties, in combinatie met aanpassingen gemeten bij echte menselijke bestuurders in daarvoor opgezette experimenten, gebruikt worden om de MCAB af te leiden, te corrigeren, en te verifiëren. De meeste experimenten die in dit proefschrift worden gebruikt voor het ontwikkelen en verifiëren van de opgezette computersimulaties en de daaruit afgeleide MCAB zijn uitgevoerd in de (fixed-base) cockpit simulatieopstelling van het Human-Machine-Interaction (HMI) laboratorium van de Faculteit Luchtvaart- en Ruimtevaarttechniek van de Technische Universiteit Delft. Voor de experimenten waarbij ook de fysieke voertuigbewegingen voelbaar moesten zijn voor de proefpersonen is de met een bewegingssysteem uitgeruste SIMONA Research Simulator (SRS) gebruikt.

In het eerste hoofdstuk van dit proefschrift wordt een experiment, waar menselijke stuurders een gierhoekstuurtaak uitvoerden, gebruikt om te laten zien dat de gebruikte cybernetische benadering met succes kan worden toegepast voor het kwantificeren van stuur-

gedragsaanpassingen op verschillende soorten gecontroleerde dynamica (positie-, snelheids- en versnellingsbesturing), zowel met als zonder fysieke bewegingsterugkoppeling van de simulator. Voor zowel positie- en snelheidsbesturingsdynamica werden geen significante verschillen in taakprestatie en besturingsactiviteit tussen condities met en zonder beweging gevonden. In het algemeen, lijken menselijk stuurders bewegingsterugkoppeling bij dit soort dynamica vrijwel niet te gebruiken. Bij versnellingssturing werd bewegingsterugkoppeling duidelijk gebruikt om de volgprestaties te verbeteren, visuele voorspellingstijdscontante te verlagen en de visuele tijdvertraging te verhogen. Deze resultaten suggereerden dat bij versnellingsbesturing en andere hogere orde bestuurde dynamica (zoals vliegtuigen) bewegingsterugkoppeling een belangrijke bijkomende factor zou kunnen zijn in het bestuderen van menselijke aanpassingen aan bestuurde dynamica.

Aangezien extra *toegevoegde* dynamica in dit proefschrift wordt gebruikt als experimentele techniek om menselijke controleaanpassing te induceren, was het cruciaal om in een vroeg stadium alle mogelijke effecten van toegevoegde dynamica op het menselijke stuurgedrag te karakteriseren. Ten tweede was het noodzakelijk om te onderzoeken in hoeverre menselijke stuurgedragsaanpassingen door toegevoegde dynamica afhankelijk zijn van de bandbreedte van de gekozen basis vliegtuigdynamica, omdat dit ook de formulering en geldigheid van de MCAB zou beïnvloeden. Om deze factoren te onderzoeken is een experiment uitgevoerd waarin proefpersonen een standhoeksstuurtaak uitvoerden met basisvliegtuigdynamica die representatief zijn voor conventionele vliegtuigen. Zowel basisvliegdynamica met hoge als lage bandbreedte zijn getest, beiden met dezelfde set van toegevoegde dynamica: zeven dempingsinstellingen van een dipool gecentreerd op een frequentie van 3 rad/s. De resultaten laten zien dat met toenemende sterkte van de toegevoegde dipooldynamica de stuurprecisie en de stuuractiviteit afnemen, net als de versterkingsfactor van de geschatte menselijke stuurdynamica. De gevonden veranderingen in menselijke stuurprestaties en stuurdynamica bij het besturen van vliegdynamica met lage als met hoge bandbreedte waren zeer vergelijkbaar, wat aangeeft dat voor de geteste variatie in basisvliegdynamica geen direct effect op de relatieve veranderingen in deze variabelen door het toevoegen van extra dynamica kon worden aangetoond. Op basis van deze resultaten is besloten dat het ontwikkelen van de MCAB in dit proefschrift in eerste instantie gedaan kon worden met één enkele representatieve set van basisvliegdynamica, zonder in te boeten op de toepasbaarheid van het eindresultaat.

Na deze twee exploratieve experimenten richt de rest van dit proefschrift zich op het ontwikkelen van de MCAB, via computersimulaties met menselijke stuurmodellen en door de mens gestuurde ("human-in-the-loop") experimenten ter verificatie. De computersimulaties zijn opgezet om aanpassingen in menselijke stuurprestaties, stuuractiviteit, en stuurgedrag als gevolg van toegevoegde stuurdynamica te voorspellen met menselijke stuurmodellen en niet-lineaire optimalisatietechnieken. Om kritieke parameters van de simulatieopzet op representatieve waarden te kunnen instellen en dus de gegeneerde simulatiedata te valideren is een experiment met menselijke proefpersonen uitgevoerd. In dit experiment is gekeken naar een standhoeksstuurtaak waar proefpersonen als basisvliegdynamica een model van standhoekdsdynamica van een Cessna Citation I bestuurden, met een variatie in toegevoegde versterkende ("up") en afzwakkende ("down") dipooldynamica, gecentreerd op frequenties van 1, 3, en 7 rad/s. Een hoge correlatie tussen de simulatie- en experimentresultaten is verkregen door het precies afstemmen van de sterkte van de ruisbijdrage ("remnant") aan de

gesimuleerde menselijke stuursignalen. Deze zelfde basisvliegdynamica, de vorm van de toegevoegde (dipool)dynamica, en ook de sterkte van de gesimuleerde remnantbijdrage zijn ook voor de verdere simulaties en stappen die beschreven zijn in dit proefschrift gebruikt. Naast objectieve stuurdata zijn in het gedane experiment ook subjectieve beoordelingen over de merkbaarheid van de toegevoegde dynamica verzameld. Deze beoordelingen bleken echter onnauwkeurig en inconsistent te zijn, zowel binnen als tussen proefpersonen, en zijn dus in dit proefschrift verder niet gebruikt als extra metriek of om de objectief gemeten gedragsveranderingen mee te correleren.

De ontwikkelde en gevalideerde simulatieopzet is vervolgens gebruikt om de geplande simulatie-gebaseerde MCAB te genereren. Dit is gedaan op basis van voorspelde relatieve veranderingen in menselijke stuurprestaties, stuuractiviteit en stuurgedragsparameters ten opzichte van het sturen van de basisvliegdynamica, voor een totaal aantal van 505 variaties in toegevoegde bestuurde dynamica. De simulatieresultaten tonen aan dat van alle menselijke parameters de stuuractiviteit het meest gevoelig is voor het toevoegen van extra dynamica, met zelfs sterke variaties voor toegevoegde dynamica die binnen de MUAD-criteria vallen. De relatieve veranderingen in vier kwantitatieve stuurgedragsmetrieken zijn uiteindelijk geselecteerd om de MCAB te bepalen: de precisie van sturen, de stuuractiviteit, verhouding van de visuele versterkingsfactor en de visuele vertragingstijdsconstante, en de visuele voorspellingstijdsconstante. Door een zekere maximaal toelaatbare relatieve verandering in deze stuurgedragsmetrieken te vast te stellen, vervolgens te kijken welke van de geteste toegevoegde dipooldynamica daaraan voldoen en vervolgens op elke frequentie in het frequentiedomein te kijken welke dipolen de “buitenste” grenzen stelden in zowel absolute waarde als faseverdraaiing, is voor elke afzonderlijke metriek een MCAB bepaald. Om het eindresultaat te kunnen toepassen en te kunnen vergelijken met de originele MUAD-criteria zijn de vier MCAB vervolgens gecombineerd tot één enkele set grenzen, die in dit proefschrift de *Integrated Manual Control Adaptation Boundaries* (IMCAB) zijn genoemd. De uiteindelijke IMCAB zijn bepaald uit de combinatie van alle MCAB, waar de ruimste MCAB in absolute waarde en fase de IMCAB definieert. Net als de originele MUAD-criteria zijn de IMCAB “zandlopervormig” en het nauwst rond de 3 rad/s, dus in de buurt van het crossover-gebied.

Ook is onderzocht in hoeverre de bepaalde MCAB en IMCAB afhankelijk zouden kunnen zijn van de aanwezigheid van bewegingsterugkoppeling. Om dit te verifiëren is een experiment met een standhoeksstuurtaak uitgevoerd in de SRS, met wederom een variatie aan toegevoegde dipool-dynamica. Elke conditie werd zowel zonder als met bewegingsterugkoppeling van de simulator getest. De gemeten relatieve veranderingen in stuurprestaties, stuuractiviteit en stuurgedragsparameters waren zeer vergelijkbaar voor de twee bewegingsinstellingen, waaruit de conclusie is getrokken dat de MCAB niet sterk zouden veranderen als de invloed van bewegingsterugkoppeling expliciet zou worden meegenomen. Om die reden zijn in dit proefschrift de MCAB verder ontwikkeld en geverifieerd voor stuurtaken zonder bewegingsterugkoppeling.

Voor experimentele verificatie van de uit simulatiedata afgeleide MCAB is gekozen voor een experiment met zowel versterkende (“up”) als verzwakkende (“down”) dipolen met een hoge resolutie aan geteste dempingsverhoudingen, allemaal gecentreerd op een frequentie van 1 rad/s. Voor alle vier de metrieken die ten grondslag liggen aan de MCAB was voor de up-dipolen de overeenkomst tussen de voorspellende simulatiedata en de expe-

riment gegevens uitermate goed. Voor de down-dipolen werden echter de relatieve veranderingen in stuuractiviteit en de verhouding van de visuele versterkingsfactor en de visuele vertragingstijdsconstante in de simulatiedata onderschat. Om voor het effect hiervan te compenseren in het bepalen van de MCAB zijn twee correctiecoëfficiënten ingevoerd voor deze twee metrieken. Vervolgens zijn voor het bepalen van *aangepaste* (I)MCAB alle simulatiedata voor de stuuractiviteit en de verhouding van de visuele versterkingsfactor en de visuele vertragingstijdsconstante vermenigvuldigd met de respectievelijke correctiecoëfficiënten. Aangezien de verschillen tussen de simulatievoorspellingen en de experimentele data consistent, maar in absolute waarde beperkt, waren, zijn de uiteindelijke verschillen tussen de aangepaste (I)MCAB en de originele op simulatiedata gebaseerde (I)MCAB zeer beperkt. Als laatste zijn ook de frequentiedomein beschrijvingen van alle geteste up- en down-dipolen expliciet vergeleken met de aangepaste MCAB. Hieruit kon geconcludeerd worden dat bij 1 rad/s de aangepaste MCAB de relatieve veranderingen in stuurprestaties, stuuractiviteit en stuurgedragsparameters van de menselijke operator ten opzichte van het besturen van de basisvliegtuigdynamica nauwkeurig beschrijven.

De in dit proefschrift bepaalde MCAB zijn ontwikkeld op basis van een objectieve cybernetische benadering en daardoor vergeleken met de oorspronkelijke MUAD-criteria kwantitatiever, flexibeler en herhaalbaarder te bepalen, en ook eenvoudiger te controleren. De MCAB zijn gebaseerd op een expliciet menselijk stuurgedragsmodel en objectieve stuurmetrieken, wat garandeert dat de bepaalde grenzen niet worden beïnvloed door een subjectief oordeel. Zolang de taakvariabelen voor de stuurtaak hetzelfde zijn, moeten de in dit proefschrift gepresenteerde MCAB via dezelfde aanpak ook door anderen gegenereerd kunnen worden. Daarnaast is het mogelijk om volgens exact dezelfde stappen die in dit proefschrift zijn doorlopen ook MCAB te bepalen voor andere basisvliegtuidynamica, andere types toegevoegde dynamica, en andere taakbandbreedtes (“forcing functions”). Daardoor kunnen de (I)MCAB potentieel worden gebruikt als een hulpmiddel om bijvoorbeeld de benodigde betrouwbaarheid van vliegtuigmodellen voor vluchtsimulatoren te bepalen en de effecten van verbeterde automatische vliegtuigbesturingssystemen op stuurprecisie, stuuractiviteit en expliciete stuurgedragsparameters van menselijke bedieners te kwantificeren. In het verleden was men voor dit soort onderzoeken veelal afhankelijk van subjectieve methoden, met de daarbij horende betrouwbaarheid.

In de vervolgstappen voor dit onderzoek zal moeten worden onderzocht of, en hoe, de vorm van de (I)MCAB zou kunnen veranderen als verschillende soorten basisvliegtuigdynamica en toegevoegde dynamica worden gecombineerd. Daarnaast is het de moeite waard om ook (I)MCAB af te leiden voor toelaatbare veranderingen in de parameters van de basisvliegtuigdynamica zelf, in plaats van voor het toevoegen van bepaalde extra bestuurde dynamica. Dit zou van direct nut kunnen zijn voor het verder onderzoeken van de relatie tussen objectief menselijk stuurgedrag en de besturingseigenschappen van vliegtuigen Hoewel de (I)MCAB die zijn ontwikkeld in dit proefschrift zijn bepaald uit menselijk stuurgedrag in relatief eenvoudige vaardigheidsgebaseerde compenserende (“compensatory”) stuurtaken, staat dit niet direct de toepassing van de (I)MCAB voor meer gecompliceerde stuurtaken, zoals “pursuit” of “preview” volgtaken, in de weg. De uitdagingen die voor ons liggen, zijn vooral om grondiger inzicht te krijgen in de menselijke capaciteit voor aanpassingen in het stuurgedrag en dat proces beter in kwantitatieve mensmodellen te vangen. Dit zou in de zeer nabije toekomst, volgens de stappen beschreven in dit proefschrift, ook het ont-

wikkelen van (I)MCAB voor dergelijke meer realistische en relevante stuurtaken eenvoudig mogelijk maken.

CONTENTS

1

INTRODUCTION

1.1. BACKGROUND

1.1.1. MANUAL CONTROL IS INDISPENSABLE

This thesis investigates how humans manually control vehicles and how human manual control behavior is influenced when the vehicle dynamics change. Manual control tasks are very normal activities that people carry out every day: on the road people ride bikes and drive cars from home to their workplace, on the water people go boating and rowing, in the sky pilots fly aircraft transporting goods and passengers. While these activities can take place at different places with different types of vehicles, they have one thing in common: humans fulfill a mostly critical task in directly manually controlling these vehicles.

At the early age of automotive and aviation, in order to travel farther, faster and higher, we were willing and dared to spend hours steering a wheel, pushing the pedals and pulling the cables with our muscles to manually control cars and aircraft. Meanwhile, with the fast development of technologies, vehicles gained much more maneuverability and operational range. However, without taking human factors into account during the design phase, these vehicles became very difficult or even impossible to control for humans, which led to system failures and accidents. To solve these problems, an understanding of how humans control vehicles, and what their limitations are in manual control tasks became crucial.

Some of the pioneering research on human manual control behavior started from military applications, for example, to investigate how to lay a gun both quickly and accurately on a moving target by manually controlled power operation [1], and how to both fast and accurately track the hostile aircraft flying ahead during air combat. From many similar studies, manual control theory has been developed to help us gain insights into how indeed humans control vehicles, and how to utilize the theory to improve the task efficiency and safety. The developed technologies have been broadly applied in the aerospace [2–11], automotive [12–16], and medical domains [17–20].

In modern days, with the development of computer technologies, a car can almost drive automatically between two places and an airplane can take off from one airport and land

on another almost without pilot intervention. The pace of automation technology development is so fast that many people believe that soon automation will take over all tasks currently carried out manually by humans. However, whether and when this full automation era would be eventually realized is still unknown. Furthermore, even with so many automation technologies, humans still enjoy manual control tasks in their lives, such as in sports. In Formula One, regulations forbid techniques such as active suspension, steering-by-wire, traction control or anti-lock braking system (ABS) on the racing cars, to prevent such techniques from causing excessive and unfair advantages to different racing drivers and teams[21]. This ensures that it is the driver rather than the control systems that pushes the racing car to its performance limit. Furthermore, today most of the cars are still driven by human drivers and aircraft are still flown by human pilots, whether the general public would accept, for example, fully automated passenger aircraft without pilots is still uncertain [22].

A common misunderstanding is that, since pilot errors are considered the main cause for aviation accidents [23], fully automated aircraft without pilots could be a solution to prevent similar accidents from happening. However, in reality it is difficult to guarantee that automatic control systems do not make mistakes (since these systems are designed and produced by humans who can make mistakes). In these cases where (part of) automatic systems fail, humans' adaptation ability is essentially crucial for safety. For example, Chesley Sullenberger successfully landed an A320 airplane after loss of thrust in both engines on the Hudson River and saved 155 people's lives [24].

In domains where high performance and high safety are needed, none of the state-of-the-art automatic control systems can fully mimic the adaptive and intelligent control behavior of humans. To design automatic control systems which are able to compete with a highly nonlinear [25, 26], time-varying [27, 28] and adaptive [29, 30] human is still extremely challenging. For example, in the racing industry, driving simulators are widely used in the development phase of the racing cars. Human drivers are able to adapt himself/herself to many different circuits, weather conditions and vehicle settings while consistently minimizing their lap time. The "adaptive" and "intelligent" human drivers are helpful for engineers to design both a drivable and fast car. In aviation, during the design phase of aircraft, it is difficult to know in advance whether the aircraft would be able to be flown with ease and enough stability by the pilot. Human-in-the-loop tests in flight simulators are still the dominant approach to tackle these problems [6, 31–33].

In summary, considering the crucial demands for safety and performance in driving and flying, human manual control is still quite indispensable. More importantly, knowing what the potential factors are that influence manual control behavior, and how humans react to changes in these elements, is crucial for the design of future human-machine systems and interfaces.

1.1.2. MANUAL CONTROL TASK AND INFLUENCING FACTORS

Manual control tasks have been investigated by many researchers [1, 29, 34–36] to study the mechanisms of the human manual control behavior and develop corresponding human control theories. As a typical example, the figure used in [29], showing the general structure of a manual control task and the potential factors which influence the human manual control behavior is reproduced in Figure 1.1.

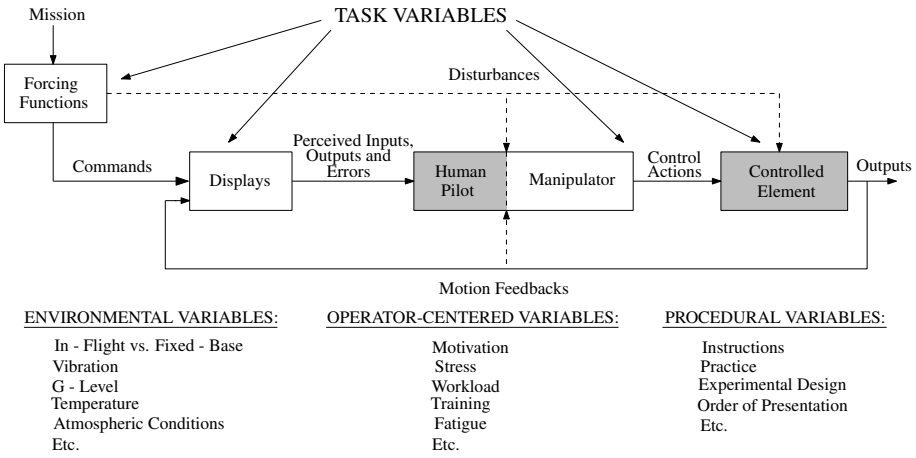

Figure 1.1: A schematic representation of a manual tracking task and the variables that affect a pilot-vehicle system. This figure is reproduced from [29], with adjustment to emphasize the relation between the human pilot and the controlled element, which is the main focus of this thesis.

In Figure 1.1, the human pilot (or operator) receives visual information from the displays and uses a control manipulator to steer the controlled element, typically to match the controlled element's output with the reference set up by the forcing functions. Forcing functions are commanded signals which the human operator needs to track and follow, it can be the position of the aircraft flying ahead or the position of a far-away runway on which the aircraft needs to land. Displays can be a screen, an instrument indicator or the outside-view of the cockpit which present visual information to the human operator.

In general, the displays can be categorized into *compensatory* [11], where only the error signal of the difference between the commanded signals and the controlled system's output, is presented; *pursuit* [37], where both the commanded signals and controlled element's output at current time instant are provided; and *preview* [38], besides the commanded signals and controlled system's output at current time instant, the future commanded signals in space and time are also presented, for example, the road ahead of the current position of a moving car can be taken as the future signal.

The manipulator is the inceptor through which the human operator gives control input to the controlled element. It can be a joystick, pedal or steering wheel, or similar devices. Finally, the controlled element is typically the vehicle that the human operator controls, which can, for example, be aircraft or a car. As can be seen in Figure 1.1, the forcing functions, displays, manipulator and controlled element are categorized into the *task variables*, which are considered the most important factors influencing human manual control behavior in this closed-loop manual control task [29, 39–45].

Similar to the *task variables* in Figure 1.1, other factors can also make a difference on human manual control behavior. For example, for the *environmental variables*, the presence of physical motion feedback can affect pilot control behavior, thus the state-of-the-art flight simulators are usually equipped with high-fidelity motion platforms [11, 46, 47]; the *operator-centered variables* such as training (and its interaction with the motion feedback) can also significantly influence the task performance and human operator control behavior

[48–51]. The same holds for the *procedural variables*, for example, how the instructions are provided and whether there is practice of the control task also make a difference.

No matter how these factors are varied and how they influence human manual control behavior, to successfully fulfill the task, system stability is usually the prior concern for the human operator. For example, when driving a car on the road, the driver has to first safely steer the car from one place to another without a crash; when landing an airplane, the pilot would usually control it smoothly without becoming trapped in pilot-induced-oscillations [52–54]. Once the vehicle can be controlled in a stable and safe manner, to improve the task performance is often the next step. For example, a racing car driver always aims to minimize his/her lap time; during air combat a fighter pilot has to track the airplane flying ahead as fast and as accurate as possible to shoot it down; and an airline pilot strives for comfortable, consistent and safe maneuvers and landings. In any environment, humans must adapt their own control dynamics to the given tasks by meeting the stability and performance requirements [29].

1.1.3. ADAPTATION TO THE CONTROLLED ELEMENT

Among all the factors which may influence human manual control behavior, the relationship between the human operator and the controlled element is of critical interest and is the main focus of this thesis (see Figure 1.1). Humans' inherent adaptation ability to different controlled elements is the essential reason that we are able to control so many different vehicles in our daily life. It is very likely that the corresponding manual control behaviors for these control tasks are completely different from each other [11, 55, 56]. Since humans can automatically solve the "how to control" problems over a wide variety of vehicles and control tasks, manual control and humans' adaptation ability were once utilized by control system engineers to help design automatic control systems [30].

To better understand the mechanisms of the humans' adaptation to the controlled element in manual control tasks, skill-based *compensatory tracking tasks* were widely used [1, 29, 34–36]. The well-known *crossover model* [29] states that in compensatory tracking tasks with any controlled element (dynamics), the human operator *adapts* and *optimizes* his/her own control dynamics to make the total human-vehicle system a single integrator with an effective time delay term at the *crossover frequency*. It was also found that the crossover frequency is a key parameter, which depends on the controlled element dynamics (for example, gain, single integrator and double integrator, which correspond with position, velocity and acceleration control, respectively) [29, 36]. The ways in which human operator *adapts* and *optimizes* his/her own control dynamics are reflected in the various forms of the equalization and the values of the internal parameters [29, 36], which will be introduced in detail in Section 1.4.2.

As can be seen in Figure 1.1, motion feedback can affect human control behavior in manual control tasks. Previous research [57–62] found that for controlled dynamics such as aircraft, motion feedback can significantly improve task performance, lower human operator's control activity, increase human operator's visual time delay and decrease the visual lead time constant. For more stable controlled elements, the effects of motion feedback are less strong [58, 59, 63, 64]. In this thesis, it is of interest to investigate the humans' adaptation to different controlled elements both with and without motion feedback.

1.1.4. MAXIMUM UNNOTICEABLE ADDED DYNAMICS (MUAD)

Humans' adaptation ability is a natural gift that allows us to carry out many different kinds of manual control tasks, however, obviously this ability does not guarantee that we can control all vehicles in the same manner. Our inherent limitations, such as the delay between signal observation and control action output, can severely degrade the task performance and even jeopardize the task safety. In aviation, being able to know what designs of aircraft are safe and able to be controlled with ease is crucial, not only because making aircraft is very expensive but also because flight accidents should be prevented at all costs.

Aircraft *handling qualities* involve the study and evaluation of the low-level stability and control characteristics of aircraft, which are critical for flight safety and the ease of controlling an airplane in steady flight and in maneuvers. Aircraft handling qualities are considered as a pilot-perceived qualitative description of the adequacy of the aircraft responses to controls in the execution of the flight task [6, 65]. Previous studies [34, 36] have pointed out that to acquire proper aircraft handling qualities, a satisfactory match between the aircraft characteristics and the human pilot's characteristics is required.

According to the well-known crossover model [29], for example, by adjusting the damping and natural frequency of aircraft short-period dynamics, in addition with pilot's own limited adaptation, a single integrator like pilot-aircraft system dynamics can be achieved. These aircraft modes parameters were strictly constrained in criteria MIL-F-8785 [66] for aircraft design. However, the introduction of flight control systems caused problems, for example, the existing criteria considering only aircraft simple modes of motion cannot fully characterize the responses of newer aircraft with control augmentation [54].

Augmented flight control systems can introduce high-order effects, deviating the pilot-aircraft system from the flight with un-augmented aircraft with classical flight control systems, for which an extensive body of handling qualities criteria was developed [66, 67]. For example, the inevitable time delay associated with computer-controlled systems [67] can significantly degrade aircraft handling qualities. New criteria which could help engineers design and analyze augmented aircraft were necessary. One of the solutions was to match the high-order responses of the augmented aircraft with their low-order equivalent systems (LOES) [54, 68] in order to keep utilizing the existing handling qualities criteria. The equivalent system parameters were then used for assessment of the overall handling qualities, as described in MIL-F-8785C. However, a major difficulty with equivalent systems was that *acceptable levels* of mismatch between a high-order system and its low-order equivalent had not been clearly defined.

Between 1970 and 1980, the Equivalent System Program (ESP) [67, 69–72] was thus proposed to define the acceptable levels of mismatch between high-order systems and their LOES. The Neal-Smith [69, 70] and the Landing Approach High Order System (LAHOS) experiments [71] served as the database for this study. In both projects, the variable stability NT-33 aircraft was used as the testing aircraft. Multiple configurations of aircraft short-period dynamics were used as the baseline. The flight control systems were represented by the *added dynamics* which were cascaded with the baseline aircraft dynamics during the flight test. The tested added dynamics in these two projects included first-order lag, first-order lead-lag, second-order lag, fourth-order lag, second-order lag combined with first order lead-lag [69–71]. These added dynamics were also used to test pilots' subjective noticeability on the differences between the modified and the original aircraft dynamics.

In both projects, aircraft pitch attitude compensatory tracking tasks were performed using instrument flight rules (IFR), in which pilots adopted a high-frequency control behavior [6] to gain useful insight into the handling qualities of the augmented aircraft. The Cooper-Harper rating scale [73] was used to evaluate the handling qualities of the aircraft with different added dynamics. A schematic representation of these tracking tasks is shown in Figure 1.2.

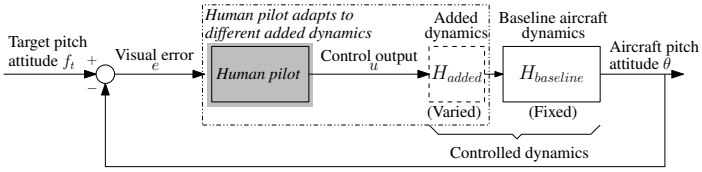

Figure 1.2: A schematic representation of the aircraft pitch attitude tracking tasks performed in Neal-Smith and Landing Approach High Order (LAHOS) System projects [69–71].

In Figure 1.2, the pilot controls the aircraft pitch attitude θ to minimize the visual error e seen from the attitude indicator on the dashboard in the cockpit [69–71]. The visual error e is the difference between the designed target pitch attitude f_t (discrete or random [69–71]) and the aircraft pitch attitude θ. Control output u can be the deflection of the manipulator (for example, a control yoke or a joystick) given by the pilot. The pilot's adaptation to different controlled dynamics was studied by varying the added dynamics H_{added} with fixed baseline aircraft dynamics $H_{baseline}$. The "critical added dynamics" were chosen as the strongest ones (as the parameters of the added dynamics changed gradually) that showed no difference from baseline system's pilot rating. The critical dynamics of all tested added dynamics were found and overlaid on a common Bode plot, and envelopes were drawn by fairing smooth curves either through or tangent to parts of the various added dynamics [67, 72]. The resulting envelopes were then matched by transfer functions for convenience and repeatability [67], and were referred to as the *Maximum Unnoticeable Added Dynamics (MUAD) envelopes* by Wood et al. [67], illustrated in Figure 1.3.

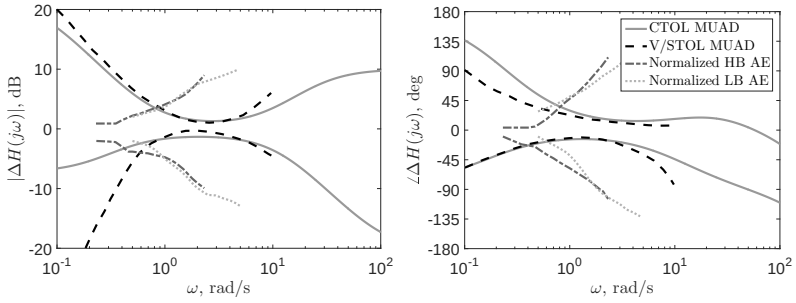

(a) Magnitude (b) Phase

Figure 1.3: Comparisons among CTOL Maximum Unnoticeable Added Dynamics (MUAD) envelopes [67], V/STOL MUAD [72], normalized high-bandwidth (HB) Allowable Error (AE) envelopes and normalized low-bandwidth (LB) AE [74].

In Figure 1.3, ΔH represents the mismatch between the "total" dynamics and baseline dynamics, which with the setup of Figure 1.2 equals H_{added}:

$$\Delta H = \frac{H_{total}}{H_{baseline}} = \frac{H_{baseline} H_{added}}{H_{baseline}} = H_{added}, \tag{1.1}$$

where $H_{baseline}$ is the baseline (aircraft) dynamics, H_{added} is the added dynamics, and H_{total} is the total controlled dynamics ($H_{baseline} H_{added}$). In Figure 1.3, the CTOL MUAD magnitude and phase envelopes define boundaries, within (or on) which any dynamics added to the baseline aircraft dynamics would not affect the handling qualities of the modified aircraft compared with the baseline aircraft, and the pilot would not notice the difference. If any added dynamics fall outside either the magnitude or phase envelope, the handling qualities with the total controlled dynamics are assumed to change (either improve or degrade) compared with the baseline, and the pilot can notice the difference.

In Figure 1.3a, for example, it can be noted that the "hourglass-shaped" CTOL MUAD magnitude envelop is narrowest between 1 rad/s and 10 rad/s, indicating that within this frequency range the pilot is most sensitive (or least tolerable) to a change in controlled dynamics. This corresponds well with manual control theory [29], which states that human manual control behavior is most critical near the crossover frequency (usually between 2 rad/s and 5 rad/s). In Figure 1.3, the V/STOL MUAD envelopes from[72] are also shown for reference. These envelopes were developed for vertical and/or short take-off and landing (V/STOL) lateral aircraft dynamics. Compared with the CTOL MUAD envelopes (between 0.1 rad/s and 100 rad/s), the V/STOL MUAD envelopes are defined over a narrower frequency range, i.e., between 0.1 rad/s to 10 rad/s. It can be seen that the V/STOL and CTOL MUAD envelopes are noticeably different at low frequencies ($\omega < 1$ rad/s).

These MUAD envelopes have become ubiquitous and have been used in many applications such as evaluating (simulator) aircraft model fidelity [75–81] and developing flight control systems [77, 82, 83] due to their straightforward interpretation. For example, if the mismatches between the identified aircraft frequency response and the aircraft model are within the MUAD, this aircraft model is assumed to have a "high fidelity". If the frequency responses of flight control systems are within the MUAD, it is assumed that these flight control systems do not affect the aircraft handling qualities and would be safe to fly with.

A more recent study by Mitchell et al. [74] suggested that the MUAD envelopes developed in the early 1980s [67, 72] may not be universal, because the bandwidth of the baseline aircraft dynamics (for example, responsive versus sluggish aircraft) would affect the shapes of the MUAD envelopes. In this research [74], pilots conducted the ADS-33E-PRF hover mission task in a fixed-base flight simulator, for both low-bandwidth (LB) and high-bandwidth (HB) lateral cyclic-to-roll attitude helicopter baseline dynamics, cascaded with added dipole dynamics (second-order lead-lag or second-order lag-lead). As was described in [74], because LB baseline dynamics naturally filter more responses of the added dynamics than high-bandwidth dynamics, a "LB MUAD" would be likely wider than an "HB MUAD", which would greatly complicate the task of defining a set of universal envelopes. As a tentative study to see whether universal envelopes existed, *Allowable Error (AE) envelopes* were derived by normalizing the original LB and HB envelopes with the bandwidth of their corresponding baseline dynamics [74], which are also shown in Figure 1.3. It can be seen that the AE envelopes are notably different from the MUAD, which

may be contributed by the factors of different (and the limited number of) pilots, control tasks, baseline aircraft dynamics and added dynamics.

1.2. THESIS MOTIVATION

Humans' adaptation ability in manual control tasks is indispensable. In aviation, to better understand how humans carry out manual control tasks and adapt to different aircraft dynamics is crucial for improving aircraft handling qualities and flight safety. Pioneering research such as [67, 69–72] systematically investigated how human pilots adapt to different aircraft configurations with various flight control system dynamics. The results of these pioneering research were the MUAD envelopes [67, 72], which qualitatively describe the pilots' subjective noticeability boundaries on the changes of aircraft dynamics. However, there are several concerns about the current available MUAD envelopes [67, 72]:

- First, these envelopes were purely based on subjective ratings, which are known to vary strongly among different subjects. Furthermore subjective and objective metrics are often not fully consistent with each other [84–86]. In addition, there was no quantitative information available such as to what extent task performance, control activity or control behavior would change for the modified aircraft dynamics.
- Second, the "noticeability" represents pilots' evaluations of the changes in aircraft handling qualities, which are based on a discrete rating scale and "Yes" or "No" comments [73]. Thus these "not noticeable" and "noticeable" areas divided by the MUAD envelopes could be too arbitrary. For example, for added dynamics which are partly inside and partly outside the envelopes, the actual noticeability is difficult to judge.
- Third, the MUAD envelopes are difficult to re-evaluate, partially due to the fact that they were based on unique real flight test data, and there is no well-established approach which can consistently create similar envelopes based on any different baseline or added dynamics.
- Fourth, even though these MUAD envelopes have been widely used in evaluating (simulator) aircraft model fidelity [75–81, 87] and developing flight control systems [77, 82, 83], it is unknown whether the MUAD envelopes [67, 72] are still valid for the purposes in these investigations, for example, with different baseline dynamics and added flight control systems [74].

Instead of relying on the subjective "noticeability" approach as used in developing the MUAD envelopes [67, 72], a new metric is proposed for describing the objective adaption of human operator control behavior to the changes of controlled dynamics. This metric is desired to be able to: first, *objectively* quantify human operator's sensitivities to different controlled dynamics; second, describe the adaption of manual control behavior in a *continuously changing* way (for example, the metric can vary by specifying any given amount of behavioral changes); third, be able to be replicated and also generated for different combinations of baseline and added dynamics.

It can be imagined that, similar to the MUAD envelopes [67, 72], to develop this new metric may also need a large amount of added dynamics, which cover a wide range of

frequencies with different levels of perturbations on the baseline system. Given limited time and resources, to conduct such a large scale human-in-the-loop experiment is infeasible, as such experiments can only deal with a limited number of conditions. To overcome this drawback, offline simulations of the tracking task such as the one shown in Figure 1.2 are necessary. The simulations can facilitate predicting human control adaptation to many more different added dynamics, part of which can be experimentally verified later. During a tracking task, the human operator is instructed to alway minimize the visual error signal (see Figure 1.2). In the offline simulation, it is thus assumed that the human operator controlled dynamics are optimized to minimize an objective function, which can be a combination of both weighed σ_e^2 and σ_u^2, representing a trade-off between tracking performance and control activity [88].

1.3. THESIS GOAL

Inspired by the concept of the MUAD [67, 72] and the AE envelopes [74], the goal of this thesis is to develop a new objective metric, called the *Manual Control Adaptation Boundaries* (MCAB), to objectively quantify humans' adaption to different controlled dynamics in manual control tasks. For example, given the MCAB and the mismatches between the modified and the baseline controlled dynamics, it would be possible to know to what extent the task performance, control activity and objective human operator control behavior would change compared with those of the baseline system.

To achieve the goal of this thesis, three key objectives are defined:

- Use compensatory tracking tasks to develop and validate a computer offline simulation, where the tracking performance, control activity and human operator control behavior can be accurately predicted;
- Gather objective tracking performance, control activity and control behavior data based on the validated offline simulation, and generate simulation-based MCAB;
- Modify and verify the simulation-based MCAB using experiment data.

In this thesis, the effects of added dynamics on human operator control behavior are also investigated with simulator motion feedback, since previous research stated that motion feedback can significantly affect human operator control behavior with specific controlled dynamics, such as the double integrator [57–62]. This is done for gaining insights into whether the motion feedback could further influence developing the MCAB. Moreover, in some experiments, subjective ratings and comments on the noticeability of added dynamics will be collected next to the objective tracking data for reference. This is to investigate, for example, whether the subjective ratings are consistent with the objective dependent measures. However, if the ratings are found to be inaccurate, no further correlation will be made between the subjective ratings and the objective dependent measures.

1.4. APPROACH

1.4.1. COMPENSATORY TRACKING TASKS

In both the previous Neal-Smith [69, 70] and LAHOS [71] projects, compensatory tracking tasks (see Figure 1.2) were performed. As was pointed out in these two projects, "*although*

these tasks do not have direct analogy in the real world of the fighter airplane, they did provide the pilot with useful insight into the capabilities of the configuration to perform precise, rapid tracking maneuvers" [69–71].

Skill-based [89] compensatory tracking tasks have been used in many pioneering research projects [1, 29, 34–36] to measure and better understand how humans perform closed-loop manual control tasks, by investigating the dynamic relationship between the perceived visual error signal and human operator control outputs. Previous research [29] found that, for example, by using quasi-random multi-sine signals [11, 69, 70, 90] as the forcing functions, the human operator's control behavior can be sufficiently linear, time-invariant and can be well described by the *quasi-linear control-theoretical models*. Such quasi-linear models describe human control dynamics in control engineering terms, and they have been successfully applied to analyze, for example, human-machine issues involving human manual control [91–96] and evaluated flight simulator motion fidelity [7, 9–11].

As was stated in [29], "*the purposes of these models were to summarize behavioral data, to provide a basis for rationalization and understanding of pilot control actions, and, most important of all, to be used in conjunction with vehicle dynamics in forming predictions or in explaining the behavior of pilot-aircraft systems*". Thus these quasi-linear models are powerful tools for predicting and analyzing human manual control adaptation to different controlled dynamics. For these same reasons, using compensatory tracking tasks and quasi-linear models can also facilitate the formulation of MCAB.

1.4.2. CYBERNETIC APPROACH

The cybernetic approach is a method to study the human manual control behavior using modeling [29], system identification [97, 98] and objective parameter estimation [90] techniques. According to the well-known crossover model [29], if the controlled dynamics change, for example, with noticeable added dynamics cascaded to the baseline system, the human operator's own control dynamics would change correspondingly. Using an aircraft pitch attitude tracking task with no motion feedback as an example, Figure 1.4 shows an example of the human operator model [29] used in this thesis, to quantify human manual control behavior in compensatory tracking tasks.

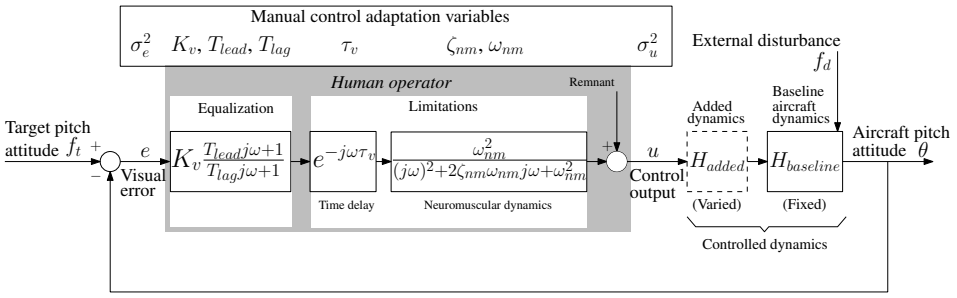

Figure 1.4: An example of the human operator model quantifying manual control behavior in a compensatory tracking task.

As an extension to Figure 1.2, Figure 1.4 shows the details of the analytical human operator model. In this thesis, except for specific descriptions, the term *human operator*

is used instead of *human pilot* in Figure 1.2 (in this thesis, both pilots and non-pilots are used as subjects in the experiment). Moreover, in Figure 1.4, an external disturbance f_d is added to perturb the controlled dynamics, to mimic the situation in which aircraft fly in turbulence. In Figure 1.4, it can be seen that the human operator model mainly consists of the equalization and human operator limitations.

The equalization term represents the way that the visual error signal is processed and utilized by the human operator for the purpose of control. The visual gain K_v is a scaling factor for processing the visual error signal. In general, a high visual gain corresponds with a high control activity and good tracking performance. The lead time constant T_{lead} represents to what extent the human operator cues both of the visual error and the rate of the visual error. T_{lead} is often generated to stabilize the human-vehicle system [29, 30, 60, 61]. T_{lag} is lag time constant which is the scaling factor for the integral of the visual error signal. By generating T_{lag} the human operator can raise his/her low frequency amplitude ratio for tight control and filter out high frequency noise [30].

According to [29], the *adaptation* of human operator dynamics in a compensatory tracking task is mainly reflected in the form of the equalization. The form can be a pure gain K_v if the controlled dynamics are a single integrator, or $K_v(T_{lead}j\omega+1)$ without the term $(T_{lag}j\omega+1)$ for a double integrator controlled dynamics, or like $K_v(T_{lead}j\omega+1)^2/(T_{lag}j\omega+1)$ for specific aircraft dynamics [11]. Meanwhile, based on further *optimization* of the equalization parameters (K_v, T_{lead} or T_{lag}), the human operator can stabilize the closed-loop system and achieve good tracking performance [29].

In Figure 1.4, the limitations include the visual time delay τ_v (representing the lumped total time delay between the input visual error signal and the human operator control output) and the neuromuscular dynamics, which are modeled as a second-order spring-damper system, with ζ_{nm} the damping ratio and ω_{nm} the undamped natural frequency [99].

For a compensatory tracking task, the target (f_t) and disturbance (f_d) forcing functions are usually designed as the sum of multiple sine waves, of which the phases are randomized so that these signals seem random and are thus unpredictable to the human operator during the tracking task. It is assumed that the human operator responds to these specific frequency components of the input signals and a stable control from the operator can be achieved. Thus the equalization and limitations are modeled as linear time-invariant functions (see Figure 1.4) [29]. However, it is known that human manual control behavior is usually nonlinear [25, 26, 100] and time-variant [27, 28, 101], so describing manual control behavior with purely linear and time-invariant transfer functions can never be 100% accurate. Noise from potential sources of randomness, in the processes of human operator information perception, processing, and action degrade the accuracy of the model [11, 29]. To account for all these nonlinearities, time-variations and noises, remnant is added as a component to describe the inaccuracy of the modeling. Research results [11, 90] show that the proportion of the remnant for compensatory tracking tasks is usually between 10% to 30%, meaning that 90% to 70% of the measured control of the human operator can be described by the linear time-invariant part of the model.

The visual gain K_v, lead time constant T_{lead}, lag time constant T_{lag}, visual time delay τ_v, neuromuscular damping ratio ζ_{nm} and undamped natural frequency ω_{nm} can well describe the human operator control behavior in compensatory tracking tasks without motion feedback. For tasks with motion feedback, human operator model with both visual and mo-

tion channels can be used to investigate the independent contributions of these two channels to the human operator control output [91, 97, 98], which will be discussed in later chapters in this thesis. As can be seen in Figure 1.4, these human operator model parameters can thus be used as *manual control adaptation variables*, i.e., to quantify the adaptation of manual control behavior to changes of controlled dynamics. Moreover, tracking performance and human operator control activity, for example, represented by the variance of error signal σ_e^2 and the variance of control output σ_u^2 respectively, are also important objective variables which will show the adaptation effects.

In this thesis, to analyze experiment data, both system identification and parameter estimation techniques are used to quantify human operator control behavior. In a traditional two-step approach, the human operator frequency describing function is first identified using spectral methods [97, 98]. The describing function is nonparametric since no model structure is priorly assumed during the identification. In the second step, the human operator model (see Figure 1.4) is fit to the describing function in the frequency domain and the values of the parameters can be estimated. However, the bias and variance of the nonparametric describing function can cause inaccuracies in the model parameter estimation process [90]. In this thesis, a one-step time-domain parameter estimation method is used to estimate the human operator model parameters based on the measured visual error signal, human operator control output signal and controlled dynamics' output signal [90]. This time-domain parameter estimation method has been successfully applied to similar human manual control research and yielded more accurate and robust results than the two-step approach [11, 90, 102]. The nonparametric describing function is still estimated to provide an indication of the human operator model structure and the quality of the model (identified using time-domain approach) fits.

1.4.3. MANUAL CONTROL ADAPTATION BOUNDARIES

Figure 1.5 shows the main steps of formulating and verifying the MCAB followed in this thesis. In Step 1, a tracking task is performed in both human-in-the-loop experiment and offline simulation. Conditions of baseline dynamics $H_{baseline}$ and a limited number (n) of added dynamics H_{added} are tested. The simulation is tuned by correlating the *manual control adaptation variables* (see Figure 1.4) from simulations with those obtained from human-in-the-loop experiments. Step 1 provides a validated offline simulation toolbox, which is then later used in Step 2 and Step 3.

In Step 2, a tracking task similar to the one in Step 1 is simulated using the validated offline simulation toolbox obtained from the previous step. Since Step 2 is purely simulation-based, many more added dynamics (N) can be tested in the simulation in order to obtain the database for the *manual control adaptation variables*. For each configuration, the tracking performance σ_e^2, control activity σ_u^2 and human operator parameters P_{H_p} (which represents K_v, T_{lead}, T_{lag}, τ_v, ζ_{nm}, ω_{nm}, or any forms of combinations of these parameters) are categorized separately and compared with those of the baseline. The MCAB is obtained by investigating the relative differences between the configurations with H_{added} and the baseline (represented by Δ in Step 2), for each individual dependent measure. Finally, these MCAB for performance, control activity and human operator model parameters are then combined into one single set of MCAB (for example, by seeking the intersection parts of all the MCAB), called the Integrated Manual Control Adaptation Boundaries (IMCAB).

Step 3 aims to modify and verify the simulation-based MCAB and IMCAB obtained from Step 2 using experiment data. Conditions with baseline dynamics $H_{baseline}$ and a limited number (m) of added dynamics H_{added}, different from the ones tested in Step 1, are tested. The *manual control adaptation variables* obtained from both experiment and simulation are compared, and the discrepancies between them (for example, in the form of a "correction coefficient") are used to modify the MCAB and IMCAB from Step 2. Finally, the verified MCAB and IMCAB are generated.

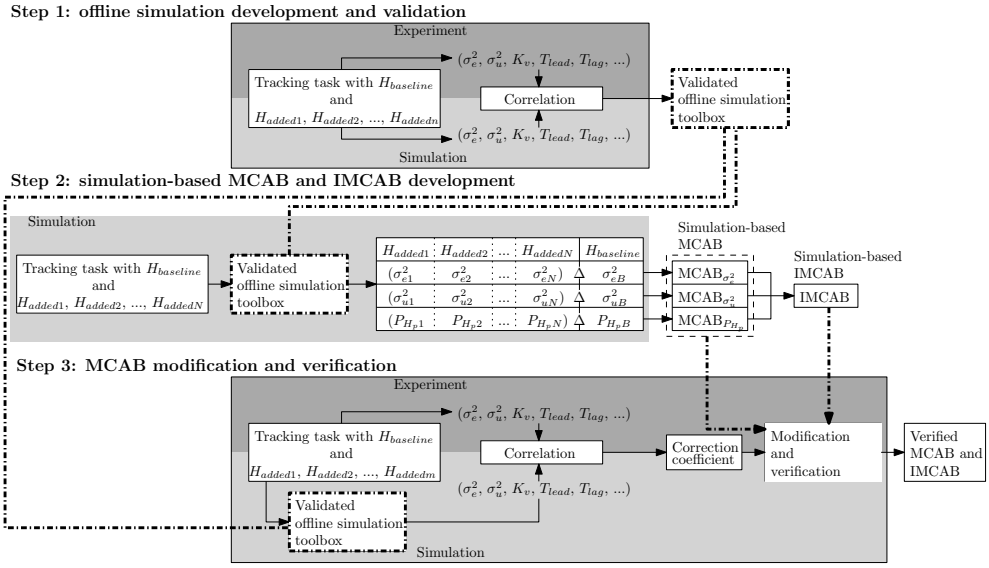

Figure 1.5: A schematic representation of formulating and verifying the MCAB based on simulation and experiment. The dark grey represents the work related with experiment, and the light grey represents the work related with offline simulation.

1.5. THESIS OUTLINE

In total three parts and seven chapters are included in this thesis, as can be seen in Figure 1.6.

Part I describes the cybernetic approach used throughout this thesis and the general approach to study the effects of added dynamics on human operator control behavior. Part II focuses on developing the simulation-based MCAB and IMCAB. Part III describes an experiment modifying and verifying the MCAB and IMCAB developed in Part II.

In Chapter 2, a human-in-the-loop yaw tracking experiment is described, which demonstrates the capabilities of the cybernetic approach modeling human manual control behavior over a wide range of controlled dynamics, under conditions with and without (simulator) physical motion feedback. The results of this chapter provide information about for which types of controlled dynamics, simulator motion feedback is necessary. Moreover, if these types of controlled dynamics are used as baseline, it would be necessary to investigate the MCAB both with and without motion.

Chapter 3 describes a human-in-the-loop pitch attitude tracking task with both low and high-bandwidth baseline dynamics perturbed by added dynamics. This chapter shows the

general approach for analyzing human operator control behavior adaptation to the different combinations of baseline and added dynamics. The methodology is utilized in the later chapters in this thesis to develop MCAB and IMCAB using similar experiment.

Chapter 4 (Step 1 in Figure 1.5) describes a human-in-the-loop aircraft pitch attitude tracking experiment, in which the baseline aircraft dynamics are perturbed by added dynamics locating over a wide range of frequency. The main goals of this chapter are to develop and also validate a computer offline simulation to predict task performance, human operator control activity and control behavior. The simulation toolbox is used in Chapter 5 to collect a large amount of human operator control behavior data, which are key to formulate the simulation-based MCAB and IMCAB.

In Chapter 5 (Step 2 in Figure 1.5), based on the simulation developed and validated in Chapter 4, human operator control behavior is simulated with a large amount of added dynamics, which cover a wide range of frequency with different levels of perturbations on the baseline system. Based on the *manual control adaptation variables* including tracking performance, control activity and human operator control behavior data, simulation-based MCAB and IMCAB are developed.

Chapter 6 (Step 3 in Figure 1.5) describes a human-in-the-loop aircraft pitch attitude tracking experiment similar to the one performed in Chapter 4, aiming to verify the MCAB and IMCAB developed in Chapter 5. Modifications on the MCAB and IMCAB are made, based on the observed discrepancies between the simulation and experiment results. As an extension to Chapter 6, Appendix D describes a tracking experiment similar to Chapter 6, to show the combined effects of motion feedback and added dynamics on the human operator control behavior. It provides information on whether and how much the MCAB would change if motion feedback is considered.

Finally, Chapter 7 draws conclusions on the results obtained in all previous chapters and provides recommendations for future studies.

In this thesis, Chapters 2, 3 and 4 have been published as conference papers. The contents of the other chapters will be submitted later for publication in conferences or scientific journals. The first page of each chapter contains a brief overview of that chapter and how it is connected with other thesis chapters.

REFERENCES

[1] A. Tustin, *The Nature of the Operator's Response in Manual Control, and its Implications for Controller Design,* Journal of the Institution of Electrical Engineers – Part IIA: Automatic Regulators and Servo Mechanisms **94**, 190 (1947).

[2] I. L. Ashkenas and D. T. McRuer, *A Theory of Handling Qualities Derived from Pilot-Vehicle System Considerations,* Aerospace Engineering **21**, 60 (1962).

[3] R. A. Hess, *Unified Theory for Aircraft Handling Qualities and Adverse Aircraft-Pilot Coupling,* Journal of Guidance, Control, and Dynamics **20**, 1141 (1997).

[4] D. H. Klyde, D. T. McRuer, and T. T. Myers, *Pilot-induced Oscillation Analysis and Prediction with Actuator Rate Limiting,* Journal of Guidance, Control, and Dynamics **20**, 81 (1997).

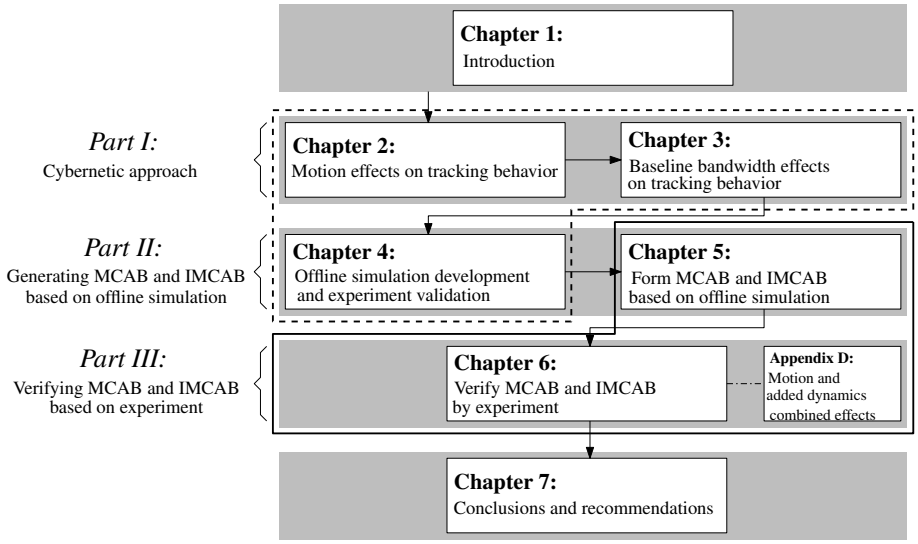

Figure 1.6: Structure of this thesis. The dashed-line box includes chapters focusing on investigating human manual control behavior adaptation to different controlled dynamics and presence of motion feedback. The solid-line box includes chapters focusing on the MCAB and IMCAB.

[5] R. A. Hess and F. Marchesi, *Analytical Assessment of Flight Simulator Fidelity Using Pilot Models,* Journal of Guidance, Control, and Dynamics **32**, 760 (2009).

[6] H. J. Damveld, *A Cybernetic Approach to Assess the Longitudinal Handling Qualities of Aeroelastic Aircraft*, Ph.D. thesis, Delft University of Technology, Faculty of Aerospace Engineering (2009).

[7] R. A. Hess and T. Malsbury, *Closed-loop Assessment of Flight Simulator Fidelity,* Journal of Guidance, Control, and Dynamics **14**, 191 (1991).

[8] Y. Zeyada and R. A. Hess, *Computer-Aided Asessment of Flight Simulator Fidelity,* Journal of Aircraft **40**, 173 (2003).

[9] M. Steurs, M. Mulder, and M. M. van Paassen, *A Cybernetic Approach to Assess Flight Simulator Fidelity,* in *Proceedings of the AIAA Modelling and Simulation Technologies Conference and Exhibit, Providence (RI)*, AIAA-2004-5442 (2004).

[10] A. T. Van Wieringen, *Effects of Aircraft Size on Motion Cues in Flight Simulation – A Cybernetic Analysis of Motion Cueing for a Boeing 747 in the Simona Research Simulator*, Master's thesis, Delft University of Technology (2011).

[11] D. M. Pool, *Objective Evaluation of Flight Simulator Motion Cueing Fidelity Through a Cybernetic Approach*, Ph.D. thesis, Delft University of Technology, Faculty of Aerospace Engineering (2012).

[12] C. V. Kroll, *Preview-Predictor Model of Driver Behavior in Emergency Situations,* Highway research record , 16 (1971).

[13] G. O. Burnham, J. Seo, and G. A. Bekey, *Identification of Human Driver Models in Car Following,* IEEE Transactions on Automatic Control **19**, 911 (1974).

[14] D. T. McRuer, R. W. Allen, D. H. Weir, and R. H. Klein, *New Results in Driver Steering Control Models,* Human Factors: The Journal of the Human Factors and Ergonomics Society **19**, 381 (1977).

[15] G. Prokop, *Modeling Human Vehicle Driving by Model Predictive Online Optimization,* Vehicle System Dynamics **35**, 19 (2001).

[16] A. M. C. Odhams and D. J. Cole, *Application of Linear Preview Control to Modelling Human Steering Control,* Proceedings of the Institution of Mechanical Engineers, Part D: Journal of Automobile Engineering **223**, 835 (2009).

[17] R. D. Jones, I. M. Donaldson, and N. B. Sharman, *A Technique for Removal of the Visuoperceptual Component from Tracking Performance and Its Application to Parkinson's Disease,* IEEE Transactions on Biomedical Engineering **43**, 1001 (1996).

[18] P. Soliveri, R. G. Brown, M. Jahanshahi, T. Caraceni, and C. D. Marsden, *Learning manual pursuit tracking skills in patients with Parkinson's disease,* Brain **120**, 1325 (1997).

[19] C. R. H. Innes, R. D. Jones, T. J. Anderson, S. G. Hollobon, and J. C. Dalrymple-Alford, *Performance in normal subjects on a novel battery of driving-related sensory-motor and cognitive tests,* Behavior Research Methods **41**, 284 (2009).

[20] M. M. K. Oishi, P. TalebiFard, and M. J. McKeown, *Assessing Manual Pursuit Tracking in Parkinson's Disease Via Linear Dynamical Systems,* Annals of Biomedical Engineering **39** (2011), 10.1007/s10439-011-0306-5.

[21] FIA, *2017 Formula One Technical Regulations*, Tech. Rep. (Technical report of Fédération Internationale de l'Automobile, 2016).

[22] S. Rice, K. Kraemer, S. R. Winter, R. Mehta, V. Dunbar, T. G. Rosser, and J. C. Moore, *Passengers from India and the United States Have Differential Opinions about Autonomous Auto-Pilots for Commercial Flights,* International Journal of Aviation, Aeronautics, and Aerospace **1**, 3 (2014).

[23] G. Li, S. P. Baker, J. G. Grabowski, and G. W. Rebok, *Factors Associated with Pilot Error in Aviation Crashes,* Aviation, Space, and Environmental Medicine **72**, 52 (2001).

[24] *Aircraft Accident Report: Loss of Thrust in Both Engines After Encountering a Flock of Birds and Subsequent Ditching on the Hudson River: US Airways Flight 1549*, Tech. Rep. (National Transportation Safety Board, 2009).

[25] D. M. Pool, A. R. Valente Pais, A. M. de Vroome, M. M. van Paassen, and M. Mulder, *Identification of Nonlinear Motion Perception Dynamics Using Time-Domain Pilot Modeling,* Journal of Guidance, Control, and Dynamics **35**, 749 (2012).

[26] A. R. Valente Pais, *Perception Coherence Zones in Vehicle Simulation*, Ph.D. thesis, Delft University of Technology, Faculty of Aerospace Engineering (2013).

[27] R. A. Hess, *Modeling Pilot Detection of Time-Varying Aircraft Dynamics,* Journal of Aircraft **49**, 2100 (2012).

[28] P. M. T. Zaal, *Manual Control Adaptation to Changing Vehicle Dynamics in Roll–Pitch Control Tasks,* Journal of Guidance, Control, and Dynamics **39**, 1046 (2016).

[29] D. T. McRuer and H. R. Jex, *A Review of Quasi-Linear Pilot Models,* IEEE Transactions on Human Factors in Electronics **HFE-8**, 231 (1967).

[30] L. R. Young, *On Adaptive Manual Control,* IEEE Transactions on Man-Machine Systems **10**, 292 (1969).

[31] D. G. Mitchell and D. C. Hart, *Effects of simulator motion and visual characteristics on rotorcraft handling qualities evaluations,* in *American Helicopter Society Conference on Piloting Vertical Flight Aircraft* (American Helicopter Society, 1993).

[32] R. A. Hess, *Analytical Assessment of Performance, Handling Qualities, and Added Dynamics in Rotorcraft Flight Control,* IEEE Transactions on Systems, Man, and Cybernetics — Part A: Systems and Humans **39**, 262 (2009).

[33] E. J. Field, T. R. Pinney, M. M. van Paassen, O. Stroosma, and R. A. Rivers, *Effects of Implementation Variations on the Results of Piloted Simulator Handling Qualities Evaluations,* in *Proceedings of the AIAA Atmospheric Flight Mechanics Conference and Exhibit 16 - 19 August 2004, Providence, Rhode Island*, AIAA 2004-4703 (2004) pp. 1–16.

[34] J. I. Elkind, *Characteristics of Simple Manual Control Systems*, Ph.D. thesis, Massachusetts Institute of Technology (1956).

[35] D. T. McRuer and E. S. Krendel, *The human operator as a servo system element,* Journal of the Franklin Institute **267**, 381 (1959).

[36] D. T. McRuer, D. Graham, E. S. Krendel, and W. J. Reisener, *Human Pilot Dynamics in Compensatory Systems, Theory Models and Experiments with Controlled Element and Forcing Function Variations*, Tech. Rep. AFFDL-TR-65-15 (Air Force Flight Dynamics Laboratory, Wright-Patterson Air Force Base (OH), 1965).

[37] F. M. Drop, *Control-Theoretic Models of Feedforward in Manual Control*, Ph.D. thesis, Delft University of Technology, Faculty of Aerospace Engineering (2016).

[38] K. van der El, D. M. Pool, M. M. van Paassen, and M. Mulder, *Effects of Linear Perspective on Human Use of Preview in Manual Control,* IEEE Transactions on Human-Machine Systems (2017), 10.1109/THMS.2017.2736882.

[39] H. J. Damveld, G. C. Beerens, M. M. van Paassen, and M. Mulder, *Design of Forcing Functions for the Identification of Human Control Behavior,* Journal of Guidance, Control, and Dynamics **33**, 1064 (2010).

[40] K. van der El, D. M. Pool, and M. Mulder, *Measuring and modeling driver steering behavior: From compensatory tracking to curve driving,* Transportation Research Part F (2017), 10.1016/j.trf.2017.09.011.

[41] M. Yamaguchi and R. W. Proctor, *Compatibility of Motion Information in Two Aircraft Attitude Displays for a Tracking Task,* American Journal of Psychology **123**, 81 (2010).

[42] S. R. Dodd, J. Lancaster, S. Grothe, B. DeMers, B. Rogers, and A. Miranda, *Touch on the flight deck: The impact of display location, size, touch technology & turbulence on pilot performance,* in *Proceedings of the IEEE/AIAA 33rd Digital Avionics Systems Conference (DASC)* (2014).

[43] D. A. Abbink and M. Mulder, *Exploring the Dimensions of Haptic Feedback Support in Manual Control,* Journal of Computing and Information Science in Engineering **9**, 011006 (2009).

[44] F. Bufalo, M. Olivari, S. Geluardi, C. A. Gerboni, L. Pollini, and H. H. Bülthoff, *Variable Force-Stiffness Haptic Feedback for Learning a Disturbance Rejection Task,* in *Proceedings of the IEEE International Conference on Systems, Man, and Cybernetics, Banff, Canada* (2017).

[45] K. van der El, D. M. Pool, M. M. van Paassen, and M. Mulder, *Effects of Preview on Human Control Behavior in Tracking Tasks With Various Controlled Elements,* IEEE Transactions on Cybernetics (2017), 10.1109/TCYB.2017.2686335.

[46] Y. Huang, D. M. Pool, O. Stroosma, and Q. P. Chu, *Incremental Nonlinear Dynamic Inversion Control for Hydraulic Hexapod Flight Simulator Motion Systems,* in *Proceedings of the the 20th IFAC World Congress, Toulouse, France* (2017) pp. 4378–4383.

[47] F. M. Nieuwenhuizen, *Changes in Pilot Control Behaviour Across Stewart Platform Motion Systems*, Ph.D. thesis, Delft University of Technology, Faculty of Aerospace Engineering (2012).

[48] E. L. Martin and W. L. Waag, *Contributions of Platform Motion to Simulator Training Effectiveness: Study I – Basic Contact*, Tech. Rep. AFHRL-TR-78-15 (Air Force Human Resources Laboratory, Brooks Air Force Base (TX, 1978).

[49] C. D. Wickens, S. Hutchins, T. Carolan, and J. Cumming, *Effectiveness of Part-Task Training and Increasing-Difficulty Training Strategies: A Meta-Analysis Approach,* Human Factors **55**, 461 (2013).

[50] P. M. T. Zaal and B. T. Sweet, *The Challenges of Measuring Transfer of Stall Recovery Training,* in *Proceedings of the IEEE International Conference on Systems, Man, and Cybernetics, San Diego (CA)* (2014) pp. 3138–3143.

[51] D. M. Pool and P. M. T. Zaal, *A Cybernetic Approach to Assess the Training of Manual Control Skills,* in *Proceedings of the 13th IFAC/IFIP/IFORS/IEA Symposium on Analysis, Design, and Evaluation of Human-Machine Systems, Kyoto, Japan* (2016).

[52] A. M. Wasei, O. Stroosma, H. J. Damveld, M. Mulder, and M. M. van Paassen, *Investigating the Role of Simulator Motion Cues during Simulation of In-Flight PIOs,* in *Proceedings of the AIAA Modeling and Simulation Technologies Conference and Exhibit, Honolulu, Hawaii, Aug. 18-21, 2008*, AIAA-2008-6538, American Institute (American Institute of Aeronautics and Astronautics, 2008).

[53] H. C. Oelker and O. Brieger, *Flight Test Experiences with Eurofighter Typhoon during High Bandwidth PIO Resistance Testing,* in *Proceedings of the AIAA Atmospheric Flight Mechanics Conference and Exhibit 21 - 24 August 2006, Keystone, Colorado*, AIAA 2006-6496 (2006) pp. 1–12.

[54] J. Hodgkinson, *History of Low-Order Equivalent Systems for Aircraft Flying Qualities,* Journal of Guidance, Control, and Dynamics **28**, 577 (2005).

[55] R. A. Hess, J. K. Moore, and M. Hubbard, *Modeling the Manually Controlled Bicycle,* IEEE Transactions on Systems, Man and Cybernetics, Part A: Systems and Humans **42**, 545 (2012).

[56] K. van der El, D. M. Pool, H. J. Damveld, M. M. van Paassen, and M. Mulder, *An Empirical Human Controller Model for Preview Tracking Tasks,* IEEE Transactions on Cybernetics **46**, 2609 (2016).

[57] R. S. Shirley and L. R. Young, *Motion Cues in Man-Vehicle Control – Effects of Roll-Motion Cues on Human Operator's Behavior in Compensatory Systems with Disturbance Inputs,* IEEE Transactions on Man-Machine Systems **9**, 121 (1968).

[58] R. L. Stapleford, R. A. Peters, and F. R. Alex, *Experiments and a Model for Pilot Dynamics with Visual and Motion Inputs*, Tech. Rep. NASA CR-1325 (Systems Technology, Inc., Hawthorne (CA), 1969).

[59] R. F. Ringland and R. L. Stapleford, *Motion Cue Effects on Pilot Tracking,* in *Seventh Annual Conference on Manual Control* (1971) pp. 327–338.

[60] J. C. van der Vaart, *Modelling of Perception and Action in Compensatory Manual Control Tasks*, Ph.D. thesis, Delft University of Technology, Faculty of Aerospace Engineering (1992).

[61] R. J. A. W. Hosman, *Pilot's Perception and Control of Aircraft Motions*, Ph.D. thesis, Delft University of Technology, Faculty of Aerospace Engineering (1996).

[62] T. L. Dehouck, M. Mulder, and M. M. van Paassen, *The Effects of Simulator Motion Filter Settings on Pilot Manual Control Behaviour,* in *Proceedings of the AIAA Modeling and Simulation Technologies Conference and Exhibit, Keystone (CO)*, AIAA-2006-6250 (2006).

[63] H. P. Bergeron, *Investigation of Motion Requirements in Compensatory Control Tasks,* IEEE Transactions on Man-Machine Systems **MMS-11**, 123 (1970).

[64] A. M. Junker and C. R. Replogle, *Motion Effects on the Human Operator in a Roll Axis Tracking Task,* Aviation, Space, and Environmental Medicine **46**, 819 (1975).

[65] M. Cook, *Flight Dynamics Principles: A Linear Systems Approach to Aircraft Stability and Control* (Butterworth-Heinemann, 2012).

[66] M. Specification, *MIL-F-8785 (ASG),* Flying Qualities of Piloted Airplanes **1** (1954).

[67] J. R. Wood and J. Hodgkinson, *Definition of Acceptable Levels of Mismatch for Equivalent Systems of Augmented CTOL Aircraft*, Tech. Rep. MDC A6792 (McDonnell Aircraft Company, St. Louis (MO), 1980).

[68] M. F. Shafer, *Low-Order Equivalent Models of Highly Augmented Aircraft Determined from Flight Data,* Journal of Guidance, Control, and Dynamics (1980).

[69] T. P. Neal and R. E. Smith, *An In-flight Investigation to Develop Control System Design Criteria for Fighter Airplanes*, Tech. Rep. AFFDL-TR-70-74, Volume 1 (Air Force Flight Dynamics Laboratory, 1970).

[70] T. P. Neal and R. E. Smith, *An In-flight Investigation to Develop Control System Design Criteria for Fighter Airplanes*, Tech. Rep. AFFDL-TR-70-74, Volume 2 (Air Force Flight Dynamics Laboratory, 1970).

[71] R. E. Smith, *Effects of Control System Dynamics on Fighter Approach and Landing Longitudinal Flying Qualities*, Tech. Rep. AFFDL-TR-78-122, Volume 1 (CALSPAN ADVANCED TECHNOLOGY CENTER BUFFALO NY, 1978).

[72] C. G. Carpenter and J. Hodgkinson, *V/STOL Equivalent Systems Analysis*, Tech. Rep. NADC-79141-60 (McDonnell Aircraft Company, St. Louis (MO), 1980).

[73] G. E. Cooper and R. P. Harper, Jr., *The Use of Pilot Rating in the Evaluation of Aircraft Handling Qualities*, Tech. Rep. NASA TN D-5153 (National Aeronautics and Space Administration, 1969).

[74] D. G. Mitchell, R. H. Hoh, C. He, and K. Strope, *Determination of Maximum Unnoticeable Added Dynamics,* in *Proceedings of the AIAA Atmospheric Flight Mechanics Conference and Exhibit, Keystone (CO)*, AIAA-2006-6492 (2006).

[75] J. T. Bosworth and P. S. Williams-Hayes, *Flight Test Results from the NF-15B Intelligent Flight Control System (IFCS) Project with Adaptation to a Simulated Stabilator Failure,* in *Proceedings of the AIAA Infotech at Aerospace 2007 Conference and Exhibit, Rohnert Park (CA)*, AIAA-2007-2818 (2007).

[76] S. Geluardi, F. M. Nieuwenhuizen, L. Pollini, and H. H. Bülthoff, *Frequency Domain Identification of a Light Helicopter in Hover,* in *Proceedings of the AHS 70th Annual Forum, Montreal, Canada* (2014).

[77] M. B. Tischler, *System Identification Methods for Aircraft Flight Control Development and Validation*, NASA Technical Memorandum 110369 (NASA Ames Research Center, Moffett Field (CA), 1995).

[78] P. G. Hamel and K. Jürgen, *Advances in Rotorcraft System Identification,* Progress in Aerospace Sciences **33**, 259 (1997).

[79] Cicolani and Luigi, *Flight Test Identification and Simulation of a UH-60A Helicopter and Slung Load*, Tech. Rep. NASA/TM-2001-209619 (NASA, Ames Research Center Moffett Field, California, 2001).

[80] P. G. Hamel and R. V. Jategaonkar, *Evolution of flight vehicle system identification,* Journal of aircraft **33**, 9 (1996).

[81] P. G. Hamel, *In-Flight Simulators and Fly-by-Wire/Light Demonstrators: A Historical Account of International Aeronautical Research* (Springer, 2017).

[82] C. J Miller, *Nonlinear Dynamic Inversion Baseline Control Law: Flight-Test Results for the Full-scale Advanced Systems Testbed F/A-18 Airplane,* (AIAA Guidance, Navigation, and Control Conference, 2011) pp. 1–25.

[83] M. R. Anderson, *Robustness evaluation of a flexible aircraft control system,* Journal of guidance, control, and dynamics **16**, 564 (1993).

[84] S. D. Beard, S. E. Reardon, E. L. Tobias, and B. L. Aponso, *Simulation System Fidelity Assessment at the Vertical Motion Simulator,* in *Proceedings of the AHS 69th Annual Forum, Phoenix, Arizona* (2013).

[85] H. J. Damveld, M. M. van Paassen, and M. Mulder, *Cybernetic Approach to Assess Aircraft Handling Qualities,* Journal of Guidance, Control, and Dynamics **34**, 1886 (2011).

[86] C. M. Wiskemann, F. M. Drop, D. M. Pool, M. M. van Paassen, M. Mulder, and H. H. Bülthoff, *Subjective and Objective Metrics for the Evaluation of Motion Cueing Fidelity for a Roll-Lateral Reposition Maneuver,* in *AHS 70th Annual Forum* (2014).

[87] M. Li, *Effects of Helicopter Degree of Freedom and Motion Cues On Allowable Error Envelopes*, Master's thesis, Delft University of Technology (2016).

[88] P. M. T. Zaal, D. M. Pool, J. de Bruin, M. Mulder, and M. M. van Paassen, *Use of Pitch and Heave Motion Cues in a Pitch Control Task,* Journal of Guidance, Control, and Dynamics **32**, 366 (2009).

[89] J. Rasmussen, *Skills, Rules, and Knowledge; Signals, Signs, and Symbols, and Other Distinctions in Human Performance Models,* IEEE Transactions on Systems, Man, and Cybernetics **SMC-13**, 257 (1983).

[90] P. M. T. Zaal, D. M. Pool, Q. P. Chu, M. M. van Paassen, M. Mulder, and J. A. Mulder, *Modeling Human Multimodal Perception and Control Using Genetic Maximum Likelihood Estimation,* Journal of Guidance, Control, and Dynamics **32**, 1089 (2009).

[91] M. Mulder, *Cybernetics of Tunnel-in-the-Sky Displays*, Ph.D. thesis, Delft University of Technology, Faculty of Aerospace Engineering (1999).

[92] M. Mulder, P. M. T. Zaal, D. M. Pool, H. J. Damveld, and M. M. van Paassen, *A Cybernetic Approach to Assess Simulator Fidelity: Looking back and looking forward,* in *Proceedings of the AIAA Modeling and Simulation Technologies Conference, Boston (MA)*, AIAA-2013-5225 (2013).

[93] P. van den Berg, P. M. T. Zaal, M. Mulder, and M. M. van Paassen, *Conducting of Multi-modal Pilot Model Identification - Results of a Simulator Experiment,* in *AIAA Modelling and Simulation Technologies Conference, South Carolina*, AIAA-2007-6892 (2007).

[94] P. M. T. Zaal, D. M. Pool, M. Mulder, and M. M. van Paassen, *New Types of Target Inputs for Multi-Modal Pilot Model Identification,* in *Proceedings of the AIAA Modeling and Simulation Technologies Conference and Exhibit, Honolulu (HI)*, AIAA-2008-7106 (2008).

[95] P. M. T. Zaal, D. M. Pool, M. Mulder, M. M. van Paassen, and J. A. Mulder, *Identification of Multimodal Pilot Control Behavior in Real Flight,* Journal of Guidance, Control, and Dynamics **33**, 1527 (2010).

[96] D. M. Pool, M. M. van Paassen, and M. Mulder, *Modeling Human Dynamics in Combined Ramp-Following and Disturbance-Rejection Tasks,* in *Proceedings of the AIAA Guidance, Navigation, and Control Conference, Toronto, Canada, Aug. 2-5*, AIAA-2010-7914, edited by M. Silvestro (American Institute for Aeronautics and Astronautics, 2010).

[97] R. L. Stapleford, D. T. McRuer, and R. E. Magdaleno, *Pilot Describing Function Measurements in a Multiloop Task,* IEEE Transactions on Human Factors in Electronics **8**, 113 (1967).

[98] M. M. van Paassen and M. Mulder, *Identification of Human Operator Control Behaviour in Multiple-Loop Tracking Tasks,* in *Proceedings of the Seventh IFAC/IFIP/IFORS/IEA Symposium on Analysis, Design and Evaluation of Man-Machine Systems, Kyoto Japan* (Pergamon, 1998) pp. 515–520.

[99] M. M. van Paassen, *Biophysics in Aircraft Control, A Model of the Neuromuscular System of the Pilot's Arm*, Ph.D. thesis, Delft University of Technology, Faculty of Aerospace Engineering (1994).

[100] A. R. Valente Pais, D. M. Pool, A. M. de Vroome, M. M. van Paassen, and M. Mulder, *Pitch Motion Perception Thresholds During Passive and Active Tasks,* Journal of Guidance, Control, and Dynamics **35**, 904 (2012).

[101] E. R. Boer and R. V. Kenyon, *Estimation of Time-Varying Delay Time in Nonstationary Linear Systems: An Approach to Monitor Human Operator Adaptation in Manual Tracking Tasks,* IEEE Transactions on Systems, Man, and Cybernetics – Part A: Systems and Humans **28**, 89 (1998).

[102] M. Mulder, D. M. Pool, D. A. Abbink, E. R. Boer, P. M. T. Zaal, F. M. Drop, K. van der El, and M. M. van Paassen, *Manual Control Cybernetics: State-of-the-Art and Current Trends,* IEEE Transactions on Human-Machine Systems (2017), 10.1109/THMS.2017.2761342.

2

THE EFFECTS OF MOTION FEEDBACK WITH DIFFERENT TYPES OF CONTROLLED DYNAMICS

This chapter describes a yaw tracking task with gain, single integrator and double integrator controlled dynamics all with and without simulator motion feedback. The first objective of this chapter is to demonstrate that the cybernetic approach can be successfully applied in analyzing the objective human operator control behavior over a wide variety of controlled dynamics both with and without simulator motion feedback. The second objective is to identify for which types of controlled dynamics the simulator motion feedback is crucial to the adaptation and optimization of human operator's control dynamics. Experiment results show that the cybernetic approach can fully capture the objective human operator control behavior in manual control tasks, thus it will be used as a fundamental approach in the following chapters of this thesis to investigate the sensitivities of performance, control activity and human operator control behavior to the change of controlled dynamics.

Part of this chapter has been published as the following conference paper:
T. Lu, D. M. Pool, M. M. van Paassen, and M. Mulder, Use of Simulator Motion Feedback for Different Classes of Vehicle Dynamics in Manual Control Tasks, in Proceedings of the 5th CEAS Air & Space Conference, Delft, The Netherlands, 2015.

2.1. INTRODUCTION

In continuous manual control tasks, human operators are known to adjust their control behavior to a myriad of different internal and external factors [1, 2], and these adjustments can be divided into two categories [1]: *adaptation* and *optimization*. *Adaptation* involves the operator's selection of a feedback control structure and suitable control dynamics (e.g., lead or lag) for each active control response. Following adaptation, the human operator *optimizes* the parameters (e.g., gains, time-constants) of the control dynamics to the specifics and demands of the performed task. A key adjustment of human operators' control dynamics occurs as a function of the dynamics of the controlled element; human operators are known to match their own control dynamics to those of the controlled element such that adequate performance of the combined system is obtained [1, 3]. Similarly, numerous studies have also found evidence of changes in human operators' control behavior due to the presence of physical motion feedback [4–8]. Detailed knowledge of adaptation and optimization of the human operators' control dynamics due to the presence of physical motion feedback is important to, for example, evaluations of flight simulation fidelity [9–11] and vehicle handling qualities [12–14].

The extent to which human operators adapt and optimize their control dynamics to the presence of motion feedback, and thereby improve their level of task performance, is known to be dependent on the dynamics of the controlled element. In general, the lower the inherent stability of the controlled system is, the larger effects of motion feedback will be [5, 15]. For control of marginally stable systems with K/s^2 dynamics in the crossover region, availability of motion results in much-improved task performance and the underlying changes in human operator dynamics are well-documented [5, 6, 16–19]. In this case, human operator adaptation occurs as an added feedback response to the sensed motion. In parallel, human operators also adjust some of the key parameters of their control dynamics to the presence of motion feedback, for which reduced visual lead and increased control gains are reported consistently [6–8]. For more stable controlled elements, the conclusions on the effects of added motion feedback are much less consistent. For example, for controlled elements with K/s dynamics in the crossover region, Bergeron [20] found no changes when motion was available, but other researchers reported similar changes in tracking behavior as observed for K/s^2 control [6, 16] or even a detrimental effect and degraded performance [21].

For sufficiently stable controlled elements that require no lead equalization by the human operator, the exact nature of possible adaptation and optimization of human operators' control dynamics in the presence of motion feedback is not yet fully clear. Most studies agree that the highly *positive* effects (better performance, reduced workload) of added motion feedback observed for less stable systems and the underlying adaptations and optimization of human operator control dynamics may not be present [5, 15, 21]. However, knowing for which controlled elements the possibly *negative* effects of motion feedback may be present (e.g., motion hinders the human operator), such as those reported by Junker and Replogle [21], can be equally important to investigate. Also, even if only relatively small adjustments of operators' control dynamics (e.g., only optimization of parameters of operators' control dynamics) occur for such controlled elements, it still implies that distinct differences in human operator control exist between motion and no-motion cases.

The goal is therefore to objectively determine human operators' adaptation and optimization of their control dynamics to the presence of physical motion feedback for a wide

range of controlled elements. To this end, a human-in-the-loop experiment, performed in the SIMONA Research Simulator at Delft University of Technology, is described. In this experiment human operators' behavior in a yaw-axis compensatory tracking task with feedback was measured. To tie in with the landmark compensatory tracking experiments of [3], double integrator dynamics, as well as single integrator and gain dynamics were evaluated. In the experiment, all controlled elements were tested both without and with motion feedback to allow for direct comparison. In addition, to allow for objective measurement of human operators' adaptation and optimization of their control dynamics, the target dominant yaw tracking task was set up to allow for multimodal modeling and identification of human operators' responses to both visual and motion channels using available describing function estimation and model fitting techniques [6, 22, 23]. The contribution of the modeled human operator motion feedback channel to the model output is considered for quantifying human operators' utilization of this potential pathway and human operators' adaptation to the presence of motion feedback. Furthermore, closed-loop analyses on the error-to-tracking signal responses are used to provide more insights into the attenuation of the error signal.

This chapter is structured as follows. First, Section 2.2 provides the details of the yaw attitude tracking experiment as well as the specifics of the human operator model-based method for detecting adaptation and optimization of manual control behavior and quantifying motion utilization. The results of the experiment are presented in Section 2.3. This chapter ends with a discussion and conclusions.

2.2. METHODS

2.2.1. CONTROL TASK

THE YAW ATTITUDE TRACKING TASK

A yaw attitude tracking task was used to evaluate the effects of motion feedback on human operator control behavior with different controlled elements. The yaw attitude tracking task was preferred rather than pitch or roll attitude tracking task because the effect of the otoliths can be neglected in yaw tracking task, that is, the rotation induces no coupled change in specific force. A schematic representation of this yaw attitude tracking task is shown in Figure 2.1: the human operator controls the yaw angle ψ of the controlled element H_c by tracking the target signal f_t to minimize the error signal e shown on a compensatory display (Figure 2.2). In addition to the visual error signal, continuous motion response from the controlled element H_c is fed back to the human operator when the motion base is turned on in the experiment. Thus the human operator's output signal u comprises signal u_e of the human operator's visual response H_p, the signal u_ψ of the motion response H_m and the remnant n representing the nonlinearities. Signal u_d (sum of the control signal u and disturbance signal f_d) is directly input into the controlled element H_c. In the mean time, the controlled element H_c is disturbed by the disturbance signal f_d acting ahead of the controlled element, which is necessary for the multimodal human operator model identification techniques [8, 24, 25] .

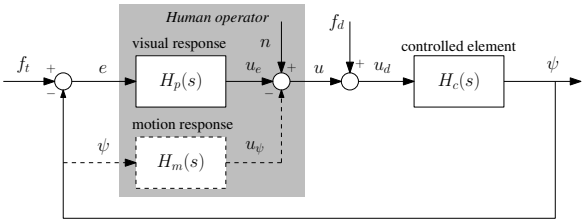

Figure 2.1: The closed-loop yaw attitude tracking task.

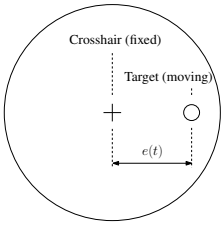

Figure 2.2: Compensatory visual display.

FORCING FUNCTIONS

For the yaw attitude tracking task shown in Figure 2.1, the human operator tracks the target signal f_t to minimize the error signal e as well as to reject the external disturbance defined by f_d. These two signals (typically referred to as forcing functions) are also needed for the multimodal human operator model identification techniques that will be applied later[8, 24, 25]. Both of these forcing functions are chosen to be the sums of 10 sine waves with independent frequencies, as given by:

$$f_{t,d}(t) = \sum_{k=1}^{10} A_{t,d}[k]\sin(\omega_{t,d}[k]\,t + \phi_{t,d}[k]), \tag{2.1}$$

where $A_{t,d}[k]$, $\omega_{t,d}[k]$ and $\phi_{t,d}[k]$ are the amplitude, frequency and phase of the kth sine wave in the target forcing function f_t and disturbance forcing function f_d, respectively.

The effective disturbance $f_{d,e}$ is a disturbance directly acting on the controlled element's output yaw angle ψ. It should be noted that the effective disturbance forcing function is the same for all controlled elements. However, as can be seen in Figure 2.1, the disturbance is inserted before the controlled element H_c in the experiment for practical reasons. Thus the amplitude and phase components of the actual f_d are pre-shaped from $f_{d,e}$ with the inverse dynamics of each controlled element H_c. The amplitude, frequency and phase components of the target and effective disturbance forcing functions are listed in Table 2.1.

Table 2.1: Multi-sine forcing function properties

		f_t				$f_{d,e}$		
k	n_t	ω_t,rad/s	A_t,deg	ϕ_t,rad	n_d	ω_d,rad/s	$A_{d,e}$,deg	$\phi_{d,e}$,rad
1	6	0.460	4.277	1.288	5	0.383	2.057	-0.269
2	13	0.997	2.991	6.089	11	0.844	1.555	4.016
3	27	2.071	1.350	5.507	23	1.764	0.775	-0.806
4	41	3.145	0.727	1.734	37	2.838	0.395	4.938
5	53	4.065	0.488	2.019	51	3.912	0.240	5.442
6	73	5.599	0.302	0.441	71	5.446	0.146	2.274
7	103	7.900	0.192	5.175	101	7.747	0.091	1.636
8	139	10.661	0.140	3.415	137	10.508	0.066	2.973
9	194	14.880	0.109	1.066	171	13.116	0.055	3.429
10	229	17.564	0.100	3.479	226	17.334	0.047	3.486

The experimental measurement time of a tracking run was 81.92 s, thus the measurement base frequency is $\omega_m = 2\pi/81.92$ s = 0.077 rad/s. To allow for the use of spectral

analysis, the frequency of each sine wave component of both forcing functions was defined as an integer multiple of the base frequency, $\omega_{t,d} = n_{t,d}\omega_m$. The integer factors n_t and n_d are shown in Table 2.1, respectively.

For both forcing functions the amplitudes of the sine components are generated by a second-order low-pass filter, defined in Eq. (2.2):

$$H_A(j\omega) = \frac{(1 + T_{A1}\, j\omega)^2}{(1 + T_{A2}\, j\omega)^2}. \tag{2.2}$$

The same amplitude distribution has been used by Zaal et al.[8], and it ensures that the control task is realistic and not too difficult for the subjects as it uses lower power for the high frequency components. Then the amplitudes are scaled to make the root mean square (RMS) of f_t 3.873 deg and RMS of $f_{d,e}$ 1.925 deg, respectively. Thus the selected scaling ensures that the control task in the experiment is mainly a target tracking task, as was designed by McRuer [1]. The phases $\phi_{t,d}$ were selected to yield signals with an approximately Gaussian distribution and without excessive peaks[26].

Considering the smoothness movement of the motion base of the simulator, a cosine form fade-in function and a cosine form fade-out function are multiplied with both f_t and f_d during the first and last 5 s of the total experimental run time 95 s, respectively.

CONTROLLED ELEMENTS

In this experiment, to approximate the perfect systems, a gain-like controlled element $H_{c,g}$, a single integrator-like controlled element $H_{c,si}$ and a double integrator controlled element $H_{c,di}$ are considered as the controlled element H_c in Figure 2.1, respectively. The gain of each controlled elements is chosen based on the human operator control activity, the sidestick deflection limitation and accurate control inputs. The first controlled element, Eq. (2.3), within the human manual control bandwidth, approximates a gain. Two break frequencies (10 rad/s and 30 rad/s) are added in the denominator for both computing the yaw acceleration $\ddot{\psi}$ needed by simulator motion base and suppressing the motion at high frequencies. The second controlled element, Eq. (2.4) approximates a single integrator within the human manual control bandwidth. The denominator with break frequency 30 rad/s is added for the same reason of the gain-like controlled element. The third controlled element, Eq. (2.5), is a pure double integrator. Since the double integrator itself suppresses the motion at high frequencies well, and the yaw acceleration $\ddot{\psi}$ is easy to deduce directly, no extra term is added. For convenience, in the later part of this chapter, Eqs. (2.3), (2.4) and (2.5) are referred as gain, single integrator and double integrator controlled elements, respectively. The transfer functions of these controlled elements are given as:

$$H_{c,g} = \frac{1}{(\frac{1}{10}s + 1)^2(\frac{1}{30}s + 1)} \approx 1, \tag{2.3}$$

$$H_{c,si} = \frac{4}{s(\frac{1}{30}s + 1)^2} \approx \frac{4}{s}, \tag{2.4}$$

$$H_{c,di} = \frac{15}{s^2}. \tag{2.5}$$

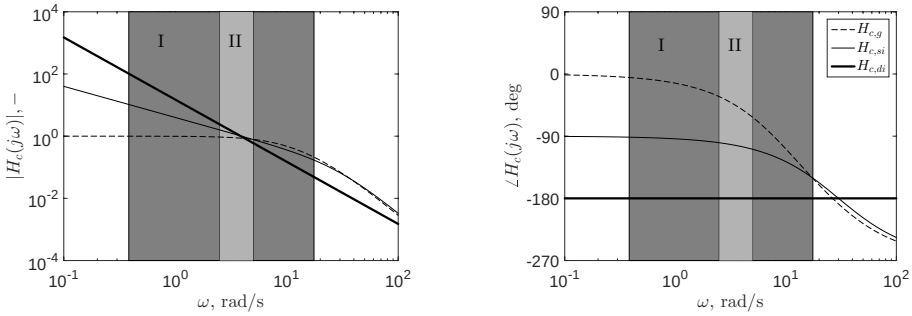

(a) Magnitude (b) Phase

Figure 2.3: Bode of three different controlled elements. I: forcing function frequency range; II: crossover region for compensatory tracking.

Figure 2.3 shows the frequency responses of the controlled elements. The light gray area indicates the frequency range where the crossover frequency is expected, which is usually 2 rad/s to 5 rad/s [3], and the darker gray area indicates the frequency range of the target and disturbance signals designed for this experiment, which can be found in Table 2.1.

HUMAN OPERATOR MODEL

A quasi-linear multimodal human operator model [23, 24, 27] is used in this research to study the effects of motion feedback on human operator control behavior. The human operator model consists of a visual channel transfer function H_p, a motion channel transfer function H_m, and a remnant signal n representing all the other nonlinearities [3]. In this section, H_p is written as $H_p(j\omega)$ to represent the response in frequency domain, and this applies to other transfer functions as well. In general, the model for the visual channel frequency response $H_p(j\omega)$ is given by:

$$H_p(j\omega) = H_{eq}(j\omega)e^{-j\omega\tau_v}H_{nm}(j\omega), \tag{2.6}$$

where $H_{eq}(j\omega)$ is the visual equalization term representing the visual cues processing, and τ_v is the visual time delay. The term $H_{eq}(j\omega)e^{-j\omega\tau_v}$ here is equivalent to the crossover model [3]. $H_{nm}(j\omega)$ represents the dynamics of the neuromuscular system, modeled as a second-order mass-spring-damper system with the damping ratio ζ_{nm} and undamped natural frequency ω_{nm} [25]:

$$H_{nm}(j\omega) = \frac{\omega_{nm}^2}{(j\omega)^2 + 2\zeta_{nm}\omega_{nm}j\omega + \omega_{nm}^2}. \tag{2.7}$$

It is well known that the human operator adapts his/her equalization term $H_{eq}(j\omega)$ in Eq. (2.6) to make the dynamics of the combined human operator-vehicle system H_pH_c a single integrator for any controlled element [3]. Thus, the expected equalization terms H_{eq} corresponding with the controlled elements of Eqs. (2.3), (2.4) and (2.5) are given as, respectively:

$$H_{eq,g}(j\omega) = K_v \frac{T_{lead} j\omega + 1}{T_{lag} j\omega + 1}, \tag{2.8}$$

$$H_{eq,si}(j\omega) = K_v, \tag{2.9}$$

$$H_{eq,di}(j\omega) = K_v(T_{lead} j\omega + 1), \tag{2.10}$$

where K_v is the visual gain, T_{lead} is the lead time constant and T_{lag} is the lag time constant. The human operator models for C1, C2 and C3 (see Table 2.2), which have no motion feedback, consist of Eq. (2.6) and Eq. (2.7) with Eq. (2.8), Eq. (2.9) and Eq. (2.10), respectively.

It should be noted that Eq. (2.8), which is chosen as the equalization term of the human operator model corresponding with the gain controlled element, differs from the pure lag equalization that McRuer et al. [3] implemented for the gain controlled element. In order to fit the model in a wider frequency range than the crossover model [3] (2 rad/s to 5 rad/s), the lead term ($T_{lead} j\omega + 1$) is necessary (the value of the identified T_{lead} is also small for the gain controlled element, see the results section, which means the lead term only takes effect at relatively high frequencies). A similar correction for the equalization term can be found in other research, for example, the double lead term of the human operator model proposed for specific aircraft pitch dynamics [27].

For yaw motion feedback, according to Hosman [18], Van der Vaart [17], Nieuwenhuizen et al. [24] and Zaal et al. [8], the motion channel frequency response function $H_m(j\omega)$ in Figure 2.1 is given as:

$$H_m(j\omega) = (j\omega)^2 H_{sc}(j\omega) K_m e^{-j\omega\tau_m} H_{nm}(j\omega), \tag{2.11}$$

where K_m is the motion gain, τ_m is the motion time delay and H_{sc} is the dynamics of semicircular canals, which is modeled as:

$$H_{sc}(j\omega) = \frac{T_{sc1} j\omega + 1}{(T_{sc2} j\omega + 1)(T_{sc3} j\omega + 1)}, \tag{2.12}$$

where $T_{sc1} = 0.11$ s, $T_{sc2} = 5.9$ s and $T_{sc3} = 0.005$ s [18]. These values are fixed for experimental conditions with motion feedback during the human operator model identification process. Since the experiment is a pure yaw tracking control task, modeling a response to the output of the semicircular canals is sufficient.

INDEPENDENT VARIABLES

The experiment was designed to evaluate the effects of motion feedback on human operator control behavior with three different controlled elements. It had a full-factorial design which means all the combinations of the independent variables motion on/off and three different controlled elements were evaluated. Thus a total of six experimental conditions were tested. All conditions and the symbols used on the reminder of the chapter to refer to these conditions are listed in Table 2.2.

Table 2.2: Experimental conditions

Controlled element	Motion off	Motion on
Gain, $H_{c,g}$	C1	C4
Single integrator, $H_{c,si}$	C2	C5
Double integrator, $H_{c,di}$	C3	C6

2.2.2. MOTION UTILIZATION FACTOR

As the multimodal human operator model is used to evaluate the effects of motion feedback on human operator control behavior with different controlled elements, it is important to verify that the motion channel of the multimodal human operator model is indeed utilized when motion is provided. In this chapter, this verification is performed in two steps. At first, the multimodal human operator models for C4, C5 and C6 are identified assuming that the motion channel transfer function H_m is always in-the-loop. Then the motion utilization factor M_u is calculated as a measure of how much the estimated H_m contributes to the control input u based on the multimodal human operator model identification results:

$$M_u = \frac{\sigma^2(u_\psi)}{\sigma^2(u_e)}, \tag{2.13}$$

where M_u is the ratio between the variance of the estimated signal u_ψ and the variance of the estimated signal u_e, which have been shown in Figure 2.1 as the components of the total control signal u. Both u_ψ and u_e are calculated from the identified multimodal human operator models.

2.2.3. EXPERIMENT

DEPENDENT MEASURES AND DATA ANALYSIS

The measured variables in the experiment include the time histories of the tracking error e, the control signal u and the yaw angle ψ during each run, see Figure 2.1. From these measurements the variance of e and the variance of u are calculated as the measures of tracking performance and control activity, respectively. Based on the measures of e, u, ψ and f_d, the Fourier coefficient (FC) method [23, 25] is used to identify the nonparametric open-loop describing functions at the target frequency ω_t and disturbance frequency ω_d, respectively:

$$\hat{H}_{ol,t}(j\omega_t) = \frac{\Psi(j\omega_t)}{E(j\omega_t)}, \tag{2.14}$$

$$\hat{H}_{ol,d}(j\omega_d) = -\frac{U(j\omega_d)}{U_d(j\omega_d)}, \tag{2.15}$$

where $\hat{H}_{ol,t}(j\omega_t)$ is the nonparametric target open-loop describing function at target frequency ω_t, $\Psi(j\omega_t)$ is the Fourier transform of the yaw angle ψ at target frequency ω_t, $E(j\omega_t)$ is the Fourier transform of the error signal e at target frequency ω_t; $\hat{H}_{ol,d}(j\omega_d)$ is the nonparametric disturbance open-loop describing function at disturbance frequency ω_d, $U(j\omega_d)$ is the Fourier transform of the control signal u at disturbance frequency ω_d, and $U_d(j\omega_d)$ is the Fourier transform of the signal u_d (which is the sum of the control signal

u and disturbance forcing function f_d) at disturbance frequency ω_d. Then the open-loop target crossover frequency $\omega_{c,t}$, target phase margin $\phi_{m,t}$, open-loop disturbance crossover frequency $\omega_{c,d}$ and disturbance phase margin $\phi_{m,d}$ representing the manual control bandwidth and the stability are calculated from these nonparametric open-loop describing functions (see Appendix E). Similarly, for the conditions without motion feedback (C1-C3, see Table 2.2), based on the measures of e and u, the nonparametric frequency response function (FRF) estimate of the human operator dynamics H_p at the frequencies of ω_t and ω_d is obtained as:

$$\hat{H}_p(j\omega_{t,d}) = \frac{U(j\omega_{t,d})}{E(j\omega_{t,d})}. \tag{2.16}$$

For conditions with motion feedback (C4-C6, see Table 2.2), for information on the nonparametric human operator visual response $\hat{H}_p(j\omega)$ and motion response $\hat{H}_m(j\omega)$, the reader is referred to [22].

The human operator model parameters in Eqs. (2.6-2.11) are estimated using the time-domain parameter estimation method of [23]. To evaluate the quality-of-fit for all fitted human operator models, the Variance Accounted For (VAF) is calculated. The VAF expresses the model quality in the percentage of the variance in the control signal u that is captured by the model [23] and [24].

In order to further compare how the tracking of f_t and the rejection of f_d are affected by the presence of motion feedback, the FRF between error signal e and target forcing function f_t and the FRF between error signal e and effective disturbance forcing function $f_{d,e}$ are estimated from the measured data according to:

$$\hat{H}_{e,f_t}(j\omega_t) = \frac{E(j\omega_t)}{F_t(j\omega_t)}, \tag{2.17}$$

$$\hat{H}_{e,f_{d,e}}(j\omega_d) = \frac{E(j\omega_d)}{F_d(j\omega_d)H_c(j\omega_d)}, \tag{2.18}$$

where $F_t(j\omega_t)$ is the Fourier transform of the target forcing function f_t at frequency of ω_t, $F_d(j\omega_d)$ is the Fourier transform of the disturbance forcing function f_d at frequency of ω_d, $H_c(j\omega_d)$ is the frequency response of the controlled element at frequency of ω_d. In order to better analyze the continuous changing trends of target-to-error and disturbance-to-error dynamics and to observe its fitting with the discrete frequency response functions Eqs. (2.17) and (2.18), the continuous frequency response functions are derived:

$$H_{e,f_t}(j\omega) = \frac{1 + H_m(j\omega)H_c(j\omega)}{1 + [H_p(j\omega) + H_m(j\omega)]H_c(j\omega)}, \tag{2.19}$$

$$H_{e,f_{d,e}}(j\omega) = \frac{-1}{1 + [H_p(j\omega) + H_m(j\omega)]H_c(j\omega)}, \tag{2.20}$$

where for the conditions without motion, $H_m = 0$.

Finally, a two-way repeated-measures analysis of variance (ANOVA) and a paired t-test are applied to reveal any significant effect of the independent variables on the tracking performance, control activity, target and disturbance crossover frequencies, target and disturbance phase margins, and all human operator parameters.

APPARATUS

The experiment was performed in the SIMONA Research Simulator (SRS) of Delft University of Technology (see Figure 2.4). During the experiment, the subjects were seated in the right seat in SRS and a sidestick was used for giving inputs to the controlled element. Only the roll axis of the sidestick was active during the experiment; the pitch axis of the sidestick was fixed at the neutral position. The tracking error e in Figure 2.1 was presented to the subject through the primary flight display (PFD) directly in front of the right seat, as shown in Figure 2.2. The display shows the yaw attitude tracking error e as the distance between the center reference cross and the follower circle. The reference cross was static, and the follower circle was in motion. Note that this display is an "inside-out" display: to compensate for the tracking error the subject needs to give a (positive) sidestick control input to the right, towards the follower circle. No other visual cues were presented during the experiment, that is, the secondary flight displays and the outside visual system were switched off.

The yaw motion cues around subject's vertical axis were provided through the motion system for C4, C5 and C6. The time delay of the motion system is less than 30 ms [28].

To make sure that the subjects only utilized and responded to the visual information and the motion feedback provided by the motion system, a noise-canceling headset was used to prevent subjects hearing the noise produced by the motion system's actuators. Additionally, aircraft engine noise was played over the headset to further keep the subjects from hearing the actuator sliding noise. The subjects wore the headset for all conditions, which included those conditions performed without motion feedback (C1, C2 and C3).

Figure 2.4: The SIMONA Research Simulator (SRS).

SUBJECTS AND EXPERIMENTAL PROCEDURES

Six male subjects aged between 25 and 53 years old were invited to perform this experiment, all students or staff of the Faculty of Aerospace Engineering of Delft University of Technology. All subjects had experience with similar manual control tasks from previous human-in-the-loop experiments. Each subject received an experimental briefing on the overview and objective of the experiment. The subjects were informed the nature of the different experimental conditions (Table 2.2) without providing the details of the dynamics of the controlled elements. The subjects were instructed to minimize the yaw attitude tracking error e presented on the PFD as best as possible. Finally, all the subjects gave written

informed consent before the start of the experiment.

For each subject, the experiment started with an initial familiarization. During this phase, the subject was allowed to familiarize himself with the different controlled elements both with and without motion. For each condition, two familiarization runs were carried out, hence in total 12 runs were performed in the familiarization phase.

The training and measurement runs were conducted after the familiarization phase. The order of the testing was determined for each subject by a Latin square. There was no predefined number of training and measurement runs. The root mean square (RMS) of the error signal e during the testing was tracked by experimenter for the entire experiment. When the RMS(e) of the subject clearly stabilized and five repetitions were collected at this performance level of one condition, the testing of this condition was completed. Generally, around 10 tracking runs were sufficient for each experimental condition to complete the training and measurement phase.

Each testing run lasted for 95 s. In order to get a stable control output from the subject, the first 8.08 s data were cut off considering the transitional period, and the last 5 s data were also cut off due to the fade-out function. Thus 81.92 s was used for measurement. The sampling frequency of the data in the experiment was set at 100 Hz.

HYPOTHESES

Shirley et al. [5] indicated that unstable vehicle dynamics causes the human operator to generate lead in order to increase the performance of the closed-loop human operator-vehicle system without destabilizing it. Thus the motion feedback which aids the human operator in generating lead is beneficial. Based on this, the hypotheses for the double integrator controlled element (which is marginally stable) in the experiment of this chapter are:

- (H1) *Compared with condition without motion feedback, the tracking performance is significantly better, the control activity is significantly lower, human operator-vehicle system target crossover frequency is significantly lower, the human operator-vehicle system target phase margin is significantly higher and the human operator's visual lead time constant is significantly lower under the condition with motion feedback.*

According to Shirley et al. [5], for a single integrator controlled element with motion cues, the tracking performance increased and the human operator increased the gain for the whole experimental frequency range. However, it should be noted that this result came from the single integrator controlled element with a pure time delay term with 100 ms. As a comparison, Bergeron et al. [20] pointed out that in the single-axis tests of pitch, roll, and yaw, neither significant performance improvement nor different human operator control behavior was observed (no adaptation or optimization of control behavior) when motion cues were added. Additionally, Junker et al. [21] reported that the degraded tracking performance was observed in a roll axis tracking task when motion is added. Even though these results on the human operator's adaptation and optimization are uncertain and inconsistent, in order to make the research of this chapter complete, the hypotheses for the single integrator controlled element in the experiment of this chapter are:

- (H2) *The motion feedback makes no significant difference on tracking performance, control activities, human operator-vehicle system target and disturbance crossover*

frequencies, target and disturbance phase margins or human operator control behavior between the conditions without and with motion in the single integrator control tasks.

- (H3) For the gain controlled element, due to the fact that it is stable, the hypotheses for it *are the same with the ones of the single integrator controlled element stated above*.

2.3. RESULTS

In this section the results of the yaw attitude tracking experiment are presented. All results are analyzed using a repeated-measures analysis of variance (ANOVA) to test for significant effects of the independent variables.

TRACKING PERFORMANCE AND CONTROL ACTIVITIES

Figure 2.5a provides the variance decomposition of the error signal e for each condition averaged over the six subjects. The error bars show the 95% confidence intervals of the total $\sigma^2(e)$. The data have been corrected for between-subject variability. As can be seen in Figure 2.5a, there is no obvious difference in $\sigma^2(e)$ between C1 and C4 or between C2 and C5, which indicates that the motion feedback is not helpful in improving tracking performance when the controlled element is a gain or single integrator. For the double integrator, compared with C3, an improvement in tracking performance can be easily seen when motion feedback is added in C6. The nearly identical values of $\sigma^2(e)$ between C1 and C4 (and between C2 and C5) and the obviously different values of $\sigma^2(e)$ between C3 and C6 correspond with the statistic results in Table 2.3, where the motion Mot ($F(1,5) = 21.6, p < 0.05$) significantly affects $\sigma^2(e)$. Overall, due to the different stability of the controlled elements, the double integrator is the most difficult to control. As can be seen in Figure 2.5a, the $\sigma^2(e)$ of C3 and C6 is higher than those of other conditions, and it can be verified in Table 2.3 that the effect of controlled element H_c on $\sigma^2(e)$ is significant ($F(2,10) = 32.7, p < 0.05$). As to the variance components (shown with different color bars in Figure 2.5a), for each condition the target forcing function component is the main contribution to $\sigma^2(e)$ and is much larger than the disturbance forcing function component. This is due to the fact that the target forcing function has larger power than that of the disturbance forcing function in this experiment. It is verified that both the controlled element H_c ($F(2,10) = 21.5, p < 0.05$) and the motion Mot ($F(1,5) = 7.8, p < 0.05$) have significant effects on the target forcing function component of $\sigma^2(e)$. Similarly, both the controlled element H_c ($F(2,10) = 22.2, p < 0.05$) and the motion Mot ($F(1,5) = 17.6, p < 0.05$) have significant effects on the disturbance forcing function component, and both the controlled element H_c ($F(1.0,5.1) = 22.2, p < 0.05$) and motion Mot ($F(1,5) = 19.2, p < 0.05$) have significant effects on the remnant component.

Figure 2.5b provides the variance decomposition of the human operator control input u for each condition averaged over the six subjects. The error bars show the 95% confidence intervals of the total $\sigma^2(u)$. As can be seen in Figure 2.5b, the average $\sigma^2(u)$ of C4 is slightly higher than that of C1. There is no obvious difference of $\sigma^2(u)$ between C2 and C5. The average $\sigma^2(u)$ of C6 is lower than that of C3, and the spread for C6 is also narrower than that for C3, indicating that the motion helps decrease the control activities

in the double integrator control task. However, from Table 2.3 it can be observed that the motion Mot has no significant effect on $\sigma^2(u)$. The controlled element H_c is the only factor with a significant effect on $\sigma^2(u)$ ($F(2,10) = 101.1, p < 0.05$). This can be seen in Figure 2.5b that the $\sigma^2(u)$ of C1 and C4 is higher than those of other conditions. But it should be noted that this is directly related with the gains chosen for the different controlled elements (see Eqs. (2.3-2.5)). As to the variance components, similar to Figure 2.5a, for each condition the target forcing function component is the main contribution to the total variance. Meanwhile, the controlled element H_c is the only main effect on the target forcing function component ($F(2,10) = 143.3, p < 0.05$) and disturbance forcing function component ($F(2,10) = 103.9, p < 0.05$), respectively. For the remnant component, neither the controlled element H_c nor the motion Mot has a significant effect.

Additionally, Table 2.4 shows the paired t-test results for both $\sigma^2(e)$ and $\sigma^2(u)$. It can be seen that only in the double integrator control task, the effect of motion Mot is significant for $\sigma^2(e)$ ($t(5) = 4.9, p < 0.05$) and for $\sigma^2(u)$ ($t(5) = 2.7, p < 0.05$).

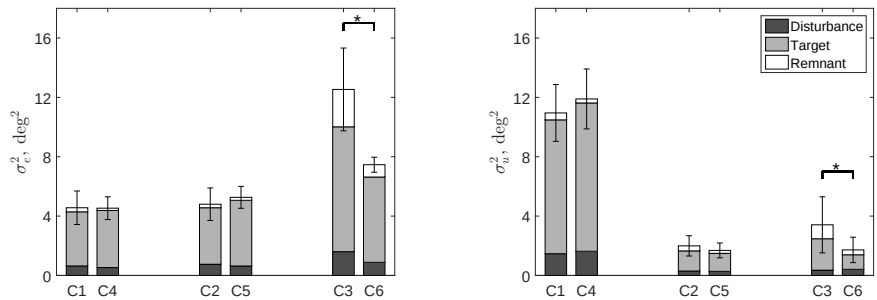

(a) Performance (b) Control activity

Figure 2.5: Variance decompositions of the error signal e and control signal u for each condition averaged over six subjects.

Table 2.3: ANOVA results for $\sigma^2(e)$ and $\sigma^2(u)$, where * is significant ($p < 0.05$), - is not significant ($p \geq 0.05$).

	$\sigma^2(e)$			$\sigma^2(u)$		
Factor	df	F	Sig.	df	F	Sig.
Hc	2,10	32.7	*	2,10	101.1	*
Mot	1,5	21.6	*	1,5	0.6	-
$Hc \times Mot$	2,10	19.5	*	2,10	3.7	-

Table 2.4: Paired t-test results for $\sigma^2(e)$ and $\sigma^2(u)$, * is significant ($p < 0.05$), - is not significant ($p \geq 0.05$).

	$\sigma^2(e)$			$\sigma^2(u)$		
Conditions	df	t	Sig.	df	t	Sig.
C1-C4	5	0.1	-	5	-0.9	-
C2-C5	5	-1.4	-	5	1.2	-
C3-C6	5	4.9	*	5	2.7	*

CROSSOVER FREQUENCIES AND PHASE MARGINS

Figure 2.6 provides the error-bar plots of the target and disturbance open-loop crossover frequencies $\omega_{c,t}$ and $\omega_{c,d}$, and target and disturbance open loop phase margins $\phi_{m,t}$ and $\phi_{m,d}$ for all conditions. The error bars give the 95% confidence intervals of the means over six subjects. The data have been corrected for between-subject variability. From Figure 2.6a it can be seen that for the gain dynamics there is no obvious difference of $\omega_{c,t}$ (or $\omega_{c,d}$) between C1 and C4, indicating that the motion may not make any difference on $\omega_{c,t}$ (or $\omega_{c,d}$). It can be verified from Table 2.6 that neither $\omega_{c,t}$ nor $\omega_{c,d}$ between C1 and C4 is significant. For the single integrator, the average value of $\omega_{c,t}$ of C5 is lower than that of C2, and the average value of $\omega_{c,d}$ of C5 is higher than that of C2. In the meantime, both of the variances of the crossover frequencies become smaller in C5 than in C2. However, Table 2.6 shows that there is no significant difference of $\omega_{c,t}$ (or $\omega_{c,d}$) between C2 and C5, even though the significance value of $\omega_{c,t}$ is already very small ($t(5) = 2.465, p = 0.057$). For the double integrator, the average value of $\omega_{c,t}$ of C6 is lower than that of C3 and the average value of $\omega_{c,d}$ of C6 is higher than that of C3. Table 2.6 shows that there is no significant difference of $\omega_{c,t}$ between C3 and C6, however, the difference of $\omega_{c,d}$ between C3 and C6 is significant ($t(5) = -2.720, p < 0.05$), which indicates that the motion makes a difference on the disturbance crossover frequency when the controlled element is double integrator.

In Figure 2.6b, for gain dynamics, there is no obvious difference of $\phi_{m,t}$ (or $\phi_{m,d}$) between C1 and C4, indicating that the motion may not make any difference on target and disturbance phase margins, and this can be verified from Table 2.6 that the paired t-test results for $\phi_{m,t}$ (and $\phi_{m,d}$) between C1 and C4 are not significant. For single integrator, in Figure 2.6b, $\phi_{m,t}$ of C5 is nearly identical with C2, the average value of $\phi_{m,d}$ of C5 is lower than that of C2 and the variance of $\phi_{m,d}$ of C5 is smaller than that of C2. According to Table 2.6, however, there is no significant difference of $\phi_{m,t}$ (or $\phi_{m,d}$) between C2 and C5, indicating that motion feedback does not essentially change the phase margins. For double integrator, in Figure 2.6b, there is an obvious difference of $\phi_{m,t}$ between C3 and C6, and the $\phi_{m,d}$ of C6 is nearly identical with C3. Table 2.6 verifies that only for $\phi_{m,t}$ the motion effect is significant between C3 and C6 ($t(5) = -6.200, p < 0.05$), which suggests that the motion feedback influences the target phase margin significantly in double integrator control task.

MOTION UTILIZATION ANALYSIS

In Table 2.7 the motion utilization factor M_u calculated from the fitted multimodal human operator models is shown for each condition and subject. For reference, the average over all subjects is also given for each condition.

In Table 2.7 it should be noted that the motion utilization factor M_u is also calculated for conditions without motion feedback for all subjects. For C1, C2 and C3, even though in the experiment there was no motion feedback at all, the multimodal human operator model including H_m is still used for identifying the human operator control behavior for reference. For these conditions, the nonzero motion utilization factor M_u results from noise and model fitting inaccuracies. As can be seen in Table 2.7, for the conditions without motion feedback (C1 – C3) M_u is always lower than 5%, suggesting a non-activated motion channel for such M_u values. For C4 and C5 which had motion feedback, M_u is less than 5% as well except

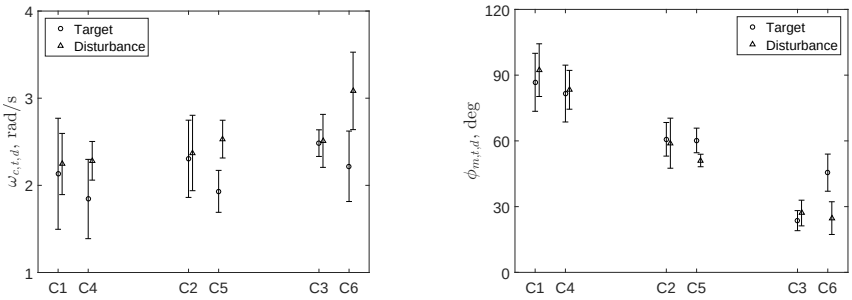

(a) Target and disturbance crossover frequencies

(b) Target and disturbance phase margins

Figure 2.6: Target, disturbance crossover frequencies and phase margins for each condition averaged over six subjects.

Table 2.5: ANOVA results of the target and disturbance crossover frequencies and phase margins, where * is significant ($p < 0.05$), and - is not significant ($p \geq 0.05$).

	$\omega_{c,t}$			$\omega_{c,d}$			$\phi_{m,t}$			$\phi_{m,d}$		
Factor	df	F	Sig.	df	F	Sig.	df	F	Sig.	df	F	Sig.
Hc	2,10	1.4	-	2,10	6.0	*	2,10	57.8	*	2,10	97.9	*
Mot	1,5	5.0	-	1,5	3.8	-	1,5	2.4	-	1,5	6.9	*
$Hc \times Mot$	2,10	0.1	-	2,10	2.6	-	2,10	11.0	*	2,10	0.6	-

Table 2.6: Paired t-test results of the target and disturbance crossover frequencies and phase margins, where * is significant ($p < 0.05$), and - is not significant ($p \geq 0.05$).

	$\omega_{c,t}$			$\omega_{c,d}$			$\phi_{m,t}$			$\phi_{m,d}$		
Conditions	df	t	Sig.	df	t	Sig.	df	t	Sig.	df	t	Sig.
C1-C4	5	1.0	-	5	-0.3	-	5	0.7	-	5	2.0	-
C2-C5	5	2.5	-	5	-0.7	-	5	0.2	-	5	1.5	-
C3-C6	5	1.7	-	5	-2.7	*	5	-6.2	*	5	0.7	-

Table 2.7: Motion utilization factor

M_u, %	C1	C2	C3	C4	C5	C6
Subject 1	0.3	2.8	0.5	0.1	0.9	22.4
Subject 2	0.3	0.7	0.2	1.1	2.5	44.1
Subject 3	0.2	0.4	0.4	0.2	0.2	19.0
Subject 4	0.1	0.02	0.2	0.2	1.8	35.0
Subject 5	0.3	1.6	4.1	1.7	10.3	58.6
Subject 6	0.2	2.4	1.7	1.3	4.1	27.3
Average	**0.2**	**1.3**	**1.2**	**0.8**	**3.3**	**34.4**

for C5 of Subject 5. This suggests that even though the motion feedback was provided for C4 and C5, it was not used by the human operators. That is, the human operators mainly used the visual channel rather than the motion channel to provide control input u for these conditions.

For C6 control of the double integrator with motion, M_u is seen to be much higher than 5% for each subject, indicating that the motion feedback was indeed utilized and the motion channel of the multimodal human operator model was active.

Based on the analysis of M_u, it is assumed that for C1 – C5 the subjects only used the visual feedback to generate control input u, thus the motion channel was not active in these conditions. For C6, the motion channel was clearly active.

HUMAN OPERATOR MODEL VALIDATION

Figure 2.7 to Figure 2.9 show representative human operator model fits for all conditions of Subject 4 with the controlled element dynamics for reference (equivalent results were obtained for all other subjects). For model verification, the describing functions obtained using Fourier coefficient estimation method [25] are also shown for reference, with the error bars showing the sample standard deviations of the FRF estimates over the five measurement runs. The VAF (Variance Accounted For) value is also shown in the legend of the figures, it is a measure indicating the percentage of the variance in the measured control signal u that can be explained by the model. It should be noted for C4 and C5 the single channel human operator model (without H_m) is used in identification based on the negligible motion utilization for these conditions (see Table 2.7). The results for C6 are obtained from the full multimodal human operator model.

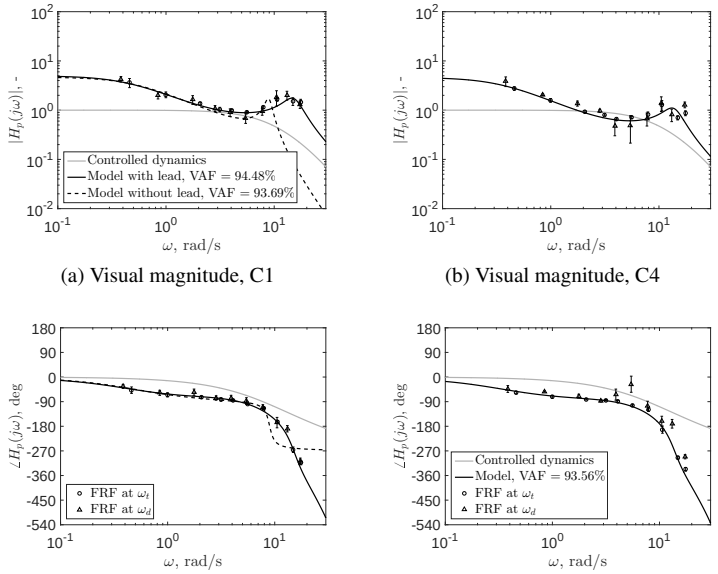

(a) Visual magnitude, C1

(b) Visual magnitude, C4

(c) Visual phase, C1

(d) Visual phase, C4

Figure 2.7: Example of human operator model fitting results for C1 and C4 (Subject 4).

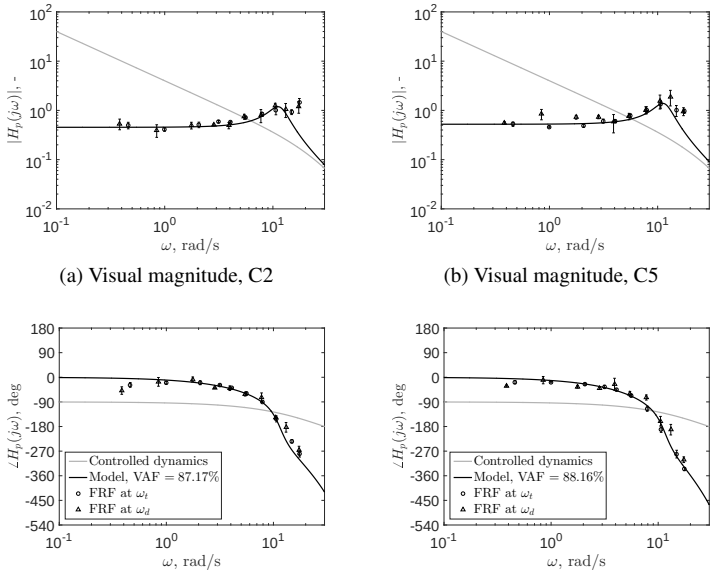

(a) Visual magnitude, C2 (b) Visual magnitude, C5

(c) Visual phase, C2 (d) Visual phase, C5

Figure 2.8: Example of human operator model fitting results for C2 and C5 (Subject 4).

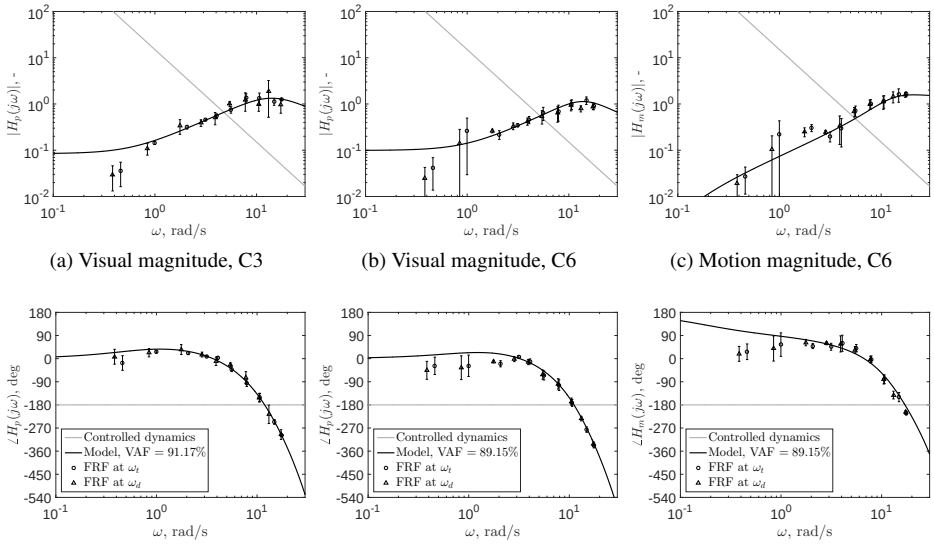

(a) Visual magnitude, C3 (b) Visual magnitude, C6 (c) Motion magnitude, C6

(d) Visual phase, C3 (e) Visual phase, C6 (f) Motion phase, C6

Figure 2.9: Example of human operator model fitting results for C3 and C6 (Subject 4).

In Figure 2.7a and Figure 2.7c, the solid curve represents the human operator identi-

fication result using the equalization term from Eq. (2.8), and the dashed curve represents the identification result using the equalization term with only gain and lag. It can be seen that by using the equalization term from Eq. (2.8), the model fits the describing functions obtained using Fourier coefficient estimation method [25] better, which proves that the additional lead term in Eq. (2.8) compared with an equalization with only gain and lag is necessary for modeling the human operator's control behavior in this gain control task. And this phenomenon is found for all other subjects as well.

As can be seen from Figure 2.7 to Figure 2.9, in the crossover frequency range (2 rad/s to 5 rad/s), the frequency responses of the human operator for C1 and C4, C2 and C5, C3 and C6, are lag, gain and lead, respectively, which correspond with the conclusions of McRuer et al. [3]. Meanwhile, the estimated human operator model fits the nonparametric describing function well for each condition. The average VAF value over all subjects and conditions is 86.9%, ranging between 73.5% and 94.5%. The average VAF values over all subjects for C4 and C5 are 90.5% and 85.5%, respectively, which suggest that modeling the human operator control behavior with only visual channel for the gain and single integrator controlled elements is sufficient. Meanwhile, the similarity of the frequency responses between C1 and C4 (also C2 and C5) also proves this. In both Figure 2.7a and Figure 2.7b it can be seen that within a very narrow frequency range around 5 rad/s, the frequency responses approximate a gain, and this is due to the lead term added in Eq. (2.8).

HUMAN OPERATOR MODEL PARAMETERS

Figure 2.10 shows the error-bar plots of the corresponding parameters of the human operator model for all conditions. The error-bars indicate the 95% confidence intervals of the means over the six subjects. Tables 2.8 and 2.9 provide the corresponding ANOVA results for the human operator model parameters.

As can be seen in Figure 2.10a, the average visual gain K_v of C1 is lower than that of C4, and there is no obvious difference in K_v between C2 and C5, or between C3 and C6, indicating that the motion may only cause the difference on K_v in the gain control task. Table 2.8 shows that only the effect of the controlled element H_c on K_v is significant ($F(1.0, 5.1) = 53.6, p < 0.05$), which may be a result of the choice of the gains for the different controlled elements. Motion Mot is not found to significantly affect K_v, even though the average K_v of C4 is higher than that of C1 observed in Figure 2.10a. Note that as the Mauchly's test indicated a violation of the sphericity assumption here, the Greenhouse-Geisser correction (indicated with a superscript "gg" in Table 2.8 and 2.9) was applied.

Figure 2.10c shows that the average lead time constant T_{lead} of C4 is slightly lower than that of C1. And T_{lead} of C6 is lower than that of C3, indicating that the control task of the double integrator needs less lead with motion, which is consistent with earlier findings [5, 15, 21]. From Table 2.8 it can be observed that the effects of both the controlled element H_c ($F(1,5) = 19.4, p < 0.05$) and the motion Mot ($F(1,5) = 13.1, p < 0.05$) are significant on T_{lead}, which corresponds with the observations in Figure 2.10c. Moreover, from the paired t-test results in Table 2.10 it can be seen that the effect of motion MOT is only significant ($t(5) = 3.2, p < 0.05$) in double integrator control task.

As the lag time constant T_{lag} is only modeled in C1 and C4, there is no controlled element effect. Figure 2.10d shows that T_{lag} of C4 is much higher than that of C1, and it is significantly affected by motion Mot ($F(1,5) = 49.7, p < 0.05$) (see Table 2.8), indicating

that the human operators integrate the error signal e more and the response is somewhat slower in the gain control task with motion. Additionally, from the paired t-test results in Table 2.10 it can be seen that the effect of motion MOT is significant ($t(5) = -7, p < 0.05$) in gain control task.

From Figure 2.10b it can be seen that the average visual time delay τ_v of C4 is a little bit lower than that of C1, the average τ_v of C5 is higher than that of C2, and the average τ_v of C6 is higher than that of C3. On average, τ_v of C3 and C6 is higher than other conditions. From Table 2.8 it can be observed that the effects of both the controlled element H_c ($F(2,10) = 115.6, p < 0.05$) and the interaction between the controlled element and motion $Hc{\times}Mot$ ($F(2,10) = 5.6, p < 0.05$) are significant on τ_v. Table 2.10 shows that the effect of motion MOT in both single integrator control task ($t(5) = -3, p < 0.05$) and double integrator control task ($t(5) = -4.5, p < 0.05$) are significant.

As can be seen in Figure 2.10e, for each controlled element (C1 and C4, C2 and C5, C3 and C6), there is no obvious difference of the neuromuscular damping ζ_{nm} between the conditions without and with motion. The average ζ_{nm} of C3 and C6 is slightly higher than that of other conditions. It can be verified in Table 2.9 that only the effect of the controlled element H_c is significant on ζ_{nm} ($F(1.1,5.6) = 6.2, p < 0.05$). In Figure 2.10f it can be seen that the average neuromuscular frequency ω_{nm} of C4 is lower than that of C1, but there is no obvious difference of ω_{nm} between C2 and C5, or between C3 and C6. Table 2.9 shows that the effect of controlled element H_c is significant on ω_{nm} ($F(2,10) = 8.2, p < 0.05$), verifying the observations in Figure 2.10f. The high ω_{nm} of C1 and C4 may be caused by an increase in arm and hand muscle tension when subjects control the gain controlled element. In Figure 2.10g it can be seen that for C6, the order of K_m is near the order of K_v. Additionally, the value of τ_m is lower than τ_v, which has also been found by Zaal et al.[8]. Since the motion gain K_m and the motion time delay τ_m are estimated only for C6, no statistics were performed on these two parameters.

Table 2.8: ANOVA results of the visual parameters, where * is significant ($p < 0.05$), and - is not significant ($p \geq 0.05$).

	K_v			T_{lead}			T_{lag}			τ_v		
Factor	df	F	Sig.	df	F	Sig.	df	F	Sig.	df	F	Sig.
Hc	1.0,5.1^{gg}	53.6	*	1,5	19.4	*				2,10	115.6	*
Mot	1,5	2.9	-	1,5	13.1	*	1,5	49.7	*	1,5	4.3	-
$Hc{\times}Mot$	1.0,5.0^{gg}	3.4	-	1,5	6.8	*				2,10	5.6	*

Table 2.9: ANOVA results of the neuromuscular parameters, where * is significant ($p < 0.05$), and - is not significant ($p \geq 0.05$).

	ζ_{nm}			ω_{nm}		
Factor	df	F	Sig.	df	F	Sig.
Hc	1.1,5.6^{gg}	6.2	*	2,10	8.2	*
Mot	1,5	0.3	-	1,5	2.1	-
$Hc{\times}Mot$	2,10	0.3	-	1.1,5.4^{gg}	2.5	-

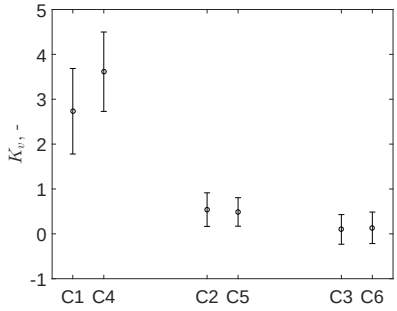

(a) Visual gain

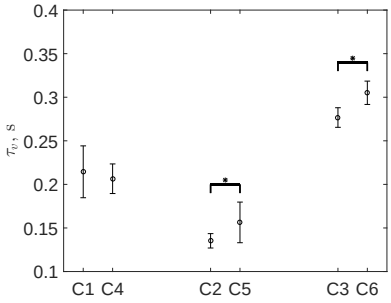

(b) Visual time delay

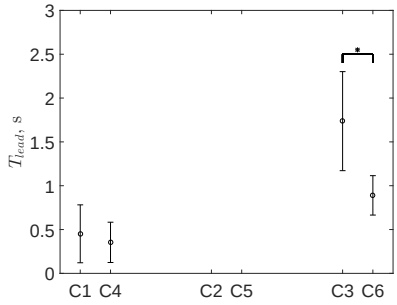

(c) Lead time constant

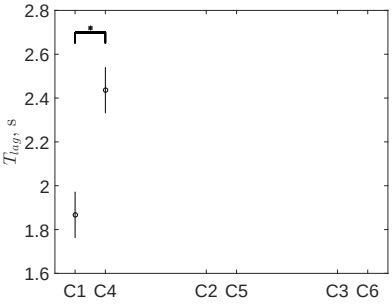

(d) Lag time constant

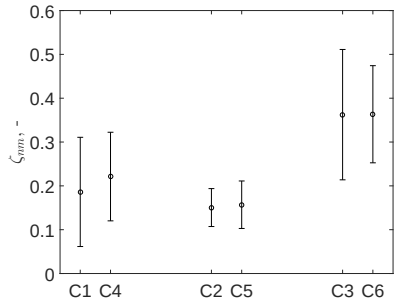

(e) Neuromuscular damping

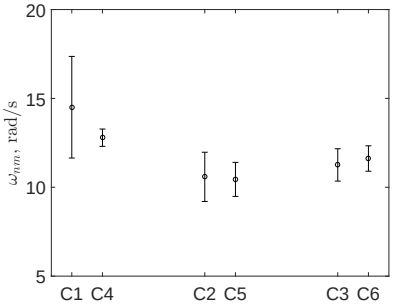

(f) Neuromuscular frequency

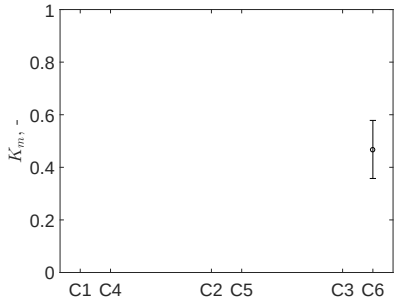

(g) Motion gain

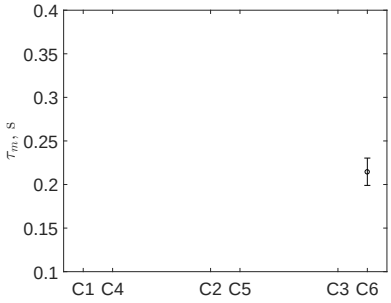

(h) Motion time delay

Figure 2.10: Estimated human operator model parameters.

Table 2.10: Paired t-test results of the visual parameters, where * is significant ($p < 0.05$), and - is not significant ($p \geq 0.05$).

	K_v			T_{lead}			T_{lag}			τ_v		
Conditions	df	t	Sig.	df	t	Sig.	df	t	Sig.	df	t	Sig.
C1-C4	5	-1.8	-	5	1.2	-	5	-7	*	5	0.6	-
C2-C5	5	1.1	-							5	-3	*
C3-C6	5	-1.8	-	5	3.2	*				5	-4.5	*

Table 2.11: Paired t-test results of the neuromuscular parameters, where * is significant ($p < 0.05$), and - is not significant ($p \geq 0.05$).

	ζ_{nm}			ω_{nm}		
Conditions	df	t	Sig.	df	t	Sig.
C1-C4	5	-0.7	-	5	1.6	-
C2-C5	5	-0.4	-	5	0.6	-
C3-C6	5	-0.03	-	5	-1.6	-

ANALYSIS OF CLOSED-LOOP ATTENUATION OF TRACKING ERRORS

Figure 2.11 shows the results of the closed-loop attenuation of tracking errors with respect to both the target (a-c) and (effective) disturbance (d-f) forcing functions of the three controlled elements. In Figures 2.11a and 2.11d, for example, the error bars with squares and asterisks represent the averages and 95% confidence intervals of the magnitude of the discrete frequency response functions estimated using Eqs. (2.17) and (2.18) for all subjects. The dashed and solid curves represent the magnitude of the averaged subject calculated by Eqs. (2.19) and (2.20) for no-motion and motion conditions, respectively. Finally, the dashed and solid vertical lines mark the average target (or disturbance) crossover frequencies for conditions without and with motion, respectively. It can be seen that attenuation of the tracking errors induced by the target (or disturbance) forcing function is only achieved below a certain frequency. For higher frequencies, the magnitude of the closed-loop responses overshoots and forms a peak, the height of which varies with the stability of the closed-loop system. As can be seen, the discrete frequency responses derived from Eqs. (2.17) and (2.18) match well with the continuous ones derived from Eqs. (2.19) and (2.20) in each plot.

In Figure 2.11c (and Figure 2.11f), obvious differences between the dashed and solid curves can be observed, especially around the frequencies of the peak. In Figure 2.11c, the peak of C6 is much lower than that of C3, indicating that the closed-loop system becomes more stable when motion feedback is provided, and this accounts for the better performance of C6 compared with C3 in Figure 2.5a.The lower target crossover frequency for C6 than for C3 is seen to result in slightly worse error attenuation at low frequencies ($\omega < 1.6$ rad/s), but result in a coupled significant reduction in the peak magnitude. In Figure 2.11f, even though the difference of the peaks between C3 and C6 is not as large as the one of Figure 2.11c, it still seems evident here in comparison with the results for the other controlled elements. The lowering of the closed-loop resonance peak between C3 and C6 in both Figure 2.11c and Figure 2.11f strongly influence the target and disturbance components of the performance $\sigma^2(e)$, as presented in Figure 2.5a, and causes both the target and disturbance components of C6 to be lower than those of C3.

Compared with the double integrator, in Figure 2.11a (and Figure 2.11d), the dashed and solid curves show less difference, which indicates that for the gain control tasks, the error signal attenuation does not change much as a result of motion feedback. This is consistent with Figure 2.5a, where the target and disturbance components for C1 nearly equal to those for C4. Furthermore, the nearly identical dashed and solid vertical lines in Figure 2.11d show that the disturbance crossover frequencies of C1 and C4 are almost the same. Even though in Figure 2.11a that the target crossover frequency for C4 is lower than that of C1, the error attenuation of C4 is worse than that of C1 when $\omega < 5.2$ rad/s but becomes better when $5.2 < \omega < 12$ rad/s, which cancel out with each other. All observations from Figure 2.11a and Figure 2.11d indicate that for the gain controlled element the motion feedback is not helpful in improving task performance.

In Figure 2.11b, compared with the dashed curve, the solid curve slightly shifts to the left, meaning that for frequencies below the peak, the error attenuation becomes marginally worse. As can be seen in Figure 2.5a, the target component of C5 is also slightly higher than for C2. Meanwhile, in Figure 2.11b, the target crossover frequency of C5 is lower than that of C2, and this difference is nearly same with that of the gain controlled element in Figure 6(a). In Figure 2.11e, the difference of the disturbance crossover frequencies between C2 and C5 is smaller than that of the target crossover frequencies in Figure 2.11b. Figure 2.11b and Figure 2.11e suggest that for the single integrator, the motion may slightly degrade the task performance and decrease target crossover frequency. However, the t-tests in Table 2.4 and Table 2.6 show no significant difference of task performance and target crossover frequencies between C2 and C5.

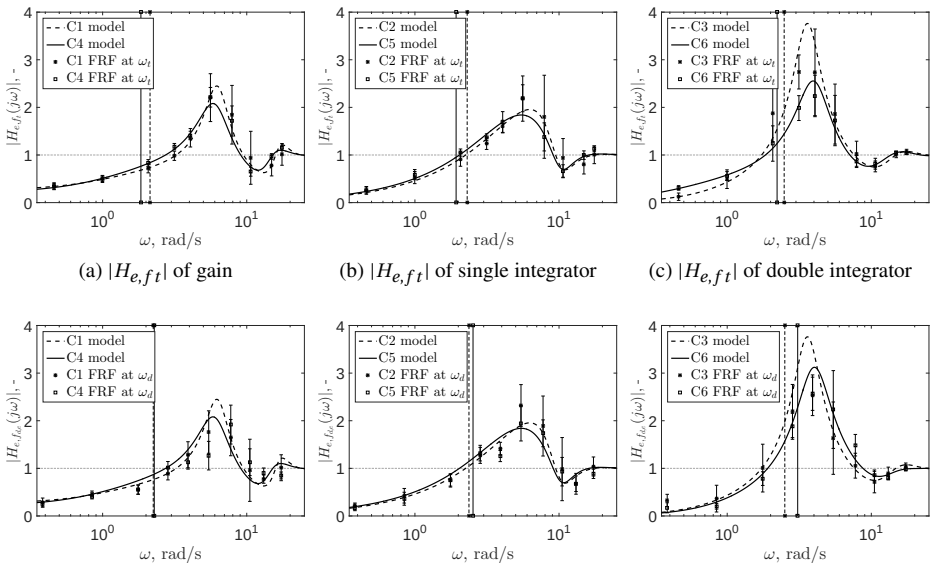

(a) $|H_{e,ft}|$ of gain (b) $|H_{e,ft}|$ of single integrator (c) $|H_{e,ft}|$ of double integrator

(d) $|H_{e,f_{d,e}}|$ of gain (e) $|H_{e,f_{d,e}}|$ of single integrator (f) $|H_{e,f_{d,e}}|$ of double integrator

Figure 2.11: Frequency responses of target-to-error and disturbance-to-error dynamics.

2.4. DISCUSSION

In this chapter, the effects of motion feedback on human operator control behavior with different controlled elements were studied in a yaw attitude tracking task. A gain controlled element, a single integrator controlled element and a double integrator controlled element were evaluated both without and with motion feedback in a within-subjects experiment with six subjects. The data were analyzed with human operator modeling techniques to evaluate the utilization of motion feedback by the human operators and the human operator control behavior.

For the double integrator controlled element, the motion feedback is utilized by the human operators, indicated by the motion utilization factor and model fitting results, which is clear evidence for the adaption of the human operator control dynamics. The visual lead time constant drops around 56% and the visual time delay increases around 13% when motion feedback is added, indicating that the double integrator control task becomes easier for the human operators with motion feedback and the optimization of the human operator control dynamics exist, too. Meanwhile, the motion feedback significantly improves the tracking performance, decreases the control activity, and increases the target phase margin. In summary, the results for the double integrator controlled element are consistent with previous studies by other researchers [5, 6, 16–19]. However, the target crossover frequencies show no significant difference between conditions without and with motion, and this may be caused by the limited numbers of subjects in this experiment.

For the gain controlled element, through the analysis of the motion utilization factor, it was concluded that the motion feedback was not utilized by the human operators. This may be due to the fact that for the gain control task the human operator does not need to generate lead to stabilize the system. The lead term in the equalization of the human operator model serves to improve the model fit. Since the value of this lead time constant is very low, it indicates that this lead term only influences human operator model at high frequencies. From the human operator modeling results, a significant increase in the lag time constant (around 33% compared to the condition without motion) for the condition with motion can be observed. There is also a slight increase in the visual gain for the condition with motion, but it is not significant compared to the condition without motion feedback. So even though there is no adaption of the human operator control dynamics between conditions with and without motion feedback, the optimization of the human operator control dynamics still exists. However, the motion feedback is not useful in improving tracking task performance.

Similar to the gain controlled element, the human operator does not need to generate lead to stabilize the system in the single integrator control task, and according to the motion utilization factor, the motion feedback is also not utilized by the human operators for this controlled element. The human operator modeling results show that the visual time delay slightly increases with motion feedback, which is the only indication for the optimization of human operator control behavior. As to the tracking performance, control activities, target crossover frequencies and target phase margins, there is no difference between conditions without and with motion.

Closed-loop analyses of the target-to-error and disturbance-to-error frequency responses show that for the double integrator control tasks the human operators improve the tracking performance mainly by increasing the stability of the human-vehicle system and decreasing the target crossover frequency. For both gain and single integrator control tasks, the

closed-loop frequency responses are very similar between no motion and motion conditions, meaning that the performance is not improved by the presence of motion feedback.

All of these suggest that a fixed-base simulator may be sufficient for human operator to do a gain or a single integrator tracking task, but for a double integrator tracking task, a moving-base simulator is indispensable.

It should be noted that the method to verify the activeness of the motion channel of the human operator model is by the motion utilization factor, which depends on the parameter identification results where the multimodal human operator model is assumed no matter whether the motion channel is really active or not. Then by assessing the values of the motion utilization factor and compare with each condition, it was arbitrarily concluded that for conditions of C4 (gain) and C5 (single integrator), the motion channel was not activated. However, objective criteria to judge the activeness of the motion channel based on the value of the motion utilization factor would be still needed. Moreover, a new metric which does not rely on the identification results of the assumed multimodal human operator model is preferred in the future.

2.5. CONCLUSIONS

A yaw attitude tracking experiment was performed to investigate the effects of motion feedback on human operator control behavior with gain, single integrator and double integrator controlled element dynamics. This experiment confirms the conclusions of previous studies that for the double integrator control tasks, both adaption and optimization of the human operator control dynamics exist: the motion feedback is utilized, and compared with the ones without motion, the visual time delay is higher and the lead time constant is lower when motion feedback is provided. Meanwhile, the tracking performance is better, the control activity is lower, the target phase margin is higher and the disturbance crossover frequency is higher with motion feedback. For the single integrator control tasks, only the visual time delay increases when motion feedback is present. For the gain control tasks, no adaption of the human operator control dynamics is observed between the conditions without and with motion feedback, but the lag time constant is higher when motion feedback is provided. For both gain and single integrator control tasks, there is no significant difference in tracking performance and control activities between conditions without and with motion. Therefore it is recommended that for control tasks of double integrator or higher order dynamics, motion feedback is necessary for both improving task performance and for properly evaluating human operator control behavior. For controlled elements with low order, motion may still cause differences in human operator control behavior but is not helpful in improving task performance.

REFERENCES

[1] D. T. McRuer and H. R. Jex, *A Review of Quasi-Linear Pilot Models,* IEEE Transactions on Human Factors in Electronics **HFE-8**, 231 (1967).

[2] L. R. Young, *On Adaptive Manual Control,* IEEE Transactions on Man-Machine Systems **10**, 292 (1969).

[3] D. T. McRuer, D. Graham, E. S. Krendel, and W. J. Reisener, *Human Pilot Dynamics*

in Compensatory Systems, Theory Models and Experiments with Controlled Element and Forcing Function Variations, Tech. Rep. AFFDL-TR-65-15 (Air Force Flight Dynamics Laboratory, Wright-Patterson Air Force Base (OH), 1965).

[4] W. E. Feddersen, *The Role of Motion Information and Its Contribution to Simulation Validity*, Report D228-429-001 (Bell Helicopter Company, 1962).

[5] R. S. Shirley and L. R. Young, *Motion Cues in Man-Vehicle Control – Effects of Roll-Motion Cues on Human Operator's Behavior in Compensatory Systems with Disturbance Inputs,* IEEE Transactions on Man-Machine Systems **9**, 121 (1968).

[6] R. L. Stapleford, R. A. Peters, and F. R. Alex, *Experiments and a Model for Pilot Dynamics with Visual and Motion Inputs*, Tech. Rep. NASA CR-1325 (Systems Technology, Inc., Hawthorne (CA), 1969).

[7] H. R. Jex, R. E. Magdaleno, and A. M. Junker, *Roll Tracking Effects of G-vector Tilt and Various Types of Motion Washout,* in *Proceedings of the Fourteenth Annual Conference on Manual Control* (1978) pp. 463–502.

[8] P. M. T. Zaal, D. M. Pool, J. de Bruin, M. Mulder, and M. M. van Paassen, *Use of Pitch and Heave Motion Cues in a Pitch Control Task,* Journal of Guidance, Control, and Dynamics **32**, 366 (2009).

[9] R. A. Hess and F. Marchesi, *Analytical Assessment of Flight Simulator Fidelity Using Pilot Models,* Journal of Guidance, Control, and Dynamics **32**, 760 (2009).

[10] P. R. Grant and J. A. Schroeder, *Modelling Pilot Control Behaviour for Flight Simulator Design and Assessment,* in *Proceedings of the AIAA Guidance, Navigation, and Control Conference, Toronto, Canada*, AIAA-2010-8356 (2010).

[11] P. M. T. Zaal, D. M. Pool, M. M. van Paassen, and M. Mulder, *Comparing Multimodal Pilot Pitch Control Behavior Between Simulated and Real Flight,* Journal of Guidance, Control, and Dynamics **35**, 1456 (2012).

[12] I. L. Ashkenas and D. T. McRuer, *A Theory of Handling Qualities Derived from Pilot-Vehicle System Considerations,* Aerospace Engineering **21**, 60 (1962).

[13] R. A. Hess, *Unified Theory for Aircraft Handling Qualities and Adverse Aircraft-Pilot Coupling,* Journal of Guidance, Control, and Dynamics **20**, 1141 (1997).

[14] H. J. Damveld, M. M. van Paassen, and M. Mulder, *Cybernetic Approach to Assess Aircraft Handling Qualities,* Journal of Guidance, Control, and Dynamics **34**, 1886 (2011).

[15] L. R. Young, *Some Effects of Motion Cues on Manual Tracking,* in *Second Annual NASA-University Conference on Manual Control, Massachusetts Institute of Technology, Cambridge (MA), February 28 – March 2, 1966* (1966) pp. 231–240.

[16] R. F. Ringland and R. L. Stapleford, *Motion Cue Effects on Pilot Tracking,* in *Seventh Annual Conference on Manual Control* (1971) pp. 327–338.

[17] J. C. van der Vaart, *Modelling of Perception and Action in Compensatory Manual Control Tasks*, Ph.D. thesis, Delft University of Technology, Faculty of Aerospace Engineering (1992).

[18] R. J. A. W. Hosman, *Pilot's Perception and Control of Aircraft Motions*, Ph.D. thesis, Delft University of Technology, Faculty of Aerospace Engineering (1996).

[19] T. L. Dehouck, M. Mulder, and M. M. van Paassen, *The Effects of Simulator Motion Filter Settings on Pilot Manual Control Behaviour,* in *Proceedings of the AIAA Modeling and Simulation Technologies Conference and Exhibit, Keystone (CO)*, AIAA-2006-6250 (2006).

[20] H. P. Bergeron, *Investigation of Motion Requirements in Compensatory Control Tasks,* IEEE Transactions on Man-Machine Systems **MMS-11**, 123 (1970).

[21] A. M. Junker and C. R. Replogle, *Motion Effects on the Human Operator in a Roll Axis Tracking Task,* Aviation, Space, and Environmental Medicine **46**, 819 (1975).

[22] M. M. van Paassen and M. Mulder, *Identification of Human Operator Control Behaviour in Multiple-Loop Tracking Tasks,* in *Proceedings of the Seventh IFAC/IFIP/IFORS/IEA Symposium on Analysis, Design and Evaluation of Man-Machine Systems, Kyoto Japan* (Pergamon, 1998) pp. 515–520.

[23] P. M. T. Zaal, D. M. Pool, Q. P. Chu, M. M. van Paassen, M. Mulder, and J. A. Mulder, *Modeling Human Multimodal Perception and Control Using Genetic Maximum Likelihood Estimation,* Journal of Guidance, Control, and Dynamics **32**, 1089 (2009).

[24] F. M. Nieuwenhuizen, P. M. T. Zaal, M. Mulder, M. M. van Paassen, and J. A. Mulder, *Modeling Human Multichannel Perception and Control Using Linear Time-Invariant Models,* Journal of Guidance, Control, and Dynamics **31**, 999 (2008).

[25] M. M. van Paassen, *Biophysics in Aircraft Control, A Model of the Neuromuscular System of the Pilot's Arm*, Ph.D. thesis, Delft University of Technology, Faculty of Aerospace Engineering (1994).

[26] T. Groot, H. J. Damveld, M. Mulder, and M. M. van Paassen, *Effects of Aeroelasticity on the Pilot's Psychomotor Behavior,* in *Proceedings of the AIAA Atmospheric Flight Mechanics Conference and Exhibit, Keystone, Colorado, Aug. 21-24, 2006*, AIAA-2006-6494 (American Institute of Aeronautics and Astronautics, 2006).

[27] D. M. Pool, *Objective Evaluation of Flight Simulator Motion Cueing Fidelity Through a Cybernetic Approach*, Ph.D. thesis, Delft University of Technology, Faculty of Aerospace Engineering (2012).

[28] W. R. Berkouwer, O. Stroosma, M. M. van Paassen, M. Mulder, and J. A. Mulder, *Measuring the Performance of the SIMONA Research Simulator's Motion System,* in *Proceedings of the AIAA Modeling and Simulation Technologies Conference and Exhibit, San Francisco, California, Aug. 15-18, 2005*, AIAA 2005-6504 (2005) pp. 1–12.

3

THE EFFECTS OF BASELINE DYNAMICS BANDWIDTH ON MANUAL CONTROL BEHAVIOR

The Maximum Unnoticeable Added Dynamics (MUAD) [1, 2] have been used for (simulator) aircraft model fidelity [3–7] and flight control system validations [5, 8]. However, these envelopes were developed purely based on subjective ratings on aircraft handling qualities and cannot quantify the sensitivity of human operator control behavior to the change of the controlled dynamics. Moreover, recent research [9] indicated that the MUAD envelopes [1, 2] may depend on the bandwidth of the baseline aircraft dynamics, arguing that the MUAD envelopes corresponding to low-bandwidth baseline dynamics are wider than those obtained for the high-bandwidth baseline, which may worsen the generalizability of the MUAD envelopes for any applications with different baseline aircraft dynamics. This chapter describes a pitch tracking experiment of which both low and high-bandwidth aircraft-representative baseline dynamics are perturbed by extra added dipole dynamics. The experiment aims to investigate whether the measured performance, control activity and identified objective human operator control behavior would correspond with the MUAD [1, 2], and whether these dependent measures depend on the interaction between the baseline and added dynamics, which could affect the formulation of the Manual Control Adaptation Boundaries.

Part of this chapter has been published as the following conference paper:
I. Matamoros, T. Lu, M. M. van Paassen, D. M. Pool, A Cybernetic Analysis of Maximum Unnoticeable Added Dynamics for Different Baseline Controlled Systems, in Proceedings of the 20th IFAC World Congress, Toulouse, France, 16417-16422 (2017).

3.1. INTRODUCTION

The Maximum Unnoticeable Added Dynamics (MUAD) envelopes [1, 2] are boundaries defined in the frequency domain within which the handing qualities of modified aircraft dynamics are equivalent to those of the baseline aircraft dynamics. By keeping the discrepancy between the modified aircraft dynamics (for example, with extra augmented control system) and the baseline aircraft dynamics within the MUAD envelopes, existing handling qualities criteria for the low-order equivalent systems (LOES) [10] can be applied to the new high-order system.

The existing MUAD envelopes were determined from extensive human-in-the-loop experiments, where subjective ratings were used to determine the noticeability of different types of added dynamics [1, 2]. It is known that the main drawback of subjective assessment methods is their poor reproducibility. Some other concerns exist about the MUAD envelopes, for example, there was no further experimental validation and the baseline aircraft dynamics which were used to develop the MUAD envelopes are very different from the ones used in recent literature. Even though these concerns exist, these envelopes are stilll used for aircraft model fidelity [3–7] and flight control system validations [5, 8]. Recent research on MUAD envelopes has shown that the sensitivity to added dynamics may be strongly dependent on the baseline [9] aircraft dynamics, where in the frequency domain the MUAD envelopes of high-bandwidth baseline aircraft dynamics (responsive) are narrower than those of low-bandwidth baseline aircraft dynamics (sluggish). This bandwidth-dependent characteristic would make it more difficult to generalize the MUAD envelopes for handling qualities assessment and human operator control behavior sensitivity analysis.

In recent years, a "*cybernetic approach*" has been successfully applied for objective analysis of human-machine issues involving human manual control [11–15]. Instead of relying on human operators' subjective feedback, the cybernetic approach focuses on objective measurements of task performance, control activity and especially identified human operator control behavior. For example, such methods have been applied to obtain objective measures for the fidelity of the flight simulators [16–19]. This approach can thus be further applied to validate the MUAD envelopes, for example, to see whether the changes in human operator's objective control behavior with respect to the added dynamics correspond with the MUAD envelopes, and whether the bandwidth of the baseline dynamics has an effect on the changes of the human operator control behavior.

In this chapter, an aircraft-representative pitch attitude tracking experiment was performed with added dipole dynamics of increasing magnitude added to the baseline dynamics. To tie in with [9], this was done for two baseline dynamics, representative for low-bandwidth (sluggish) and high-bandwidth (responsive) aircraft. From the experiment data, the individual and combined effects of the variation in the baseline and added dynamics on human operator control behavior can be determined, which provides further indications on whether the objective manual control behavior corresponds with the MUAD envelopes and whether the baseline dynamics make a difference.

This chapter is structured as follows. In Section 3.2 the experiment setup, procedures and methodologies are presented. The obtained results are given in Section 3.3. This chapter ends with a discussion and conclusions.

3.2. METHODS

3.2.1. CONTROL TASK

THE PITCH ATTITUDE TRACKING TASK

A pitch attitude tracking task is used to study human operator control behavior with different baseline and added dynamics. A schematic representation of this tracking task is shown in Figure 3.1. The total controlled dynamics consist of the baseline dynamics $H_{baseline}$, cascaded with the added dynamics H_{added}. The human operator (represented by a linear transfer function H_p and the remnant n) controls the pitch angle θ of these total dynamics ($H_{baseline}H_{added}$) by tracking the target signal f_t to minimize the error signal e, which is the difference between the target signal f_t and the pitch angle θ. In Figure 3.1, u is the human operator control signal, u_e is the linear part of the control signal contributed by H_p, K_s (= 1) is the stick gain, u_s is the control signal from the stick, and δ_e is the signal directly feeding into the baseline dynamics.

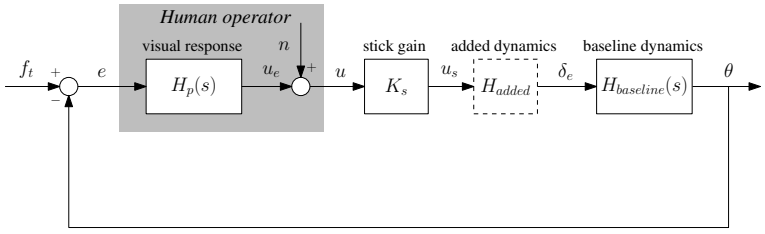

Figure 3.1: A schematic representation of the pitch attitude tracking task.

FORCING FUNCTIONS

For the pitch attitude tracking task shown in Figure 3.1, the human operator tracks the target signal f_t to minimize the error signal e. The target signal is also typically referred to as the forcing function, which here is chosen to be the sums of 10 sine waves with independent frequencies, as given by:

$$f_t(t) = \sum_{k=1}^{10} A_t[k] \sin(\omega_t[k]\, t + \phi_t[k]), \tag{3.1}$$

where $A_t[k]$, $\omega_t[k]$ and $\phi_t[k]$ are the amplitude, frequency and phase of the kth sine wave in f_t, respectively. The amplitude, frequency and phase components of the target forcing function are listed in Table 3.1:

Table 3.1: Multi-sine forcing function properties

		f_t		
k	n_t	ω_t,rad/s	A_t,deg	ϕ_t,rad
1	6	0.460	1.397	1.288
2	13	0.997	0.977	6.089
3	27	2.071	0.441	5.507
4	41	3.145	0.237	1.734
5	53	4.065	0.159	2.019
6	73	5.599	0.099	0.441
7	103	7.900	0.063	5.175
8	139	10.661	0.046	3.415
9	194	14.880	0.036	1.066
10	229	17.564	0.033	3.479

The experimental measurement time of a tracking run was 81.92 s, thus the measurement base frequency is $\omega_m = 2\pi/81.92$ s = 0.077 rad/s. To allow for the use of spectral analysis, the frequency of each sine wave component was defined as an integer multiple of the base frequency, $\omega_t = n_t\omega_m$. The integer factors n_t are listed in Table 3.1.

The amplitudes of the sine components are defined by a second-order low-pass filter:

$$H_A(j\omega) = \frac{(1 + T_{A_1} j\omega)^2}{(1 + T_{A_2} j\omega)^2}, \tag{3.2}$$

where $T_{A_1} = 0.1$ s and $T_{A_2} = 0.8$ s [20]. This filter ensures that the tracking task is realistic and not too difficult for the subjects. Performing such a control task would correspond to a high-gain flying task, therefore making this a situation under which changes in controlled system dynamics that affect handling qualities would be noticeable. The phases ϕ_t were selected to yield signals with an approximately Gaussian distribution and without excessive peaks [21].

A fade-in function was applied to the target forcing function during the first 5 s of the experimental run. The total experiment time for one run is 90 s.

BASELINE DYNAMICS

The baseline dynamics $H_{baseline}$ are a simplified low-order equivalent system (LOES) of aircraft pitch dynamics, as for instance also considered in [9]:

$$H_{baseline}(s) = M_{\delta_e} \frac{M_q}{s(s + M_q)}, \tag{3.3}$$

where M_q and M_{δ_e} are the pitch damping and elevator control effectiveness coefficients, respectively. To study the effects of the bandwidth of baseline dynamics on human operator control behavior, two baseline dynamics were considered in the experiment (see Table 3.2). The dynamics are different in terms of M_q, for which values equivalent to those tested in [9] were chosen to achieve a low-bandwidth baseline (LBB, $M_q = 1.5$ rad/s) and high-bandwidth baseline (HBB, $M_q = 3$ rad/s). These dynamics are representative of sluggish (large) aircraft [22], and fast-responding (small) aircraft [19], respectively. The frequency responses of both tested baseline dynamics are shown in Figure 3.2. In Figure 3.2, it can be seen that both the magnitude and phase of the high-bandwidth baseline dynamics are

higher than those of the low-bandwidth baseline. The dashed vertical line indicates M_q of the low-bandwidth baseline, and the solid vertical line indicates M_q of the high-bandwidth baseline.

Table 3.2: Parameters of low and high-bandwidth baseline dynamics

Baseline dynamics	M_q, rad/s	M_{δ_e},-
Low-bandwidth baseline (LBB)	1.5	1.5
High-bandwidth baseline (HBB)	3	1.5

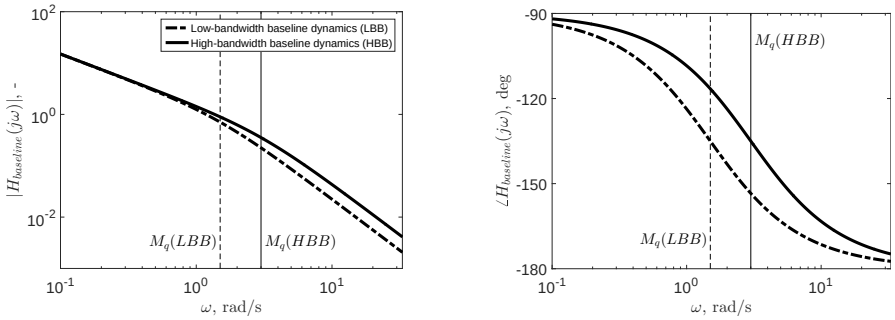

(a) Magnitude (b) Phase

Figure 3.2: Frequency responses of low and high-bandwidth baseline dynamics.

HUMAN OPERATOR MODEL

It is well-known that in manual control, human operators adapt and optimize their own control dynamics H_p to those of the controlled dynamics $H_{baseline} \cdot H_{added}$ to ensure adequate closed-loop stability and tracking performance [23]. For the baseline dynamics considered in this experiment (Eq. (3.3)), human operators are required to generate lead equalization to counter the controlled dynamics' lag due to M_q. Thus the frequency response of the model for H_p is:

$$H_p(j\omega) = K_v(T_{lead}\, j\omega + 1)e^{-j\omega\tau_v} H_{nm}(j\omega), \tag{3.4}$$

where K_v is the visual gain, T_{lead} is the lead time constant, τ_v is the inherent visual time delay, and $H_{nm}(j\omega)$ represents the dynamics of the neuromuscular system, which is modeled as a second-order spring-damper system [24]:

$$H_{nm}(j\omega) = \frac{\omega_{nm}^2}{(j\omega)^2 + 2\zeta_{nm}\omega_{nm} j\omega + \omega_{nm}^2}, \tag{3.5}$$

where ζ_{nm} is the damping ratio and ω_{nm} is the undamped natural frequency.

It is assumed that the lead equalization form (see Eq. (3.4)) also applies to the controlled dynamics with the added dipoles, and this assumption will be verified with the identified human frequency response functions in Section 3.3.

ADDED DYNAMICS AND INDEPENDENT VARIABLES

To be able to intuitively vary the magnitude of the perturbation of $H_{baseline}$, the added dynamics in the experiment were chosen as dipoles with magnitude $|H_{added}| > 1$, also previously used in [2], given by:

$$H_{added}(s) = \frac{(\frac{s}{\omega_{dp}})^2 + 2\frac{\zeta_1}{\omega_{dp}}s + 1}{(\frac{s}{\omega_{dp}})^2 + 2\frac{\zeta_2}{\omega_{dp}}s + 1}, \tag{3.6}$$

where ω_{dp} is the natural frequency of both the numerator and denominator second-order terms in Eq. (3.6), ζ_1 is the numerator damping ratio, and ζ_2 is the damping ratio of the second-order denominator term. Eq. (3.6) therefore represents dipole dynamics, which are characterized by a clear magnitude perturbation centered on the natural frequencies of the numerator and denominator terms.

The natural frequency of dipole dynamics ω_{dp} is set to 3 rad/s, which is in the range of predominant frequencies of manual control [23] and, consequently, in the region where the MUAD envelopes are the most narrow [2]. The denominator damping ratio ζ_2 is fixed at 0.2, where the numerator damping ratio ζ_1 is an independent variable varying from 0.2 to 0.7. The six added dipole dynamics and baseline dynamics are shown in Figure 3.3, with the MUAD envelopes [2] for reference. In Figure 3.3, it can be seen that for $\zeta_1 \geq 0.5$ the added dynamics H_{added} are outside of the MUAD envelopes in both magnitude and phase. Table 3.3 lists all conditions, where C1 represents the low-bandwidth baseline (LBB) condition, C8 represents the high-bandwidth baseline (HBB) condition, "LB" indicates the conditions with added dynamics with the low-bandwidth baseline, and "HB" represents the conditions with added dynamics with the high-bandwidth baseline.

Table 3.3: Experiment conditions

	Conditions	ω_{dp}, rad/s	ζ_1,-	ζ_2,-
Low-bandwidth baseline (LBB)	C1	-	-	-
Low-bandwidth (LB)	C2	3	0.22	0.2
	C3	3	0.24	0.2
	C4	3	0.28	0.2
	C5	3	0.35	0.2
	C6	3	0.5	0.2
	C7	3	0.7	0.2
High-bandwidth baseline (HBB)	C8	-	-	-
High-bandwidth (HB)	C9	3	0.22	0.2
	C10	3	0.24	0.2
	C11	3	0.28	0.2
	C12	3	0.35	0.2
	C13	3	0.5	0.2
	C14	3	0.7	0.2

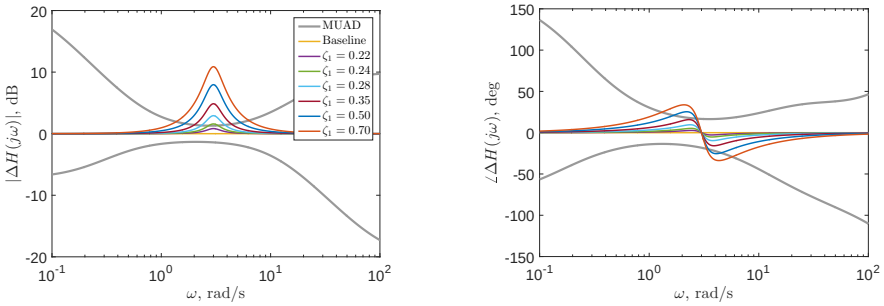

(a) Magnitude (b) Phase

Figure 3.3: MUAD and all added dynamics.

3.2.2. EXPERIMENT

DEPENDENT MEASURES AND DATA ANALYSIS

The measured variables in the experiment include the time histories of the tracking error e, the control signal u and the pitch angle θ during each run, see Figure 3.1. From these measurements the variance of e and the variance of u are calculated as the measures of tracking performance and control activity, respectively. Based on the measures of e and θ, the Fourier coefficient (FC) method [24, 25] is used to identify the nonparametric open-loop describing functions at the target signal frequencies ω_t:

$$\hat{H}_{ol,t}(j\omega_t) = \frac{\Theta(j\omega_t)}{E(j\omega_t)}, \tag{3.7}$$

where $\hat{H}_{ol,t}(j\omega)$ is the nonparametric target open-loop describing function, Θ is the Fourier transform of the pitch angle θ and E is the Fourier transform of the error signal e. Then the open-loop target crossover frequency $\omega_{c,t}$ and phase margin $\phi_{m,t}$ representing the manual control bandwidth and the stability are calculated from this nonparametric open-loop describing function.

Similarly, based on the measures of e and u, a nonparametric frequency response function (FRF) estimate of the human operator dynamics H_p at the frequencies of f_t is also obtained as:

$$\hat{H}_p(j\omega_t) = \frac{U(j\omega_t)}{E(j\omega_t)}, \tag{3.8}$$

where $\hat{H}_p(j\omega_t)$ represents the estimated FRF and U is the Fourier transform of the control signal u, see Figure 3.1. Finally, the human operator model parameters in Eqs. (3.4) and (3.5) are estimated using a time-domain parameter estimation method [25].

To verify the statistical significance of observed trends in all dependent measures, statistical analyses are performed. A two-way repeated-measures analysis of variance (ANOVA) is used to check for significant variations due to the baseline bandwidth (LBB and HBB) and different added dynamics (H_{added}) over all experimental conditions for all dependent measures. In addition, only for the dependent measures affected significantly by H_{added},

six paired t-tests (at a Bonferroni corrected significance level of $\alpha = 0.0083$) are used to compare conditions with the added dynamics and the baseline condition.

APPARATUS

The experiment was performed in the fixed-base simulator setup of the Human-Machine Interaction Laboratory (HMI Lab) at the Faculty of Aerospace Engineering of Delft University of Technology (see Figure 3.4). During the experiment, subjects were seated in the right cockpit seat and a right-handed sidestick was used for giving inputs to the controlled dynamics. Only the pitch axis of the sidestick was active during the experiment; the roll axis of the sidestick was fixed at the neutral position. The tracking error e in Figure 3.1 was presented to the subject through the primary flight display (PFD) directly in front of the right seat, as shown in Figure 3.4b. The display shows the pitch attitude tracking error e as the distance between the center fixed aircraft symbol and the moving target line. The aircraft symbol was static, and the target line moved to indicate the current tracking error e. Note that this display is an "inside-out" display: to compensate for the tracking error shown in Figure 3.4b, the subject needs to give a (positive) pitch input, i.e., pull the stick. No other visual cues were presented during the experiment, that is, the secondary flight displays and the outside visual system were switched off.

(a) The Human-Machine Interaction Laboratory (HMI Lab) Simulator.

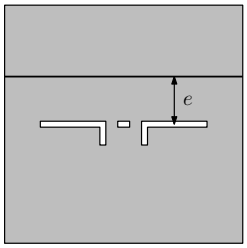

(b) Compensatory pitch tracking display.

Figure 3.4: The Human-Machine-Interaction Laboratory (HMI Lab) simulator and compensatory pitch tracking display.

SUBJECTS AND EXPERIMENTAL PROCEDURES

Seven male subjects were invited to perform the experiment, all students of the Aerospace Engineering Faculty of Delft University of Technology. All subjects had experience with similar manual control tasks from previous experiments. The subjects received an experimental briefing on the overview and objective of the experiment. Subjects were instructed to minimize the pitch attitude tracking error e presented on the PFD as best as possible, without providing the details of the characteristics of the controlled aircraft dynamics or added dynamics. Finally, all subjects gave written informed consent before the start of the experiment.

The experiment was performed in two sessions, one for each baseline dynamics setting. For each subject at the beginning of each session, the experiment started with an initial familiarization. During this phase, subjects were allowed to familiarize themselves with

the baseline aircraft dynamics for a total of 4 tracking runs. Following this initial familiarization, the testing runs for all experiment conditions were performed. The order of the testing was determined for each subject by a Latin square. The order testing for the LB and HB dynamics was balanced, for example, four subjects tested the HB conditions in the first session, while the other three controlled the LB conditions in the first session. For each condition, a total of 4 repeated runs were performed, followed by a single tracking run with the corresponding baseline dynamics only (no added dynamics). The root mean square (RMS) of the error signal e was recorded by the experimenter and reported to the subject after each run.

HYPOTHESES

In Figure 3.2, it can be seen that HBB has both higher gain and phase compared with those of LBB, indicating that HBB is more responsive than LBB. Moreover, according to [23], human operator would generate more lead to stabilize the controlled system with lower phase (LBB). Considering both the high gain of HBB and potentially less needed lead generated by the human operator, the control activity with HBB may be less than that with LBB. Based on these, the hypotheses for the baseline dynamics are:

- (H1) *For a certain added dynamics, the tracking performance with HBB is better than that with LBB, the control activity with HBB is lower than that with LBB, and the lead time constant with HBB is lower than that with LBB.*

In Figure 3.3, the added dynamics with $\zeta_1 = 0.22$ have the lowest perturbation and added dynamics with $\zeta_1 = 0.7$ have the highest perturbation on the baseline dynamics. According to [23], tracking performance and human operator control behavior are most sensitive near the crossover region. Thus with increasing perturbations by the added dynamics, the performance could become worse. Moreover, with increasing ζ_1, the gain of the controlled dynamics increases and human operator may lower his own visual gain and corresponding control activity. Based on these, the hypotheses for the added dynamics are:

- (H2) *For a certain baseline dynamics, the tracking performance worsens, control activity decreases and human operator visual gain decreases when ζ_1 increases.*

According to [9], the MUAD envelopes depend on the bandwidth of the baseline dynamics, for example, low-bandwidth baseline dynamics naturally filter more responses of the added dynamics than the high-bandwidth baseline dynamics do, thus the MUAD envelopes of low-bandwidth baseline are more "tolerable" (wider in frequency domain) than those of the high-bandwidth baseline. Thus it is possible that certain added dynamics could have obvious effects on tracking performance, control activity and/or human operator control behavior for the high-bandwidth baseline case but have no effect on those of the low-bandwidth baseline case. Thus the hypotheses for the interaction between the baseline and added dynamics are:

- (H3) *The interaction between the baseline dynamics and added dipole dynamics $H_{baseline} \times H_{added}$ has significant effects on tracking performance, control activity and human operator control behavior. For the high-bandwidth (HB) case, an added*

dipole can be found that has significant effects on tracking performance, control activity or human operator control behavior, but this same dipole has no effect on those measured in the LB conditions.

3.3. RESULTS

TRACKING PERFORMANCE AND CONTROL ACTIVITY

Figure 3.5 provides the variances of the error signal e and control signal u for each condition averaged over the seven subjects, respectively. In Figure 3.5a, for example, the error bars show the 95% confidence intervals of the means of σ_e^2. To facilitate comparison with the baseline condition, the shaded areas indicate the 95% confidence intervals for both baseline conditions where $H_{added} = 1$. The data have been corrected for between-subject variability.

In Figure 3.5a, it can be seen that the performance for the HB conditions is in general better than for the LB conditions. This is due to the fact that the HB dynamics are more responsive due to the lower phase lag. In Table 3.4, it can be seen that $H_{baseline}$ ($F(1,6) = 12.2, p < 0.05$) has a significant effect on σ_e^2. Meanwhile, in Figure 3.5a, it can be seen that for both LB and HB conditions the performance degrades when ζ_1 increases, for example, for more prominent dipoles. This confirms that the control task becomes more difficult when the perturbation of the added dynamics increases. Table 3.4 shows that H_{added} ($F(6,36) = 12, p < 0.05$) has significant effect on σ_e^2. However, Table 3.5 shows that for both LB and HB dynamics none of the performance with the added dynamics is significantly different from that with the baseline dynamics. In Table 3.4 it can be seen that the interaction between the baseline and added dynamics $H_{baseline} \times H_{added}$ has no significant effect on σ_e^2.

In Figure 3.5b, it can be seen that the control activity for the HB conditions is in general lower than for the LB conditions. This is due to the fact that the gain of the HB dynamics is higher than that of the LB dynamics. Table 3.4 shows that $H_{baseline}$ ($F(1,6) = 10.2, p < 0.05$) has significant effect on σ_u^2. Meanwhile, in Figure 3.5b, it can be seen that when ζ_1 increases the control activity decreases for both LB and HB cases. This may be also due to the fact that the gain of the controlled system increases when ζ_1 increases, thus the human operators may lower their own gain. Table 3.4 shows that H_{added} ($F(6,36) = 12.9, p < 0.05$) has significant effect on σ_u^2. However, Table 3.5 shows that for both LB and HB dynamics none of the σ_u^2 of the added dynamics is significantly different from that of the baseline dynamics, respectively. In Table 3.4 it can be seen that the interaction between the baseline and added dynamics $H_{baseline} \times H_{added}$ has no significant effect on σ_u^2.

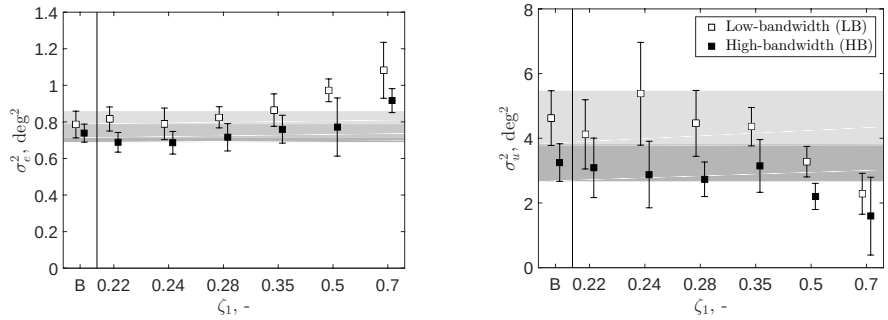

(a) Performance (b) Control activity

Figure 3.5: Variance of the error signal e and control signal u for each condition averaged over seven subjects.

Table 3.4: ANOVA results for σ_e^2 and σ_u^2, where * is significant ($p < 0.05$), and - is not significant ($p \geq 0.05$).

	σ_e^2			σ_u^2		
Factor	df	F	Sig.	df	F	Sig.
$H_{baseline}$	1, 6	12.2	*	1, 6	10.2	*
H_{added}	6, 36	12	*	6, 36	12.9	*
$H_{baseline} \times H_{added}$	6, 36	1.3	-	6, 36	1.7	-

Table 3.5: Paired t-test results for σ_e^2 and σ_u^2, where * is significant ($p < 0.0083$), and - is not significant ($p \geq 0.0083$).

		σ_e^2			σ_u^2		
	Factor	df	t	Sig.	df	t	Sig.
Low-bandwidth (LB)	C2-LBB	11.7	0.3	-	12	-0.4	-
	C3-LBB	12	0.1	-	11	0.5	-
	C4-LBB	11.4	0.4	-	12	-0.1	-
	C5-LBB	12	0.8	-	12	-0.2	-
	C6-LBB	11	0.6	-	11.6	-1.2	-
	C7-LBB	9	2	-	11.5	-2.1	-
High-bandwidth (HB)	C9-HBB	11.6	-0.5	-	12	-0.1	-
	C10-HBB	11.7	-0.5	-	11.8	-0.3	-
	C11-HBB	12	-0.2	-	10.6	-0.5	-
	C12-HBB	12	0.19	-	12	-0.1	-
	C13-HBB	11.5	0.3	-	10.7	-1	-
	C14-HBB	11.9	1.5	-	9.8	-1.6	-

CROSSOVER FREQUENCIES AND PHASE MARGINS

Figure 3.6 shows the means of the target crossover frequencies $\omega_{c,t}$ and phase margins $\phi_{m,t}$ over seven subjects for all conditions. In Figure 3.6a, for example, the error bars show the 95% confidence intervals of the means of $\omega_{c,t}$. To facilitate comparison with the baseline condition, the shaded areas indicate the 95% confidence intervals for both baseline conditions where $H_{added} = 1$. The data have been corrected for between-subject variability.

In Figure 3.6a it can be seen that the target crossover frequencies for the HB conditions are in general higher than for the LB conditions. This may be due to the fact that the gain of the HB dynamics is higher than that of the LB conditions, thus the HB dynamics are more responsive and easier to control than the LB dynamics. The higher target crossover frequencies of the HB dynamics correspond with better performance (see Figure 3.5a). Table 3.6 shows that $H_{baseline}$ ($F(1,6) = 14, p < 0.05$) has significant effect on $\omega_{c,t}$. Meanwhile, in Figure 3.6a, it can be seen that for both LB and HB conditions $\omega_{c,t}$ generally increases when ζ_1 increases (except for $\zeta_1 = 0.7$ for HB). This is in part due to the fact that the gain of the controlled system increases when ζ_1 increases. However, Table 3.6 shows that H_{added} ($F(1.5, 9.2) = 1.6, p \geq 0.05$) has no significant direct effect on $\omega_{c,t}$. Note that as the Mauchly's test indicated a violation of the sphericity assumption here, the Greenhouse-Geisser correction (indicated with a superscript "gg" in Table 3.6) was applied. Table 3.6 also shows that the interaction between the baseline and added dynamics $H_{baseline} \times H_{added}$ is not significant for $\omega_{c,t}$.

In Figure 3.6b it can be seen that there is no difference between the target phase margins between the LB and HB conditions. There is also no trend on the target phase margins when ζ_1 increases and the average phase margin over all conditions is around 55 deg. Table 3.6 shows that neither $H_{baseline}$ ($F(1,6) = 0.3, p \geq 0.05$), H_{added} ($F(1.5, 9.1) = 0.3, p \geq 0.05$), nor $H_{baseline} \times H_{added}$ ($F(6,36) = 1.4, p \geq 0.05$) has significant effect on $\phi_{m,t}$. Thus no t-test was conducted to compare the differences between conditions of added dynamics and baseline dynamics due to the insignificant effects of H_{added} for both $\omega_{c,t}$ and $\phi_{m,t}$.

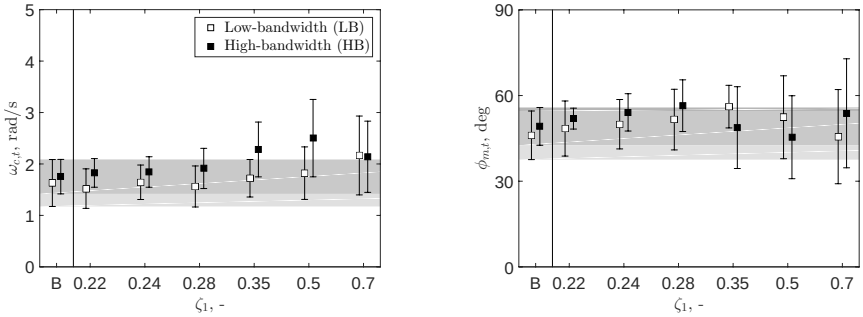

(a) Target crossover frequencies

(b) Target phase margins

Figure 3.6: Target crossover frequencies and phase margins for each condition averaged over seven subjects.

Table 3.6: ANOVA results of the target crossover frequencies and phase margins, where * is significant ($p < 0.05$), and - is not significant ($p \geq 0.05$).

	$\omega_{c,t}$			$\phi_{m,t}$		
Factor	df	F	Sig.	df	F	Sig.
$H_{baseline}$	1, 6	14	*	1, 6	0.3	-
H_{added}	1.5, 9.2^{gg}	1.6	-	1.5, 9.1^{gg}	0.3	-
$H_{baseline} \times H_{added}$	6, 36	1	-	6, 36	1.4	-

HUMAN OPERATOR MODEL VALIDATION

As an example of the results of the human operator modeling and identification, Figure 3.7 shows the human operator modeling results for Subject 7 for C7 (see Table 3.3). The frequency response functions at target forcing function frequencies are shown with circular markers. The error bars show the sample standard deviations of the FRF estimates over three measurement runs. Finally, the frequency response of the total controlled dynamics is also shown, for reference.

As can be verified from Figure 3.7, the fitted human operator models in general show very good agreement with (independently estimated) FRFs. Also, the attained VAF values are high (>80%), which means that the human operator model output accurately describes the measured output u. The results in Figure 3.7 are representative for all collected data, i.e., for all other subjects and conditions, the avearge VAF value is around 70%.

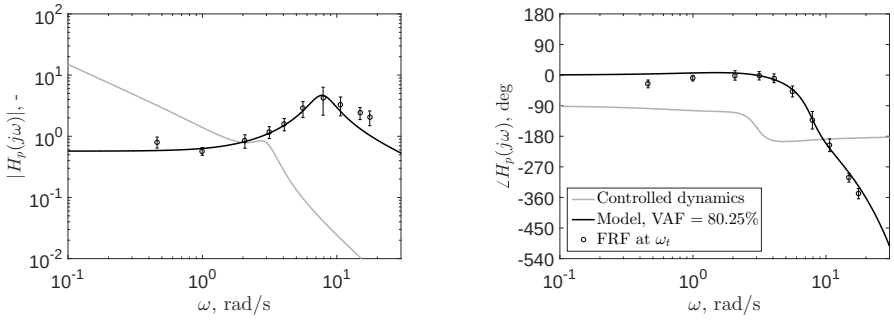

(a) Magnitude, C7 (b) Phase, C7

Figure 3.7: Example of human operator model fitting results for C7 (Subject 7).

HUMAN OPERATOR MODEL PARAMETERS

Figure 3.8 provides the means of the human operator model parameters for each condition averaged over the seven subjects. In Figure 3.8a, for example, the error bars show the 95% confidence intervals of the means of K_v. To facilitate comparison with the baseline condition, the shaded areas indicate the 95% confidence intervals for both baseline conditions where $H_{added} = 1$. The data have been corrected for between-subject variability.

In Figure 3.8a, it can be seen that there is no obvious difference in the visual gain between LB and HB conditions, and Table 3.7 indeed shows that $H_{baseline}$ ($F(1,6) = 0.1, p \geq 0.05$) has no significant effect on K_v. Meanwhile, in Figure 3.8a, it can be seen that K_v decreases when ζ_1 increases, which was expected based on the fact that the gain of the controlled system increases with increasing ζ_1. Table 3.7 confirms that H_{added} ($F(6,36) = 35.3, p < 0.05$) has a significant effect on K_v. Table 3.9 shows that for the LB conditions, K_v for both C6 ($\zeta_1 = 0.5$) and C7 ($\zeta_1 = 0.7$) is significantly different from the low-bandwidth baseline data; for HB conditions, only K_v of C14 ($\zeta_1 = 0.7$) is significantly different from that of the high-bandwidth baseline (HBB).

Figure 3.8c shows that the lead time constant of HB is lower than that of LB conditions. This is due to the fact that the phase of the LB controlled system is in general lower than that of the HB controlled system, which makes the LB dynamics less stable than the HB

dynamics, thus the human operators need to generate more lead to stabilize the system. Table 3.7 shows that $H_{baseline}$ ($F(1,6) = 30, p < 0.05$) has a significant effect on T_{lead}. Figure 3.8c shows no trend in T_{lead} with increasing ζ_1 and Table 3.7 indeed confirms that H_{added} ($F(6,36) = 0.9, p \geq 0.05$) has no significant effect on T_{lead}.

In Figure 3.8d, it can be seen that the neuromuscular damping ratio does not differ between LB and HB conditions, and Table 3.8 indeed shows that $H_{baseline}$ ($F(1,6) = 0.01, p \geq 0.05$) has no significant effect on ζ_{nm}. Figure 3.8d does show that ζ_{nm} decreases as ζ_1 increases, and Table 3.8 confirms a significant effect of H_{added} ($F(6,36) = 3.5, p < 0.05$). Table 3.9 shows that for both LB and HB conditions, ζ_{nm} for any of the added dynamics conditions is not significantly different from that of the baseline.

As is clear from Figures 3.8b and 3.8e, the visual time delay τ_v and the neuromuscular frequency ω_{nm} are seen to remain approximately constant, at around 0.25 s and 9 rad/s on average respectively, for all experiment conditions. Table 3.7 and Table 3.8 also confirm that neither $H_{baseline}$ nor H_{added} has significant effect on τ_v and ω_{nm}.

Finally, Table 3.7 and Table 3.8 show that the interaction between $H_{baseline} \times H_{added}$ has no significant effect on any of the human operator model parameters.This implies that all variations due to the added dynamics are equivalent for both the LB and HB conditions in this experiment. The human operator data thus show no evidence for a combination effect of the baseline dynamics and the added dynamics. Table 3.9 shows the t-test results for the visual gain and neuromuscular damping ratio, which are the only human operator model parameters significantly affected by the added dynamics, as can be seen in Table 3.7 and Table 3.8.

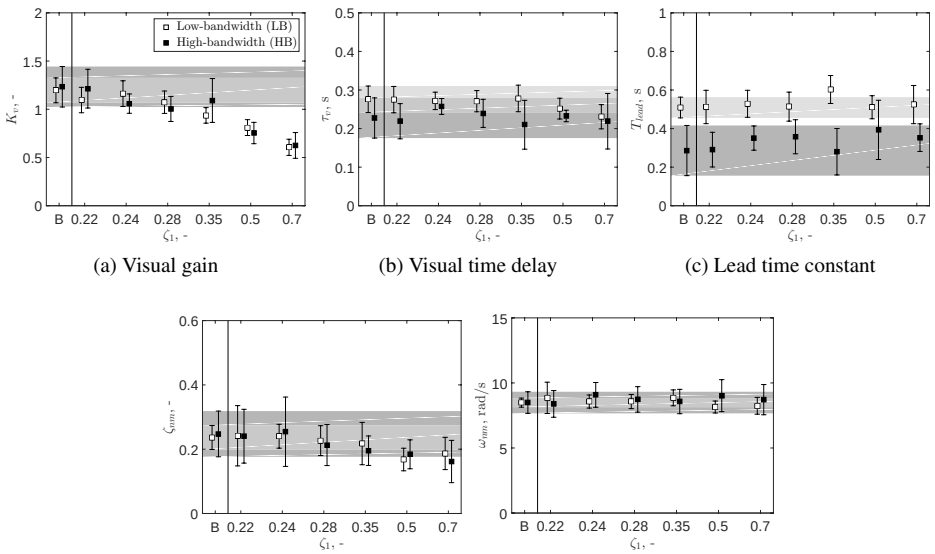

(a) Visual gain (b) Visual time delay (c) Lead time constant

(d) Neuromuscular damping ratio (e) Neuromuscular frequency

Figure 3.8: Estimated human operator model parameters.

Table 3.7: ANOVA results of the human operator model visual parameters, where * is significant ($p < 0.05$), and - is not significant ($p \geq 0.05$).

	K_v			t_v			T_{lead}		
Factor	df	F	Sig.	df	F	Sig.	df	F	Sig.
$H_{baseline}$	1, 6	0.1	-	1,6	3.5	-	1, 6	30	*
H_{added}	6, 36	35.3	*	1.6,9.7[gg]	2.8	-	6, 36	0.9	-
$H_{baseline} \times H_{added}$	6, 36	1.4	-	2.3,14.1[gg]	0.8	-	6, 36	1.4	-

Table 3.8: ANOVA results of the human operator model neuromuscular parameters, where * is significant ($p < 0.05$), and - is not significant ($p \geq 0.05$).

	ζ_{nm}			ω_{nm}		
Factor	df	F	Sig.	df	F	Sig.
$H_{baseline}$	1, 6	0.01	-	1, 6	0.2	-
H_{added}	6, 36	3.5	*	6, 36	0.3	-
$H_{baseline} \times H_{added}$	6, 36	0.3	-	6, 36	1	-

Table 3.9: Paired t-test results for visual gain K_v and neuromuscular damping ratio ζ_{nm}, where * is significant ($p < 0.0083$), and - is not significant ($p \geq 0.0083$).

		K_v			ζ_{nm}		
	Factor	df	t	Sig.	df	t	Sig.
Low-bandwidth (LB)	C2-LBB	11.4	-0.9	-	10.9	0.1	-
	C3-LBB	11.1	-0.3	-	11.8	0.1	-
	C4-LBB	11.9	-1.3	-	11.8	-0.2	-
	C5-LBB	12	-2.7	-	12	-0.3	-
	C6-LBB	11.4	-4.4	*	9.6	-1.4	-
	C7-LBB	11.9	-6.3	*	11.9	-0.9	-
High-bandwidth (HB)	C9-HBB	12	-0.1	-	11.6	-0.1	-
	C10-HBB	8.8	-1.1	-	11.8	0.1	-
	C11-HBB	8.9	-1.4	-	11.2	-0.5	-
	C12-HBB	12	-0.7	-	8.6	-0.9	-
	C13-HBB	7.9	-3.1	-	8.1	-1.1	-
	C14-HBB	7.8	-3.9	*	8	-1.5	-

3.4. DISCUSSION

This chapter investigated whether the MUAD envelopes [1] correspond with measured changes in tracking performance, control activity and human operator control behavior when extra dynamics are added to the system and whether these changes depend on the bandwidth of the baseline dynamics. For this purpose, a dedicated aircraft-representative pitch attitude tracking experiment with two different baseline dynamics (low and high bandwidth) cascaded with six different added dipole dynamics with increasing dipole damping ratio was performed. Adaptations in manual control dynamics, as determined from a human operator model fitted to collected measurement data, was used to verify human operator's sensitivity to the changes of the controlled system.

For the considered variations in baseline and added dynamics, three hypotheses were formulated. For *Hypothesis 1*, it was expected that the tracking performance for conditions

with high-bandwidth baseline (HBB) is better than that for conditions with low-bandwidth baseline (LBB), the control activity for conditions with HBB is lower than that for conditions with LBB, and the lead time constant with HBB is lower than that with LBB. Based on the experiment data, this hypothesis is confirmed. The better performance for high-bandwidth (HB) conditions is due to the fact that the HBB has both higher gain and phase compared with those of the LBB, thus the dynamics of HB conditions are more responsive than the low-bandwidth (LB) conditions. The higher lead for LB conditions is mainly due to the fact that the human operators need to generate more lead to stabilize the controlled system for LB conditions with lower phases, which further contributes to the higher control activity for the LB conditions than for the HB conditions.

For *Hypothesis 2*, it was expected that the tracking performance worsens, control activity decreases and human operator visual gain decreases when the perturbation of the added dynamics on the baseline increases (ζ_1 increases). Based on the experiment data, this hypothesis is confirmed. Experiment results indeed show that in general the control activity decreases when ζ_1 increases, which corresponds to the decrease of human operator visual gain. The tracking performance becomes worse with increasing ζ_1. This is due to the fact that when ζ_1 increases, the added dynamics not only increase the gain but also decrease the stability of the controlled system, and the human operator could not be able to further increase his own visual gain and lead time constant to improve the performance.

Hypothesis 3 stated that the interaction between the baseline and added dynamics has significant effects on tracking performance, control activity and human operator control behavior in a way that an added dipole can be found which has significant effects on the tracking performance, control activity or human operator control behavior for the HB conditions but has no effect on the LB conditions. Based on the experiment data, this hypothesis has to be rejected. For all the dependent measures, even though expected differences can be seen between the LB and HB conditions, for example, performance, control activity and lead time constant, the trends due to the added dynamics are very similar between the LB and HB cases. This leads to the conclusion that, based on the current experiment and range of tested conditions, the interaction between the baseline and added dynamics in fact does not influence the tracking performance, control activity and human operator control behavior. ANOVA results show that for performance, control activity, visual gain and neuromuscular damping ratio the added dynamics H_{added} has significant effects. However, t-test results show that for performance, control activity and neuromuscular damping ratio no significant differences were observed between the added dynamics conditions and the baseline (for both LB and HB cases). The visual gain of LB cases becomes significantly different at C6 ($\zeta_1 = 0.5$), however, the visual gain of HB cases becomes significantly different only at C7 ($\zeta_1 = 0.7$), which means that the HB case is more "tolerable" than LB (different from [9]).

However, for both of the tracking performance and control activity (Figure 3.5), the changing trends can be seen when damping ratio ζ_1 increases (compared with the baseline dynamics). The lack of significant results by t-test may be due to the limited number of subjects. If the average objective measurements that fall near and outside of the 95% confidence interval of the corresponding baseline condition measurement are taken to imply a noticeable change in controlled dynamics, the limit of both tracking performance and control activity would be around between $\zeta_1 = 0.35$ and $\zeta_1 = 0.5$. Similarly for the visual gain (Figure 3.8a), the limit would be around between $\zeta_1 = 0.28$ and $\zeta_1 = 0.5$. Since the added

dipole dynamics of $\zeta_1 = 0.5$ and $\zeta_1 = 0.7$ are outside both the magnitude and phase MUAD envelopes [1], and if $\zeta_1 = 0.35$ is chosen to indicate the boundary of MUAD, the objectively noticeable limits of the tracking performance, control activity and human operator visual gain would be very close with the MUAD envelopes [1].

The experiment of this chapter studied the effects of the added dipole dynamics on the human operator control behavior only for a representative aircraft dynamics at the frequency of 3 rad/s. The independence of performance, control activity and human operator control behavior on the interaction between the baseline dynamics and added dynamics indicates that the Manual Control Adaptation Boundaries may not be affected by the bandwidth of the baseline, which allows to choose a more accurate baseline aircraft dynamics for the research in the following chapters of this thesis. Moreover, the following chapters will also focus on investigating the effects of added dynamics on human operator control behavior at various frequencies.

3.5. CONCLUSIONS

An aircraft-representative pitch attitude compensatory tracking experiment with dipole dynamics added to both low and high-bandwidth baseline dynamics was performed by seven subjects in order to study whether the measured changes of tracking performance, control activity and objective human operator control behavior correspond with the MUAD envelopes and whether these changes depend on the bandwidth of the baseline dynamics. For the considered variations in the baseline and added dynamics, experiment results show that performance is better, control activity is lower and human operator lead time constant is lower for the conditions with high-bandwidth baseline; performance worsens, control activity decreases and human operator visual gain decreases with increasing perturbations from the added dipole dynamics. The interaction between the baseline and added dynamics has no significant effect on tracking performance, control activity or human operator control behavior. Furthermore, the objective limits on the changes of tracking performance, control activity and human operator visual gain correspond well with the MUAD envelopes from literature. All these findings indicate that the Manual Control Adaptation Boundaries may not be affected by the bandwidth of the baseline dynamics.

REFERENCES

[1] J. R. Wood and J. Hodgkinson, *Definition of Acceptable Levels of Mismatch for Equivalent Systems of Augmented CTOL Aircraft*, Tech. Rep. MDC A6792 (McDonnell Aircraft Company, St. Louis (MO), 1980).

[2] C. G. Carpenter and J. Hodgkinson, *V/STOL Equivalent Systems Analysis*, Tech. Rep. NADC-79141-60 (McDonnell Aircraft Company, St. Louis (MO), 1980).

[3] J. T. Bosworth and P. S. Williams-Hayes, *Flight Test Results from the NF-15B Intelligent Flight Control System (IFCS) Project with Adaptation to a Simulated Stabilator Failure,* in *Proceedings of the AIAA Infotech at Aerospace 2007 Conference and Exhibit, Rohnert Park (CA)*, AIAA-2007-2818 (2007).

[4] S. Geluardi, F. M. Nieuwenhuizen, L. Pollini, and H. H. Bülthoff, *Frequency Domain*

Identification of a Light Helicopter in Hover, in *Proceedings of the AHS 70th Annual Forum, Montreal, Canada* (2014).

[5] M. B. Tischler, *System Identification Methods for Aircraft Flight Control Development and Validation*, NASA Technical Memorandum 110369 (NASA Ames Research Center, Moffett Field (CA), 1995).

[6] P. G. Hamel and K. Jürgen, *Advances in Rotorcraft System Identification,* Progress in Aerospace Sciences **33**, 259 (1997).

[7] Cicolani and Luigi, *Flight Test Identification and Simulation of a UH-60A Helicopter and Slung Load*, Tech. Rep. NASA/TM-2001-209619 (NASA, Ames Research Center Moffett Field, California, 2001).

[8] C. J Miller, *Nonlinear Dynamic Inversion Baseline Control Law: Flight-Test Results for the Full-scale Advanced Systems Testbed F/A-18 Airplane,* (AIAA Guidance, Navigation, and Control Conference, 2011) pp. 1–25.

[9] D. G. Mitchell, R. H. Hoh, C. He, and K. Strope, *Determination of Maximum Unnoticeable Added Dynamics,* in *Proceedings of the AIAA Atmospheric Flight Mechanics Conference and Exhibit, Keystone (CO)*, AIAA-2006-6492 (2006).

[10] J. Hodgkinson, *History of Low-Order Equivalent Systems for Aircraft Flying Qualities,* Journal of Guidance, Control, and Dynamics **28**, 577 (2005).

[11] M. Mulder, P. M. T. Zaal, D. M. Pool, H. J. Damveld, and M. M. van Paassen, *A Cybernetic Approach to Assess Simulator Fidelity: Looking back and looking forward,* in *Proceedings of the AIAA Modeling and Simulation Technologies Conference, Boston (MA)*, AIAA-2013-5225 (2013).

[12] P. van den Berg, P. M. T. Zaal, M. Mulder, and M. M. van Paassen, *Conducting of Multi-modal Pilot Model Identification - Results of a Simulator Experiment,* in *AIAA Modelling and Simulation Technologies Conference, South Carolina*, AIAA-2007-6892 (2007).

[13] P. M. T. Zaal, D. M. Pool, M. Mulder, and M. M. van Paassen, *New Types of Target Inputs for Multi-Modal Pilot Model Identification,* in *Proceedings of the AIAA Modeling and Simulation Technologies Conference and Exhibit, Honolulu (HI)*, AIAA-2008-7106 (2008).

[14] P. M. T. Zaal, D. M. Pool, M. Mulder, M. M. van Paassen, and J. A. Mulder, *Identification of Multimodal Pilot Control Behavior in Real Flight,* Journal of Guidance, Control, and Dynamics **33**, 1527 (2010).

[15] D. M. Pool, M. M. van Paassen, and M. Mulder, *Modeling Human Dynamics in Combined Ramp-Following and Disturbance-Rejection Tasks,* in *Proceedings of the AIAA Guidance, Navigation, and Control Conference, Toronto, Canada, Aug. 2-5*, AIAA-2010-7914, edited by M. Silvestro (American Institute for Aeronautics and Astronautics, 2010).

[16] R. A. Hess and T. Malsbury, *Closed-loop Assessment of Flight Simulator Fidelity,* Journal of Guidance, Control, and Dynamics **14**, 191 (1991).

[17] M. Steurs, M. Mulder, and M. M. van Paassen, *A Cybernetic Approach to Assess Flight Simulator Fidelity,* in *Proceedings of the AIAA Modelling and Simulation Technologies Conference and Exhibit, Providence (RI)*, AIAA-2004-5442 (2004).

[18] A. T. Van Wieringen, *Effects of Aircraft Size on Motion Cues in Flight Simulation – A Cybernetic Analysis of Motion Cueing for a Boeing 747 in the Simona Research Simulator*, Master's thesis, Delft University of Technology (2011).

[19] D. M. Pool, *Objective Evaluation of Flight Simulator Motion Cueing Fidelity Through a Cybernetic Approach*, Ph.D. thesis, Delft University of Technology, Faculty of Aerospace Engineering (2012).

[20] P. M. T. Zaal, D. M. Pool, J. de Bruin, M. Mulder, and M. M. van Paassen, *Use of Pitch and Heave Motion Cues in a Pitch Control Task,* Journal of Guidance, Control, and Dynamics **32**, 366 (2009).

[21] T. Groot, H. J. Damveld, M. Mulder, and M. M. van Paassen, *Effects of Aeroelasticity on the Pilot's Psychomotor Behavior,* in *Proceedings of the AIAA Atmospheric Flight Mechanics Conference and Exhibit, Keystone, Colorado, Aug. 21-24, 2006*, AIAA-2006-6494 (American Institute of Aeronautics and Astronautics, 2006).

[22] H. J. Damveld, *A Cybernetic Approach to Assess the Longitudinal Handling Qualities of Aeroelastic Aircraft*, Ph.D. thesis, Delft University of Technology, Faculty of Aerospace Engineering (2009).

[23] D. T. McRuer and H. R. Jex, *A Review of Quasi-Linear Pilot Models,* IEEE Transactions on Human Factors in Electronics **HFE-8**, 231 (1967).

[24] M. M. van Paassen, *Biophysics in Aircraft Control, A Model of the Neuromuscular System of the Pilot's Arm*, Ph.D. thesis, Delft University of Technology, Faculty of Aerospace Engineering (1994).

[25] P. M. T. Zaal, D. M. Pool, Q. P. Chu, M. M. van Paassen, M. Mulder, and J. A. Mulder, *Modeling Human Multimodal Perception and Control Using Genetic Maximum Likelihood Estimation,* Journal of Guidance, Control, and Dynamics **32**, 1089 (2009).

4

Quantifying Human Operator Control Behavior with Simulations

The original Maximum Unnoticeable Added Dynamics (MUAD) envelopes [1, 2] are based on subjective ratings, and only provide qualitative noticeability to the change of controlled dynamics. This chapter aims to develop an offline computer simulation tool to objectively predict the performance, control activity and human operator control behavior in compensatory tracking tasks. The simulation is a basis to form the Manual Control Adaptation Boundaries (the main goal of this thesis). For this chapter, an aircraft pitch attitude tracking task with added dipole dynamics perturbing the baseline aircraft dynamics was performed. The results of the simulation performing the same tracking task were compared with the experiment results. By tuning the remnant-to-control activity ratio, high correlations between simulation and experiment for tracking performance, control activity and human operator control behavior could be obtained. The validated simulation will be used in Chapter 5 to further develop the Manual Control Adaptation Boundaries.

This chapter has been published as the following conference paper:
T. Lu, D. M. Pool, M. M. van Paassen, and M. Mulder, Quantifying the Effects of Added Dynamics with Human Operator Control Behavior Measurements and Simulations, in Proceedings of the AIAA Modeling and Simulation Technologies Conference, Denver (CO), AIAA-2017-3667 (2017).

4.1. INTRODUCTION

Maximum Unnoticeable Added Dynamics (MUAD) envelopes [1, 2] are boundaries, defined in the frequency domain, within which the handing qualities of modified aircraft dynamics have no degradation compared with the baseline aircraft dynamics. By keeping the discrepancy between the modified aircraft dynamics and the baseline aircraft dynamics within the MUAD envelope, existing handling quality criteria can be applied to the augmented aircraft. MUAD envelopes are also applied in the assessment of aircraft model fidelity [3–7]. Recent research on MUADs has shown that the sensitivity to added dynamics strongly depends on the baseline [8] aircraft dynamics, leading to the definition of proposed normalized MUAD, referred to as the "*allowable error envelope*"[8].

Still, some concerns exist about the validity and applicability of previously developed MUAD envelopes. For example, the original MUAD envelopes that were derived in the 1980s [1, 2] have seen little further (experimental) validation. Furthermore, these envelopes were derived from experiments with baseline aircraft dynamics that, in terms of their handling qualities, are likely very different from the dynamics of current modern aircraft [8]. Finally, the original MUAD envelopes were defined based on subjective ratings regarding the noticeability of added dynamics [1, 2], and no objective metrics were used to quantify task performance or the required human pilot compensation. As subjective ratings may vary strongly among different human operators, subjective and objective metrics are often not very consistent [9–11]. This opens the possibility that the objective human operator control behavior shows clear variations between the baseline and the modified aircraft dynamics, however, the handling qualities of these two dynamics could be the same, and the human operator would not be able to subjectively distinguish any differences between these two dynamics.

In recent years, the "*cybernetic approach*" has been successfully applied for objective analysis of human-machine issues involving human manual control [12–16]. Instead of relying on human operators' subjective feedback, the cybernetic approach focuses on objective measurements of task performance, control activity and especially identified human operator control behavior. For example, such methods have been applied to obtain objective measures for the fidelity of the flight simulators [17–20]. This approach can thus objectively quantify changes in the control behavior of human operators due to changes in the controlled dynamics, and avoids the possible ambiguity of the subjective methods. This chapter aims to develop a new methodology for defining Manual Control Adaptation Boundaries (MCAB), using the objective approach enabled by cybernetics. These new *Manual Control Adaptation Boundaries* (MCAB) will reflect the differences in human operator control behavior between the manipulated aircraft dynamics and the considered baseline dynamics. Moreover, it is expected to help engineers to better judge the fidelity of their aircraft dynamics model in their flight simulators, without the need to perform a human-in-the-loop experiment.

To develop this Manual Control Adaptation Boundary, this chapter tests a combined experimental and analytical (computer simulation based) methodology. An aircraft pitch attitude tracking experiment was performed, to study human operator control adaptations for different added (dipole) dynamics. In addition, an offline computer simulation was set up to predict the human control behavior adaptations and perform validation with the experiment data. The presented experiment and simulation predictions are used as a preliminary

study for the development of the Manual Control Adaptation Boundary.

This chapter starts by introducing the aircraft pitch tracking task and the cybernetic method on which the experiment and simulation are based, in Section 4.2. The simulation routine and the experiment design will also be introduced in detail. Experiment results are discussed in Section 4.3, and compared with the computer offline simulation predictions. The chapter ends with a discussion and conclusions.

4.2. METHODS

4.2.1. CONTROL TASK

AIRCRAFT PITCH ATTITUDE TRACKING TASK

An aircraft pitch attitude tracking task is used to study human operator control behavior with different added dynamics. A schematic representation of this tracking task is shown in Figure 4.1. The total controlled aircraft dynamics consist of the baseline dynamics $H_{baseline}$, cascaded with the added dynamics H_{added}. The human operator (represented by a linear transfer function H_p and the remnant n) controls the pitch angle θ of these total aircraft dynamics ($H_{baseline}H_{added}$) by tracking the target signal f_t to minimize the error signal e, which is the difference between the target signal f_t and the aircraft pitch angle θ. In Figure 4.1, u is the human operator control signal, K_s is the stick gain, u_s is the control signal from the stick, u_a is the signal out from the added dynamics, and δ_e is the signal directly feeding into the baseline aircraft dynamics. Besides the target forcing function f_t, a disturbance signal f_d is also added into the loop.

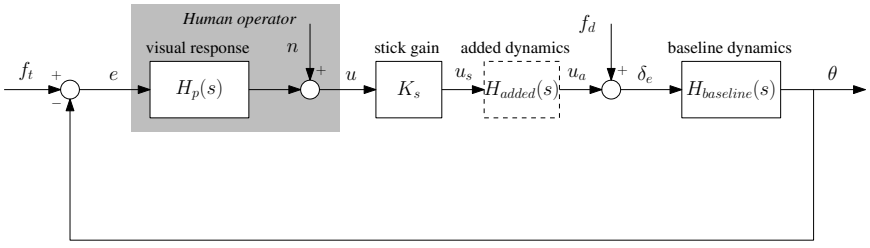

Figure 4.1: A schematic representation of the aircraft pitch attitude tracking task.

FORCING FUNCTIONS

For the pitch attitude tracking task shown in Figure 4.1, the human operator tracks the target signal f_t to minimize the error signal e as well as to reject the disturbance f_d. These two signals (typically referred to as forcing functions) are also necessary to be able to apply multimodal human operator model identification techniques [21–23], even though the motion feedback is not used in the current experiment. However, for compatibility of the method and data with future experiments, which are planned to be performed with physical motion feedback, the disturbance forcing function f_d is still added in the current experiment. In order to obtain the same effective disturbance on the aircraft pitch attitude, considering different added dynamics that will be tested in the experiment, the disturbance forcing function is added between the added dynamics and the baseline aircraft dynamics, see Fig. 4.1. Both of these forcing functions are chosen to be the sums of 10 sine waves

with independent frequencies, as given by:

$$f_{t,d}(t) = \sum_{k=1}^{10} A_{t,d}[k] \sin(\omega_{t,d}[k]\, t + \phi_{t,d}[k]), \tag{4.1}$$

where $A_{t,d}[k]$, $\omega_{t,d}[k]$ and $\phi_{t,d}[k]$ are the amplitude, frequency and phase of the kth sine wave in the target forcing function f_t and the disturbance forcing function f_d, respectively. The amplitude, frequency and phase components of the target and disturbance forcing functions are listed in Table 4.1:

Table 4.1: Multi-sine forcing function properties

	f_t				f_d			
k	n_t	ω_t,rad/s	A_t,deg	ϕ_t,rad	n_d	ω_d,rad/s	A_d,deg	ϕ_d,rad
1	6	0.460	1.397	1.288	5	0.383	0.601	-2.069
2	13	0.997	0.977	6.089	11	0.844	0.788	2.065
3	27	2.071	0.441	5.507	23	1.764	0.48	-2.612
4	41	3.145	0.237	1.734	37	2.838	0.313	3.759
5	53	4.065	0.159	2.019	51	3.912	0.331	4.739
6	73	5.599	0.099	0.441	71	5.446	0.411	1.856
7	103	7.900	0.063	5.175	101	7.747	0.55	1.376
8	139	10.661	0.046	3.415	137	10.508	0.753	2.792
9	194	14.880	0.036	1.066	171	13.116	0.992	3.288
10	229	17.564	0.033	3.479	226	17.334	1.481	3.381

The experimental measurement time of a tracking run was 81.92 s, thus the measurement base frequency is $\omega_m = 2\pi/81.92$ s = 0.077 rad/s. To allow for the use of spectral analysis, the frequency of each sine wave component of both forcing functions was defined as an integer multiple of the base frequency, $\omega_{t,d} = n_{t,d}\omega_m$. The integer factors n_t and n_d are shown in Table 4.1.

For both forcing functions, the amplitudes of the sine components were defined by a second order low-pass filter:

$$H_A(j\omega) = \frac{(1 + T_{A_1} j\omega)^2}{(1 + T_{A_2} j\omega)^2}, \tag{4.2}$$

where $T_{A_1} = 0.1$ s and $T_{A_2} = 0.8$ s [22]. This filter ensures that the tracking task is realistic and not too difficult for the subjects. Then the amplitudes were scaled to make the variance of f_t 1.6 deg^2 and the variance of f_d a quarter of that, i.e., 0.4 deg^2. The scaling ensures that the control task in the experiment was mainly a target tracking task. Performing such a control task, with two forcing functions present, would correspond to a high-gain flying task under turbulent conditions, therefore making this a situation under which changes in controlled system dynamics that affect handling qualities would be noticeable. The phases $\phi_{t,d}$ were selected to yield signals with an approximately Gaussian distribution and without excessive peaks [24].

A fade-in function and a fade-out function were applied to both the target and disturbance forcing functions during the first and last 5 s of the experimental run. The total experiment time for one run is 95 s.

BASELINE AIRCRAFT DYNAMICS AND ADDED DYNAMICS

In this chapter, the controlled baseline aircraft dynamics ($H_{baseline}$ in Fig. 4.1) are set to be a low-order linearization of a Cessna Citation I's aircraft pitch dynamics. The main reasons are that these dynamics have also been considered in many earlier investigations [20, 22]. The transfer function of the baseline aircraft pitch dynamics is:

$$H_{baseline}(s) = \frac{K_{\theta,\delta_e}(T_{\theta_2}s+1)}{s\left((\frac{s}{\omega_{sp}})^2 + \frac{2\zeta_{sp}}{\omega_{sp}}s+1\right)}, \tag{4.3}$$

where $K_{\theta,\delta_e} = 0.3959$, $T_{\theta_2} = 1.0095$ s, $\omega_{sp} = 2.759$ rad/s, $\zeta_{sp} = 0.4995$. The aircraft pitch dynamics represent the aircraft in a trimmed horizontal flight condition at 10,000 ft and 160 kt [20, 22]. The stick gain K_s in Figure 4.1 is set to 1.

In this study, the effects of the addition of different dipole added dynamics (H_{added} in Fig. 4.1) are analyzed. The transfer function of these added dynamics is given by:

$$H_{added}(s) = \frac{(\frac{s}{\omega_{dp}})^2 + 2\frac{\zeta_1}{\omega_{dp}}s+1}{(\frac{s}{\omega_{dp}})^2 + 2\frac{\zeta_2}{\omega_{dp}}s+1}, \tag{4.4}$$

where ω_{dp} is the natural frequency of both the numerator and denominator second-order terms in Eq. (4.4), ζ_1 is the numerator damping ratio, and ζ_2 is the damping ratio of the second-order denominator term. Eq. (4.4) represents dipole dynamics, which are characterized by a clear magnitude peak and dip centered on the natural frequencies of the numerator and denominator terms, respectively. In this chapter, dipole added dynamics are used to evaluate the frequency dependence of additions to controlled system dynamics. Therefore, the natural frequencies of the numerator and denominator are both set equal to ω_{dp}, to have added dynamics whose effects are focused on a specific frequency ω_{dp} and whose characteristics and strength are controlled with the chosen values of ζ_1 and ζ_2. If $0 < \zeta_1 < \zeta_2 < 1$, H_{added} is a "down dipole" with a dip in magnitude and induced phase lag and lead at frequencies below and above ω_{dp}, respectively. When $0 < \zeta_2 < \zeta_1 < 1$, H_{added} is an "up dipole" with a peak in magnitude and induced phase lead and lag below and above ω_{dp}. Finally, if $\zeta_2 = \zeta_1$, the numerator and denominator are equal and hence $H_{added} = 1$. The frequency responses of the baseline aircraft dynamics $H_{baseline}$, an example dipole added dynamics H_{added} ($\omega_{dp} = 3$ rad/s, $\zeta_1 = 0.7$, $\zeta_2 = 0.2$) and the total resulting controlled dynamics are shown in Figure 4.2.

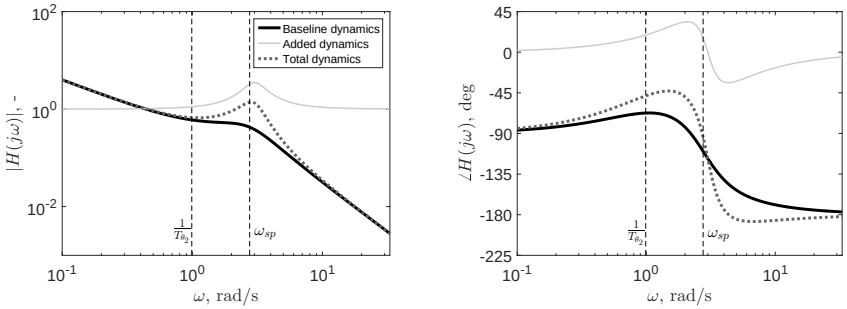

(a) Magnitude (b) Phase

Figure 4.2: Bode plot of the baseline aircraft dynamics, the added dynamics, and the total controlled dynamics.

4

HUMAN OPERATOR MODEL

A quasi-linear human operator model [20, 25] is used to both predict (offline simulations) and quantify (experiment data) human operator control behavior with different added dynamics. Here $H_p(j\omega)$ represents the frequency response of the human operator model:

$$H_p(j\omega) = K_v \frac{(T_{lead} j\omega + 1)^2}{T_{lag} j\omega + 1} e^{-j\omega\tau_v} H_{nm}(j\omega), \tag{4.5}$$

where K_v is the visual gain, T_{lead} is the lead time constant and T_{lag} is the lag time constant, τ_v is the inherent visual time delay, and $H_{nm}(j\omega)$ represents the dynamics of the neuromuscular system, which is modeled as a second order spring-damper system [23]:

$$H_{nm}(j\omega) = \frac{\omega_{nm}^2}{(j\omega)^2 + 2\zeta_{nm}\omega_{nm} j\omega + \omega_{nm}^2}, \tag{4.6}$$

where ζ_{nm} is the damping ratio and ω_{nm} is the undamped natural frequency.

It is known that the human operators can adapt and optimize their equalization term $K_v \frac{(T_{lead} j\omega+1)^2}{T_{lag} j\omega+1}$ in Eq. (4.5) to make the dynamics of the combined human operator-vehicle system approximate a single integrator in the crossover region [26]. To better describe the human operator control behavior with the aircraft pitch dynamics, the double lead and single lag equalization form in Eq. (4.5) is needed in modeling the adopted equalization dynamics [20, 25]. Moreover, it is assumed that this equalization form also applies to the controlled dynamics with the added dipoles, and this assumption will be verified with the identified human operator model.

SIMULATION AND EXPERIMENT CONDITIONS

The same conditions – that is, added dynamics settings – were considered in both of the human-in-the-loop experiment and the offline simulations. The baseline aircraft dynamics remain constant for all conditions, and the added dynamics are different for each condition. For the added dynamics H_{added}, in total there are three parameters that can be modified: the natural frequency ω_{dp}, the damping ratio ζ_1, and the damping ratio ζ_2. The natural frequency ω_{dp} determines the frequency on which the dipole, and hence the perturbation

of $H_{baseline}$, is centered. Since the crossover frequency of the manual control task is usually between 2 and 5 rad/s [26], in order to cover a relatively wide range of frequencies, the selected natural frequencies of ω_{dp} are 1,3, and 7 rad/s, respectively. Then at each frequency ω_{dp}, two combinations of the numerator and denominator damping ratios are tested: $\zeta_1 = 0.2$ and $\zeta_2 = 0.7$ for a "down" and $\zeta_1 = 0.7$ and $\zeta_2 = 0.2$ for an "up" dipole, respectively [2]. Moreover, to enable a direct comparison with human operator control behavior of the baseline aircraft dynamics, the baseline aircraft without any added dynamics are also tested. Table 4.2 lists all conditions, where "B" represents the baseline condition. The frequency responses of all added dynamics conditions are shown in Figure 4.3, plotted against the MUAD envelope [2] for reference.

Table 4.2: Simulation and experiment conditions

	Conditions	ω_{dp}, rad/s	ζ_1,-	ζ_2,-
Down	C1	1	0.2	0.7
Up	C2	1	0.7	0.2
Down	C3	3	0.2	0.7
Up	C4	3	0.7	0.2
Down	C5	7	0.2	0.7
Up	C6	7	0.7	0.2
Baseline	C7 (B)	-	-	-

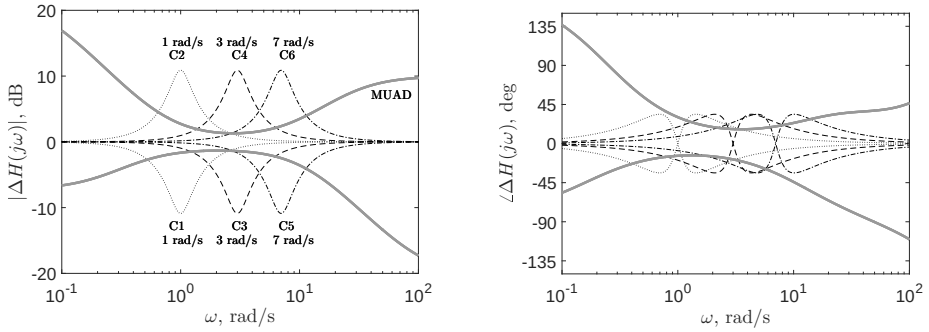

(a) Magnitude (b) Phase

Figure 4.3: MUAD and all added dynamics.

4.2.2. COMPUTER SIMULATION

FORCING FUNCTIONS

The forcing functions for computer offline simulation are the same as used in the experiment (see Eq. (4.1)), including both target and disturbance forcing functions. To allow for the use of spectral analysis, the time duration of both forcing functions used in the simulation is 81.92 s, which is the same as the experimental measurement time. The frequency range of the simulation is:

$$\omega_{sim} = \omega_m N_{sim}, \tag{4.7}$$

where $\omega_m = 2\pi/81.92$ s = 0.077 rad/s is the measurement base frequency, and N_{sim} is an equal spaced integer sequence: $N_{sim} = 1, 2, 3, ..., 4096$.

DECISION VARIABLES

According to Eqs. (4.5,4.6), the human operator control behavior is quantified by five parameters for the compensatory tracking task, which are K_v, T_{lead}, T_{lag}, τ_v, ζ_{nm} and ω_{nm}. However, it is known that human operators mainly adapt and optimize their equalization terms K_v, T_{lead} and T_{lag} to achieve optimal tracking performance. Parameters such as τ_v, ζ_{nm} and ω_{nm} represent the inherent physical visual and neuromuscular limit of human operators, and thus are treated as constants throughout the simulation: $\tau_v = 0.25$ s, $\zeta_{nm} = 0.2$ and $\omega_{nm} = 10$ rad/s. These parameters values were referred to [20] for the tracking task with the same aircraft dynamics. Since the visual gain K_v depends largely on the stick gain and the gain of the controlled dynamics, it is not selected as the decision variable for optimization. However, in a compensatory tracking task the ranges of the target crossover frequency $\omega_{c,t}$ and the target phase margin $\phi_{m,t}$ are better known [26]. Thus it is convenient to use both $\omega_{c,t}$ and $\phi_{m,t}$ as the decision variables for the optimization. However, by the definitions of target crossover frequency and target phase margin, only two constraint equations are not enough to derive the extra three parameters (K_v, T_{lead}, T_{lag}). Thus T_{lag} is chosen as an extra decision variable. Summarizing, there are three decision variables for the optimization:

$$P_{sim} = [\omega_{c,t}, \phi_{m,t}, T_{lag}], \tag{4.8}$$

where another two human operator model parameters K_v and T_{lead} will be derived using the variables in Eq. (4.8).

OBJECTIVE

As the goal of the compensatory tracking task is to minimize the error signal e in Figure 4.1, it is assumed that the objective of the simulation is to minimize the variance of the error signal while keeping the control activity at an acceptable level:

$$J_{sim} = \underset{P_{sim}}{\arg\min}\ [(\frac{\sigma_e^2}{\sigma_{f_t}^2}|P_{sim}) + C_W(\frac{\sigma_u^2}{\sigma_{f_t}^2}|P_{sim})], \tag{4.9}$$

where σ_e^2 is the variance of the error signal representing the performance of the tracking task: the lower the value, the better the performance, σ_u^2 is the variance of the control signal: the lower the value, the less the control activity, $\sigma_{f_t}^2$ is the variance of the target forcing function, and C_W is a weighing factor balancing the tracking performance and control activity. Both σ_e^2 and σ_u^2 are normalized by $\sigma_{f_t}^2$, which is used to cancel out the effects of the power of the target forcing function. Preliminary simulations with various C_W values have been done in order to study the effects of the weighing factor on simulated human operator control behavior. Compared with the experiment results, it was found that for all the tested conditions a common value of the weighing factor cannot be found. Moreover, for any added dynamics without experiment test, the trade-off between tracking performance and control activity cannot be known in advance. To keep things simple, it was decided to keep $C_W = 0$ throughout all simulations.

DERIVATION OF T_{lead}

Using the decision variables in Eq. (4.8), the lead time constant T_{lead} can be derived based on the definition of the target phase margin. The frequency responses of the baseline dynamics, added dynamics and human operator dynamics in Figure 4.1 are:

$$H_{baseline}(j\omega) = \frac{K_{\theta,\delta_e}(T_{\theta_2} j\omega + 1)}{j\omega[(\frac{j\omega}{\omega_{sp}})^2 + \frac{2\zeta_{sp}}{\omega_{sp}} j\omega + 1]}, \tag{4.10}$$

$$H_{added}(j\omega) = \frac{(\frac{j\omega}{\omega_{dp}})^2 + 2\frac{\zeta_1}{\omega_{dp}} j\omega + 1}{(\frac{j\omega}{\omega_{dp}})^2 + 2\frac{\zeta_2}{\omega_{dp}} j\omega + 1}, \tag{4.11}$$

$$H_p(j\omega) = K_v \frac{(T_{lead} j\omega + 1)^2}{T_{lag} j\omega + 1} e^{-j\omega\tau_v} \frac{\omega_{nm}^2}{(j\omega)^2 + 2\zeta_{nm}\omega_{nm} j\omega + \omega_{nm}^2}, \tag{4.12}$$

where $[K_v, T_{lead}]$ are the only unknown variables.

When $\omega = \omega_{c,t}$, the phases of Eqs. (4.10,4.11,4.12) are:

$$\angle H_{baseline}|_{\omega_{c,t}} = \arctan(T_{\theta_2}\omega_{c,t}) - \frac{\pi}{2} - \arctan(\frac{\frac{2\zeta_{sp}}{\omega_{sp}}\omega_{c,t}}{1 - (\frac{\omega_{c,t}}{\omega_{sp}})^2}), \tag{4.13}$$

$$\angle H_{added}|_{\omega_{c,t}} = \arctan(\frac{\frac{2\zeta_1}{\omega_{dp}}\omega_{c,t}}{1 - (\frac{\omega_{c,t}}{\omega_{dp}})^2}) - \arctan(\frac{\frac{2\zeta_2}{\omega_{dp}}\omega_{c,t}}{1 - (\frac{\omega_{c,t}}{\omega_{dp}})^2}), \tag{4.14}$$

$$\angle H_p|_{\omega_{c,t}} = -\omega_{c,t}\tau_v + 2\arctan(T_{lead}\omega_{c,t}) - \arctan(T_{lag}\omega_{c,t}) - \arctan(\frac{2\zeta_{nm}\omega_{nm}\omega_{c,t}}{\omega_{nm}^2 - \omega_{c,t}^2}). \tag{4.15}$$

According to the definition of the open loop target phase margin:

$$\phi_{m,t} = \angle H_{t,ol}|_{\omega_{c,t}} + \pi, \tag{4.16}$$

where $\phi_{m,t}$ is the target phase margin, and $\angle H_{t,ol}|_{\omega_{c,t}}$ is the phase of the open loop system at crossover frequency $\omega_{c,t}$:

$$\angle H_{t,ol}|_{\omega_{c,t}} = \angle H_p|_{\omega_{c,t}} + \angle H_{added}|_{\omega_{c,t}} + \angle H_{baseline}|_{\omega_{c,t}}. \tag{4.17}$$

In Eq. (4.17) T_{lead} is the only unknown variable and can be derived as:

$$T_{lead} = \frac{\tan\frac{\phi_{m,t} - \pi - \angle H_{added}|_{\omega_{c,t}} - \angle H_{baseline}|_{\omega_{c,t}} - \angle H_{p,part}|_{\omega_{c,t}}}{2}}{\omega_{c,t}}, \tag{4.18}$$

where $\angle H_{p,part}|_{\omega_{c,t}}$ is the phase of H_p at crossover frequency $\omega_{c,t}$ except the term of T_{lead}:

$$\angle H_{p,part}|_{\omega_{c,t}} = \angle H_p|_{\omega_{c,t}} - 2\arctan(T_{lead}\omega_{c,t}). \tag{4.19}$$

DERIVATION OF K_v

The visual gain K_v is derived using the definition of the target crossover frequency. When $\omega = \omega_{c,t}$, the gain of the baseline aircraft dynamics $H_{baseline}$, the added dynamics H_{added} and the human operator dynamics H_p are:

$$|H_{baseline}|_{\omega_{c,t}} = |\frac{K_{\theta,\delta_e}(T_{\theta_2} j\omega_{c,t} + 1)}{j\omega[(\frac{j\omega_{c,t}}{\omega_{sp}})^2 + \frac{2\zeta_{sp}}{\omega_{sp}} j\omega_{c,t} + 1]}|, \tag{4.20}$$

$$|H_{added}|_{\omega_{c,t}} = |\frac{(\frac{j\omega_{c,t}}{\omega_{dp}})^2 + 2\frac{\zeta_1}{\omega_{dp}} j\omega_{c,t} + 1}{(\frac{j\omega_{c,t}}{\omega_{dp}})^2 + 2\frac{\zeta_2}{\omega_{dp}} j\omega_{c,t} + 1}|, \tag{4.21}$$

$$|H_p|_{\omega_{c,t}} = |K_v \frac{(T_{lead} j\omega_{c,t} + 1)^2}{T_{lag} j\omega_{c,t} + 1} e^{-j\omega_{c,t}\tau_v} \frac{\omega_{nm}^2}{(j\omega_{c,t})^2 + 2\zeta_{nm}\omega_{nm} j\omega_{c,t} + \omega_{nm}^2}|, \tag{4.22}$$

where subscript $_{\omega_{c,t}}$ represents $\omega = \omega_{c,t}$.

According to the definition of the open loop target crossover frequency:

$$|H_p|_{\omega_{c,t}} \cdot |H_{added}|_{\omega_{c,t}} \cdot |H_{baseline}|_{\omega_{c,t}} = 1. \tag{4.23}$$

In Eq. (4.23) K_v is the only unknown variable and can be derived as:

$$K_v = \frac{1}{|H_{added}|_{\omega_{c,t}} \cdot |H_{baseline}|_{\omega_{c,t}} \cdot |H_{p,part}|_{\omega_{c,t}}}, \tag{4.24}$$

where $|H_{p,part}|_{\omega_{c,t}}$ is the gain of H_p at crossover frequency $\omega_{c,t}$ except K_v

$$|H_{p,part}|_{\omega_{c,t}} = |\frac{(T_{lead} j\omega_{c,t} + 1)^2}{T_{lag} j\omega_{c,t} + 1} e^{-j\omega_{c,t}\tau_v} \frac{\omega_{nm}^2}{(j\omega_{c,t})^2 + 2\zeta_{nm}\omega_{nm} j\omega_{c,t} + \omega_{nm}^2}|. \tag{4.25}$$

FREQUENCY RESPONSES OF RELATED TRANSFER FUNCTIONS

The frequency responses of the transfer functions related with the error signal e and the control signal u are needed for the derivation of $\sigma_e^2/\sigma_{f_t}^2$ and $\sigma_u^2/\sigma_{f_t}^2$:

$$H_{e,f_t}(j\omega) = \frac{1}{1 + K_s H_p(j\omega) H_{added}(j\omega) H_{baseline}(j\omega)}, \tag{4.26}$$

$$H_{e,f_d}(j\omega) = \frac{-H_{baseline}(j\omega)}{1 + K_s H_p(j\omega) H_{added}(j\omega) H_{baseline}(j\omega)}, \tag{4.27}$$

$$H_{e,n}(j\omega) = \frac{-K_s H_{added}(j\omega) H_{baseline}(j\omega)}{1 + K_s H_p(j\omega) H_{added}(j\omega) H_{baseline}(j\omega)}, \tag{4.28}$$

where $H_{e,f_t}(j\omega)$, $H_{e,f_d}(j\omega)$, $H_{e,n}(j\omega)$ are frequency responses of the transfer functions between the error signal e, target forcing function f_t, disturbance forcing function f_d and remnant n, respectively.

$$H_{u,f_t}(j\omega) = \frac{H_p(j\omega)}{1 + K_s H_p(j\omega) H_{added}(j\omega) H_{baseline}(j\omega)}, \tag{4.29}$$

$$H_{u,f_d}(j\omega) = \frac{-H_p(j\omega) H_{baseline}(j\omega)}{1 + K_s H_p(j\omega) H_{added}(j\omega) H_{baseline}(j\omega)}, \tag{4.30}$$

$$H_{u,n}(j\omega) = \frac{1}{1 + K_s H_p(j\omega) H_{added}(j\omega) H_{baseline}(j\omega)}, \tag{4.31}$$

where $H_{u,f_t}(j\omega)$, $H_{u,f_d}(j\omega)$, $H_{u,n}(j\omega)$ are frequency responses of the transfer functions between the control signal u, target forcing function f_t, disturbance forcing function f_d and remnant n, respectively.

DERIVATION OF K_n

The remnant n of the human operator in Figure 4.1 is modeled as filtered white noise, as can be seen in Figure 4.4:

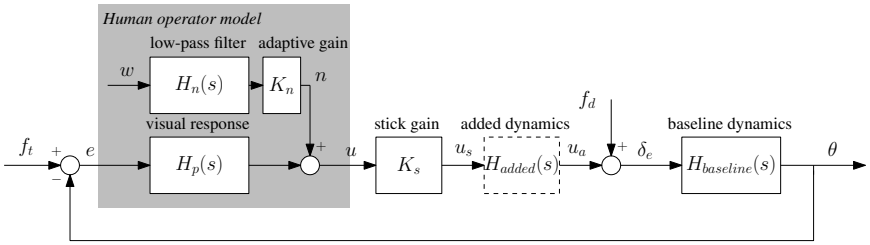

Figure 4.4: A schematic representation of the simulation remnant.

In Figure 4.4, w is Gaussian white noise, and H_n is a third order low pass filter [25]:

$$H_n(s) = \frac{\omega_n^3}{(s^2 + 2\zeta_n \omega_n s + \omega_n^2)(s + \omega_n)}, \tag{4.32}$$

where $\zeta_n = 0.26$ and $\omega_n = 12.7$ rad/s. In Figure 4.4, K_n is an adaptive gain in order to keep the ratio between the variance of the remnant n and the variance of the control signal u constant:

$$\frac{\sigma_n^2}{\sigma_u^2} = r, \tag{4.33}$$

where σ_n^2 is the variance of the remnant and σ_u^2 is the variance of the control signal. Multiple remnant ratios will be simulated and compared with the experiment results in order to select a most suitable remnant ratio for future experiment predictions. For the following derivation, $(j\omega)$ representing frequency responses is omitted for simplicity.

From Figure 4.4 it is known that:

$$N = K_n H_n W, \tag{4.34}$$

where N is the Fourier transform of the remnant n, and W is the Fourier transform of the white noise w. The square of the magnitude of the Fourier transform of remnant is:

$$N\overline{N} = |H_n W|^2 K_n^2, \tag{4.35}$$

where the over-line above N represents the complex conjugate of corresponding Fourier transforms.

The Fourier transform of the control signal u is:

$$U = F_t \cdot H_{u,f_t} + F_d \cdot H_{u,f_d} + N \cdot H_{u,n}, \tag{4.36}$$

where F_t is the Fourier transform of the target forcing function f_t, F_d is the Fourier transform of the disturbance forcing function f_d.

The square of the magnitude of the Fourier transform of control signal is:

$$U\overline{U} = A_{ww}K_n^2 + (A_{K_n f_t} + A_{K_n f_d})K_n + (A_{f_t f_t} + A_{f_d f_d} + A_{f_t f_d}), \tag{4.37}$$

where:

$$A_{ww} = |H_{u,n} H_n W|^2, \tag{4.38}$$

$$A_{K_n f_t} = F_t H_{u,f_t} \overline{H_{u,n} H_n W} + \overline{F_t H_{u,f_t}} H_{u,n} H_n W, \tag{4.39}$$

$$A_{K_n f_d} = F_d H_{u,f_d} \overline{H_{u,n} H_n W} + \overline{F_d H_{u,f_d}} H_{u,n} H_n W, \tag{4.40}$$

$$A_{f_t f_t} = |H_{u,f_t} F_t|^2, \tag{4.41}$$

$$A_{f_d f_d} = |H_{u,f_d} F_d|^2, \tag{4.42}$$

$$A_{f_t f_d} = F_t H_{u,f_t} \overline{F_d H_{u,f_d}} + \overline{F_t H_{u,f_t}} F_d H_{u,f_d}. \tag{4.43}$$

The ratio between the variance of the remnant n and the variance of the control signal u is:

$$\frac{\sigma_n^2}{\sigma_u^2} = \frac{\int S_{nn} d\omega}{\int S_{uu} d\omega} \approx \frac{\int N\overline{N} d\omega}{\int U\overline{U} d\omega} = r, \tag{4.44}$$

where S_{nn} is the power spectral density of the remnant, and S_{uu} is the power spectral density of the control signal.

Substituting Eq. (4.35) – Eq. (4.43) into Eq. (4.44) yields:

$$\frac{E_4 K_n^2}{E_1 K_n^2 + E_2 K_n + E_3} = r, \tag{4.45}$$

where:

$$E_1 = \int A_{ww} d\omega, \tag{4.46}$$

$$E_2 = \int (A_{K_n f_t} + A_{K_n f_d}) d\omega, \tag{4.47}$$

$$E_3 = \int (A_{f_t f_t} + A_{f_d f_d} + A_{f_t f_d}) d\omega, \tag{4.48}$$

$$E_4 = \int |H_n W|^2 d\omega. \tag{4.49}$$

The adaptive gain K_n in Figure 4.4 can be derived from Eq. (4.45):

$$K_n = \frac{-E_2 r - \sqrt{(E_2 r)^2 - 4(E_1 r - E_4)(E_3 r)}}{2(E_1 r - E_4)}, \tag{4.50}$$

where a minus sign is put in front of the square root in Eq. (4.50) to select the positive solution K_n of Eq. (4.45).

DERIVATION OF PERFORMANCE AND CONTROL ACTIVITY

Similarly, the square of the magnitude of the Fourier transform of error signal e is:

$$E = F_t \cdot H_{e,f_t} + F_d \cdot H_{e,f_d} + N \cdot H_{e,n}, \tag{4.51}$$

$$E\overline{E} = B_{ww} K_n^2 + (B_{K_n f_t} + B_{K_n f_d}) K_n + (B_{f_t f_t} + B_{f_d f_d} + B_{f_t f_d}), \tag{4.52}$$

where E is the Fourier transform of the error signal e, and:

$$B_{ww} = |H_{e,n} H_n W|^2, \tag{4.53}$$

$$B_{K_n f_t} = F_t H_{e,f_t} \overline{H_{e,n} H_n W} + \overline{F_t H_{e,f_t}} H_{e,n} H_n W, \tag{4.54}$$

$$B_{K_n f_d} = F_d H_{e,f_d} \overline{H_{e,n} H_n W} + \overline{F_d H_{e,f_d}} H_{e,n} H_n W, \tag{4.55}$$

$$B_{f_t f_t} = |H_{e,f_t} F_t|^2, \tag{4.56}$$

$$B_{f_d f_d} = |H_{e,f_d} F_d|^2, \tag{4.57}$$

$$B_{f_t f_d} = F_t H_{e,f_t} \overline{F_d H_{e,f_d}} + \overline{F_t H_{e,f_t}} F_d H_{e,f_d}. \tag{4.58}$$

The normalized tracking performance of the simulation is:

$$\frac{\sigma_e^2}{\sigma_{f_t}^2} = \frac{\int S_{ee} d\omega}{\int S_{f_t f_t} d\omega} \approx \frac{\int E\overline{E} d\omega}{\int F_t \overline{F_t} d\omega}, \tag{4.59}$$

where S_{ee} is the power spectral density of the error signal, and $S_{f_t f_t}$ is the power spectral density of the target forcing function.

The normalized control activity of the simulation is:

$$\frac{\sigma_u^2}{\sigma_{f_t}^2} = \frac{\int S_{uu} d\omega}{\int S_{f_t f_t} d\omega} \approx \frac{\int U\overline{U} d\omega}{\int F_t \overline{F_t} d\omega}. \tag{4.60}$$

CONSTRAINTS

In the simulation a set of linear constraints is used to limit the ranges of all three decision variables in Eq. (4.8):

$$\begin{aligned} 0 &\leq \omega_{c,t} \leq \omega_{c,t,max} \\ 0 &\leq \phi_{m,t} \leq \phi_{m,t,max} \\ 0 &\leq T_{lag} \leq T_{lag,max}, \end{aligned} \tag{4.61}$$

where $\omega_{c,t,max}$ is the maximum target crossover frequency, $\phi_{m,t,max}$ is the maximum target phase margin, and $T_{lag,max}$ is the maximum lag time constant. According to [26], the crossover frequency is usually between 2 rad/s and 5 rad/s. In the simulation, it is set that $\omega_{c,t,max} = 6$ rad/s and $\phi_{m,t,max} = 2.88$ rad (around 165°). The maximum lag time constant is set $T_{lag,max} = 6$ s in the case that the human operator could generate lag at very low frequencies.

Another constraint is used to limit the range of the lead time constant:

$$0 \leq T_{lead} \leq \min(T_{lag}, T_{lead,max}), \tag{4.62}$$

where $T_{lead,max}$ s is the maximum lead time constant. In Figure 4.5, a down dipole ($\omega_{dp} = 1$ rad/s, $\zeta_1 = 0.2$, $\zeta_2 = 0.7$) is added to the baseline aircraft dynamics. It can be seen that the slope of the magnitude of the total controlled dynamics starts to decrease at around $\omega = 0.4$ rad/s. According to [26], it is assumed that the lowest frequency at which the human operator could generate lead will be at $\omega = 0.4$ rad/s, meaning that $T_{lead,max} = 2.5$ s.

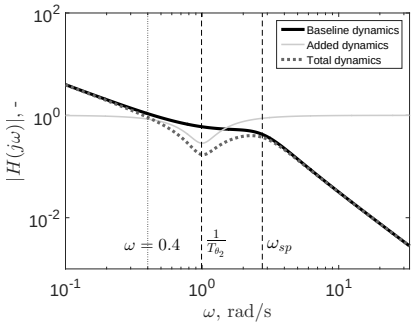

Figure 4.5: An indication of the lowest frequency for human operator to generate lead.

Meanwhile, the lead time constant should be smaller than the lag time constant. As can be seen in Figure 4.5, for the controlled dynamics such as the baseline aircraft dynamics, $\frac{1}{T_{\theta_2}} < \omega_{sp}$. To make the open loop system a single integrator, the human operator generates lag at lower frequency and generates lead at higher frequency. Thus T_{lead} should not exceed T_{lag} [20, 25]. In the simulation, T_{lead} can equal 0, meaning that the equalization term of the human operator model is a pure lag; or T_{lead} can equal T_{lag}, meaning that the equalization term of the human operator model is a pure lead.

SIMULATION ROUTINE

The inputs into the simulation include the target forcing function f_t, disturbance forcing function f_d, white noise w, aircraft baseline dynamics $H_{baseline}$, added dynamics H_{added}, human operator visual time delay τ_v, neuromuscular damping ratio ζ_{nm} and neuromuscular natural frequency ω_{nm}. The outputs of the simulation include the optimal normalized tracking performance $\sigma_e^2/\sigma_{f_t}^2$, normalized control activity $\sigma_u^2/\sigma_{f_t}^2$, visual gain K_v, lead time constant T_{lead}, lag time constant T_{lag}, target crossover frequency $\omega_{c,t}$ and target phase margin $\phi_{m,t}$, as can be seen in Figure 4.6.

The *Fmincon* function with Sequential Quadratic Programing (SQP) algorithm Integrated in MATLAB Optimization Toolbox is used to optimize the decision variables [$\omega_{c,t}$, $\phi_{m,t}$, T_{lag}] (Eq. (4.8)) in order to minimize $\sigma_e^2/\sigma_{f_t}^2$ (Eq. (4.9)), by satisfying constraints (Eqs. (4.61,4.62)). The SQP algorithm used by *Fmincon* function is a local optimum algorithm, meaning that a global optimum cannot be guaranteed. Global optimum algorithms such as the interval analysis method [27, 28] guarantee to find the global optimum, depending on the computer digital accuracy. However, these global algorithms take a lot of computation time. Considering to simulate many more conditions with potentially interesting added dynamics for the future experiment, a much faster local optimum algorithm such as SQP is used.

To increase the chance of finding a lower value of $\sigma_e^2/\sigma_{f_t}^2$, for each noise realization in total 64 sets of initial guesses for the decision variables [$\omega_{c,t}$, $\phi_{m,t}$, T_{lag}] are used for the optimization, which are the combinations of:

$$\begin{aligned} \hat{\omega}_{c,t}|_0 &= \{0.5, 1, 3, 5\} && \text{rad/s} \\ \hat{\phi}_{m,t}|_0 &= \{20, 50, 80, 110\} \cdot (\frac{\pi}{180}) && \text{rad} \\ \hat{T}_{lag}|_0 &= \{0.5, 1, 3, 5\} && \text{s,} \end{aligned} \tag{4.63}$$

where each initial guess may end up with different performance $\sigma_e^2/\sigma_{f_t}^2$ (the local optimum effect), and the lowest value of $\sigma_e^2/\sigma_{f_t}^2$ will be chosen as the final normalized tracking performance. This procedure forms the outer loop of the simulation routine, as can be seen in Figure 4.6. To maximize the computation efficiency, the *parfor* function of MATLAB is used for parallel computation for the 64 sets of initial guesses.

In the inner loop of Figure 4.6, when a certain set of initial guess of [$\omega_{c,t}$, $\phi_{m,t}$, T_{lag}] is chosen, the adaptive gain K_n is first calculated based on the initial values of the decision variables. There is a chance that the calculated K_n is a complex number (see Eq. (4.50)). The SQP algorithm can handle the situation where the first iteration of the optimization is

infeasible (for example, constraints violated), but cannot recover from the situation where complex numbers appear. If the initial K_n is a complex number, the simulation reverses back to select a new initial guess $[\omega_{c,t},\ \phi_{m,t},\ T_{lag}]$.

After the *Fmincon* routine, it is necessary to check whether the optimal $[\omega_{c,t},\ \phi_{m,t},\ T_{lag}]$ is indeed found or not (the solution should at least satisfy the optimality conditions). This depends both on the initial guess of the decision variables and the optimization settings. Through preliminary tests, the step tolerance of the decision variables is set to 10^{-7} (all decision variables are normalized by their own maximum values first) and all the other settings of optimization keep the default values of MATLAB 2015b. For one noise realization, the optimal $[\omega_{c,t},\ \phi_{m,t},\ T_{lag}]$ can be found within 20 s using a 4-core 2.6 GHz laptop computer.

To double check whether the optimal solution is feasible and keeps the system stable, the adaptive gain K_n is recalculated using the optimized $[\omega_{c,t},\ \phi_{m,t},\ T_{lag}]$, and from that calculation K_n should be a non-negative real number and the system should be stable. Otherwise the simulation reverses to select a new set of initial guess and repeats the procedure.

Finally, all the normalized tracking performance $\sigma_e^2/\sigma_{f_t}^2$ outcomes corresponding with different initial guesses are compared with each other. The minimum $\sigma_e^2/\sigma_{f_t}^2$ is chosen as the final normalized tracking performance for one single noise realization. Meanwhile the corresponding optimal $[K_v,\ T_{lead},\ T_{lag},\ \omega_{c,t},\ \phi_{m,t},\ \sigma_u^2/\sigma_{f_t}^2]$ are stored for further analysis.

A schematic representation of the simulation routine is provided in Figure 4.6.

4.2.3. EXPERIMENT

In this section, the human-in-the-loop aircraft pitch attitude compensatory tracking experiment (Figure 4.1) is introduced. First, the dependent measures and the methods of the analysis are explained. Second, the apparatus and the experiment procedures are introduced. In the end the hypotheses are stated.

DEPENDENT MEASURES AND DATA ANALYSIS

The measured variables in the experiment include the time histories of the tracking error e, the control signal u and the pitch angle θ during each run, see Figure 4.1. From these measurements the variance of e and the variance of u are calculated as the measures of tracking performance and control activity, respectively. Based on the measures of e and θ, the Fourier coefficient (FC) method [23, 25] is used to identify the nonparametric open-loop describing functions at the target signal frequencies ω_t:

$$\hat{H}_{ol,t}(j\omega_t) = \frac{\Theta(j\omega_t)}{E(j\omega_t)}, \tag{4.64}$$

where $\hat{H}_{ol,t}(j\omega)$ is the nonparametric target open-loop describing function, Θ is the Fourier transform of the aircraft pitch angle θ and E is the Fourier transform of the error signal e. Then the open-loop target crossover frequency $\omega_{c,t}$ and phase margin $\phi_{m,t}$ representing the manual control bandwidth and the stability are calculated from this nonparametric open-loop describing function.

Similarly, based on the measures of e and u, a (nonparametric) frequency response function (FRF) estimate of the human operator dynamics H_p at the frequencies of both f_t and f_d is also obtained as:

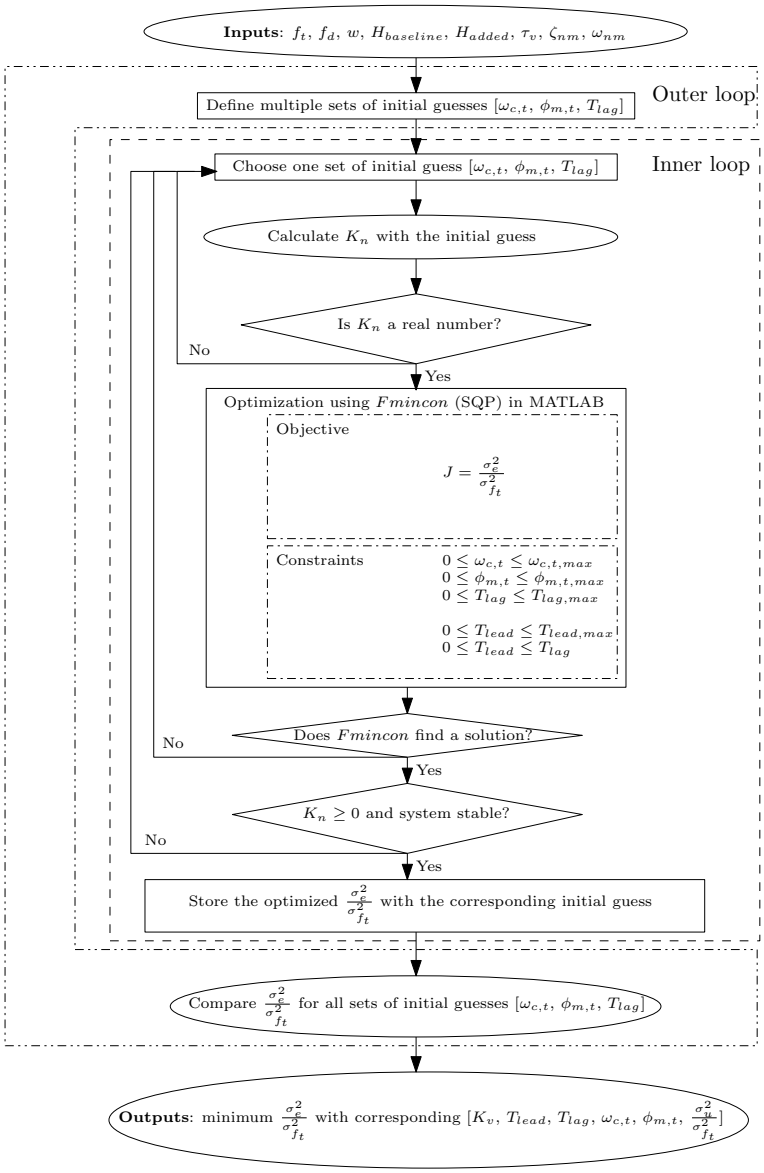

Figure 4.6: A representation of the simulation routine.

$$\hat{H}_p(j\omega_{t,d}) = \frac{U(j\omega_{t,d})}{E(j\omega_{t,d})}, \tag{4.65}$$

where $\hat{H}_p(j\omega_{t,d})$ represents the estimated FRF and U is the Fourier transform of the control signal u, see Figure 4.1. Finally, the human operator model parameters in Eqs. (4.5) and (4.6) are estimated using the time-domain parameter estimation method of [25]. To evaluate the quality-of-fit for all fitted human operator models, the Variance Accounted For (VAF) is calculated. The VAF expresses the model quality in the percentage of the variance in the control signal u that is captured by the model [21, 25].

To verify the statistical significance of observed trends in all dependent measures (performance, control activity, target crossover frequency, target phase margin and all human operator model parameters), statistical analyses are performed. First, a one-way repeated-measures analysis of variance (ANOVA) is used to check for significant variations due to the different added dynamics settings (H_{added}) over all seven experimental conditions. In addition, for each dependent measure six paired t-tests (at a Sidak corrected significance level of $\alpha = 0.0085$) are used to compare all six added dynamics conditions (C1-C6) with the data of the baseline (B).

(a) The Human-Machine-Interaction Simulator (HMI).

(b) Compensatory pitch tracking display.

Figure 4.7: The Human-Machine-Interaction Laboratory (HMI) lab and compensatory pitch tracking display.

APPARATUS

The experiment was performed in the fixed-base simulator setup of the Human-Machine Interaction Laboratory (HMILab) at the Faculty of Aerospace Engineering of Delft University of Technology (see Figure 4.7). During the experiment, subjects were seated in the right cockpit seat and a right-handed sidestick was used for giving inputs to the controlled dynamics. Only the pitch axis of the sidestick was active during the experiment; the roll axis of the sidestick was fixed at the neutral position. The tracking error e in Figure 4.1 was presented to the subject through the primary flight display (PFD) directly in front of the right seat, as shown in Figure 4.7(b). The display shows the pitch attitude tracking error e as the distance between the center fixed aircraft symbol and the moving target line. The aircraft symbol was static, and the target line moved to indicate the current tracking error e. Note that this display is an "inside-out" display: to compensate for the tracking error shown in Figure 4.7(b), the subject needs to give a (positive) pitch input, i.e., pull the stick.

No other visual cues were presented during the experiment, that is, the secondary flight displays and the outside visual system were switched off.

SUBJECTS AND EXPERIMENT PROCEDURES

Seven subjects aged between 25 and 54 years were invited to perform the experiment, all students or staff of the Aerospace Engineering Faculty of Delft University of Technology. All subjects had experience with similar manual control tasks from previous experiments. The subjects received an experimental briefing on the overview and objective of the experiment. Subjects were instructed to minimize the pitch attitude tracking error e presented on the PFD as best as possible, without providing the details of the characteristics of the controlled aircraft dynamics or added dynamics. Finally, all the subjects gave written informed consent before the start of the experiment.

For each subject, the experiment started with an initial familiarization. During this phase, subjects were allowed to familiarize themselves with the baseline aircraft dynamics (condition B) for a total of 7 tracking runs. Following this initial familiarization, the testing runs for all experiment conditions were performed. The order of the testing was determined for each subject by a Latin square. Figure 4.8 shows the run order of Subject 1 for all the conditions as an example. Note that condition of the baseline aircraft dynamics (C7(B)) is also included in the Latin Square design. Figure 4.8 also shows that each condition was tested in two stages. The first *subjective evaluation stage* covers the first 4 runs performed for each condition and was used to collect subjective feedback from the subject about the noticeability of the differences with the baseline aircraft dynamics. Among these first 4 runs, the baseline aircraft dynamics (B) is randomly inserted. However, in the experiment briefing subjects were informed that the baseline aircraft dynamics could appear at any run of the *subjective evaluation stage*, and the number of its appearances could be between 0 and 4. For example, in Figure 4.8 the first testing condition of Subject 1 is C3. After the 1st run (R1), he was not required to give any feedback. After the 2nd run (R2), he was required to give subjective feedback by comparing R2 with R1 in the aspects of: tracking performance, control activity and responsiveness of the dynamics. Moreover, a score indicating the general level of difference was also given by subjects, where "0" indicates "no difference", "1" indicates "slightly different", "2" indicates "notably different" and "3" indicates "very different". The subjective feedback was required at the end of R2, R3 and R4 for each testing condition. The results of the subjective ratings of each subject can be seen in Appendix B. After the first 4 runs, subjects were informed that the controlled dynamics would remain the same for the rest of the runs. The second *measurement stage* starts from the 5th run of each condition and is used to collect the data (i.e., five measurement runs for each conditions at a stable level of performance) for human operator model identification. The root mean square (RMS) of the error signal e was recorded by the experimenter and reported to the subject after each run. When RMS(e) clearly stabilized and five repetitions were collected, the testing of this condition was completed. In general, around 11 runs were necessary for each experimental condition to complete.

Subjective evaluation stage				Measurement stage						
R1	R2	R3	R4	R5	R6	R7	R8	R9	R10	R11
C3	B	C3	C3	C3						
C1	C1	B	C1	C1						
B	C5	C5	C5	C5						
C4	C4	C4	B	C4						
C7(B)										
B	C2	C2	C2	C2						
C6	B	C6	C6	C6						

Figure 4.8: The run order of Subject 1 for all the conditions. The baseline aircraft dynamics (B) is randomly inserted among the first 4 runs, for each condition. The added dynamics of different conditions can be seen in Table 4.2.

Each testing run lasted 95 s. In order to obtain stable control output from the subject, the first 8.08 s and the last 5 s data were cut off. Thus 81.92 s of data were used for the frequency domain analysis. The sampling frequency was set at 100 Hz.

HYPOTHESES

For the experiment, the following hypotheses were formulated:

1. *Dipoles added outside the crossover region have no effect on tracking performance, control activity and human operator control behavior.* The controlled dynamics within the crossover region are considered to be the most crucial with respect to tracking performance, control behavior and handling qualities [1, 2, 26]. Thus it is expected that for C3 and C4 ($\omega_{dp} = 3$ rad/s) the tracking performance, control activity and human operator control behavior will be different from those of the baseline. For C1 and C2 ($\omega_{dp} = 1$ rad/s) and C5 and C6 ($\omega_{dp} = 7$ rad/s), it is expected that for all the dependent measures there is no difference with the baseline.

2. *The effects of the up and down dipoles at 3 rad/s on tracking performance, control activity and human operator visual gain are opposite (mirrored) and significantly different from the baseline.* The main difference between the down and up dipoles is that the down dipole decreases the gain of the controlled dynamics (compared with the baseline) while the up dipole increases the gain of the controlled dynamics. It is expected that, compared with the baseline, the tracking performance with the down dipole (C3) is worse, that the control activity increases and that the human operator visual gain increases. In contrast, the tracking performance with the up dipole (C4) is expected to be better, with decreased control activity and human operator visual gain compared to the baseline.

4.3. RESULTS

4.3.1. EXPERIMENT RESULTS

This section first presents the subjective ratings given by our subjects regarding the noticeability of the different added dynamics compared to the baseline aircraft dynamics. Then the objective control behavioral measurements collected from the experiment are shown.

SUBJECTIVE RATINGS

In Figure 4.9, the subjective rating scores of all subjects over all conditions are shown. The original scores given by each subject are only integers: $0, 1, 2$ and 3. In Figure 4.8, it can be seen that the baseline condition (B) randomly appears among the first 4 runs of the *subjective evaluation stage*. For C3 and C1, the baseline condition (B) locates at R2 and R3 respectively. The subjective rating score is then averaged between R2 and R3. For C5, the baseline condition (B) appears at R1, thus only the subjective rating score at R2 is valid. For C4, the baseline condition (B) appears at R4, thus only the subjective rating score at R4 is valid. For C7 (B), the subjective rating score is averaged over R2, R3 and R4.

As can be seen in Figure 4.9, the scores of different subjects are not consistent, and no general trend can be observed of different subjects over different conditions. Moreover, even though the mean score of the baseline condition (B) has the lowest value, it is not expected. The subjects should not notice any difference between testing runs for the baseline condition (B), since all the controlled dynamics in C7 (B) (see Figure 4.8) are exactly the same. The details of the subjective ratings of each subject are given in Appendix B.

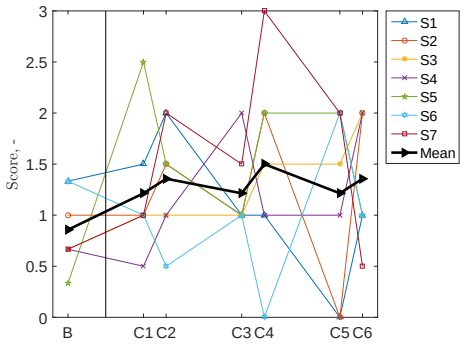

Figure 4.9: Subjective ratings for different conditions. The lines connecting different conditions are only for viewing convenience.

TRACKING PERFORMANCE AND CONTROL ACTIVITY

Figure 4.10a provides the variance decomposition of the error signal e for each condition averaged over the seven subjects. The error bars show the 95% confidence intervals of the total σ_e^2. The data have been corrected for between-subject variability. The solid line connecting C1, C3 and C5 shows the change of the means of the “down dipole" conditions ($\zeta_1 = 0.2, \zeta_2 = 0.7$), and the dashed line connecting C2, C4 and C6 shows the change of the means of the “up dipole" conditions ($\zeta_1 = 0.7, \zeta_2 = 0.2$). The baseline condition is indicated as “B” in the figure. An asterisk symbol above the data from a certain condition indicates a statistically significant difference between this condition and the baseline, as found with a t-test.

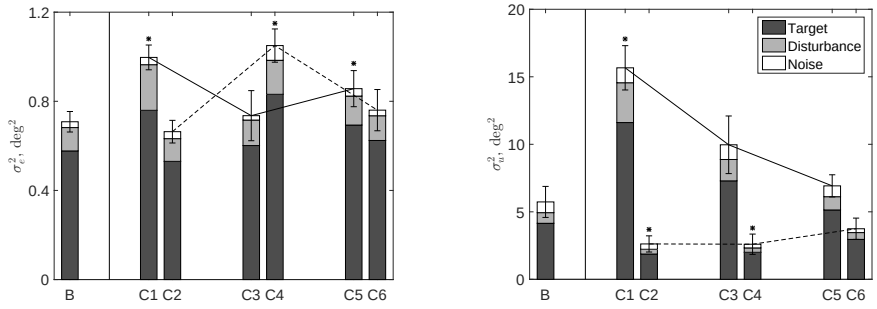

(a) Performance (b) Control activity

Figure 4.10: Variance decompositions of the error signal e and control signal u for each condition, averaged over seven subjects.

Table 4.3: ANOVA results for σ_e^2 and σ_u^2, where * is significant ($p < 0.05$), and - is not significant ($p \geq 0.05$).

	σ_e^2			σ_u^2		
Factor	df	F	Sig.	df	F	Sig.
H_c	2.3^{gg}	19.4	*	2.0^{gg}	71.2	*

Table 4.4: Paired t-test results for σ_e^2 and σ_u^2, where * is significant ($p < 0.0085$), and - is not significant ($p \geq 0.0085$).

	σ_e^2			σ_u^2		
Factor	df	t	Sig.	df	t	Sig.
C1-B	11.2	6.4	*	11.8	9.8	*
C2-B	10.9	-0.7	-	7.5	-3.6	*
C3-B	8.3	0.5	-	10	2.9	-
C4-B	10.1	6.8	*	7.1	-3.8	*
C5-B	11.7	3.3	*	9	1.4	-
C6-B	8.8	0.7	-	6.6	-2.4	-

In Figure 4.10a, performance with C1 is significantly worse than that of the baseline ($t(11.2) = 6.4, p < 0.0085$). The added down dipole at 1 rad/s reduces the gain of the controlled dynamics at frequencies where the forcing function has most of its power. The human operator has to increase his gain in order to compensate for the gain loss due to the down dipole. However, this could lead to very high control activity. The performance of C3 is close to that of the baseline, even though the down dipole is located at 3 rad/s, within the manual control crossover frequency region. The low gain with the down dipole moves away from the low frequency region (0.46 rad/s to 2.07 rad/s) where the forcing function has most of its power, and the human operator may use a similar control strategy as for the baseline to obtain an acceptable and similar performance. Performance of C5 is significantly different from that of the baseline ($t(11.7) = 3.3, p < 0.0085$), the reason may be that the performance of Subject 3 of C5 is much worse than all the other subjects. It can be seen in Figure 4.10a that the performance of C2 is close to that of the baseline. Compared with the down dipole

of C1, the up dipole increases the gain of the controlled dynamics, thus the human operator may not need to change his control behavior and a similar performance with the baseline can be obtained. The performance of C4 is significantly worse than that of the baseline ($t(10.1) = 6.8, p < 0.0085$). This is probably due to the fact that the baseline aircraft short period frequency ω_{sp} is very close to 3 rad/s, and the phase of the total controlled dynamics decreases strongly between 2 rad/s and 4.4 rad/s. The performance of C6 is close to that of the baseline. The quick phase drop due to the dipole happens beyond 7 rad/s, which is far away from the aircraft short period frequency ω_{sp} and would not destabilize the system. A similar performance as for the baseline may be obtained by the human operator.

In Figure 4.10b, the control activities σ_u^2 of all conditions are shown. The control activity of C1 is significantly higher than that of the baseline ($t(11.8) = 9.8, p < 0.0085$). This is due to the fact that the human operator has to increase his gain (thus the control activity) to compensate for the performance loss caused by the low gain with the down dipole at the frequencies where the forcing function has most of the power. Moreover, it can be seen that the mean of the control activity decreases when the down dipole moves from 1 rad/s (C1), through 3 rad/s (C3) and to 7 rad/s (C5). When the down dipole moves to a higher frequency, for example 7 rad/s, where the forcing function has less power, the low gain brought by the down dipole has less effect on the performance, and the human operator needs to compensate less. Similar reasoning can be applied to the up dipole conditions (C2, C4 and C6), where the control activity increases when the up dipole moves from low to high frequencies.

CROSSOVER FREQUENCIES AND PHASE MARGINS

Figure 4.11 shows the means of the target crossover frequencies $\omega_{c,t}$ and phase margins $\phi_{m,t}$ over seven subjects for all conditions. The error bars show the 95% confidence intervals and the data have been corrected for between-subject variability.

As can be seen in Figure 4.11a, the target crossover frequencies of C1 and C2 are close to that of the baseline. It may be due to the fact that the human operators may be able to adapt their own visual gain to compensate for the changes brought by the up and down dipoles at 1 rad/s, which is also reflected in Figure 4.10b for the control activity. For the added dynamics at 3 rad/s, the target crossover frequency of C4 is higher than that of C3 and is also the highest among all the conditions. During the experiment, most of the subjects reported that the controlled dynamics of C4 were less stable than others and difficult to control, which also corresponds with the worse performance in Figure 4.10a and low phase margin in Figure 4.11b. At 7 rad/s, the target crossover frequencies of C5 and C6 are close to that of the baseline, since at 7 rad/s the added dynamics may have less effect on control behavior. Table 4.5 shows that there is no significant difference among conditions, thus no t-test was conducted for the target crossover frequency.

In Figure 4.11b it can be seen that only the phase margin of C3 ($t(12) = -3.2, p < 0.0085$) is significantly different than that of the baseline. The average phase margin of C4 is the lowest among all the conditions but due to its wide spread Table 4.6 shows that it is not significantly different from that of the baseline. The phase margins of other conditions are relatively close to that of the baseline, indicating that these systems have similar stability.

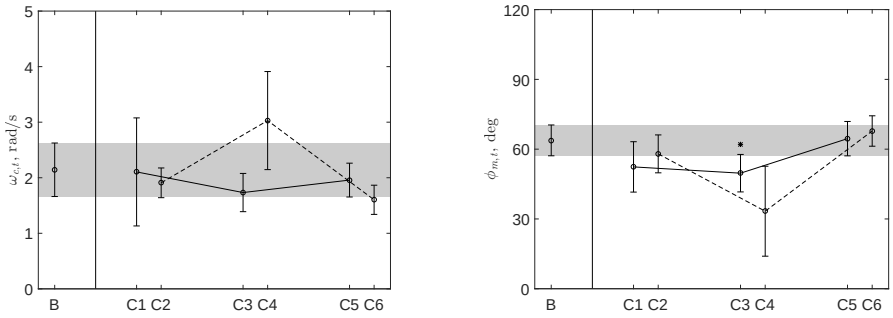

(a) Target crossover frequencies (b) Target phase margins

Figure 4.11: Target crossover frequencies and phase margins for each condition, averaged over seven subjects. The grey area marks the range of the baseline condition, and the asterisk marks the condition significantly different from the baseline condition.

Table 4.5: ANOVA results of the target crossover frequencies and phase margins, where * is significant ($p < 0.05$), and - is not significant ($p \geq 0.05$).

	$\omega_{c,t}$			$\phi_{m,t}$		
Factor	df	F	Sig.	df	F	Sig.
H_c	2.0^{gg}	3.4	-	2.3^{gg}	6.6	*

Table 4.6: Paired t-test results for the target phase margins, where * is significant ($p < 0.0085$), and - is not significant ($p \geq 0.0085$).

	$\phi_{m,t}$		
Factor	df	t	Sig.
C1-B	9.5	-1.7	-
C2-B	10.8	-1.5	-
C3-B	12	-3.2	*
C4-B	7.3	-2.9	-
C5-B	11.5	0.1	-
C6-B	11.3	1	-

HUMAN OPERATOR MODEL FITTING RESULTS

Figure 4.12 shows the human operator modeling results for Subject 7 for conditions B, C3, and C4. The frequency response functions at both target and disturbance forcing function frequencies are shown with circular and triangular markers, respectively. The error bars show the sample standard deviations of the FRF estimates over the five measurement runs. Finally, the frequency response of the total controlled dynamics is also shown, for reference.

As can be verified from Figure 4.12, the fitted human operator models in general show very good agreement with (independently estimated) FRFs. Also, the attained VAF values are high (>80%), which means that the human operator model output accurately describes the measured output u. The results in Figure 4.12 are representative for all collected data, i.e., for all other subjects and conditions, the VAF values between 75% and 95% were

attained. Only for the data of Subject 2 in conditions C2 and C4, the human operator modeling results were less accurate, with VAFs of around 61% and 68%, respectively.

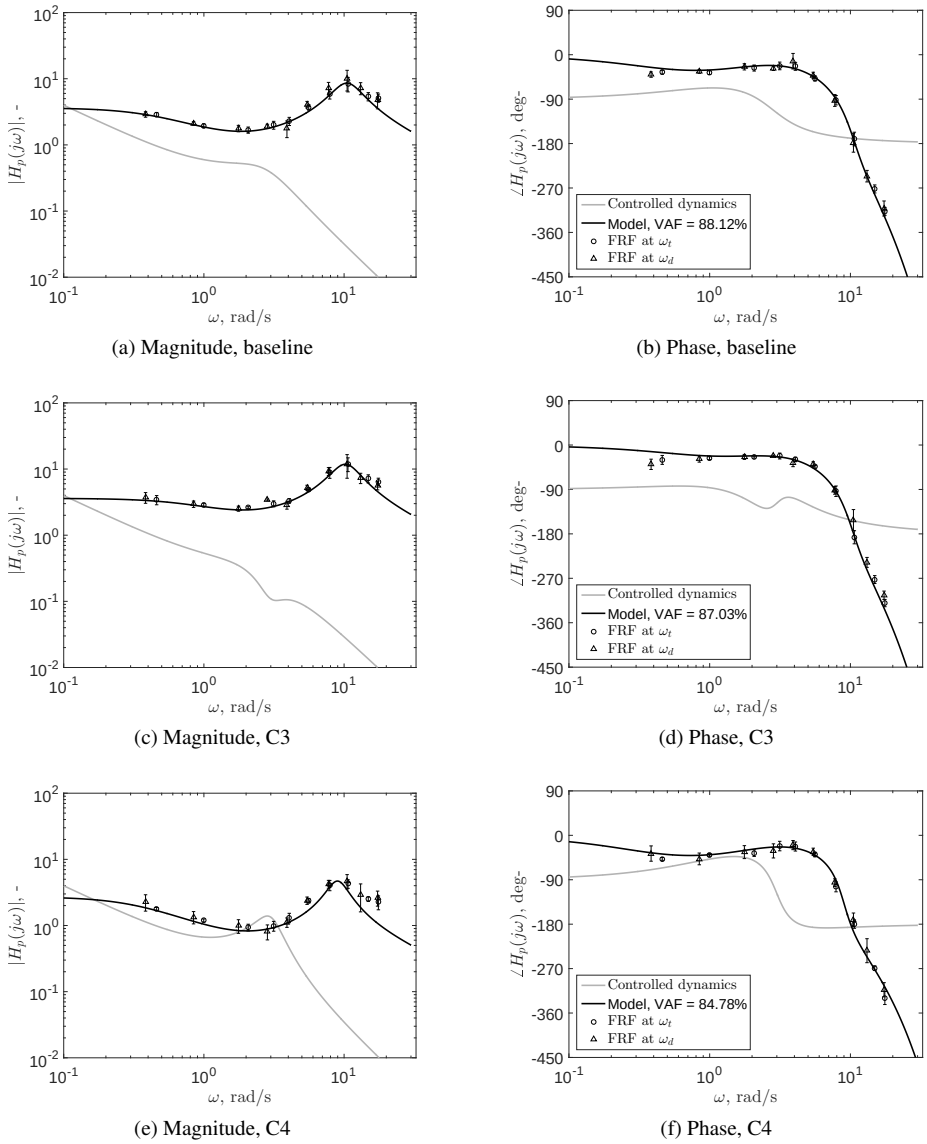

(a) Magnitude, baseline

(b) Phase, baseline

(c) Magnitude, C3

(d) Phase, C3

(e) Magnitude, C4

(f) Phase, C4

Figure 4.12: Subject 7 compensatory model fits and frequency response functions for conditions of baseline, C3 and C4.

HUMAN OPERATOR MODEL PARAMETERS

Figure 4.14 shows the error-bar plots of the human operator model parameters for all conditions. The error-bars indicate the 95% confidence intervals of the means over the seven subjects. The data have been corrected for between-subject variability.

In Figure 4.14a, it can be seen that the visual gain of C1 is significantly higher ($t(10.7) = 5, p < 0.0085$) than that of the baseline, and this corresponds with the high control activity of C1 in Figure 4.10b. Moreover, the visual gain decreases as the down dipole moves from 1 rad/s (C1), through 3 rad/s (C3) and to 7 rad/s (C5). This also corresponds with the decreasing control activity from C1 to C5 in Figure 4.10b. When the down dipole moves from 1 rad/s to 7 rad/s, the human operator needs less visual gain due to the fact that the low gain with the down dipole has less effect on the performance at higher frequencies. As the up dipole increases the gain of the controlled dynamics, the human operator could reduce his visual gain (C2 in Figure 4.14a) and the control activity (C2 in Figure 4.10b) to achieve a close performance (C2 in Figure 4.10a) with the baseline. In Figure 4.14a, when the up dipole moves to 3 rad/s (C4) and 7 rad/s (C6), the human operator needs to increase the visual gain (compared with C2) due to the fact that the gain increase due to the up dipole has less effect on the performance at higher frequencies.

In Figure 4.14b, only the visual time delay of C4 is significantly different from that of the baseline ($t(9.3) = -6.4, p < 0.0085$). This may be attributed to the fact that the controlled dynamics of C4 are much less stable than that of other conditions. A lower visual delay may help the operator stabilize the system.

In Figure 4.14c, it can be seen that the lead time constants of C1 ($t(10.1) = -5.2, p < 0.0085$) and C2 ($t(11.4) = 6.4, p < 0.0085$) are significantly different than that of the baseline, and in Figure 4.14d, the lag time constant of C1 is close to that of the baseline but the mean of the lag time constant of C2 is higher than that of the baseline. Since the value of the lag time constant T_{lag} should be higher than that of the lead time constant T_{lead} [20, 25], meaning that the human operator would first generate lag at a certain lower frequency, then the lead could be generated later at a certain higher frequency. Moreover, the open-loop system is usually a single integrator near the crossover region [26]. The changes in T_{lead} and T_{lag} for C1 and C2 are further explained in Figure 4.13 using Subject 7 as an example (similar to Figure 4.12). In Figure 4.13a, for example, two vertical dashed lines show the frequencies of $1/T_{lead}$ (generating lead) and $1/T_{lag}$ (generating lag), respectively. The shaded area indicates the frequency range within which the controlled dynamics are single integrator like. Due to the fact that both of the controlled dynamics of C1 and the baseline are close to a single integrator from very low frequency until around 0.6 rad/s, their lag time constants are close ($1/T_{lag}$ are therefore close). However, since the gain of the dynamics of C1 increases between 1 rad/s and 2.3 rad/s due to the dipole, the lead term of C1 is generated at a higher frequency of 2.83 rad/s (compared with the baseline) in order to obtain open-loop dynamics for C1 that approximate a single integrator. Thus the lead time constant of C1 (1/2.83 s) is lower than that of the baseline (1/2.06 s). As for the controlled dynamics of C2, the single integrator like part ends at frequency around 0.4 rad/s, moreover, the gain of the controlled dynamics increases between around 0.4 rad/s to 1 rad/s. Thus the human operator generates lag at 0.34 rad/s (close to 0.4 rad/s), and the lag time constant (1/0.34 s) is therefore higher than that of the baseline (1/0.45 s). Beyond 1 rad/s, the gain of the controlled dynamics of C2 decreases and in order obtain a single integrator like open-loop

response, the human operator generates lead at frequency of 1.58 rad/s which is lower than that of the baseline, thus the lead time constant of C2 (1/1.58 s) is higher than that of the baseline (1/2.06 s).

In Figure 4.14c, it can be seen that the lead time constants for conditions C3 and C4 are close, and in Figure 4.14d, the lag time constant of C3 is much lower than that found for C4. This can be verified from Figure 4.12c and Figure 4.12e. In Figure 4.12c, the single integrator like part of the controlled dynamics of C3 ends at around 2 rad/s, and in Figure 4.12e, it ends at around 0.6 rad/s. Thus the human operator needs to generate lag in C4 at lower frequency compared with C3, and the lag time constant of C4 is higher than that of C3. The lead time constants of C3 and C4 are close, and this may attribute to the fact that both the controlled dynamics of C3 and C4 change their frequency response characteristics at around 2.4 rad/s.

In Figure 4.14c, the lead time constants for conditions C2 and C5 are seen to be significantly higher (i.e., around 0.65 s) than the baseline average of around 0.49 s. On the other hand, for conditions C1 and C6, a significant drop in T_{lead} is found. These effects can be directly linked to human operator compensation for the phase lead or lag induced by the added dynamics in the crossover region. Up dipoles at low frequencies (C2) and down dipoles at high frequencies (C5) give additional lag around crossover, that operators can negate by increasing their T_{lead}. Similarly, for conditions C1 and C6 the added dynamics provide phase lead around crossover, meaning less is required from the operator to retain the same level of stability. Somewhat surprisingly, dipoles very close to the crossover region (conditions C3 and C4) do not result in any notable adaptation of T_{lead}. Figure 4.14d shows that the lag time constant data (T_{lag}) has much more spread and no significant differences with the baseline data for any of the conditions.

Figures 4.14e and 4.14f show the damping ratios and natural frequencies of the neuromuscular system for all conditions, respectively. Only the natural frequency for condition C4 is seen to be significantly different from the baseline data ($t(11.5) = -3.2, p < 0.0085$). Overall, the neuromuscular parameters thus show little primary adaptation to the different added dynamics settings.

Table 4.7: ANOVA results of the human operator model visual parameters, * is significant ($p < 0.05$), - is not significant ($p \geq 0.05$).

	K_v			T_{lead}			T_{lag}			τ_v		
Factor	df	F	Sig.	df	F	Sig.	df	F	Sig.	df	F	Sig.
H_c	6	36.1	*	2.5[gg]	58.8	*	6	12.4	*	6	22.1	*

Table 4.8: ANOVA results of the human operator model neuromuscular parameters, * is significant ($p < 0.05$), - is not significant ($p \geq 0.05$).

	ζ_{nm}			ω_{nm}		
Factor	df	F	Sig.	df	F	Sig.
H_c	3.2[gg]	7.5	*	6	7.2	*

Table 4.9: Paired t-test results of visual parameters, where * is significant ($p < 0.0085$), and - is not significant ($p \geq 0.0085$).

	K_v			T_{lead}			T_{lag}			τ_v		
Factor	df	t	Sig.	df	t	Sig.	df	t	Sig.	df	t	Sig.
C1-B	10.7	5	*	10.1	-5.2	*	10.8	-0.5	-	11	-0.2	-
C2-B	9.6	-3.1	-	11.4	6.4	*	10.8	2	-	8.4	0.5	-
C3-B	11.8	1.1	-	11.3	-2.3	-	9.2	-2.7	-	10.7	2.3	-
C4-B	12	-2	-	10.7	-1	-	10.3	2.1	-	9.3	-6.4	*
C5-B	11.6	-0.5	-	11	4.7	*	11.7	1.1	-	9.6	0.6	-
C6-B	11.1	1.2	-	11.5	-5.9	*	12	0.8	-	11	-0.5	-

Table 4.10: Paired t-test results of neuromuscular parameters, where * is significant ($p < 0.0085$), - is not significant ($p \geq 0.0085$).

	ζ_{nm}			ω_{nm}		
Factor	df	t	Sig.	df	t	Sig.
C1-B	11.5	-0.4	-	7.8	0.01	-
C2-B	11.9	1.3	-	9.4	-0.2	-
C3-B	11.3	2	-	11.9	1.3	-
C4-B	8.7	-1.7	-	11.5	-3.2	*
C5-B	11.9	1.4	-	11.6	-1.8	-
C6-B	11.5	0.3	-	8.2	1.5	-

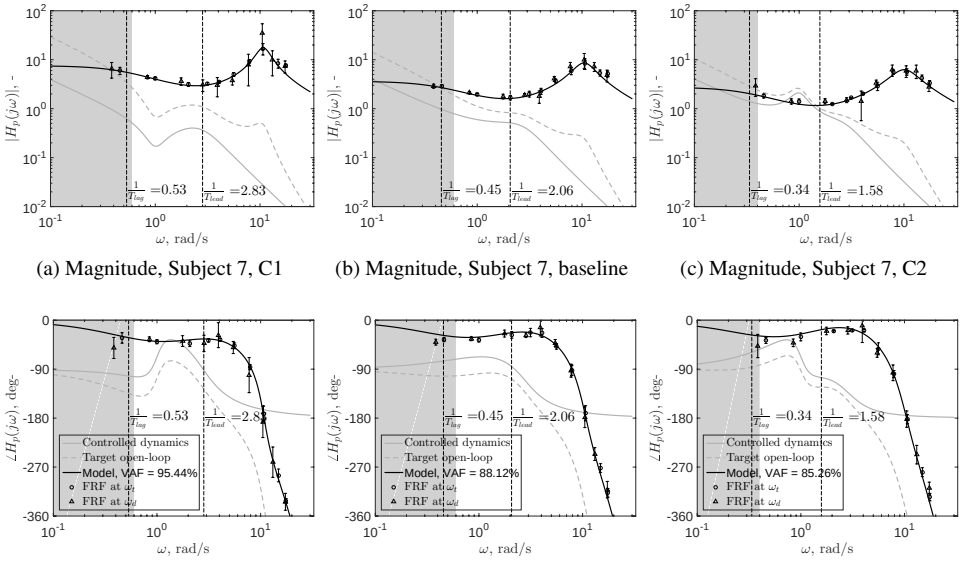

(a) Magnitude, Subject 7, C1 (b) Magnitude, Subject 7, baseline (c) Magnitude, Subject 7, C2

(d) Phase, Subject 7, C1 (e) Phase, Subject 7, baseline (f) Phase, Subject 7, C2

Figure 4.13: Subject 7 compensatory model fits and frequency response functions for conditions of C1, baseline and C2. The shaded area in each figure indicates the frequency range within which the controlled dynamics are single integrator like.

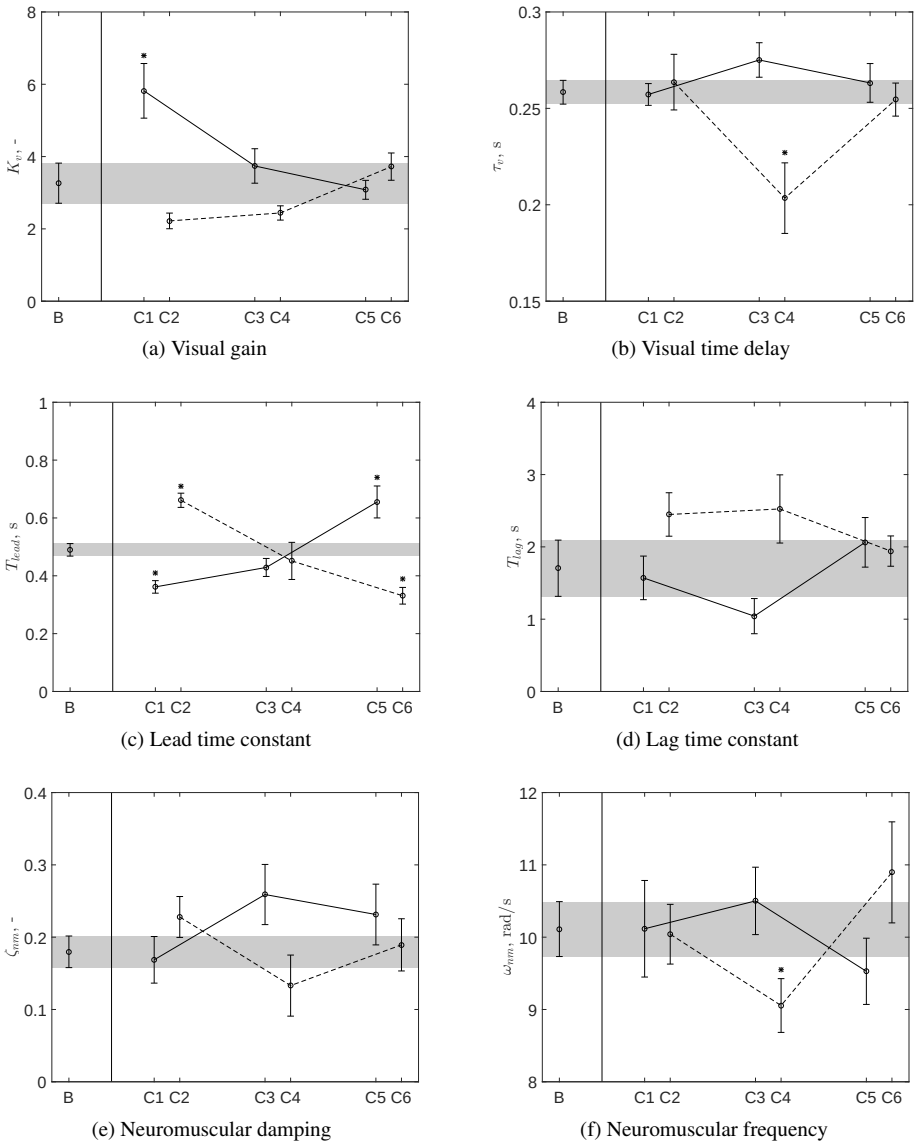

(a) Visual gain

(b) Visual time delay

(c) Lead time constant

(d) Lag time constant

(e) Neuromuscular damping

(f) Neuromuscular frequency

Figure 4.14: Human operator model parameters. The grey area marks the range of the baseline condition, and the asterisk marks the condition significantly different from the baseline condition.

4.3.2. COMPARISON WITH SIMULATION PREDICTION DATA

Figure 4.15 shows the simulation results with different remnant ratios together with the experiment data. In each condition, the median value of 100 noise realizations is plotted for the simulation (except for $r = 0$, only 1 realization is simulated for each condition), and the raw measured or identified values are plotted for the experiment.

In Figure 4.15a, large offsets between simulation and experiment data for $r = 0$ can be seen in C1, C2 and C5. The normalized tracking performance gets worse when the remnant ratio increases. In Figure 4.15b, obvious offsets between simulation and experiment data for $r = 0$ can be seen in C1, C2, C3 and C5. With $r \neq 0$ the normalized control activity does not change much with different remnant ratios, except for C2. In Figure 4.15c, large offsets between simulation and experiment data for $r = 0$ can be seen in C1, C2 and C5. When remnant ratio increases, the simulated target crossover frequency gets closer to the experiment data, especially for C1, C2 and C5. Similar trends can be seen in Figure 4.15d for the target phase margin. In Figure 4.15e, an offset between simulation and experiment data for $r = 0$ can be seen in C5. With $r \neq 0$ the visual gain decreases when the remnant ratio increases, and this trend is more obvious for the baseline condition (B) and C6. In Figure 4.15f, it can be seen that the lead time constant is overestimated for the baseline condition (B) and C5. With $r \neq 0$ the simulation matches the experiment data much better. In Figure 4.15g, the simulated lag time constant decreases when the remnant ratio increases.

In order to judge a suitable remnant ratio for the computer offline simulations, a correlation test is carried out between the medians of the simulation and the experiment data. The off-diagonal element R values are summarized in Table 4.11. The R value should be close to 1 if the correlation is significant, and $*$ is plotted along with the R value to indicate the correlation is significant. In each column of Table 4.11, the mean value of R is calculated over all independent variables to indicate the average level of correlation between the simulation and experiment. In Table 4.11, it can be seen that the mean R values of $r = 0.25$ and $r = 0.3$ are the highest, which means that for these values of r the simulation and experiment data are the most similar.

In Figure 4.16, the simulation results of $r = 0.25$ are shown as box-plots and compared with the experiment data. It can be seen that for the target crossover frequency $\omega_{c,t}$, target phase margin $\phi_{m,t}$, visual gain K_v and lag time constant T_{lag} the correlations are not significant. In Figure 4.16e, it can be seen that in C1 the simulation K_v is lower than the experiment data. If the median of the visual gain in C1 could be higher, then the change trend from the baseline to C1 could correlate better between the simulation and experiment.

Table 4.11: Correlation coefficients for experiment and simulation data with different remnant ratios, where * indicates the correlation is significant ($p < 0.05$), - is not significant ($p \geq 0.05$).

Dependent	$\sigma_n^2/\sigma_u^2 = r$					
Measures	0	0.1	0.15	0.2	0.25	0.3
$\sigma_e^2/\sigma_{f_t}^2$	0.77^*	0.95^*	0.95^*	0.95^*	0.96^*	0.96^*
$\sigma_u^2/\sigma_{f_t}^2$	0.84^*	0.74^-	0.74^-	0.76^*	0.77^*	0.76^*
$\omega_{c,t}$	0.48^-	0.56^-	0.64^-	0.69^-	0.75^-	0.76^*
$\phi_{m,t}$	-0.10^-	0.33^-	0.45^-	0.44^-	0.47^-	0.46^-
K_v	0.80^*	0.72^-	0.68^-	0.65^-	0.64^-	0.62^-
T_{lead}	0.91^*	0.87^*	0.89^*	0.92^*	0.91^*	0.92^*
T_{lag}	0.66^-	0.45^-	0.45^-	0.55^-	0.59^-	0.61^-
Mean R	0.63	0.66	0.69	0.71	0.73	0.73

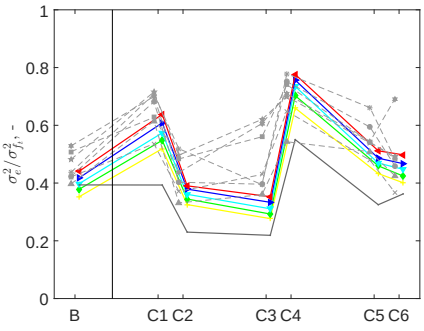

(a) Performance

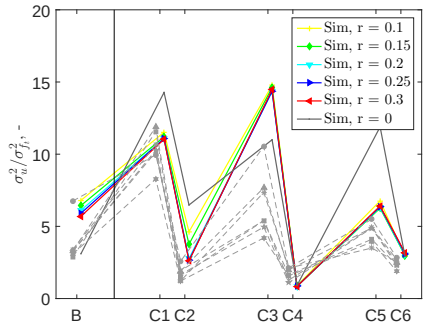

(b) Control activity

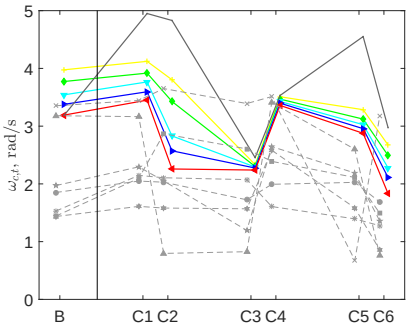

(c) Target crossover frequency

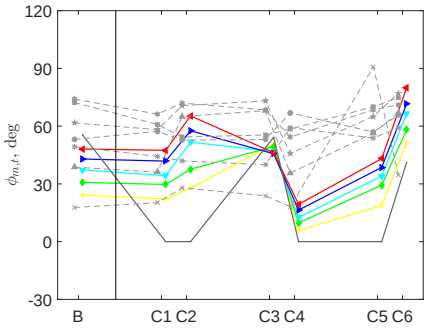

(d) Target phase margin

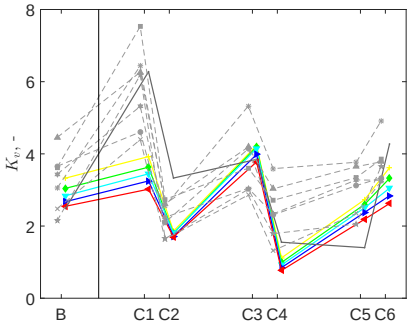

(e) Visual gain

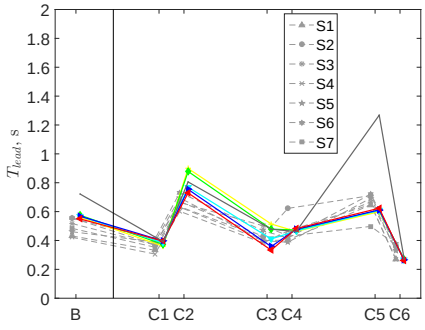

(f) Lead time constant

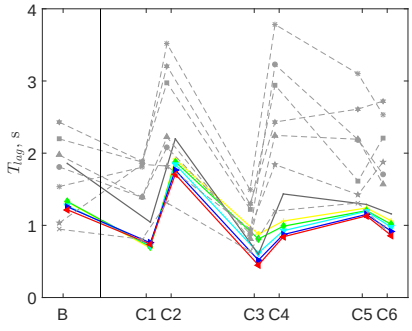

(g) Lag time constant

Figure 4.15: Comparison between experiment and simulation results with different remnant ratios.

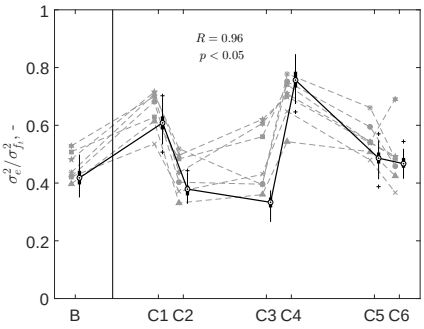

(a) Performance

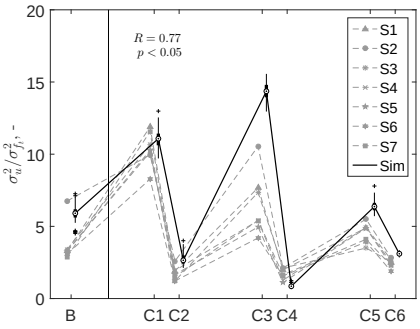

(b) Control activity

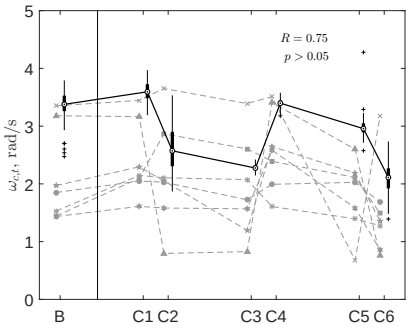

(c) Target crossover frequency

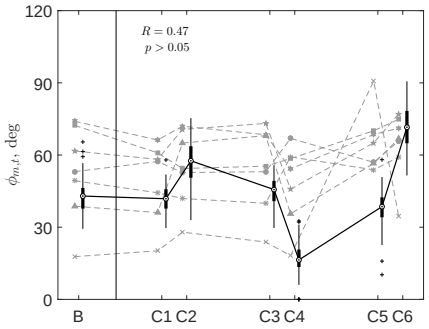

(d) Target phase margin

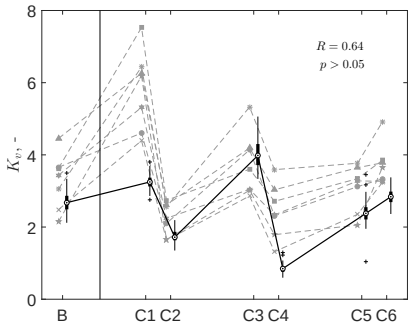

(e) Visual gain

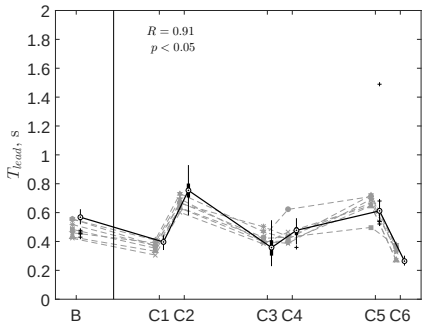

(f) Lead time constant

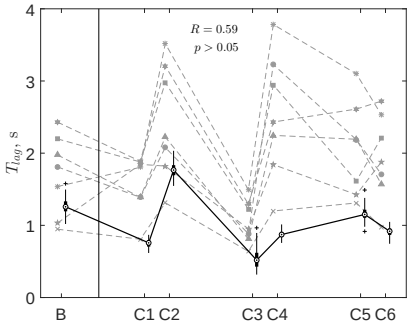

(g) Lag time constant

Figure 4.16: Comparison between experiment and simulation results (in simulation $\sigma_n^2/\sigma_u^2 = 0.25$).

4.4. DISCUSSION

In order to develop Manual Control Adaptation Boundaries that capture the sensitivity of human operator control behavior to changes in controlled dynamics, an aircraft pitch attitude compensatory tracking experiment with different added dipole dynamics was performed. In total seven conditions were tested, with "down" and "up" dipoles at 1 rad/s, 3 rad/s and 7 rad/s cascaded with the baseline aircraft pitch dynamics, as well as a reference baseline aircraft dynamics case. In addition, an offline computer simulation based on optimal performance predictions with a human operator model – using a constrained nonlinear optimization algorithm – was developed to predict tracking performance, control activity, crossover frequency, phase margin and control behavioral parameters for the same test conditions. To verify the extent to which the observed human operator adaptations could be predicted without experimentation, the simulation results were directly compared, and correlated, with the experiment data.

For the experiment and the considered variation in added dipole dynamics, two hypotheses were formulated. For *Hypothesis 1*, it was expected that dipole added dynamics centered at frequencies well outside of the crossover region (i.e., 1 and 7 rad/s) would not show a strong effect on human operator behavior and performance. Based on the experiment data, this hypothesis has to be rejected. The experiment results show that when the dipoles are added below (C1 and C2) and within the crossover region (C3 and C4), the dependent measures are not necessarily different from those of the baseline; and when the dipoles are added outside the crossover region (C5 and C6), the dependent measures are not necessarily the same as for the baseline. For example, the performance of C2 and C3 are close to that of the baseline. Even though the added dipoles of C2 and C3 are near and within the crossover frequency region, however, they do not destabilize the system; moreover, the gain change in the controlled dynamics due to the added dipoles of C2 and C3 can be easily compensated by the adaptation of the human operator. Correspondingly, the crossover frequencies of C2 and C3 are close to that of the baseline. The phase margin of C2 is also close to that of the baseline. Regarding human operator control behavior, the visual gains of C2, C3 and C4 are not significantly different from that of the baseline. The lead time constants of C3 and C4 are close to that of the baseline, and the lag time constants of C1, C2, C3 and C4 are not significantly different from that of the baseline. The visual gain, lead time constant and lag time constant determine the equalization term of the human operator dynamics, which is the main adaption term of the human operator. Added dynamics near and within the crossover frequency region do not always significantly change these three parameters, especially when the added dynamics do not affect the stability of the system and the human operator can utilize similar control activity and/or visual gain of the baseline to the new controlled system to achieve a close and acceptable performance. In contrast, the lead time constants of C5 and C6 (outside the crossover frequency region) are all significantly different from that of the baseline. Take C6 as an example, the lead term in the human operator frequency response is always generated at a higher frequency than that of the lag term, and the lag term in the human operator frequency response extends to a higher frequency (compared with the baseline) due to the fact that the dipole of C6 changes the frequency response of the baseline dynamics near the crossover frequency region.

The second hypothesis (*Hypothesis 2*) stated that opposite effects of matching magnitude were expected when comparing the "down" and "up" dipole conditions tested in the

experiment. Considering the observed variation in all dependent measures, also this hypothesis is rejected. The tracking performance of C3 is almost equal to that of the baseline, this is due to the fact that the controlled system is stable and the human operators can optimize their equalization term to achieve a close performance with the baseline, even though the added dynamics are within the crossover region. The worse performance of C4 is due to the instability of the controlled dynamics. The control activity of C3 is higher (but not significantly) than that of the baseline, and the control activity of C4 is significantly lower than that of C4. Correspondingly, the visual gain of C3 is higher than that of the baseline, and the visual gain of C4 is lower than that of the baseline, but neither is significant. Moreover, the lead time constants of both C3 and C4 are lower than those of the baseline. The inconsistent effects of the up and down dipoles at 3 rad/s on the dependent measures indicate that any Manual Control Adaptation Boundaries derived from control behavior metrics should not be derived from a single dependent measure.

Subjective ratings show no obvious change trends over different conditions. The reliability of the subjective rating scores is doubtful, since several subjects even indicated obviously notable difference between controlled dynamics which were exactly the same. No further analysis on the subjective ratings is conducted in this chapter.

The simulation predictions were validated by correlating with the experiment results of the tracking performance, control activity, target crossover frequency, target phase margin, visual gain, lead time constant and lag time constant. Simulation with remnant ratio 0.25 (and 0.3) had the highest average correlation, the remnant ratio 0.25 is selected and will be fixed for the future simulation work. The match between the simulation and experiment results shows the potential of the simulation to be used as a tool for the prediction of human operator control behavior in compensatory tracking tasks. Moreover, in order to derive a high-resolution Manual Control Adaptation Boundary, a large number of different added dynamics should be tested. Considering realistic feasible experiments, only a limited number of the possible added dynamics conditions can be tested in experiments as described in this chapter. Hence, simulation predictions can be a critical tool for increasing data resolution and the development of Manual Control Adaptation Boundaries.

4.5. CONCLUSIONS

This chapter proposed and tested a combined experimental and simulation-based methodology for deriving Manual Control Adaptation Boundaries (MCAB) which would objectively quantify human operators' sensitivity to differences in controlled system dynamics. For this, a compensatory pitch attitude tracking experiment was performed where subjects were asked to control the baseline aircraft pitch dynamics, as well as dynamics with different dipoles – "up" or "down" dipoles centered on frequencies of 1, 3, or 7 rad/s – added to this baseline system. In addition to the experiment, an offline simulation prediction of human operator adaptation to the same added dynamics was developed and verified with the experiment data. The experiment results show that, unlike expected, even added dipole dynamics located in the crossover region (3 rad/s dipoles) do not necessarily induce a significant change in tracking performance and other control behavioral parameters. Moreover, even for added dynamics well outside the crossover region (1 and 7 rad/s dipoles) still very strong changes in critical human operator parameters, such as the visual lead time constant, were observed. Finally, comparison of the effects of the up and down dipole data at the same

dipole frequency showed operators' adaptation was reflected in different performance or control behavioral metrics. Overall, these findings suggest that analysis of control behavior changes induced by added dynamics – and hence the further development of Manual Control Adaptation Boundaries – should always consider multiple control behavioral metrics (e.g., performance and human operator model parameters). Overall, the simulation prediction of changes in most considered dependent measures correlates very well with the experiment data. Therefore, such offline simulation predictions will in future work be strongly relied on in the further development of the Manual Control Adaptation Boundary, to increase its resolution and the density of tested added dynamics variations far beyond what is experimentally possible.

REFERENCES

[1] J. R. Wood and J. Hodgkinson, *Definition of Acceptable Levels of Mismatch for Equivalent Systems of Augmented CTOL Aircraft*, Tech. Rep. MDC A6792 (McDonnell Aircraft Company, St. Louis (MO), 1980).

[2] C. G. Carpenter and J. Hodgkinson, *V/STOL Equivalent Systems Analysis*, Tech. Rep. NADC-79141-60 (McDonnell Aircraft Company, St. Louis (MO), 1980).

[3] J. T. Bosworth and P. S. Williams-Hayes, *Flight Test Results from the NF-15B Intelligent Flight Control System (IFCS) Project with Adaptation to a Simulated Stabilator Failure,* in *Proceedings of the AIAA Infotech at Aerospace 2007 Conference and Exhibit, Rohnert Park (CA)*, AIAA-2007-2818 (2007).

[4] S. Geluardi, F. M. Nieuwenhuizen, L. Pollini, and H. H. Bülthoff, *Frequency Domain Identification of a Light Helicopter in Hover,* in *Proceedings of the AHS 70th Annual Forum, Montreal, Canada* (2014).

[5] M. B. Tischler, *System Identification Methods for Aircraft Flight Control Development and Validation*, NASA Technical Memorandum 110369 (NASA Ames Research Center, Moffett Field (CA), 1995).

[6] P. G. Hamel and K. Jürgen, *Advances in Rotorcraft System Identification,* Progress in Aerospace Sciences **33**, 259 (1997).

[7] Cicolani and Luigi, *Flight Test Identification and Simulation of a UH-60A Helicopter and Slung Load*, Tech. Rep. NASA/TM-2001-209619 (NASA, Ames Research Center Moffett Field, California, 2001).

[8] D. G. Mitchell, R. H. Hoh, C. He, and K. Strope, *Determination of Maximum Unnoticeable Added Dynamics,* in *Proceedings of the AIAA Atmospheric Flight Mechanics Conference and Exhibit, Keystone (CO)*, AIAA-2006-6492 (2006).

[9] S. D. Beard, S. E. Reardon, E. L. Tobias, and B. L. Aponso, *Simulation System Fidelity Assessment at the Vertical Motion Simulator,* in *Proceedings of the AHS 69th Annual Forum, Phoenix, Arizona* (2013).

[10] H. J. Damveld, M. M. van Paassen, and M. Mulder, *Cybernetic Approach to Assess Aircraft Handling Qualities,* Journal of Guidance, Control, and Dynamics **34**, 1886 (2011).

[11] C. M. Wiskemann, F. M. Drop, D. M. Pool, M. M. van Paassen, M. Mulder, and H. H. Bülthoff, *Subjective and Objective Metrics for the Evaluation of Motion Cueing Fidelity for a Roll-Lateral Reposition Maneuver,* in *AHS 70th Annual Forum* (2014).

[12] M. Mulder, P. M. T. Zaal, D. M. Pool, H. J. Damveld, and M. M. van Paassen, *A Cybernetic Approach to Assess Simulator Fidelity: Looking back and looking forward,* in *Proceedings of the AIAA Modeling and Simulation Technologies Conference, Boston (MA)*, AIAA-2013-5225 (2013).

[13] P. van den Berg, P. M. T. Zaal, M. Mulder, and M. M. van Paassen, *Conducting of Multi-modal Pilot Model Identification - Results of a Simulator Experiment,* in *AIAA Modelling and Simulation Technologies Conference, South Carolina*, AIAA-2007-6892 (2007).

[14] P. M. T. Zaal, D. M. Pool, M. Mulder, and M. M. van Paassen, *New Types of Target Inputs for Multi-Modal Pilot Model Identification,* in *Proceedings of the AIAA Modeling and Simulation Technologies Conference and Exhibit, Honolulu (HI)*, AIAA-2008-7106 (2008).

[15] P. M. T. Zaal, D. M. Pool, M. Mulder, M. M. van Paassen, and J. A. Mulder, *Identification of Multimodal Pilot Control Behavior in Real Flight,* Journal of Guidance, Control, and Dynamics **33**, 1527 (2010).

[16] D. M. Pool, M. M. van Paassen, and M. Mulder, *Modeling Human Dynamics in Combined Ramp-Following and Disturbance-Rejection Tasks,* in *Proceedings of the AIAA Guidance, Navigation, and Control Conference, Toronto, Canada, Aug. 2-5*, AIAA-2010-7914, edited by M. Silvestro (American Institute for Aeronautics and Astronautics, 2010).

[17] R. A. Hess and T. Malsbury, *Closed-loop Assessment of Flight Simulator Fidelity,* Journal of Guidance, Control, and Dynamics **14**, 191 (1991).

[18] M. Steurs, M. Mulder, and M. M. van Paassen, *A Cybernetic Approach to Assess Flight Simulator Fidelity,* in *Proceedings of the AIAA Modelling and Simulation Technologies Conference and Exhibit, Providence (RI)*, AIAA-2004-5442 (2004).

[19] A. T. Van Wieringen, *Effects of Aircraft Size on Motion Cues in Flight Simulation – A Cybernetic Analysis of Motion Cueing for a Boeing 747 in the Simona Research Simulator*, Master's thesis, Delft University of Technology (2011).

[20] D. M. Pool, *Objective Evaluation of Flight Simulator Motion Cueing Fidelity Through a Cybernetic Approach*, Ph.D. thesis, Delft University of Technology, Faculty of Aerospace Engineering (2012).

[21] F. M. Nieuwenhuizen, P. M. T. Zaal, M. Mulder, M. M. van Paassen, and J. A. Mulder, *Modeling Human Multichannel Perception and Control Using Linear Time-Invariant Models,* Journal of Guidance, Control, and Dynamics **31**, 999 (2008).

[22] P. M. T. Zaal, D. M. Pool, J. de Bruin, M. Mulder, and M. M. van Paassen, *Use of Pitch and Heave Motion Cues in a Pitch Control Task,* Journal of Guidance, Control, and Dynamics **32**, 366 (2009).

[23] M. M. van Paassen, *Biophysics in Aircraft Control, A Model of the Neuromuscular System of the Pilot's Arm*, Ph.D. thesis, Delft University of Technology, Faculty of Aerospace Engineering (1994).

[24] T. Groot, H. J. Damveld, M. Mulder, and M. M. van Paassen, *Effects of Aeroelasticity on the Pilot's Psychomotor Behavior,* in *Proceedings of the AIAA Atmospheric Flight Mechanics Conference and Exhibit, Keystone, Colorado, Aug. 21-24, 2006*, AIAA-2006-6494 (American Institute of Aeronautics and Astronautics, 2006).

[25] P. M. T. Zaal, D. M. Pool, Q. P. Chu, M. M. van Paassen, M. Mulder, and J. A. Mulder, *Modeling Human Multimodal Perception and Control Using Genetic Maximum Likelihood Estimation,* Journal of Guidance, Control, and Dynamics **32**, 1089 (2009).

[26] D. T. McRuer, D. Graham, E. S. Krendel, and W. J. Reisener, *Human Pilot Dynamics in Compensatory Systems, Theory Models and Experiments with Controlled Element and Forcing Function Variations*, Tech. Rep. AFFDL-TR-65-15 (Air Force Flight Dynamics Laboratory, Wright-Patterson Air Force Base (OH), 1965).

[27] E. van Kampen, P. M. T. Zaal, E. de Weerdt, Q. P. Chu, and J. A. Mulder, *Optimization of Human Perception Modeling Using Interval Analysis,* Journal of Guidance, Control, and Dynamics **33**, 42 (2010).

[28] E. van Kampen, *Global Optimization using Interval Analysis. Interval optimization for aerospace applications.*, Ph.D. thesis, Delft University of Technology (2010).

5

SIMULATION PREDICTION OF MANUAL CONTROL ADAPTATION BOUNDARIES

Inspired by the concept of the Maximum Unnoticeable Added Dynamics (MUAD) envelopes [1, 2], the Manual Control Adaptation Boundaries (MCAB) will be developed in this chapter. It is based on the computer offline simulation which was developed and validated in Chapter 4, to objectively quantify the sensitivity of tracking performance, control activity and human operator control behavior to the change of the controlled aircraft dynamics. In this chapter, the baseline aircraft dynamics are the same as those used in Chapter 4, and in total 504 *different added dipole dynamics over a wide frequency range and various levels of perturbation on the baseline aircraft dynamics are simulated, a number that would have been infeasible to test in the human-in-the-loop experiment. Furthermore, based on the simulation results, it can be known that how much performance, control activity and human operator control behavior would deviate from those of the baseline for the added dynamics which are within the original MUAD envelopes [1]. The Manual Control Adaptation Boundaries developed in this chapter will be partially validated in Chapter 6 by experiment.*

The content of this chapter will be submitted to the following paper:
T. Lu, D. M. Pool, M. M. van Paassen, and M. Mulder, Simulation Prediction of Objective Manual Control Adaptation Boundaries in Aircraft Pitch Tracking Tasks, Journal of Guidance, Control, and Dynamics.

5.1. INTRODUCTION

Since the development of the Maximum Unnoticeable Added Dynamics (MUAD) envelopes in 1980 [1], these have been applied to assess the aircraft model fidelity [3–7] and evaluate the effects of augmented control system on baseline aircraft dynamics [8]. The main motivation to use MUAD in these research is that as long as the mismatches of the magnitude and phase between the modified aircraft dynamics and the baseline aircraft dynamics remain within the MUAD, it is assumed that the modified aircraft dynamics have equivalent handling quality with the baseline aircraft dynamics, and the difference would not be noticed by human operators. Even though a recent research indicates that MUAD may depend on the bandwidth of the baseline aircraft dynamics, the original MUAD [1] is still widely used.

However, the baseline dynamics used to develop the MUAD [1] are different from the ones used in recent research [3–8]. It is unknown whether the shape of the MUAD envelopes would change, for example, in case different baseline dynamics or added dynamics are used. The main drawback of the MUAD [1] is that it is purely based on subjective ratings, and cannot quantify human operator control behavior. In contrast, the "*cybernetic approach*" developed in recent years [9–13] can not only identify and quantify the human operator control behavior in manual control tasks, but also can be used as a powerful tool to predict the performance, control activity and human operator control behavior with any provided controlled dynamics [14–16]. To tie in with the concept of the original MUAD [1] which provides information about qualitative noticeability on the mismatch in different dynamics in frequency domain, the Manual Control Adaptation Boundaries are desired to be developed, which could quantify the objective sensitivity of the performance, control activity and human operator control behavior to the change of the controlled dynamics. Using the cybernetic approach, the human control behavior can be predicted well for a wide range of baseline aircraft dynamics and added dynamics. Moreover, a large variations of added dynamics with a wide frequency range and various levels of perturbation on the baseline aircraft dynamics need to be simulated to form the Manual Control Adaptation Boundaries in frequency domain. It would be practically infeasible for any human-in-the-loop experiment to cover such a large number of conditions.

In this chapter the main objective is to develop the Manual Control Adaptation Boundaries (MCAB) based on the simulation developed in Chapter 4. In Chapter 3 it was also found that the interaction between the baseline (bandwidth) and added dynamics has no effect on performance, control activity or human operator control behavior (trends over different added dynamics conditions are equivalent between low and high-bandwidth baseline dynamics). In this chapter, the baseline aircraft dynamics are the same as those used in Chapter 4. The added dynamics are still dipoles as used in Chapter 4, since these provide easy modification of the magnitude of the controlled system at a selected natural frequency. Based on the simulation results to be developed in this chapter, it is of interest to know how much the human operator control behavior would deviate from the baseline for the added dynamics within the original MUAD [1]. This could provide quantitative information on performance, control activity and human operator control behavior for added dynamics which are supposed to be subjectively unnoticeable.

This chapter starts by introducing the simulation control task, simulation settings and conditions in Section 5.2. Then the methods of formulating the Manual Control Adaptation

Boundaries are introduced, and the added dynamics within the original MUAD [1] are selected. The overall simulation results, Manual Control Adaptation Boundaries and analysis on the dynamics within the original MUAD [1] are shown in Section 5.3. This chapter ends with a discussion and conclusions.

5.2. METHODS

5.2.1. CONTROL TASK

Exactly the same aircraft pitch attitude tracking task as carried out in Chapter 4 is used in this chapter for the simulation, see Figure 5.1. The human operator (model) $H_p(s)$ both tracks the target f_t and rejects the disturbance f_d in order to minimize the error e by controlling the aircraft pitch angle θ. The signal u is the human operator (model) control output, u_s is the control output after the stick gain ($K_s = 1$), u_a is the control output after the added dynamics $H_{added}(s)$, and δ_e is the input signal into the baseline aircraft dynamics $H_{added}(s)$. The target forcing function, disturbance forcing function, the structure of the human operator model, added dynamics and baseline aircraft dynamics are the same as those used in Chapter 4.

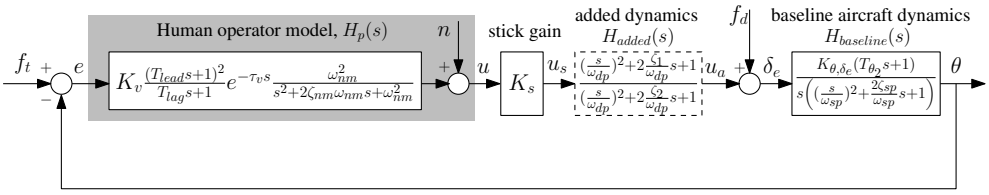

Figure 5.1: A schematic representation of the aircraft pitch attitude tracking task for simulation.

5.2.2. SIMULATION SETTINGS AND CONDITIONS

The constrained nonlinear optimization based simulation developed in Chapter 4 is used to optimize the human operator visual gain K_v, lead time constant T_{lead} and lag time constant T_{lag} (Figure 5.1) in order to minimize the normalized tracking performance $\sigma_e^2/\sigma_{f_t}^2$. Since $\sigma_{f_t}^2$ is a constant and f_t is the same for all chapters in this thesis expect Chapter 3, all the analyses in the remainder of this thesis with respect to the tracking performance will use σ_e^2. To increase the chance of finding a global optimal solution, more initial guesses for the optimization variables are added in the simulation conducted in this chapter as compared to Chapter 4, as can be seen in Eq. (5.1):

$$\begin{aligned} \hat{\omega}_{c,t,0} &= \{0.5, 1, 2, 3, 4, 5\} && \text{rad/s} \\ \hat{\phi}_{m,t,0} &= \{20, 40, 60, 80, 100, 120\} \cdot (\frac{\pi}{180}) && \text{rad} \\ \hat{T}_{lag,0} &= \{0.5, 1, 2, 3, 4, 5\} && \text{s}, \end{aligned} \tag{5.1}$$

where $\hat{\omega}_{c,t,0}$ are the initial guesses of the target crossover frequency, $\hat{\phi}_{m,t,0}$ are the initial guesses of the target phase margin, and $\hat{T}_{lag,0}$ are the initial guesses of the human operator

lag time constant. In the simulations of this chapter, in total there are 216 sets of different initial guesses for the optimization of each condition.

The constants of the simulation in Figure 5.1 include the target and disturbance forcing functions f_t and f_d, the human operator visual time delay τ_v, neuromuscular damping ratio ζ_{nm} and natural frequency ω_{nm}, stick gain K_s and all the parameters of the baseline aircraft dynamics (K_{θ,δ_e}, T_{θ_2}, ζ_{sp}, ω_{sp}). The values of these constants can all be found in Chapter 4. In the simulation, the ratio of the variance of the remnant and the variance of the control signal σ_n^2/σ_u^2 is kept at 0.25, which is one of the main tuning results of Chapter 4.

For manual control tasks, since the human manual control behavior is most sensitive in the frequency band located near the crossover frequency [17], which is also reflected in the MUAD envelopes where the boundaries are the narrowest [1, 2], it would be reasonable to select ω_{dp} near and within the crossover region. The range of the damping ratios of the dipole dynamics ζ_1 and ζ_2 are usually between 0 and 1. For these considerations the simulation conditions are the full factorial combinations of ω_{dp}, ζ_1 and ζ_2 in the ranges of:

$$\begin{aligned} \omega_{dp} &\in \{1,2,3,4,5,6,7\}, && \text{rad/s} \\ \zeta_1 &\in \{0.1,0.2,0.3,0.4,0.5,0.6,0.7,0.8,0.9\}, && \text{-} \\ \zeta_2 &\in \{0.1,0.2,0.3,0.4,0.5,0.6,0.7,0.8,0.9\}, && \text{-}, \end{aligned} \tag{5.2}$$

where for each ω_{dp}, 36 "up" dipoles ($\zeta_1 > \zeta_2$) and 36 "down" dipoles ($\zeta_2 > \zeta_1$) dynamics are simulated (excluding the combinations where $\zeta_1 = \zeta_2$). The baseline aircraft dynamics (obtained when $\zeta_1 = \zeta_2$ and the numerator and denominator of H_{added}(s) in Figure 5.1 cancel each other) are also added as the reference. In total this gives $7(\omega_{dp}) \times 72(\zeta_1, \zeta_2) + 1$(Baseline) = 505 simulation conditions, a number that is practically infeasible for any human-in-the-loop experiment. Since not only σ_n^2/σ_u^2 but also the power spectral density of the remnant n affect the simulated performance, control activity and human operator control behavior, 100 noise realizations are simulated for each condition to be able to investigate the average effect of the remnant n.

5.2.3. MANUAL CONTROL ADAPTATION BOUNDARIES FORMULATION

DEPENDENT MEASURES QUANTIFYING MCAB

The main goal of this chapter is to develop Manual Control Adaptation Boundaries (MCAB), based on the simulation results. Compared with the original MUAD envelopes [1] which only provide qualitative information on the noticeability of the change of controlled dynamics, it is desired that the Manual Control Adaptation Boundaries to be developed in this chapter could provide quantitative information on the sensitivities of tracking performance, control activity and human operator control behavior with respect to the change of controlled dynamics.

The dependent measures of the simulation developed in Chapter 4 include the performance σ_e^2, control activity σ_u^2, visual gain K_v, lead time constant T_{lead}, lag time constant TI_{lag}, target crossover frequency $\omega_{c,t}$ and target phase margin $\phi_{m,t}$. In the performed simulation predictions, the visual time delay τ_v, neuromuscular damping ratio ζ_{nm} and natural frequency ω_{nm} were treated as constants. Since $\omega_{c,t}$ and $\phi_{m,t}$ are functions of the human operator model parameters (K_v, T_{lead}, T_{lag}, τ_v, ζ_{nm}, ω_{nm}) and controlled dynamics, $\omega_{c,t}$

and $\phi_{m,t}$ are not explicitly taken as the variables quantifying the Manual Control Adaptation Boundaries. Moreover, since the visual time delay τ_v, neuromuscular damping ratio ζ_{nm} and natural frequency ω_{nm} representing the physical limits of the human operator and do not change much (treated as constants in the simulation), these parameters are not selected to quantify the Manual Control Adaptation Boundaries.

In Chapter 4, the average value of the identified lag time constant T_{lag} over selected experiment conditions was around 2 s, indicating that the gain of the frequency response of the human operator starts to decrease at $1/T_{lag} = 0.5$ rad/s, which is near the lowest frequency component 0.46 rad/s of the target forcing function f_t. Thus the estimation accuracy of T_{lag} could be low. Moreover, since the lag time constant T_{lag} is at the denominator and the visual gain K_v is at the nominator of the human operator model $H_p(s)$ (see Figure 5.1), the potential coupling between T_{lag} and K_v could result in low estimation accuracy for K_v as well. Therefore, the ratio of the visual gain and lag time constant, or the "low-frequency gain" K_v/T_{lag} is proposed as a new dependent measure replacing the individual K_v and T_{lag}.

According to Chapter 4, it is known that even though the correlations of the trends between the simulation and experiment results are high for the tracking performance, control activity and human operator model parameters, the absolute values of these dependent measures are usually not the same between the simulation and experiment. However, rather than considering the absolute values, the relative changes of these dependent measures with respect to those of the baseline dynamics are of interest for predicting the quantitative sensitivities. For example, the relative change of the performance with respective to that of the baseline dynamics can be defined as:

$$\Delta\sigma_e^2 = \frac{\sigma_e^2 - \sigma_{e,H_{baseline}}^2}{\sigma_{e,H_{baseline}}^2} \times 100\%, \tag{5.3}$$

where σ_e^2 is the performance with certain added dipole dynamics, $\sigma_{e,H_{baseline}}^2$ is the performance with the baseline dynamics. Similarly, Eq. (5.3) can also be applied to the control activity, the ratio of the visual gain and lag time constant and lead time constant, which are chosen as the dependent measures quantifying the Manual Control Adaptation Boundaries (MCAB):

$$P_{MCAB} = [\Delta\sigma_e^2, \Delta\sigma_u^2, \Delta\frac{K_v}{T_{lag}}, \Delta T_{lead}], \tag{5.4}$$

where $\Delta\sigma_u^2$ is the relative change of control activity with respect to that of the baseline, $\Delta K_v/T_{lag}$ is the relative change of the ratio of the visual gain and lag time constant with respect to that of the baseline, and ΔT_{lead} is the relative change of lead time constant with respect to that of the baseline. Strictly speaking, performance σ_e^2 and control activity σ_u^2 are also functions of the human operator model parameters and controlled dynamics. Due to the fact that human operator may first notice the change of performance and control activity when the controlled dynamics change, $\Delta\sigma_e^2$ and $\Delta\sigma_u^2$ are also included in the variables quantifying the Manual Control Adaptation Boundaries.

MCAB FOR INDIVIDUAL DEPENDENT MEASURES

Several features are desired for the Manual Control Adaptation Boundaries (MCAB). First, in the frequency domain they can provide information on the relative changes of the dependent measures (see Eq. (5.4)) with respect to the baseline dynamics based on where the added dynamics are located (within or outside the boundaries). Second, the boundaries with higher relative changes of the dependent measures should enclose the ones with lower relative changes. Third, the Manual Control Adaptation Boundaries should be automatically generated based on the simulation data, rather than the methods used in [1, 2] which provided some freedom in formulating the boundaries.

Figure 5.2a shows an example of formulating the Manual Control Adaptation Boundary of magnitude of control activity. According to the range of the allowed change on control activity, for example, $-20\% \leq \Delta\sigma_u^2 \leq 20\%$, all the qualified dipole dynamics can be found based on the simulation results obtained in this chapter. The magnitudes of these qualified dynamics are plotted in frequency domain. Frequencies of $\omega_{MCAB} = 1,2,3,4,5,6$ and 7 rad/s are chosen as the frequency nodes of the boundaries, since these frequencies were used as the dipole natural frequency ω_{dp} in the simulation and at $\omega = \omega_{dp}$ up dipole dynamics have maximum magnitude and down dipole dynamics have minimum magnitude (in dB). At $\omega_{MCAB} = 1$ rad/s, for example, the up dipole dynamics with the maximum magnitude among all the qualified up dipole dynamics of $\omega_{dp} = 1$ rad/s is chosen as the "outermost" qualified dipole dynamics. The Manual Control Adaptation Boundary of magnitude is then formulated by connecting all the peak points of these "outermost" qualified dipole dynamics, as can be seen in Figure 5.2a.

Figure 5.2b shows an example of formulating the Manual Control Adaptation Boundary of phase of control activity. Since the maximum and minimum phases of dipole dynamics do not occur at ω_{dp} and the frequencies corresponding to these maximum and minimum phases depend on the damping ratios ζ_1 and ζ_2, unlike the magnitude boundaries, the connecting points of the phase boundary are not necessary the maximum or minimum phases of the qualified dipole dynamics. Moreover, if the frequency nodes of the phase boundary were chosen based on the shifting frequencies corresponding with the maximum and minimum phases of dipole dynamics, it would be possible that part of the phase boundary of 20% relative change is outside the one of 30%. Therefore, the connecting point above the 0 degree line in Figure 5.2b, for example, at $\omega = 1$ rad/s, corresponds with the dipole dynamics with the maximum phase among all the qualified up and down dipole dynamics for $\omega_{dp} = 1,2,3,4,5,6$ and 7 rad/s.

In Figure 5.2, both magnitude and phase boundaries guarantee that for any other added dipole dynamics, if its magnitude or phase is outside the boundary(s) at $\omega = \omega_{MCAB}$, for example, the relative change of control activity is either $\Delta\sigma_u^2 < -20\%$ or $\Delta\sigma_u^2 > 20\%$. However, due to the lack of simulation data, no information can be provided between any two adjacent frequency nodes. Moreover, for any other added (dipole) dynamics totally within the boundaries, it is not guaranteed that $-20\% \leq \Delta\sigma_u^2 \leq 20\%$.

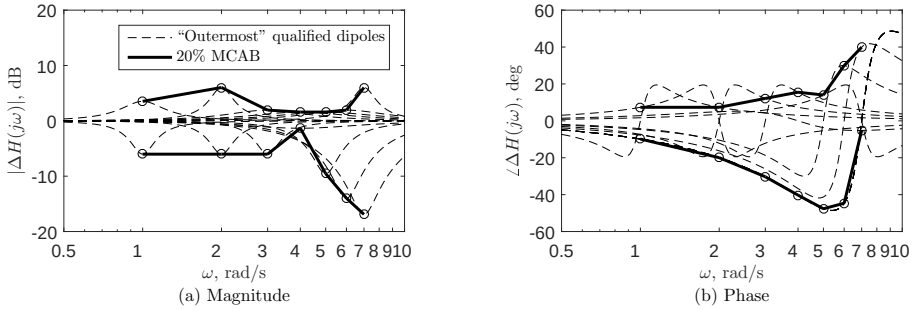

(a) Magnitude (b) Phase

Figure 5.2: An example of formulating the Manual Control Adaptation Boundaries (MCAB) for control activity based on the "outermost" qualified dipole dynamics, of which $-20\% \leq \Delta\sigma_u^2 \leq 20\%$.

INTEGRATED MANUAL CONTROL ADAPTATION BOUNDARIES

Based on the simulation data, the Manual Control Adaptation Boundaries for all the dependent measures in Eq. (5.4) can be formulated according to the approach shown in Figure 5.2, respectively. Then the *Integrated Manual Control Adaptation Boundaries* (IMCAB, for example, magnitude boundary) can be obtained by seeking the intersection part of the Manual Control Adaptation Boundaries of performance, control activity, ratio of the visual gain and lag time constant and the lead time constant (see Figures 5.3 and 5.4). If the magnitude and phase of any added dipole dynamics are within the Integrated Manual Control Adaptation Boundaries, the values of the variables in Eq. (5.4) could be constrained within the the relative change level corresponding with the boundaries.

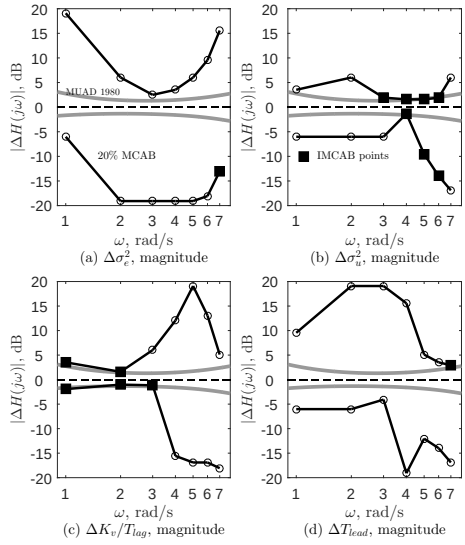

(a) $\Delta\sigma_e^2$, magnitude (b) $\Delta\sigma_u^2$, magnitude

(c) $\Delta K_v/T_{lag}$, magnitude (d) ΔT_{lead}, magnitude

Figure 5.3: An example of the Manual Control Adaptation Boundaries (MCAB) of magnitude of 20%. The solid points closest to the 0 dB line form Figure 5.4.

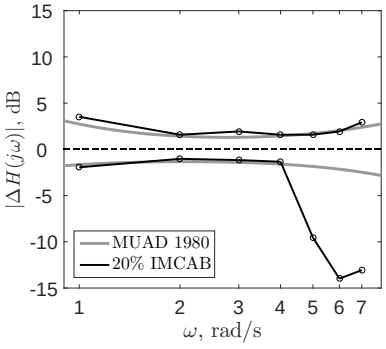

Figure 5.4: An example of the Integrated Manual Control Adaptation Boundary (IMCAB) of magnitude of 20%, based on all the solid points in Figure 5.3.

5.2.4. ADDED DYNAMICS WITHIN MUAD OF 1980

For all the simulation conditions (Eq. (5.2)), it is of interest to know which added dipole dynamics are within the previously determined MUAD envelopes [1] and how much variation in tracking performance, control activity, target crossover frequency, target phase margin and human operator control behavior is still present within this range of added dynamics. This provides a quantitative estimate of the maximum amount of the change in these objective variables when the added dynamics are supposed subjectively unnoticeable [1, 2].

MUAD OF 1980

In order to identify the added dipole dynamics within the MUAD envelopes [1], the magnitude and phase of the MUAD envelopes are needed first. According to [1], in total four transfer functions were derived to represent the MUAD Upper Gain Envelope, Lower Gain Envelope, Upper Phase Envelope and Lower Phase Envelope, respectively:

$$|H_{Upper}(s)| = |\frac{3.16s^2 + 31.61s + 22.79}{s^2 + 27.14s + 1.84}|, \tag{5.5}$$

$$|H_{Lower}(s)| = |\frac{0.0955s^2 + 9.92s + 2.15}{s^2 + 11.6s + 4.95}|, \tag{5.6}$$

$$\angle H_{Upper}(s) = \angle \frac{68.89s^2 + 1100.12s - 275.22}{s^2 + 39.94s + 9.99} e^{0.0059s}, \tag{5.7}$$

$$\angle H_{Lower}(s) = \angle \frac{475.32s^2 + 184100s + 29456.1}{s^2 + 11.66s + 0.0389} e^{-0.0072s}. \tag{5.8}$$

DIPOLE DYNAMICS WITHIN MUAD OF 1980

It is known that the up dipole dynamics ($\zeta_1 > \zeta_2$) have the maximum magnitude and the down dipole dynamics ($\zeta_1 < \zeta_2$) have the minimum magnitude (in dB) when $\omega = \omega_{dp}$. Here it is assumed that if the magnitude with the up dipole dynamics at ω_{dp} is lower than the Upper Gain Envelope, or when the magnitude with the down dipole dynamics at ω_{dp} is higher than the Lower Gain Envelope, this dipole is within the MUAD gain envelope:

$$\begin{aligned} |H_{added}(j\omega_{dp})| &\leq |H_{Upper}(j\omega_{dp})|, \forall \zeta_1 > \zeta_2 \\ |H_{added}(j\omega_{dp})| &\geq |H_{Lower}(j\omega_{dp})|, \forall \zeta_2 > \zeta_1. \end{aligned} \tag{5.9}$$

However, the maximum and minimum phases of the dipole dynamics do not occur at $\omega = \omega_{dp}$. It is assumed that if the maximum phase of the dipole dynamics is lower than the Upper Phase Envelope (at the frequency where $\angle H_{added}(j\omega)$ is maximum), and if the minimum phase of the dipole dynamics is higher than the Lower Phase Envelope (at the frequency where $\angle H_{added}(j\omega)$ is minimum), this dipole is within the MUAD phase envelope:

$$\begin{aligned} \angle H_{added}(j\omega)_{max} &\leq \angle H_{Upper}(j\omega) \\ \angle H_{added}(j\omega)_{min} &\geq \angle H_{Lower}(j\omega), \end{aligned} \tag{5.10}$$

Figure 5.5a shows an added dipole within the MUAD magnitude envelope according to Eq. (5.9), the vertical dashed line shows the natural frequency of the added dipole dynamics ω_{dp}. Figure 5.5b shows an added dipole within the MUAD phase envelope according to Eq. (5.10). The dashed vertical lines show the frequency ω_{max} corresponding with the maximum phase, the natural frequency ω_{dp} and the frequency ω_{min} corresponding with the minimum phase of the added dipole dynamics, respectively.

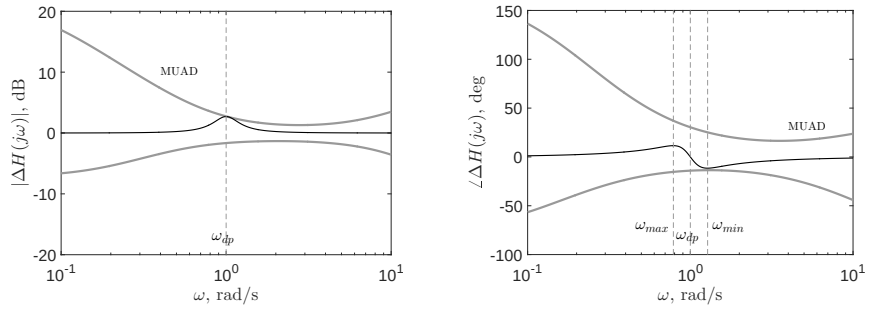

(a) Magnitude (b) Phase

Figure 5.5: An example of an added dipole within the MUAD magnitude envelope and an added dipole within the MUAD phase envelope.

For all considered added dipole dynamics for the simulation (see Eq. (5.2)), the dipoles with parameter combinations that satisfy both Eq. (5.9) and Eq. (5.10) are shown in Figure 5.6 together with the MUAD envelopes [1]. In total 59 out of 504 dipoles used in the simulation are within the MUAD. It can be seen that the magnitude envelope is more critical than the phase envelope to constrain the qualified dipole dynamics. The parameters of these dipole dynamics are summarized in Table 5.1. As can be seen in Table 5.1, with the current simulation condition resolution (Eq. (5.2)), most dipole dynamics within the MUAD envelopes are at $\omega = 1,5,6$ and 7 rad/s. At $\omega = 2,3$ and 4 rad/s, fewer dipoles can be found due to the fact that the MUAD magnitude envelope is narrowest around these frequencies. It can be also noticed that $|\zeta_1 - \zeta_2| \leq 0.2$ for all the qualified dipoles in Table 5.1.

5.3. RESULTS

To determine the model-based Manual Control Adaptation Boundaries, offline simulations are performed for all conditions listed in Section 5.2.2. The simulation results are then derived into the Manual Control Adaptation Boundaries for the individual dependent measures based on the methods introduced in Section 5.2.3, which are finally combined into the Integrated Manual Control Adaptation Boundaries. The effects of the added dipole dynamics within the original MUAD envelopes [1] are analyzed at the end of this section.

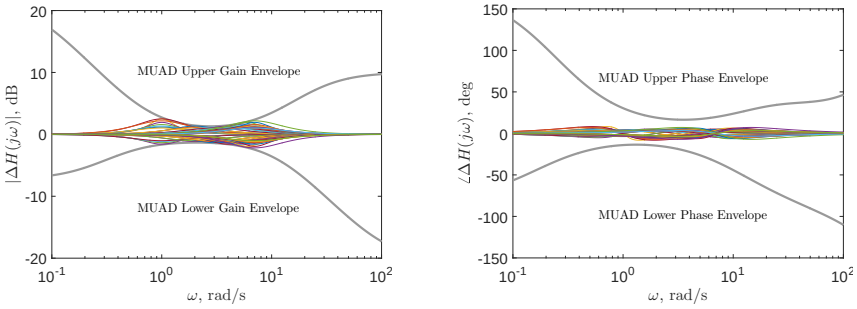

(a) Magnitude (b) Phase

Figure 5.6: MUAD [1] with the tested added dipole dynamics within the envelopes.

Table 5.1: The parameters of all added dipole dynamics within the MUAD envelopes [1].

$[\zeta_1,\zeta_2]$	1 rad/s	2 rad/s	3 rad/s	4 rad/s	5 rad/s	6 rad/s	7 rad/s
	0.4, 0.3						
	0.5, 0.4					0.5, 0.4	0.5, 0.4
Up dipole	0.6, 0.5				0.6, 0.5	0.6, 0.5	0.6, 0.5
$\zeta_1 > \zeta_2$	0.7, 0.6	0.7, 0.6		0.7, 0.6	0.7, 0.6	0.7, 0.6	0.7, 0.6
	0.8, 0.6						
	0.8, 0.7	0.8, 0.7	0.8, 0.7	0.8, 0.7	0.8, 0.7	0.8, 0.7	0.8, 0.7
							0.9, 0.7
	0.9, 0.8	0.9, 0.8	0.9, 0.8	0.9, 0.8	0.9, 0.8	0.9, 0.8	0.9, 0.8
	0.4, 0.5					0.4, 0.5	0.4, 0.5
	0.5, 0.6			0.5, 0.6	0.5, 0.6	0.5, 0.6	0.5, 0.6
Down dipole	0.6, 0.7		0.6, 0.7	0.6, 0.7	0.6, 0.7	0.6, 0.7	0.6, 0.7
$\zeta_2 > \zeta_1$	0.7, 0.8	0.7, 0.8	0.7, 0.8	0.7, 0.8	0.7, 0.8	0.7, 0.8	0.7, 0.8
							0.7, 0.9
	0.8, 0.9	0.8, 0.9	0.8, 0.9	0.8, 0.9	0.8, 0.9	0.8, 0.9	0.8, 0.9

5.3.1. OVERALL SIMULATION RESULTS

As will be seen and discussed in the later part of this section, the patterns of the tracking performance between the up and down dipole dynamics are similar for $\omega_{dp} = 2,3,4,5,6$ and 7 rad/s, and for $\omega_{dp} = 1$ rad/s, the patterns of the tracking performance between the up and down dipole dynamics are inversed compared with other dipole frequencies. Considering the representativeness and conciseness, Figures 5.8, 5.9 and 5.10 show the simulation results for $\omega_{dp} = 1,2$ and 3 rad/s, respectively. Simulation results for $\omega_{dp} = 4,5,6$ and 7 rad/s can be found in Appendix C. Each subfigure shows the optimal tracking results for all 36(down dipoles) + 1(baseline) + 36(up dipoles) = 73 conditions. The vertical line in the center indicates the baseline dynamics (B) and separates the left half of the figure with down dipole dynamics and the right half with up dipole dynamics. The horizontal dashed line indicates the median of the baseline.

In Figures 5.9a and 5.10a, it can be seen that the performance for $\omega_{dp} = 2$ and 3 rad/s shows similar patterns. The performance with the down dipole dynamics is either better than or equivalent to that of the baseline, while the performance with the up dipole dynamics is generally worse than that of the baseline. However, for $\omega_{dp} = 1$ rad/s the performance

with the down dipole dynamics in Figure 5.8a is in general worse than that with the up dipole dynamics. Comparing Figures 5.8a and 5.9a, the pattern of the performance of the up and down dipoles are inversed, where ω_{dp} only changes from 1 rad/s to 2 rad/s.

To further analyze this sudden change in the performance, the open-loop and closed-loop frequency responses of the baseline dynamics, down dipole dynamics H_{h1c1} ($\omega_{dp} = 1$ rad/s, $\zeta_1 = 0.1$, $\zeta_2 = 0.9$ with the worst performance for $\omega_{dp} = 1$ rad/s) and corresponding down dipole dynamics H_{h2c2} ($\omega_{dp} = 2$ rad/s, $\zeta_1 = 0.1$, $\zeta_2 = 0.9$) are shown in Figure 5.7. To generate Figure 5.7, the median values of the human operator visual gain K_v, lead time constant T_{lead} and lag time constant T_{lag} over 100 noise realizations were used for each set of dynamics. In each subfigure, multiple vertical lines are drawn to indicate the target crossover frequency $\omega_{c,t}$ for each dynamics. In Figure 5.7c, due to the much higher gain around between 0.3 rad/s and 1.5 rad/s, the performance of H_{h1c1} is much worse than that of the baseline. However, for H_{h2c2}, its gain is much lower than that of baseline around between 0.1 rad/s and 1 rad/s, but higher than that of the baseline around between 1 rad/s and 2.7 rad/s, which makes the performance of H_{h2c2} equivalent to that of the baseline. To investigate whether the optimal control behavior of H_{h2c2} can be applied to the controlled dynamics of H_{h1c1} to improve the performance, the human operator visual gain K_v, lead time constant T_{lead} and lag time constant T_{lag} of H_{h2c2} are applied to the controlled dynamics of H_{h1c1}, with the results indicated as H_{h2c1} in Figure 5.7. In Figure 5.7a it can be seen that the gain of H_{h2c1} is higher than that of H_{h1c1}, and the target crossover frequency of H_{h2c1} is the highest among all the dynamics. In Figure 5.7b, however, the phase margin of H_{h2c1} is so low that the system becomes marginally stable. In Figure 5.7c, the closed-loop magnitude of H_{h2c1} largely overshoots at around the target crossover frequency 4.4 rad/s, which corresponds with the low phase margin in Figure 5.7b. In short, if the control behavior of H_{h2c2} is applied to the dynamics of H_{h1c1}, the performance could become even worse since the system becomes much less stable compared with the original case of H_{h1c1}. This indicates that the performance of H_{h1c1} could hardly be further improved given the current optimal control behavior shown in Figure 5.8.

In Figures 5.8b, 5.9b and 5.10b, it can be seen that the control activity for each ω_{dp} shows similar patterns. For example, in Figure 5.8b, the control activity for the down dipole dynamics is generally higher than that of the baseline, while the control activity with the up dipole dynamics is considerably lower. This is due to the fact that the down dipole dynamics reduce the overall gain of the controlled dynamics, and the human operator needs larger control inputs to compensate. The up dipole dynamics increase the gain of the controlled dynamics, and the human operator only needs a lower gain and control activity. Expected matching variations in visual gain K_v are also found in Figures 5.8e, 5.9e and 5.10e.

The lead time constant T_{lead} is usually generated by human operators to increase the open-loop system phase around $\omega_{c,t}$. For $\omega < \omega_{dp}$, the down dipole dynamics decrease and the up dipole dynamics increase the phase of the controlled system. For $\omega > \omega_{dp}$, the down dipole dynamics increase and the up dipole dynamics decrease the phase of the controlled system. For example, as can be seen in Figures 5.8f, 5.9f and 5.10f, the lead time constant with the down dipole dynamics is generally lower than that of the baseline. This may be due to the fact that for $\omega_{dp} = 1,2$ and 3 rad/s, down dipoles increase the stability of the system. Depending on the frequency at which the dipole is located, it could either decrease the stability of the controlled system or vice versa, thus the lead time constant is expected

to vary depending on both the dipole natural frequency and damping ratios.

Figures 5.11 shows the ratio of the visual gain and lag time constant K_v/T_{lag} (a variable quantifying the Manual Control Adaptation Boundaries, see Eq. (5.4)) for $\omega_{dp} = 1, 2$ and 3 rad/s. In general, for all three frequencies of ω_{dp}, K_v/T_{lag} with the down dipole dynamics is higher than that with the up dipole dynamics. Furthermore, K_v/T_{lag} with the down dipole dynamics of $\omega_{dp} = 1$ rad/s is in general lower than that of $\omega_{dp} = 1$ and 2 rad/s.

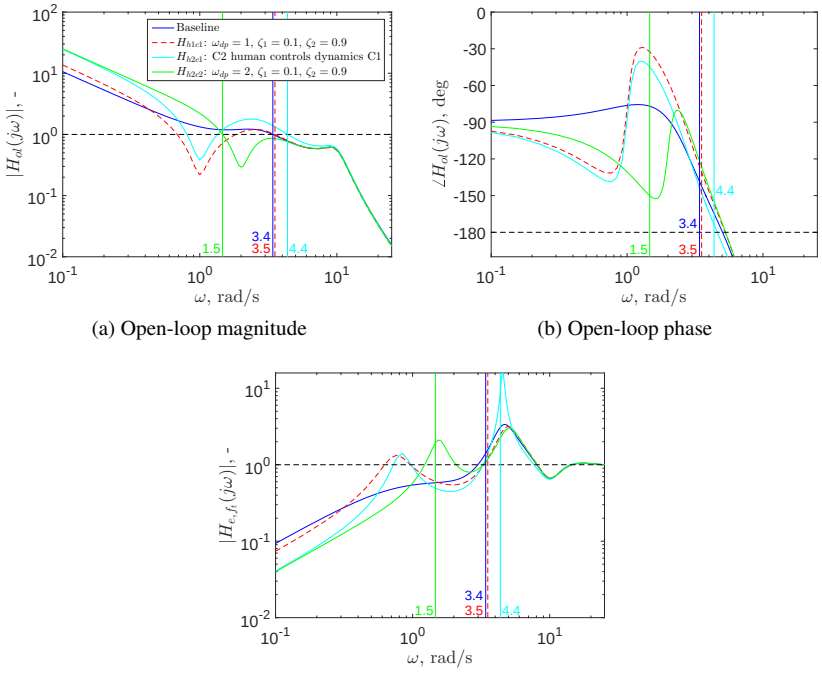

(a) Open-loop magnitude

(b) Open-loop phase

(c) Closed-loop magnitude

Figure 5.7: Open-loop and closed-loop analysis on baseline, down dipole ($\omega_{dp} = 1$ rad/s, $\zeta_1 = 0.1$, $\zeta_2 = 0.9$), and down dipole ($\omega_{dp} = 2$ rad/s, $\zeta_1 = 0.1$, $\zeta_2 = 0.9$) conditions.

5.3.2. MANUAL CONTROL ADAPTATION BOUNDARIES

OVERALL EFFECTS OF ADDED DIPOLE DYNAMICS

Table 5.2 contains 28 figures which illustrate the overall effects of the added dipole dynamics on the relative changes of performance, control activity and human operator model parameters with respect to the baseline dynamics. Each row of Table 5.2 corresponds with the natural frequency of the dipole dynamics ω_{dp}, and the columns of Table 5.2 correspond with the relative changes of performance $\Delta\sigma_e^2$, control activity $\Delta\sigma_u^2$, ratio of the visual gain and lag time constant $\Delta K_v/T_{lag}$, and lead time constant ΔT_{lead}, respectively. The size of the relative changes can be seen by referring to the color-bar (with 10% as interval). The diagonal of each figure represents the baseline condition (B) where $\zeta_1 = \zeta_2$, above the diagonal are the down dipole dynamics (Down) where $\zeta_1 < \zeta_2$ and below the diagonal are the up dipole dynamics (Up) where $\zeta_1 > \zeta_2$.

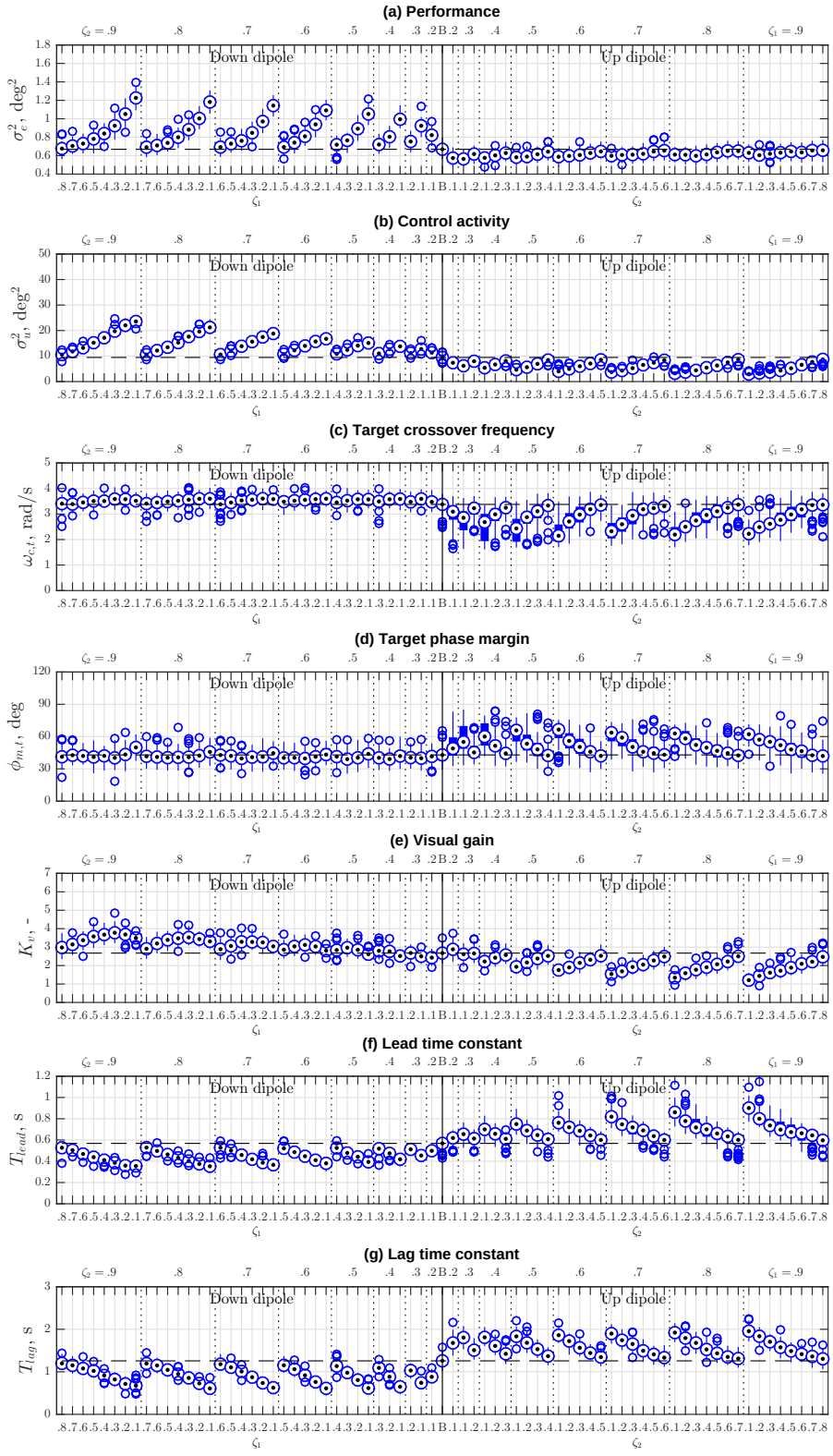

Figure 5.8: All simulation results at $\omega_{dp} = 1$ rad/s.

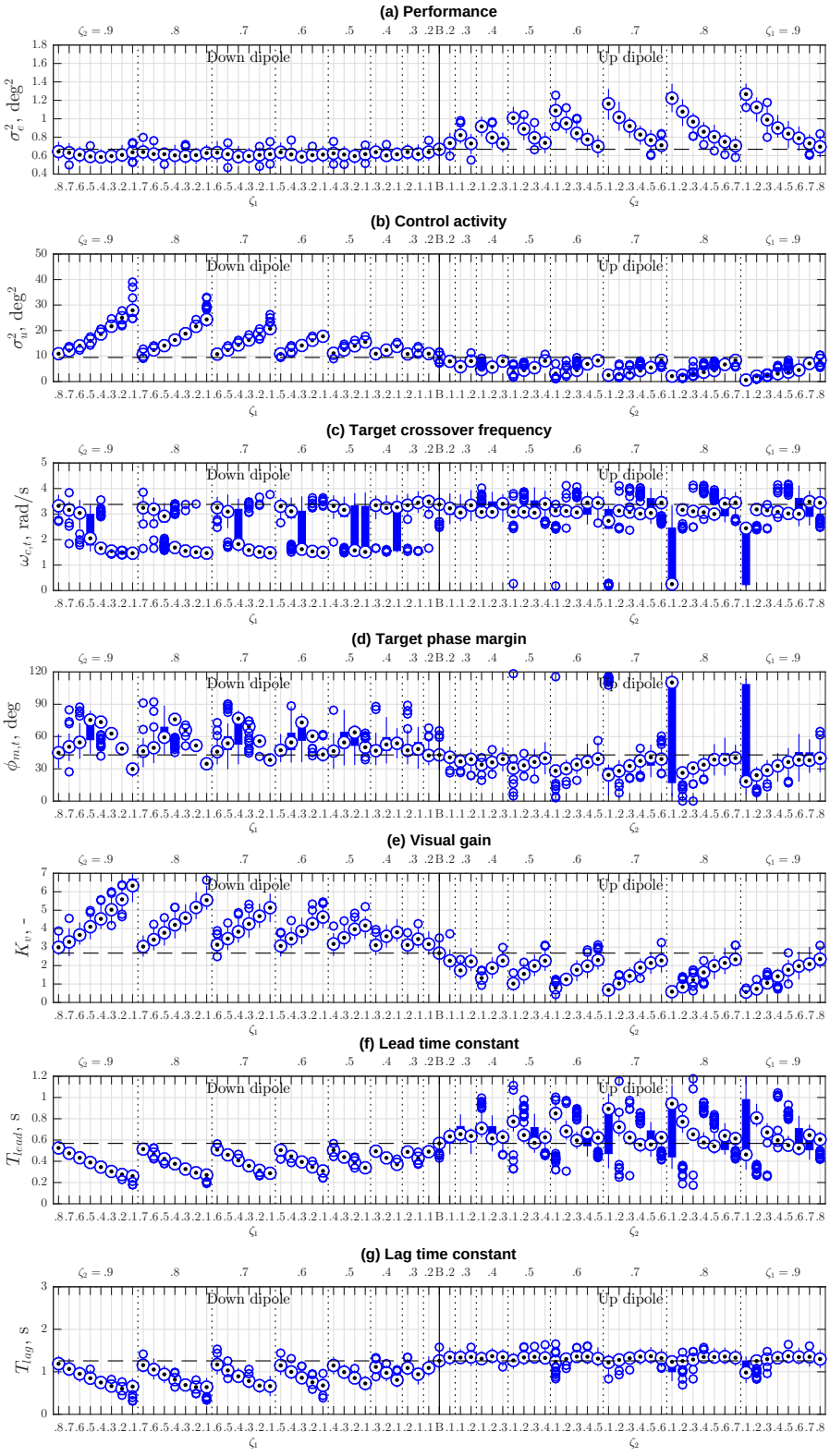

Figure 5.9: All simulation results at $\omega_{dp} = 2$ rad/s.

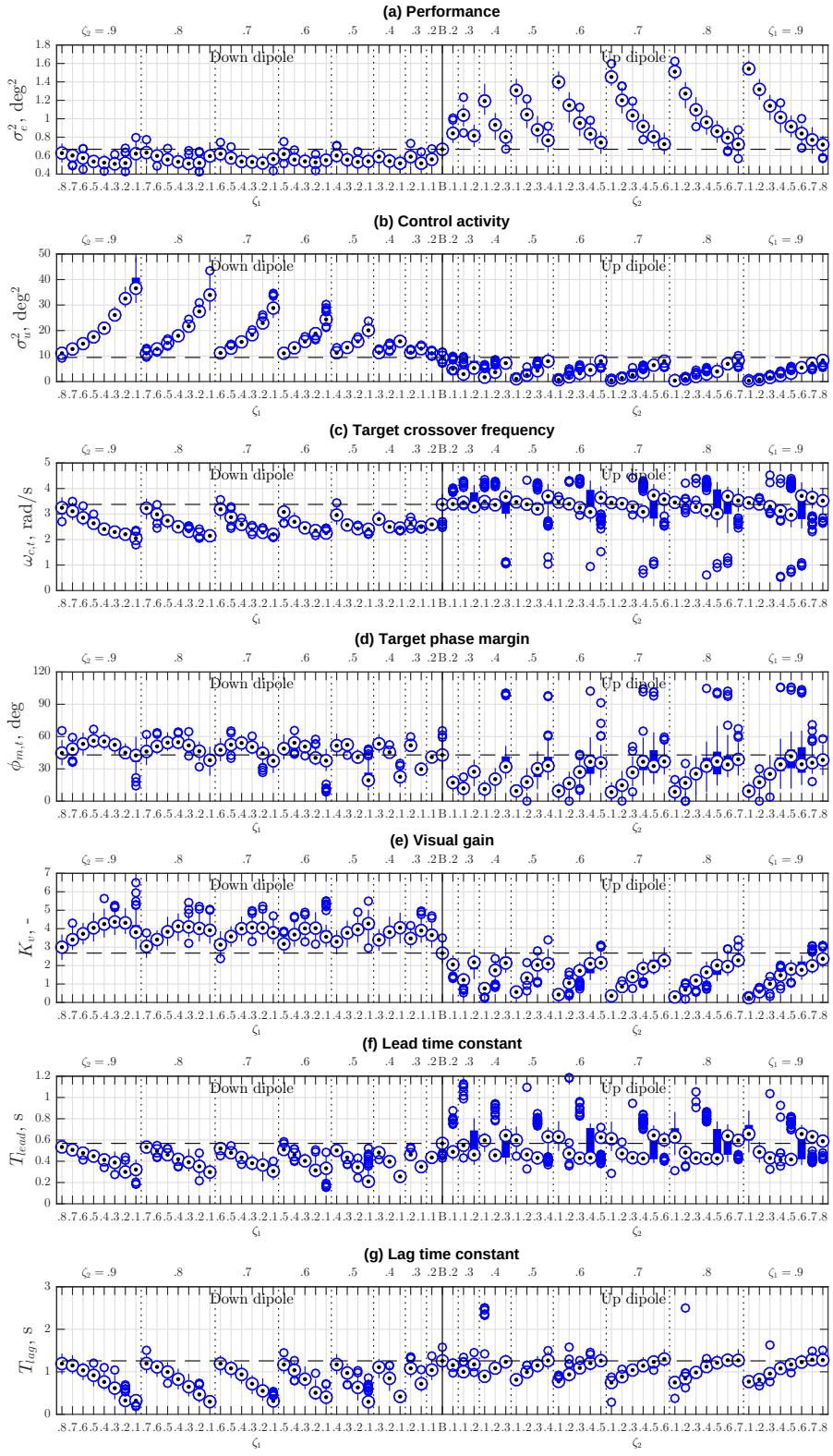

Figure 5.10: All simulation results at $\omega_{dp} = 3$ rad/s.

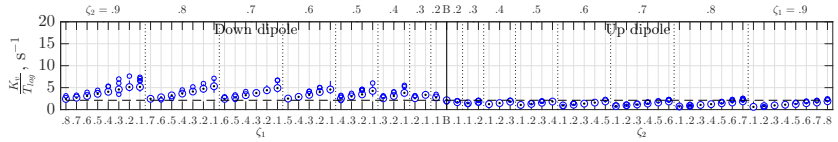

(a) ω_{dp} = 1 rad/s

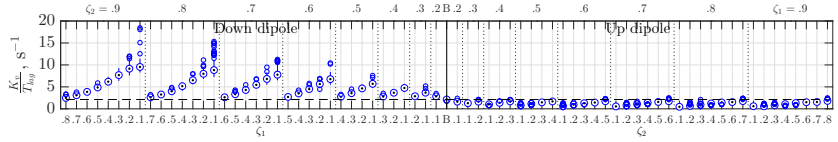

(b) ω_{dp} = 2 rad/s

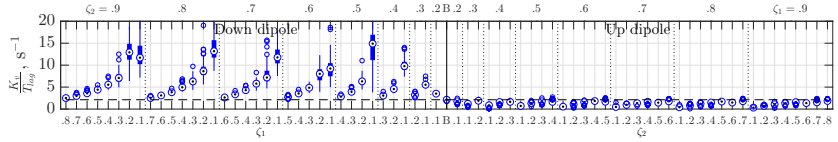

(c) ω_{dp} = 3 rad/s

Figure 5.11: Ratio between visual gain and lag time constant at different ω_{dp}.

In the first column of Table 5.2, at $\omega_{dp} = 1$ rad/s, the performance with down dipole dynamics is worse than that of other dynamics. However, for $\omega_{dp} = 2,3,4$ and 5 rad/s, the performance with up dipole dynamics is worse. At $\omega_{dp} = 6$ and 7 rad/s, the effect with up dipole dynamics on the performance weakens since here the added dynamics moved away from the frequency range where the target and disturbance forcing functions have the most power. In the second column, the control activity is very sensitive to the added dipole dynamics from $\omega_{dp} = 1$ rad/s to $\omega_{dp} = 7$ rad/s (the white areas around the baseline are narrow). In general, the control activity increases for the down dipole dynamics and decreases for the up dipole dynamics. For $\omega_{dp} = 1$ rad/s, the increased control activity for the down dipole dynamics cannot further improve the corresponding performance. However, for $\omega_{dp} = 2,3,4$ and 5 rad/s, the largely increased control activity for the down dipole dynamics makes the corresponding performance better than that of the baseline. At these same frequencies, the decreased control activity for the up dipole dynamics corresponds with worse performance compared with that of the baseline. In the third column, for $\omega_{dp} = 1,2,3$ and 4 rad/s, K_v/T_{lag} is very sensitive to the added dipole dynamics. This sensitivity may correspond with the sensitivity of the control activity at the same frequencies. At $\omega_{dp} = 5$ rad/s, K_v/T_{lag} is much less sensitive. For $\omega_{dp} = 6$ and 7 rad/s, K_v/T_{lag} with the up dipole dynamics is higher than that of the baseline, which is different for most of the other frequencies. In the fourth column, for $\omega_{dp} = 1$ and 2 rad/s, the lead time constant with the down dipole dynamics is lower than that of the baseline, and the lead time constant with the up dipole dynamics is higher than that of the baseline. In contrast, for $\omega_{dp} = 4,5,6$ and 7 rad/s, this pattern is inversed. It may be due to the fact that the up dipole dynamics decreases the stability of the system at $\omega_{dp} = 1$ and 2 rad/s, such that more lead is needed to stabilize the system; but the up dipole dynamics increases the stability of the system at $\omega_{dp} = 4,5,6$ and 7 rad/s, where less lead is needed.

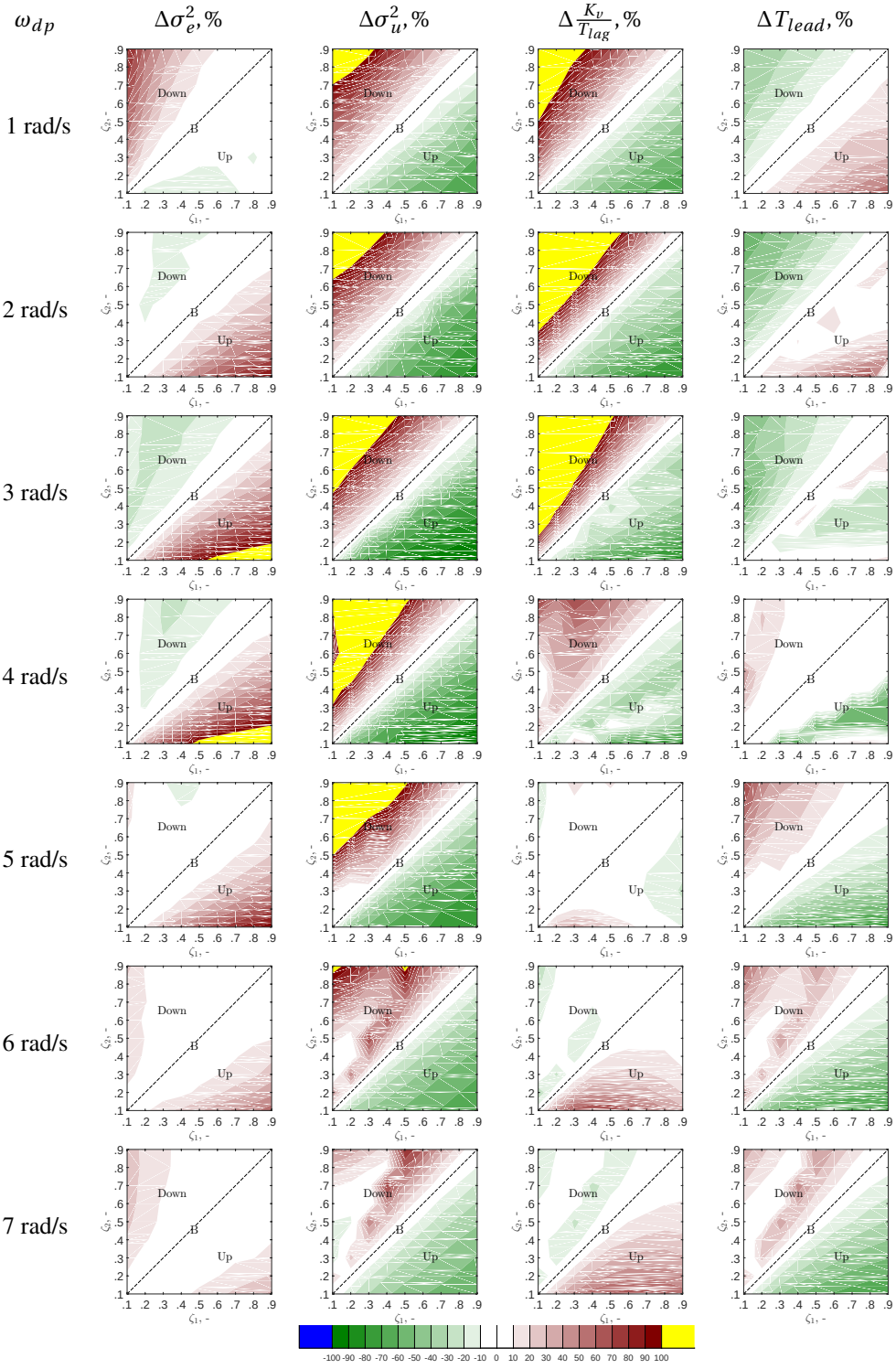

Table 5.2: The effects of added dipole dynamics on performance, control activity and control behavior.

MCAB FOR INDIVIDUAL DEPENDENT MEASURES

Figure 5.12 shows the Manual Control Adaptation Boundaries of magnitude and phase of relative changes of performance $\Delta\sigma_e^2$, control activity $\Delta\sigma_u^2$, ratio of the visual gain and lag time constant $\Delta K_v/T_{lag}$ and lead time constant ΔT_{lead} with $|\Delta| \leq 20\%$ (blue), $|\Delta| \leq 40\%$ (red), $|\Delta| \leq 60\%$ (green) compared with those of the baseline dynamics, respectively. The original MUAD envelopes of 1980 [1] are shown for comparison (grey).

It can be seen in Figure 5.12 that for all the given amount of relative changes and for all the dependent measures, the Manual Control Adaptation Boundaries of magnitude are in general wider than the original MUAD magnitude envelope. The Manual Control Adaptation Boundaries for a fixed amount of relative change, for example $|\Delta| \leq 20\%$, differ for the different dependent measures. This indicates that the dipole dynamics which cause the same amount of changes on performance, control activity, or human operator control behavior are different. The Manual Control Adaptation Boundaries expand when Δ increases from 20% to 60% due to more dipole dynamics are added into the boundaries. The effects of the up and down dipole dynamics are not mirrored in magnitude, especially for performance (see Figure 5.12a). The narrowest part of the Manual Control Adaptation Boundaries of magnitude is between 3 rad/s and 4 rad/s for the performance, control activity and ratio of the visual gain and lag time constant. The narrowest part of the Manual Control Adaptation Boundaries of phase is between 1 rad/s and 2 rad/s for performance, control activity and ratio of the visual gain and lag time constant. Due to the fact that the range of the lead time constant is relatively smaller than the range of other dependent measures, its Manual Control Adaptation Boundaries are also wider than those of other dependent measures.

INTEGRATED MANUAL CONTROL ADAPTATION BOUNDARIES

Figure 5.13 shows the Integrated Manual Control Adaptation Boundaries (IMCAB) of magnitude and phase of relative changes of performance, control activity, ratio of the visual gain and lag time constant, or lead time constant with $|\Delta| \leq 20\%$ (blue), $|\Delta| \leq 40\%$ (red), $|\Delta| \leq 60\%$ (green). For example, in Figure 5.13a the 20% Integrated Manual Control Adaptation Boundary of magnitude is the intersection of the 20% Manual Control Adaptation Boundaries of magnitude for performance, control activity, ratio of the visual gain and lag time constant and lead time constant (Figures 5.12a, 5.12b, 5.12c and 5.12d). Together the original MUAD envelopes of 1980 [1] are shown for comparison (grey).

In Figure 5.13a, it can be seen that the Integrated Manual Control Adaptation Boundaries are narrowest at 3 rad/s and wider at other frequencies. This corresponds to basic manual control theory which states that the performance and human operator control behavior is most sensitive to the controlled dynamics within the crossover region [18]. The 20% Integrated Manual Control Adaptation Boundary of magnitude seems to overlap with the original MUAD magnitude envelope, especially for the up dipole dynamics. This indicates that the relative changes on performance, control activity or human operator control behavior may be around 20% for the added dynamics which are supposed subjectively unnoticeable.

In Figure 5.13b, it can be seen that no Integrated Manual Control Adaptation Boundary of phase overlaps with the original MUAD phase envelope. Moreover, the Integrated Manual Control Adaptation Boundaries of phase are narrowest at 1 rad/s.

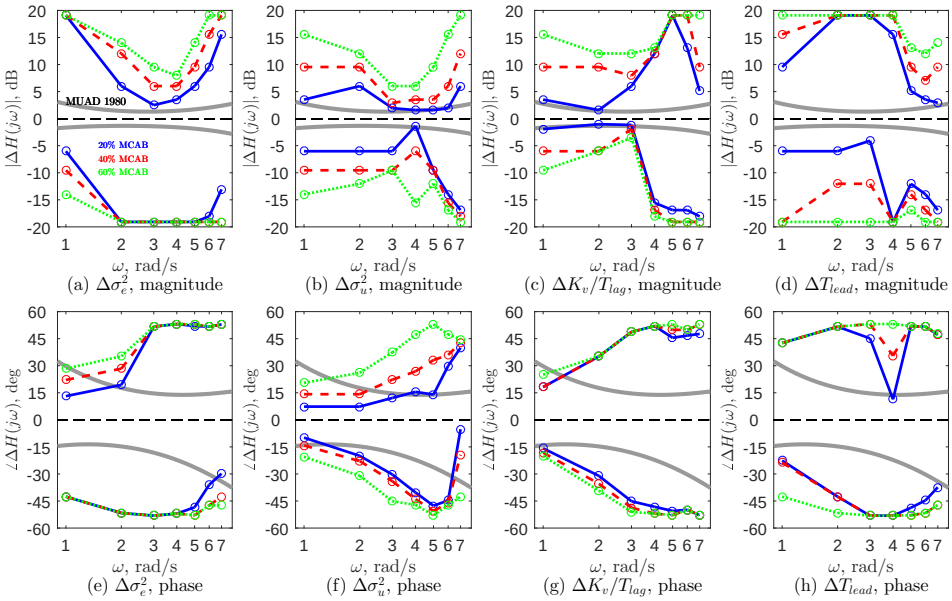

Figure 5.12: The Manual Control Adaptation Boundaries (MCAB) with various amounts of relative changes on the performance, control activity, ratio of the visual gain and lag time constant and lead time constant (blue: $|\Delta| \leq 20\%$, red: $|\Delta| \leq 40\%$, green: $|\Delta| \leq 60\%$) compared with the original MUAD envelopes [1] (grey).

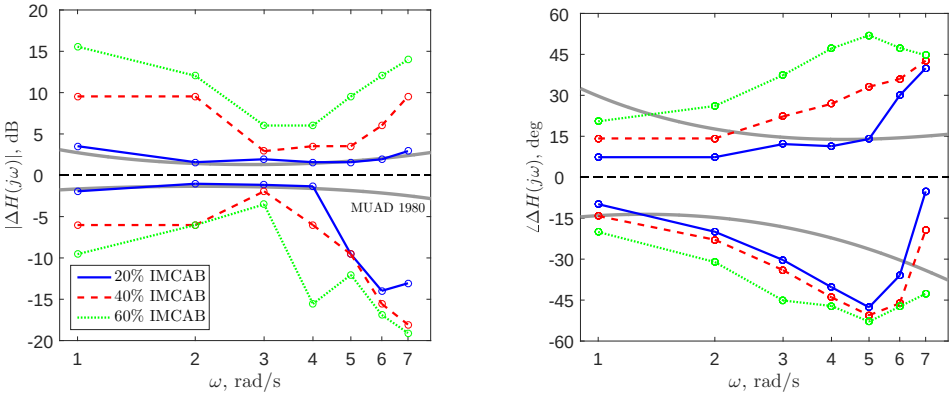

Figure 5.13: Integrated Manual Control Adaptation Boundaries (IMCAB) with different levels of relative changes on performance, control activity or control behavior. (blue: $|\Delta| \leq 20\%$, red: $|\Delta| \leq 40\%$, green: $|\Delta| \leq 60\%$) compared with the original MUAD envelopes [1] (grey).

Due to the methods of formulating the phase boundary (see section 5.2.3), the Integrated Manual Control Adaptation Boundary of phase at 1 rad/s may expand if simulation data were available for $\omega_{dp} < 1$ rad/s.

5.3.3. ADDED DYNAMICS WITHIN MUAD

In Figure 5.14, for the added dipole dynamics within the original MUAD envelopes [1] (see, Table 5.1), the performance σ_e^2, control activity σ_u^2, target crossover frequency $\omega_{c,t}$, target phase margin $\phi_{m,t}$, human operator visual gain K_v, lead time constant T_{lead}, lag time constant T_{lag} and ratio of the visual gain and lag time constant K_v/T_{lag} with the maximum deviations from the baseline are shown for each ω_{dp}. For example, in Figure 5.14a, the performance for the baseline condition (B) is shown at the very left side, with a dashed line crossing the baseline median for reference. The boxplot shown at $\omega_{dp} = 1$ rad/s represents the performance of 100 noise realizations of the dipole dynamics ($\omega_{dp} = 1$ rad/s, $\zeta_1 = 0.4$, $\zeta_2 = 0.3$) of which the median differs the most from the baseline among all the dipoles in Table 5.1 for $\omega_{dp} = 1$ rad/s. Table 5.3 shows the parameters of the corresponding added dynamics of each dependent measure plotted in Figure 5.14.

Table 5.3: The parameters of added dipole dynamics which are within the original MUAD envelopes [1] with maximum absolute deviation from the baseline dynamics for each dependent measure at each ω_{dp}.

$[\zeta_1, \zeta_2]$	1 rad/s	2 rad/s	3 rad/s	4 rad/s	5 rad/s	6 rad/s	7 rad/s
σ_e^2	0.4, 0.3	0.7, 0.6	0.8, 0.7	0.7, 0.6	0.7, 0.6	0.5, 0.4	0.4, 0.5
σ_u^2	0.8, 0.6	0.8, 0.9	0.6, 0.7	0.5, 0.6	0.5, 0.6	0.4, 0.5	0.7, 0.9
$\omega_{c,t}$	0.8, 0.6	0.7, 0.8	0.6, 0.7	0.5, 0.6	0.6, 0.5	0.5, 0.4	0.4, 0.5
$\phi_{m,t}$	0.5, 0.6	0.7, 0.6	0.6, 0.7	0.8, 0.7	0.6, 0.5	0.5, 0.6	0.4, 0.5
K_v	0.9, 0.7	0.7, 0.6	0.6, 0.7	0.6, 0.7	0.8, 0.7	0.4, 0.5	0.4, 0.5
T_{lead}	0.9, 0.7	0.7, 0.6	0.6, 0.7	0.6, 0.7	0.5, 0.6	0.4, 0.5	0.4, 0.5
T_{lag}	0.4, 0.3	0.7, 0.8	0.8, 0.9	0.7, 0.6	0.5, 0.6	0.5, 0.4	0.5, 0.4
K_v/T_{lag}	0.9, 0.7	0.7, 0.8	0.6, 0.7	0.6, 0.7	0.8, 0.7	0.4, 0.5	0.4, 0.5

Table 5.4 shows the maximum relative differences of the dependent measures between the added dipole dynamics (see Table 5.3) and the baseline at different frequencies. The last column of Table 5.4 is the average of the absolute values over all frequencies of each corresponding row. It can be seen that the control activity σ_u^2 has the maximum absolute average deviation (23.69%) and the crossover frequency $\omega_{c,t}$ has the minimum absolute average deviation (5.15%) from the baseline among all the variables. Meanwhile, the absolute average deviation of the performance is low as well (5.55%). These results indicate that for the added dynamics which are supposed subjectively unnoticeable (within the original MUAD envelopes [1]), the tracking performance and target crossover frequency may be the most distinguishable for noticeability, and human operator may not notice the change of controlled dynamics even though the control activity increases significantly.

According to Table 5.3 and Table 5.4, added dipole dynamics such as ($\omega_{dp} = 6$ rad/s, $\zeta_1 = 0.4$, $\zeta_2 = 0.5$) have relatively high control activity ($\Delta\sigma_u^2 = 29.3\%$) compared with that of the baseline. In Figure 5.15 the frequency responses of this added dynamics are shown with the 20% Integrated Manual Control Adaptation Boundaries, together with the original MUAD envelopes [1] as reference. It can be seen that this dipole is not only within the original MUAD but also within the 20% Integrated Manual Control Adaptation Boundaries. As has been mentioned in section 5.2.3, within the Manual Control Adaptation Boundaries, it is not guaranteed that the performance, control activity or human operator control behavior always obeys, for example, $\Delta \leq 20\%$. This phenomenon means that at a certain frequency ω_{dp}, with increasing magnitude perturbation of the added dipole dynamics, the perfor-

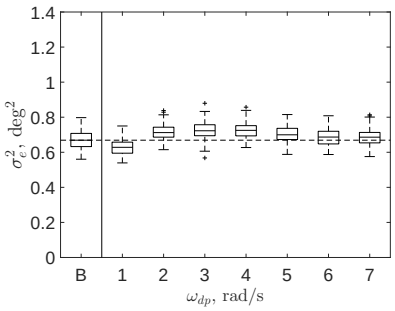

(a) Performance

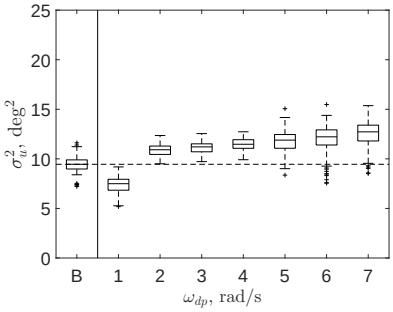

(b) Control activity

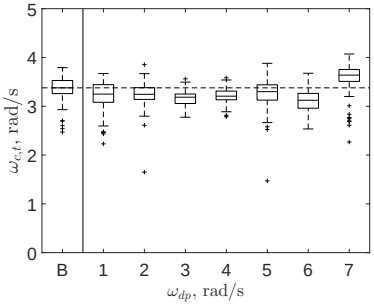

(c) Target crossover frequency

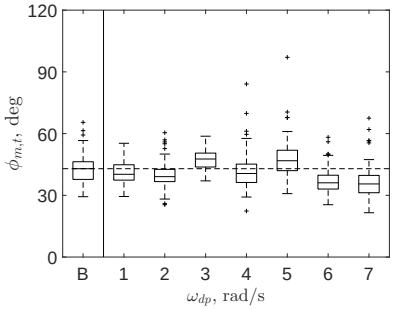

(d) Target phase margin

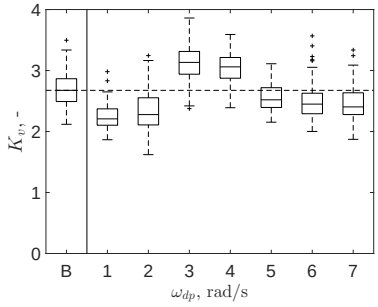

(e) Visual gain

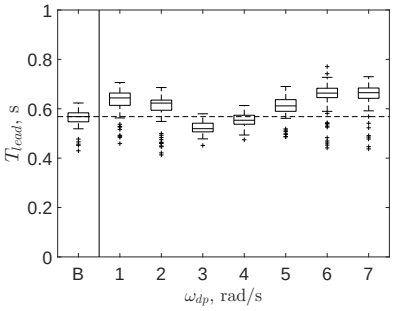

(f) Lead time constant

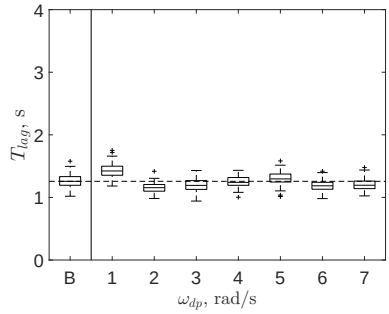

(g) Lag time constant

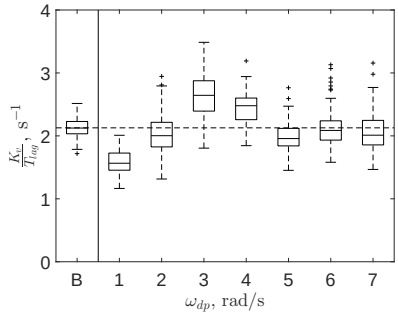

(h) Ratio between K_v and T_{lag}

Figure 5.14: Human operator parameters of maximum deviations from baseline. All added dipole dynamics are within the MUAD envelopes (Figure 5.6).

Table 5.4: Maximum deviation of human operator parameters from baseline dynamics. All added dipole dynamics are within both MUAD gain and phase envelopes.

Δ,%	1 rad/s	2 rad/s	3 rad/s	4 rad/s	5 rad/s	6 rad/s	7 rad/s	Absolute average
σ_e^2	-6.07	6.48	8.04	8.39	4.60	2.68	2.58	5.55
σ_u^2	-20.71	15.51	18.57	21.38	25.79	29.30	34.60	23.69
$\omega_{c,t}$	-3.80	-3.93	-5.69	-5.05	-2.31	-7.53	7.72	5.15
$\phi_{m,t}$	-6.34	-9	10.96	-5.42	9.02	-15.97	-17.25	10.57
K_v	-17.48	-14.86	17.13	14.40	-5.80	-8.44	-10.15	12.61
T_{lead}	13.34	9.67	-8.58	-2.57	7.66	16.77	17.07	10.81
T_{lag}	13.16	-8.08	-5.17	-1.33	3.08	-5.68	-4.98	5.92
K_v/T_{lag}	-26.33	-5.73	24.46	16.68	-7.88	-1.79	-5.35	12.60

mance, control activity or human operator control behavior may not change consistently.

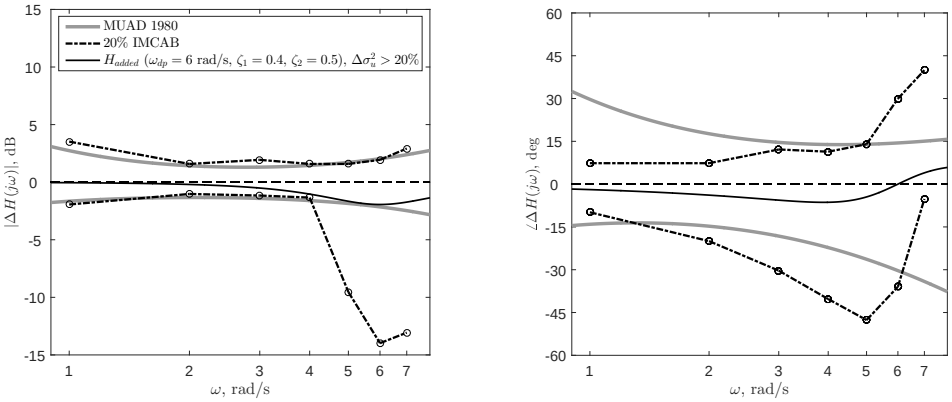

(a) Magnitude (b) Phase

Figure 5.15: Integrated Manual Control Adaptation Boundaries (IMCAB) of 20% with the added dipole dynamics (ω_{dp} = 6 rad/s, ζ_1 = 0.4, ζ_2 = 0.5) of which $\Delta\sigma_u^2 > 20\%$.

5.4. DISCUSSION

In order to develop the Manual Control Adaptation Boundaries, an aircraft pitch attitude compensatory tracking task perturbed by the added dipole dynamics was simulated based on the simulation developed and validated in Chapter 4. In the simulation, the aircraft dynamics were kept constant while the added dipole dynamics were varied over different factorial combinations of natural frequencies ω_{dp} and damping ratios ζ_1 and ζ_2. The optimal performance, control activity, target crossover frequency, target phase margin, visual gain, lead time constant and lag time constant were found for each added dynamics with 100 remnant noise realizations.

Among all the simulation results, it was found that the effects of the added dipole dynamics at ω_{dp} = 1 rad/s on the performance are distinctively different from that at other frequencies. At 1 rad/s, the performance with the down dipole dynamics is generally worse

than that of the baseline, and the performance with the up dipole dynamics is equivalent or even better than that of the baseline. However, for other values of ω_{dp}, the performance with the down dipole dynamics is better than that with the up dipole dynamics. It was found that for the down dipole dynamics at 1 rad/s, the human operator cannot further increase the visual gain to improve performance, otherwise the stability of the system decreases significantly which would further worsen the performance. For the down dipole dynamics at 2 rad/s, simulation results showed that high visual gain and high control activity do not necessarily correspond with a high crossover frequency. This may be due to the fact that, for example, the down dipole decreases the phase of the controlled system for $\omega < \omega_{dp}$ and increases the phase of the controlled system for $\omega > \omega_{dp}$, which complicates the choices of target crossover frequency for human operators.

The relative changes of the tracking performance, control activity, ratio of the visual gain and lag time constant and lead time constant with respect to those of the baseline dynamics were used as the dependent measures quantifying the Manual Control Adaptation Boundaries. The overall effects of the tested added dipole dynamics on performance, control activity and human operator control behavior were shown as contour-plots, which can be considered as a lookup table for predicting the sensitivity of the corresponding dependent measures to any other added dipole dynamics. Based on the simulation data, the Manual Control Adaptation Boundaries for performance, control activity, ratio of the visual gain and lag time constant and lead time constant were developed, respectively. The area of the Manual Control Adaptation Boundaries expands with the increase of the relative change on the corresponding dependent measure. The shape of the Manual Control Adaptation Boundaries is irregular, meaning that the effects of the up and down dipoles are not symmetric. Furthermore, the Manual Control Adaptation Boundaries of each dependent measure are different from each other.

With the expected inconsistence among the Manual Control Adaptation Boundaries among different dependent measures, the Integrated Manual Control Adaptation Boundaries were proposed, which were the intersection of the Manual Control Adaptation Boundaries for performance, control activity, ratio of the visual gain and lag time constant and the lead time constant. The Integrated Manual Control Adaptation Boundary of magnitude is narrowest at 3 rad/s and wider at other frequencies. This corresponds with manual control theory which states that the performance and human operator control behavior is most sensitive in the crossover region. It was also found that the 20% Integrated Manual Control Adaptation Boundary of magnitude overlaps well with the original MUAD magnitude envelope, indicating that for the subjectively unnoticeable added dynamics, the maximum tolerable deviation of the performance, control activity or human operator control behavior could be around 20%.

To tie in with the original MUAD envelopes, it was of interest to see to what extent the performance, control activity and human operator control behavior would change for added dynamics within the original MUAD envelopes which are hypothesized to be subjectively unnoticeable. The added dipole dynamics within the original MUAD envelopes were first selected from the tested dipoles, and their corresponding performance, control activity, target crossover frequency, target phase margin, human operator visual gain, lead time constant and lag time constant were compared with those of the baseline. On average, the performance (5.55%) and target crossover frequency (5.15%) change the least, and the

control activity (23.69%) changes the most. This indicates that performance and crossover frequency may be the most sensitive in the perspective of noticeability, and human operator may not notice the difference in the controlled system even with larger control inputs. Furthermore, it was found that for certain added dynamics within the proposed Integrated Manual Control Adaptation Boundaries, the relative change of performance, control activity or human operator control behavior could be more than the amount corresponding with the boundaries. This indicates that the proposed Manual Control Adaptation Boundaries do not guarantee that the performance, control activity or human operator control behavior of any added (dipole) dynamics within the boundaries would be consistently constrained. However, according to the proposed boundary formulating methods, it is of more confidence to say that for added dipole dynamics falling outside the Manual Control Adaptation Boundaries, the absolute relative change on performance, control activity or human operator control behavior would be more than the amount corresponding with the boundaries.

5.5. CONCLUSIONS

In this chapter, an aircraft pitch attitude tracking task with a large number of added dipole dynamics variations, over a wide frequency range and with various levels of perturbations was simulated to form the Manual Control Adaptation Boundaries. The relative changes of tracking performance, control activity, ratio of the visual gain and lag time constant and lead time constant compared with those of the baseline dynamics were chosen as the dependent measures quantifying the Manual Control Adaptation Boundaries. For each dependent measure, the proposed Manual Control Adaptation Boundaries enclose all the added dipole dynamics of which the corresponding absolute relative change of the dependent measure is within a certain range. The Integrated Manual Control Adaptation Boundaries were developed which are the intersection of the individual Manual Control Adaptation Boundaries for performance, control activity, ratio of the visual gain and lag time constant and lead time constant. The Integrated Manual Control Adaptation Boundary of magnitude is narrowest at 3 rad/s, meaning that at this frequency the performance, control activity or human operator control behavior is the most sensitive to the added dipole dynamics, which corresponds well with manual control theory. In this chapter, it was also found that for the dipoles within the original MUAD envelopes of 1980, the performance and target crossover frequency are the most sensitive to the added dynamics in the perspective of noticeability, and human operator may be less sensitive to the change of control activity. Furthermore, it was found that the proposed (Integrated) Manual Control Adaptation Boundaries do not guarantee that for any added (dipole) dynamics that within the boundaries the relative change of performance, control activity or human operator control behavior with respect to that of the baseline would be consistently constrained by the boundaries. For any added dipole dynamics falling outside the Manual Control Adaptation Boundaries, it is of more confidence to claim that the absolute relative change on performance, control activity or human operator control behavior would be more than the amount corresponding with the boundaries.

REFERENCES

[1] J. R. Wood and J. Hodgkinson, *Definition of Acceptable Levels of Mismatch for Equivalent Systems of Augmented CTOL Aircraft*, Tech. Rep. MDC A6792 (McDonnell

Aircraft Company, St. Louis (MO), 1980).

[2] C. G. Carpenter and J. Hodgkinson, *V/STOL Equivalent Systems Analysis*, Tech. Rep. NADC-79141-60 (McDonnell Aircraft Company, St. Louis (MO), 1980).

[3] J. T. Bosworth and P. S. Williams-Hayes, *Flight Test Results from the NF-15B Intelligent Flight Control System (IFCS) Project with Adaptation to a Simulated Stabilator Failure,* in *Proceedings of the AIAA Infotech at Aerospace 2007 Conference and Exhibit, Rohnert Park (CA)*, AIAA-2007-2818 (2007).

[4] S. Geluardi, F. M. Nieuwenhuizen, L. Pollini, and H. H. Bülthoff, *Frequency Domain Identification of a Light Helicopter in Hover,* in *Proceedings of the AHS 70th Annual Forum, Montreal, Canada* (2014).

[5] M. B. Tischler, *System Identification Methods for Aircraft Flight Control Development and Validation*, NASA Technical Memorandum 110369 (NASA Ames Research Center, Moffett Field (CA), 1995).

[6] P. G. Hamel and K. Jürgen, *Advances in Rotorcraft System Identification,* Progress in Aerospace Sciences **33**, 259 (1997).

[7] Cicolani and Luigi, *Flight Test Identification and Simulation of a UH-60A Helicopter and Slung Load*, Tech. Rep. NASA/TM-2001-209619 (NASA, Ames Research Center Moffett Field, California, 2001).

[8] C. J Miller, *Nonlinear Dynamic Inversion Baseline Control Law: Flight-Test Results for the Full-scale Advanced Systems Testbed F/A-18 Airplane,* (AIAA Guidance, Navigation, and Control Conference, 2011) pp. 1–25.

[9] M. Mulder, P. M. T. Zaal, D. M. Pool, H. J. Damveld, and M. M. van Paassen, *A Cybernetic Approach to Assess Simulator Fidelity: Looking back and looking forward,* in *Proceedings of the AIAA Modeling and Simulation Technologies Conference, Boston (MA)*, AIAA-2013-5225 (2013).

[10] P. van den Berg, P. M. T. Zaal, M. Mulder, and M. M. van Paassen, *Conducting of Multi-modal Pilot Model Identification - Results of a Simulator Experiment,* in *AIAA Modelling and Simulation Technologies Conference, South Carolina*, AIAA-2007-6892 (2007).

[11] P. M. T. Zaal, D. M. Pool, M. Mulder, and M. M. van Paassen, *New Types of Target Inputs for Multi-Modal Pilot Model Identification,* in *Proceedings of the AIAA Modeling and Simulation Technologies Conference and Exhibit, Honolulu (HI)*, AIAA-2008-7106 (2008).

[12] P. M. T. Zaal, D. M. Pool, M. Mulder, M. M. van Paassen, and J. A. Mulder, *Identification of Multimodal Pilot Control Behavior in Real Flight,* Journal of Guidance, Control, and Dynamics **33**, 1527 (2010).

[13] D. M. Pool, M. M. van Paassen, and M. Mulder, *Modeling Human Dynamics in Combined Ramp-Following and Disturbance-Rejection Tasks,* in *Proceedings of the AIAA Guidance, Navigation, and Control Conference, Toronto, Canada, Aug. 2-5*, AIAA-2010-7914, edited by M. Silvestro (American Institute for Aeronautics and Astronautics, 2010).

[14] P. M. T. Zaal, D. M. Pool, J. de Bruin, M. Mulder, and M. M. van Paassen, *Use of Pitch and Heave Motion Cues in a Pitch Control Task,* Journal of Guidance, Control, and Dynamics **32**, 366 (2009).

[15] T. Lu, D. M. Pool, M. M. van Paassen, and M. Mulder, *Quantifying the Effects of Added Dynamics with Human Operator Control Behavior Measurements and Simulations,* in *Proceedings of the AIAA Modeling and Simulation Technologies Conference, Denver (CO)*, AIAA-2017-3667 (2017).

[16] D. M. Pool, *Objective Evaluation of Flight Simulator Motion Cueing Fidelity Through a Cybernetic Approach*, Ph.D. thesis, Delft University of Technology, Faculty of Aerospace Engineering (2012).

[17] D. T. McRuer, D. Graham, E. S. Krendel, and W. J. Reisener, *Human Pilot Dynamics in Compensatory Systems, Theory Models and Experiments with Controlled Element and Forcing Function Variations*, Tech. Rep. AFFDL-TR-65-15 (Air Force Flight Dynamics Laboratory, Wright-Patterson Air Force Base (OH), 1965).

[18] D. T. McRuer and H. R. Jex, *A Review of Quasi-Linear Pilot Models,* IEEE Transactions on Human Factors in Electronics **HFE-8**, 231 (1967).

6

EXPERIMENTAL VERIFICATION OF MANUAL CONTROL ADAPTATION BOUNDARIES

In Chapter 4, an offline computer simulation was developed to predict the performance, control activity and human operator control adaptations for an aircraft pitch attitude tracking task when extra dynamics are added to the controlled system. The simulation was validated and tuned using a human-in-the-loop experiment, with three pairs of up and down added dipole dynamics located at three different frequencies. Chapter 5 further extended the necessary data base and defined the Manual Control Adaptation Boundaries (MCAB), based on the relative changes of performance, control activity, ratio of the visual gain and lag time constant and the lead time constant, all with respect to those of the baseline. Moreover, in Chapter 5, simulation results showed that the tracking performance and control activity with added dipoles at 1 rad/s are very different from those with dipoles at other frequencies. In this chapter, the MCAB developed in Chapter 5 are experimentally verified and further refined, by testing the added dipole dynamics with gradually changing damping ratios only around what was found to be the most critical dipole frequency, 1 rad/s.

The content of this chapter will be submitted to the following paper:
T. Lu, D. M. Pool, M. M. van Paassen, and M. Mulder, Experimental Verification of Objective Manual Control Adaptation Boundaries in Aircraft Pitch Tracking Tasks, Journal of Guidance, Control, and Dynamics.

6.1. INTRODUCTION

The goal of this thesis is to develop MCAB, which can more objectively quantify the sensitivities of tracking performance, control activity and human operator control behavior to the change of the controlled dynamics. In Chapter 4, a computer offline simulation using constrained nonlinear optimization techniques was developed, to predict the performance, control activity and human operator model parameters. It was validated by an experiment where subjects performed the same task with the same testing conditions. In Chapter 5, this control task was simulated with 504 different added dipole dynamics, located at frequencies $1, 2, 3, 4, 5, 6$ and 7 rad/s, to formulate boundaries of the MCAB. Different MCAB were formulated for performance, control activity, ratio of the visual gain and lag time constant, and the lead time constant. Then the intersections of the four MCAB for these dependent measures were defined as the Integrated Manual Control Adaptation Boundaries (IMCAB), for both magnitude and phase, respectively. In general, the IMCAB of magnitude is narrowest at 3 rad/s, corresponding with manual control theory which states that performance and human operator control behavior are the most sensitive within the crossover region [1].

In theory, the verification of the MCAB developed in Chapter 5 needs to test an infinitive amount of added dipole dynamics, or at least the 504 different added dipole dynamics which were used in the simulation. This is practically infeasible for a human-in-the-loop experiment. However, it is possible to verify the MCAB for limited testing conditions in order to gain insights into how much the measured sensitivities of performance, control activity and identified human operator control behavior would deviate from the simulation-based MCAB. Moreover, even with limited testing conditions an experiment could also serve as a reference to further tune the MCAB obtained in Chapter 5.

The goal of this chapter is to experimentally verify the MCAB developed in Chapter 5, and if necessary, to further tune the simulation-based envelopes using the experimental results. An aircraft pitch attitude tracking experiment perturbed by added "up" and "down" dipole dynamics was performed and the same "*cybernetic approach*" utilized in previous chapters was used to study the effects of the added dynamics on performance, control activity and human operator adaptation.

This chapter starts in Section 6.2, with an introduction of the aircraft pitch tracking task that forms the basis of the experiment and simulation. Experiment results will be discussed in Section 6.3, and compared to the simulation predictions in both absolute values and as relative changes with respect to the baseline. Simulation data in Chapter 5 are modified based on the experiment results, and the modified MCAB are verified by comparing with the added dipole dynamics tested in this experiment and their corresponding relative changes in tracking performance, control activity, ratio of the visual gain and lag time constant, and the lead time constant. The chapter ends with a discussion and conclusions.

6.2. METHODS

6.2.1. CONTROL TASK

AIRCRAFT PITCH ATTITUDE TRACKING TASK

In this chapter, the same aircraft pitch attitude tracking task as used in both Chapters 4 and 5 will be performed to study the tracking performance, control activity and human operator control behavior with added dynamics perturbing the baseline aircraft dynamics, as shown

in Figure 6.1. The total controlled dynamics are the combination of the baseline dynamics $H_{baseline}(s)$ and the added dynamics $H_{added}(s)$. The human operator (represented by a linear transfer function $H_p(s)$ for visual response and the remnant n) controls the pitch angle θ of the total aircraft dynamics ($H_{baseline}(s)H_{added}(s)$) to both track the target signal f_t and reject the disturbance signal f_d. The error signal e is the difference between the target signal f_t and the aircraft pitch angle θ. In Figure 6.1, u is the human operator control signal, K_s is the stick gain, u_s is the control signal from the stick, u_a is the signal out from the added dynamics, and δ_e is the signal directly feeding into the baseline aircraft dynamics. To avoid repetition, the details of the forcing functions f_t and f_d, the baseline dynamics $H_{baseline}(s)$, the added dynamics $H_{added}(s)$, the stick gain K_s and the human operator visual response $H_p(s)$ can be found in Chapter 4.

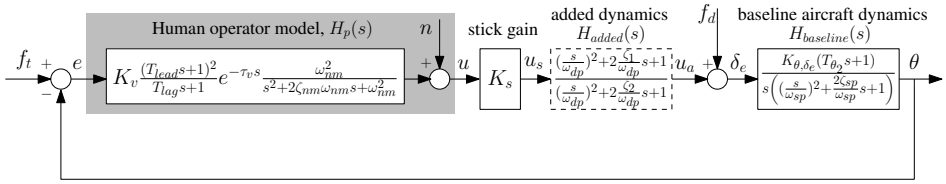

Figure 6.1: A schematic representation of the aircraft pitch attitude tracking task.

EXPERIMENT CONDITIONS

In Chapter 4, up ($\zeta_1 = 0.7$, $\zeta_2 = 0.2$) and down ($\zeta_1 = 0.2$, $\zeta_2 = 0.7$) dipole dynamics were tested at $\omega_{dp} = 1,3$ and 7 rad/s, respectively. However, since only one up and one down dipole at each frequency were tested, it was at that point unknown how much the performance, control activity and human operator model parameters would change when the perturbation of the added dynamics on the baseline system is gradually increased. Moreover, in Chapter 4 the simulation was validated only for one up and one down dipole at at $\omega_{dp} = 1,3$ and 7 rad/s respectively, it is also unknown whether the simulation is still accurate when the damping ratio changes gradually with finer resolutions. However, to increase the number of dipoles at multiple frequencies, for example, $\omega_{dp} = 1,3$ and 7 rad/s, will significantly increase the number of conditions of the experiment, which makes the experiment difficult to carry out. In this chapter, it was decided to focus on only one frequency of ω_{dp} and increase the number of added dynamics tested by varying the damping ratios ζ_1 and ζ_2.

Two main considerations were taken into account when selecting the added dynamics natural frequency ω_{dp} in this chapter. First, the frequency range of interest is between 1 rad/s and 10 rad/s, which includes the crossover frequency region [1] where the human operator control behavior is sensitive to the changes of controlled dynamics (in Figure 6.2 it can be also seen that the MUAD envelopes [2] are indeed narrowest within this frequency range). Second, in Chapter 5, based on the simulation results, it was known that the performance pattern between the up and down dipole dynamics at $\omega = 1$ rad/s is unique and different from that at other frequencies. Moreover, near $\omega = 1$ rad/s, the forcing functions have most power and the added dynamics can make a significant impact on human operator control behavior. Thus in this chapter $\omega_{dp} = 1$ rad/s is chosen as the natural frequency of the added dipole dynamics.

The selection of the damping ratios ζ_1 and ζ_2 in this chapter was mainly based on

the experiment results of Chapter 4 and Chapter 3. In Chapter 4, for both up and down dipoles at 1 rad/s, one damping ratio was kept at 0.2 and another one changed from 0.2 to 0.7. Experiment results showed that for the selected conditions, obvious changes in the performance, control activity, human operator visual gain and lag time constant were observed, compared with the baseline condition. To tie in with Chapter 4, for this chapter it was also decided, for example for the up dipole dynamics, ζ_2 is fixed 0.2 and ζ_1 changes from 0.2 to 0.7 (vice versa for the down dipole dynamics). Chapter 3 concluded that the noticeable limit of performance and control activity would be around between $\zeta_1 = 0.35$ and $\zeta_1 = 0.5$ ($\zeta_2 = 0.2$). Even though in Chapter 3 the baseline dynamics and the added dynamics natural frequency are different from the ones used in this chapter, $\zeta_1 = 0.35$ for the up dipole (or $\zeta_2 = 0.35$ for the down dipole) dynamics is selected as a damping ratio of interest. Finally in this chapter, the damping ratios with the up dipole dynamics are selected as $\zeta_1 = 0.25, 0.3, 0.35, 0.4, 0.5, 0.6$ and 0.7 with $\zeta_2 = 0.2$. The damping ratios with the down dipole dynamics are varied the other way around.

To enable a direct comparison with human operator control behavior of the baseline aircraft dynamics, the baseline aircraft without any added dynamics is also tested. Table 6.1 lists all conditions, where "B" represents the baseline condition. Conditions C7 and C14 are identical to the ones tested in Chapter 4. The performance, control activity and human operator control behavior of conditions C1, C3, C8, C10 in Table 6.1 were predicted by the simulation developed in Chapter 4 before the experiment. The performance, control activity and human operator control behavior of other conditions in Table 6.1 were directly obtained from Chapter 5.

The frequency responses of all added dynamics conditions are shown in Figure 6.2, plotted against the original MUAD envelopes [2] for reference.

Table 6.1: Simulation and experiment conditions

	Conditions	ω_{dp}, rad/s	ζ_1,-	ζ_2,-
Up dipoles $\zeta_1 > \zeta_2$	C1	1	0.25	0.2
	C2	1	0.3	0.2
	C3	1	0.35	0.2
	C4	1	0.4	0.2
	C5	1	0.5	0.2
	C6	1	0.6	0.2
	C7	1	0.7	0.2
Down dipoles $\zeta_2 > \zeta_1$	C8	1	0.2	0.25
	C9	1	0.2	0.3
	C10	1	0.2	0.35
	C11	1	0.2	0.4
	C12	1	0.2	0.5
	C13	1	0.2	0.6
	C14	1	0.2	0.7
Baseline	B	-	-	-

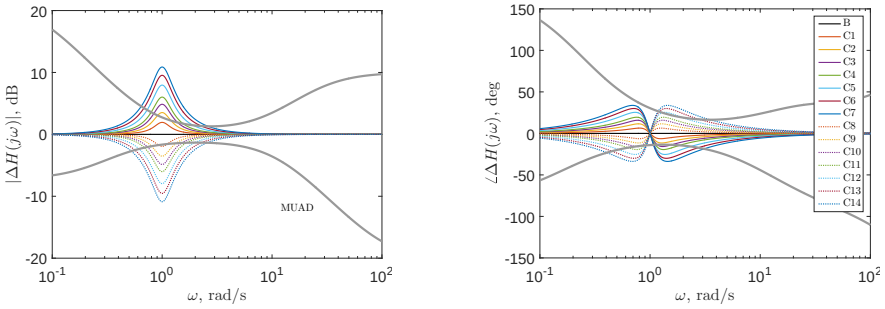

(a) Magnitude (b) Phase

Figure 6.2: MUAD and all added dynamics.

6.2.2. EXPERIMENT

In this section, the human-in-the-loop aircraft pitch attitude compensatory tracking experiment (Figure 6.1) is introduced. First, the dependent measures and the methods of the analysis are explained. Second, the apparatus and the experiment procedures are introduced. In the end the hypotheses of the experiment are stated.

DEPENDENT MEASURES AND DATA ANALYSIS

The measured variables in the experiment include the time histories of the tracking error e, the control signal u and the pitch angle θ during each run, see Figure 6.1. From these measurements the variance of e and the variance of u are calculated as the measures of performance and control activity, respectively. Based on the measures of e and θ, the Fourier coefficient (FC) method [3, 4] is used to identify the nonparametric open-loop describing functions at the target signal frequencies ω_t:

$$\hat{H}_{ol,t}(j\omega_t) = \frac{\Theta(j\omega_t)}{E(j\omega_t)}, \tag{6.1}$$

where $\hat{H}_{ol,t}(j\omega)$ is the nonparametric target open-loop describing function, Θ is the Fourier transform of the aircraft pitch angle θ and E is the Fourier transform of the error signal e. Then the open-loop target crossover frequency $\omega_{c,t}$ and phase margin $\phi_{m,t}$, representing the manual control bandwidth and the stability, respectively, are calculated from this nonparametric open-loop describing function estimate.

Similarly, based on the measures of e and u, a (nonparametric) frequency response function (FRF) estimate of the human operator dynamics H_p at the frequencies of both f_t and f_d is also obtained as:

$$\hat{H}_p(j\omega_{t,d}) = \frac{U(j\omega_{t,d})}{E(j\omega_{t,d})}, \tag{6.2}$$

where $\hat{H}_p(j\omega_{t,d})$ represents the estimated FRF and U is the Fourier transform of the control signal u, see Figure 6.1. Finally, the human operator model parameters are estimated using the time-domain parameter estimation method of [4]. To evaluate the quality-of-fit for all

fitted human operator models, the Variance Accounted For (VAF) is calculated. The VAF expresses the model quality in the percentage of the variance in the control signal u that is captured by the model [4, 5].

To verify the statistical significance of observed trends in all dependent measures, statistical analyses are performed. First, a nonparametric Friedman test is used to check for significant variations due to the different added dynamics settings (H_{added}) over all fifteen experimental conditions. In addition, for each dependent measure fourteen paired t-tests (at a Bonferroni corrected significance level of $\alpha = 0.0036$) are used to compare all fourteen added dynamics conditions (C1-C14) with the data of the baseline condition (B).

For all the experiment conditions in Table 6.1, experiment and simulation results will be compared and correlated for performance, control activity, target crossover frequency, target phase margin and human operator model parameters. The relative changes of performance, control activity, ratio of the visual gain and lag time constant and lead time constant with respect to those of the baseline dynamics (which are the dependent measures quantifying the MCAB, see Chapter 5) will be compared between the simulation and experiment. Based on these comparison results, the MCAB and IMCAB developed in Chapter 5 would be modified based on the experiment results.

APPARATUS

The experiment was performed in the fixed-base simulator called the Human-Machine Interaction Laboratory (HMILab) at the Faculty of Aerospace Engineering of Delft University of Technology (see Figure 6.3). During the experiment, subjects were seated in the right cockpit seat and a right-handed sidestick was used for giving inputs to the controlled dynamics. Only the pitch axis of the sidestick was active during the experiment; the roll axis of the sidestick was fixed at the neutral position. The tracking error e in Figure 6.1 was presented to the subject through the primary flight display (PFD) directly in front of the right seat, as shown in Figure 6.3(b). The display shows the pitch attitude tracking error e as the distance between the center fixed aircraft symbol and the moving target line. The aircraft symbol was static, and the target line moved to indicate the current tracking error e. Note that this display is an "inside-out" display: to compensate for the tracking error shown in Figure 6.3(b), the subject needs to give a (positive) pitch input, i.e., pull the stick. No other visual cues were presented during the experiment, that is, the secondary flight displays and the outside visual system were switched off.

SUBJECTS AND EXPERIMENT PROCEDURES

Fifteen subjects (twelve male and three female) aged between 22 and 50 years were invited to perform the experiment, all students or staff of Delft University of Technology. The subjects received an experimental briefing on the overview and objective of the experiment. Subjects were instructed to minimize the pitch attitude tracking error e presented on the PFD as best as possible, without providing the details of the characteristics of the controlled aircraft dynamics or added dynamics. Finally, all the subjects gave written informed consent before the start of the experiment.

The order of the testing was determined for each subject by a Latin square. Considering the large number of conditions and testing runs, the experiment for each subject was divided into two sessions on two different days. For example, Figure 6.4 shows the run order of Subject 7 of all experiment conditions on two sessions of two days.

(a) The Human-Machine-Interaction Simulator (HMI).

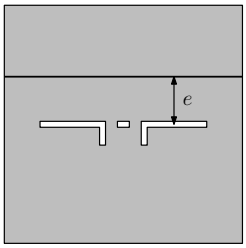

(b) Compensatory pitch tracking display.

Figure 6.3: The Human-Machine-Interaction Laboratory (HMI) lab and compensatory pitch tracking display.

Session 1 of day 1										Session 2 of day 2							
Training	C10	C14	C8	C5	C1	C6	B	C3		Training	C7	C11	C2	C12	C13	C4	C9

Figure 6.4: The run order of Subject 7 for all the conditions on two sessions. The added dynamics of different conditions can be found in Table 6.1.

For each subject, the experiment started with an initial familiarization. During this phase, subjects were allowed to familiarize themselves with the baseline aircraft dynamics (condition B) for a total of 7 tracking runs. Following this initial familiarization, the measurement runs for all experiment conditions were performed. The root mean square (RMS) of the error signal e was recorded and reported to the subject after each run. For each subject five repetitions were collected before the testing of this condition was completed.

Each testing run lasted 95 s. In order to obtain stable control output from the subject, the first 13.08 s data were cut off. Thus 81.92 s data were used for the data analysis. The sampling frequency of the experiment data was set at 100 Hz.

HYPOTHESES

For the experiment, the following hypotheses are formulated:

1. *The added dipole dynamics of C1&C2 and C8&C9 have no effect on performance, control activity, target crossover frequency, target phase margin and human operator model parameters. The added dipole dynamics of C3-C7 and C10-C14 have a significant effect on either visual gain, lead time constant or lag time constant.* In Figures 6.2a and 6.2b it can be seen that the added dynamics of C1&C2 and C8&C9 are the ones lying mostly within the MUAD envelopes. Even though the magnitude of the added dynamics of C2 and C9 are not completely within the MUAD magnitude envelopes (Figure 6.2a), they are still within the MUAD phase envelopes (Figure 6.2b). For C3-C7 and C10-C14, the added dynamics are both outside the MUAD magnitude and phase envelopes. Moreover, according to Chapter 3, the dipole of $\zeta_1 = 0.35, \zeta_2 = 0.2$ has significant effects on human operator control behavior.

2. *The effects of the up and down dipole dynamics on performance and control activity are not exactly each other's opposite.* According to Chapter 4, at $\omega_{dp} = 1$ rad/s, the performance with the down dipole is significantly worse than that of the baseline and the performance with the up dipole is very close to that of the baseline. The control activity with the down dipole is significantly higher than that of the baseline and the control activity with the up dipole is significantly lower than that of the baseline, but the differences are much smaller than those for the down dipole dynamics. Moreover, the simulation results obtained in Chapter 5 at $\omega_{dp} = 1$ rad/s also support this hypothesis.

6.3. RESULTS

6.3.1. EXPERIMENT RESULTS

This section first presents the experiment results of performance, control activity, target crossover frequency, phase margin and human operator control behavior parameters. Then the experiment results are compared with the simulation results in both values of the dependent measures and their relative changes (with respect to those of the baseline). In the end of this section, the MCAB and IMCAB are modified based on the experiment data. These modified boundaries are verified by comparing them with the tested added dipole dynamics and their corresponding relative changes in the dependent measures.

TRACKING PERFORMANCE AND CONTROL ACTIVITIES

Figure 6.5a shows the box-plot of the variance of the error signal e for each condition for the fifteen subjects. The solid line shows the change of the medians of the "up dipole" conditions when $\zeta_2 = 0.2$ and ζ_1 increases from 0.2 to 0.7, and the dashed line shows the change of the medians of the "down dipole" conditions when $\zeta_1 = 0.2$ and ζ_2 increases from 0.2 to 0.7. The baseline condition is indicated as "B" in the figure and a horizontal line is drawn to indicate its median. The asterisk mark the conditions which are significantly different from the baseline.

As can be seen in Figure 6.5a, the performance with the up dipole dynamics is similar to that of the baseline over different conditions. In contrast, the performance with the down dipole dynamics gradually gets worse when ζ_2 increases. The up dipole dynamics increase the gain of the controlled dynamics, thus the human operator may not need to change control behavior and a similar performance with the baseline can be achieved. However, the down dipole dynamics lower the gain of the controlled dynamics at frequencies ($\omega_{dp} = 1$ rad/s) where the forcing function has most of its power. Thus the human operator has to increase his/her own gain in order to compensate for it. However, this could lead to very high control activity. According to Kolmogorov-Smirnov tests, the distribution of the performance data is significantly different from normal (C0, C6 and C11), and a nonparametric Friedman test was performed instead of an ANOVA, as can be seen in Table 6.2. Furthermore, a nonparametric Wilcoxon signed-rank test was performed instead of a paired t-test in order to find the conditions which are significantly different from the baseline condition (at a Bonferroni corrected significance level of $\alpha = 0.0036$). The z-statistic of the Wilcoxon signed-rank test is not available due to the small sample size (≤ 14) with the exact-method for calculating the p-value [6]. Figure 6.5a shows that the performance of all the up dipole dynamics are not significantly different from the baseline. The performance with the down

dipole dynamics becomes significantly different from the baseline from C10 ($\zeta_1 = 0.2$, $\zeta_2 = 0.35$) to C14 ($\zeta_1 = 0.2$, $\zeta_2 = 0.7$).

In Figure 6.5b, the control activities of all conditions are shown. It can be seen that the control activity with the up dipole dynamics decreases when ζ_1 increases. In contrast, the control activity with the down dipole dynamics increases when ζ_2 increases. The up dipole dynamics increase the gain of the controlled dynamics, thus the human operator could lower his/her own gain. In contrast, the down dipole dynamics decrease the gain of the controlled dynamics, and the human operator has to increase his/her own gain to compensate for the performance. The data of control activity are not normal distributed (C4), and a nonparametric Friedman test was performed instead of an ANOVA, and a Wilcoxon signed-rank test was performed instead of a paired t-test. As can be seen in Figure 6.5b, the control activity with the up dipole dynamics becomes significantly different from the baseline from C2 ($\zeta_1 = 0.3$, $\zeta_2 = 0.2$) to C7 ($\zeta_1 = 0.7$, $\zeta_2 = 0.2$). The control activity with the down dipole dynamics becomes significantly different from the baseline from C9 ($\zeta_1 = 0.2$, $\zeta_2 = 0.3$) to C14 ($\zeta_1 = 0.2$, $\zeta_2 = 0.7$).

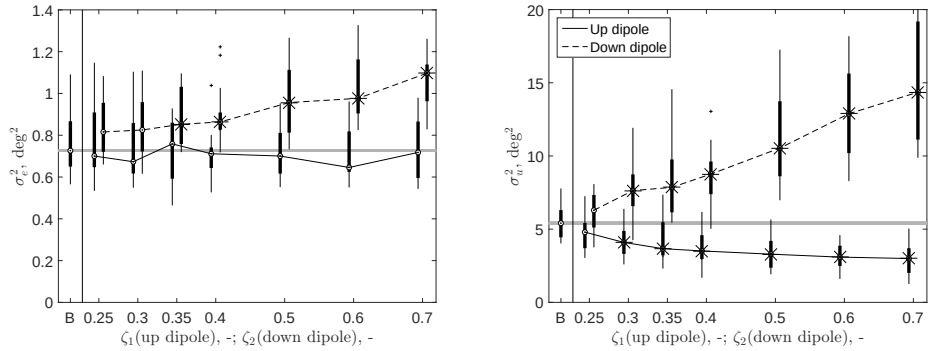

(a) Performance (b) Control activity

Figure 6.5: Variance of the error signal e and control signal u for each condition of fifteen subjects. The asterisk mark the conditions significantly different from the baseline (B) based on a Wilcoxon signed-rank test ($p < 0.0036$).

Table 6.2: Friedman test results for σ_e^2 and σ_u^2, where * is significant ($p < 0.05$), and - is not significant ($p \geq 0.05$).

	σ_e^2			σ_u^2		
Factor	df	χ^2	Sig.	df	χ^2	Sig.
H_c	14	127.3	*	14	192.4	*

CROSSOVER FREQUENCIES AND PHASE MARGINS

Figure 6.6a shows the box-plot of the target crossover frequencies $\omega_{c,t}$ for all conditions for the fifteen subjects. The solid line shows the change of the medians of the “up dipole" conditions when $\zeta_2 = 0.2$ and ζ_1 increases from 0.2 to 0.7, and the dashed line shows the

change of the medians of the "down dipole" conditions when $\zeta_1 = 0.2$ and ζ_2 increases from 0.2 to 0.7.

As can be seen in Figure 6.6a, the target crossover frequencies with the up dipole dynamics are slightly lower than that of the baseline, and the target crossover frequencies with the down dipole dynamics increase when ζ_2 increases. Because the crossover frequency data are not normally distributed (C11, C12 and C13), a nonparametric Friedman test (Table 6.3) and a nonparametric Wilcoxon signed-rank test were performed. Table 6.3 shows that there is a significant difference among conditions ($\chi^2(14) = 38.6,\ p < 0.05$). However, in Figure 6.6a, as can be seen there is no asterisk (the asterisk is used to mark a condition which is significantly different from the baseline, see Figure 6.5 as an example), meaning that none of the crossover frequency of any condition is significantly different from the baseline.

Figure 6.6b shows the box-plot of the target phase margins $\phi_{m,t}$ for all conditions of the fifteen subjects. It can be seen that the target phase margin decreases slightly when the damping ratio increases from 0.25 to 0.7. Due to the fact that the target phase margn data are not normally distributed (C13), a nonparametric Friedman test and a nonparametric Wilcoxon signed-rank test were performed. Table 6.3 shows that there there are significant differences among conditions ($\chi^2(14) = 31.8,\ p < 0.05$). However, in Figure 6.6b there is no asterisk, meaning that none of the target phase margin of any condition is significantly different from the baseline.

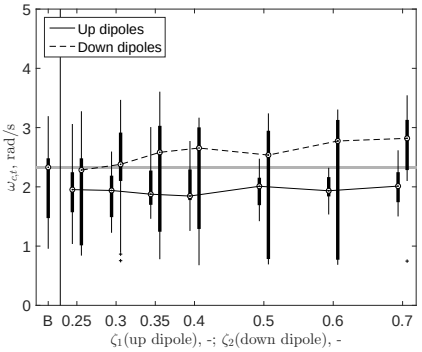

(a) Target crossover frequencies

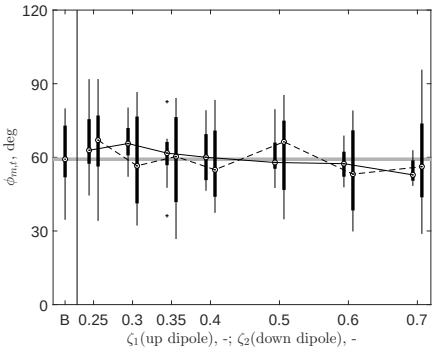

(b) Target phase margins

Figure 6.6: Target crossover frequencies and phase margins for each condition of fifteen subjects. Based on a Wilcoxon signed-rank test ($p < 0.0036$), none of the condition is significantly different from the baseline for target crossover frequency or target phase margin, respectively.

Table 6.3: Friedman test results of the target crossover frequencies and phase margins, where * is significant ($p < 0.05$), and - is not significant ($p \geq 0.05$).

	$\omega_{c,t}$			$\phi_{m,t}$		
Factor	df	χ^2	Sig.	df	χ^2	Sig.
H_c	14	38.6	*	14	31.8	*

HUMAN OPERATOR MODEL FITTING RESULTS

Figure 6.7 shows the human operator modeling results for Subject 3 for the baseline condition (B), C7, and C14. The frequency response functions at both target and disturbance forcing function frequencies are shown with circular and triangular markers, respectively. The error bars show the sample standard deviations of the FRF estimates over the three measurement runs. Finally, the frequency response of the total controlled dynamics is also shown, for reference.

As can be verified from Figure 6.7, the fitted human operator models in general show very good agreement with (independently estimated) FRFs. Also, the attained VAF values are high (>80%), which means that the human operator model output accurately describes the measured output u. The results in Figure 6.7 are representative for all collected data, i.e., for all other subjects and conditions. Overall, VAF values between 71% and 93% were attained. The human operator modeling result was less accurate only for Subject 15 in C7, with a VAF of around 67%.

HUMAN OPERATOR MODEL PARAMETERS

Figure 6.8 shows the box-plot of the human operator model parameters for all conditions of the fifteen subjects. The solid line shows the change of the medians of the “up dipole" conditions when $\zeta_2 = 0.2$ and ζ_1 increases from 0.2 to 0.7, and the dashed line shows the change of the medians of the “down dipole" conditions when $\zeta_1 = 0.2$ and ζ_2 increases from 0.2 to 0.7. The baseline condition is indicated as “B” in the figure and a horizontal line is drawn to indicate its median. The asterisk mark the conditions which are significantly different from the baseline.

In Figure 6.8a, in general the visual gain with the up dipole dynamics decreases when ζ_1 increases, and the visual gain with the down dipole dynamics increases when ζ_2 increases. The up dipole dynamics increase the gain of the controlled dynamics, thus the human operator may decrease his/her visual gain and similar performance with the baseline can be obtained (see Figure 6.5a). However, the down dipole dynamics lower the gain of the controlled dynamics at frequencies where the forcing function has most of its power. The human operator has to increase his/her gain to compensate with higher control activity (see Figure 6.5b). Figure 6.8 shows that the visual gain with the up dipole dynamics becomes significantly different from that of the baseline from C3 ($\zeta_1 = 0.35$, $\zeta_2 = 0.2$) to C7 ($\zeta_1 = 0.7$, $\zeta_2 = 0.2$), and the visual gain with the down dipole dynamics becomes significantly different from that of the baseline for C13 ($\zeta_1 = 0.2$, $\zeta_2 = 0.6$) and C14 ($\zeta_1 = 0.2$, $\zeta_2 = 0.7$).

In Figure 6.8d, the lead time constant with the up dipole dynamics increases when ζ_1 increases, and the lead time constant with the down dipole dynamics decreases when ζ_2 increases. The phase with the up dipole dynamics is positive when $\omega < 1 rad/s$ and becomes negative when $\omega > 1 rad/s$ (see Figure 6.2b). For a compensatory tracking task the up dipole dynamics may decrease the stability of the system when $\omega > 1$ rad/s. The lead time constant is thus found to increase with increasing perturbations with the up dipole dynamics. In contrast, the down dipole dynamics increase the stability of the system, and the human operators do not need to generate much lead compared with the case of up dipole dynamics. Figure 6.8d shows that for the up dipole dynamics the lead time constant becomes significantly different from that of the baseline from C5 ($\zeta_1 = 0.5$, $\zeta_2 = 0.2$) to C7

($\zeta_1 = 0.7$, $\zeta_2 = 0.2$), and the lead time constant with the down dipole dynamics becomes significantly different from that of the baseline from C12 ($\zeta_1 = 0.2$, $\zeta_2 = 0.5$) to C14 ($\zeta_1 = 0.2$, $\zeta_2 = 0.5$).

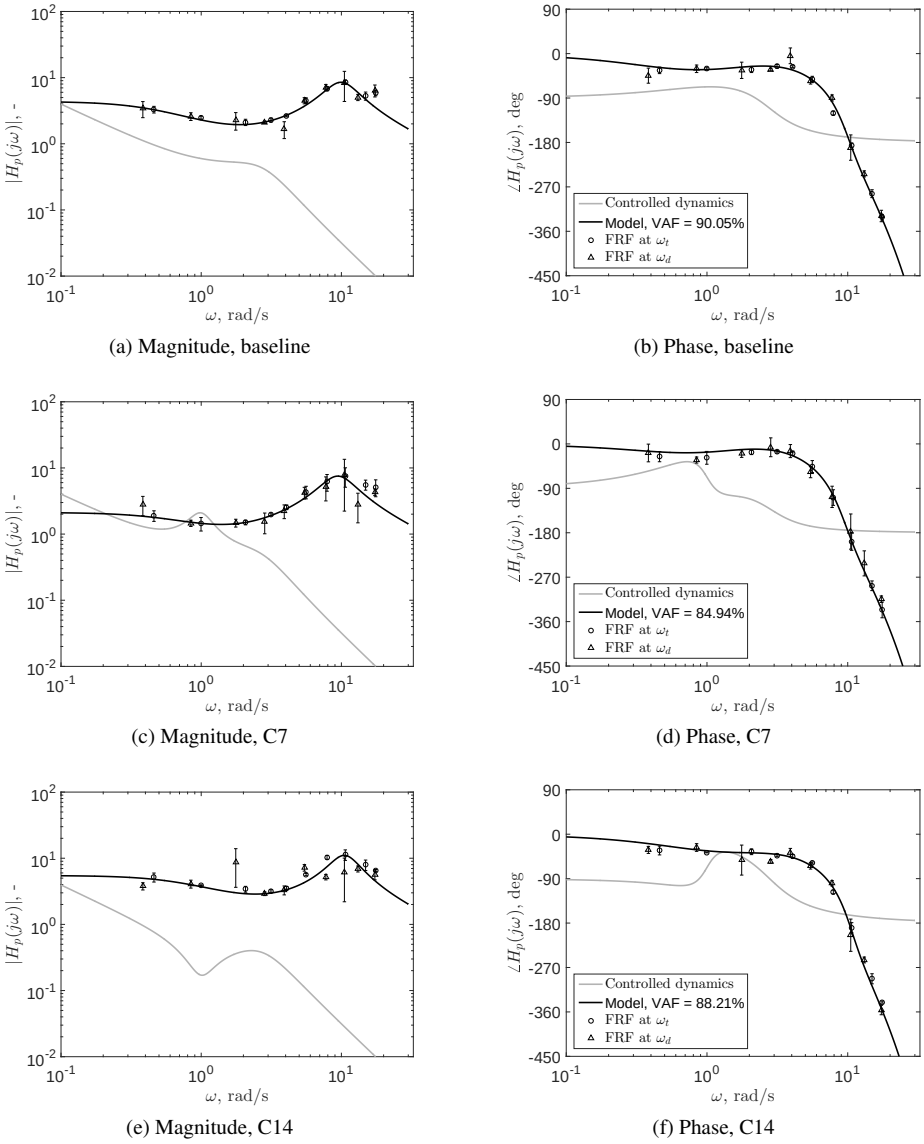

(a) Magnitude, baseline

(b) Phase, baseline

(c) Magnitude, C7

(d) Phase, C7

(e) Magnitude, C14

(f) Phase, C14

Figure 6.7: Subject 3 compensatory model fits and frequency response functions for conditions of baseline, C7 and C14.

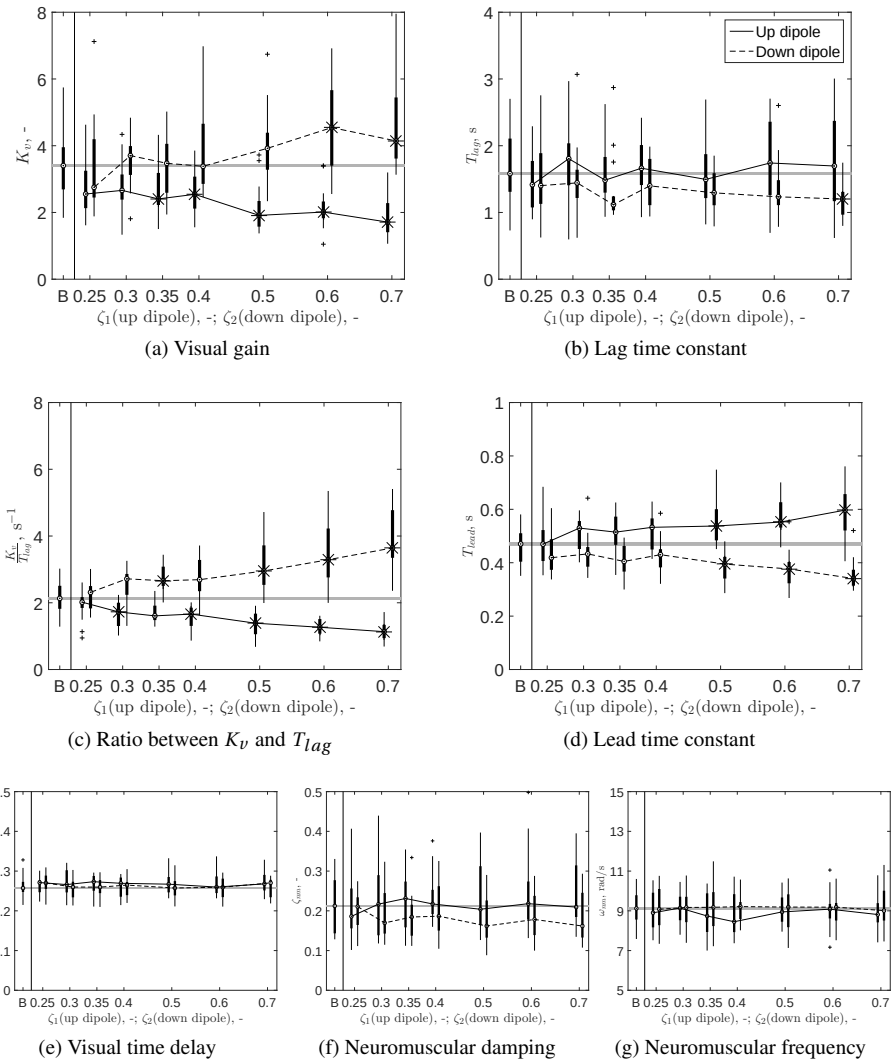

(a) Visual gain

(b) Lag time constant

(c) Ratio between K_v and T_{lag}

(d) Lead time constant

(e) Visual time delay

(f) Neuromuscular damping

(g) Neuromuscular frequency

Figure 6.8: Human operator model parameters. The asterisk mark the conditions significantly different from the baseline (B) based on a Wilcoxon signed-rank test ($p < 0.0036$).

Table 6.4: Friedman test results of the human operator model equalization parameters, * is significant ($p < 0.05$), - is not significant ($p \geq 0.05$).

	K_v			T_{lag}			K_v/T_{lag}			T_{lead}		
Factor	df	χ^2	Sig.	df	χ^2	Sig.	df	χ^2	Sig.	df	χ^2	Sig.
H_c	14	167.7	*	14	28.3	*	14	180.3	*	14	149.5	*

Table 6.5: Friedman test results of the human operator model visual time delay and neuromuscular parameters, * is significant ($p < 0.05$), - is not significant ($p \geq 0.05$).

	τ_v			ζ_{nm}			ω_{nm}		
Factor	df	χ^2	Sig	df	χ^2	Sig.	df	χ^2	Sig.
H_c	14	21.9	-	14	48.6	*	14	5.5	-

Figure 6.8b shows that the lag time constant with the up dipole dynamics is in general higher than that with the down dipole dynamics. It can be seen that for the up dipole dynamics the lag time constant is not significantly different from that of the baseline for any condition, and for the down dipole dynamics the lag time constant of C14 ($\zeta_1 = 0.2$, $\zeta_2 = 0.7$) is significantly different from that of the baseline.

Figures 6.8e, 6.8f and 6.8g show the visual time delay, neuromuscular damping ratio and neuromuscular natural frequency, respectively. None of these parameters are significantly different from those of the baseline, respectively.

According to the Wilcoxon signed-rank test for the performance, control activity (see Figure 6.5), ratio of the visual gain and lag time constant and lead time constant (see Figure 6.8), only the added dynamics of C1 and C8 (Table 6.1) are not significantly different with respect to the baseline dynamics. For any of the other tested added dynamics, at least one of the dependent measures (performance, control activity, ratio of the visual gain and lag time constant or lead time constant) is significantly different from the baseline.

6.3.2. COMPARISON WITH SIMULATION PREDICTION DATA

In Figure 6.9 the experiment results are compared with the simulation results on the same conditions. Figure 6.9a, for example, shows the baseline condition (B) in the middle. The down dipole dynamics conditions are shown on the left-hand side of the baseline condition, with $\zeta_1 = 0.2$ and ζ_2 changing from 0.25 (C8) to 0.7 (C14). The up dipole dynamics conditions are shown on the right-hand side of the baseline condition, with $\zeta_2 = 0.2$ and ζ_1 changing from 0.25 (C1) to 0.7 (C7).

In Figure 6.9a it can be seen that the performance of the simulation is better than that of the experiment. Figure 6.9b shows that the control activity of the simulation is higher than that of the experiment over different conditions. This may be due to the fact that in the simulation the objective was only to optimize the performance without limiting the control activity, which means that the control activity can become high if better performance can be achieved.

In Figure 6.9c, the target crossover frequencies of the simulation are higher than those of the experiment over different conditions. This may also be due to the fact that the objective of the simulation is only to optimize the performance without limiting the control activity, which may lead to higher crossover frequencies. In Figure 6.9d, in general the target phase margins of the simulation are lower than those of the experiment for most of the conditions. For the conditions with the up dipole dynamics, it can be seen that the changing trends between the simulation and experiment are not consistent.

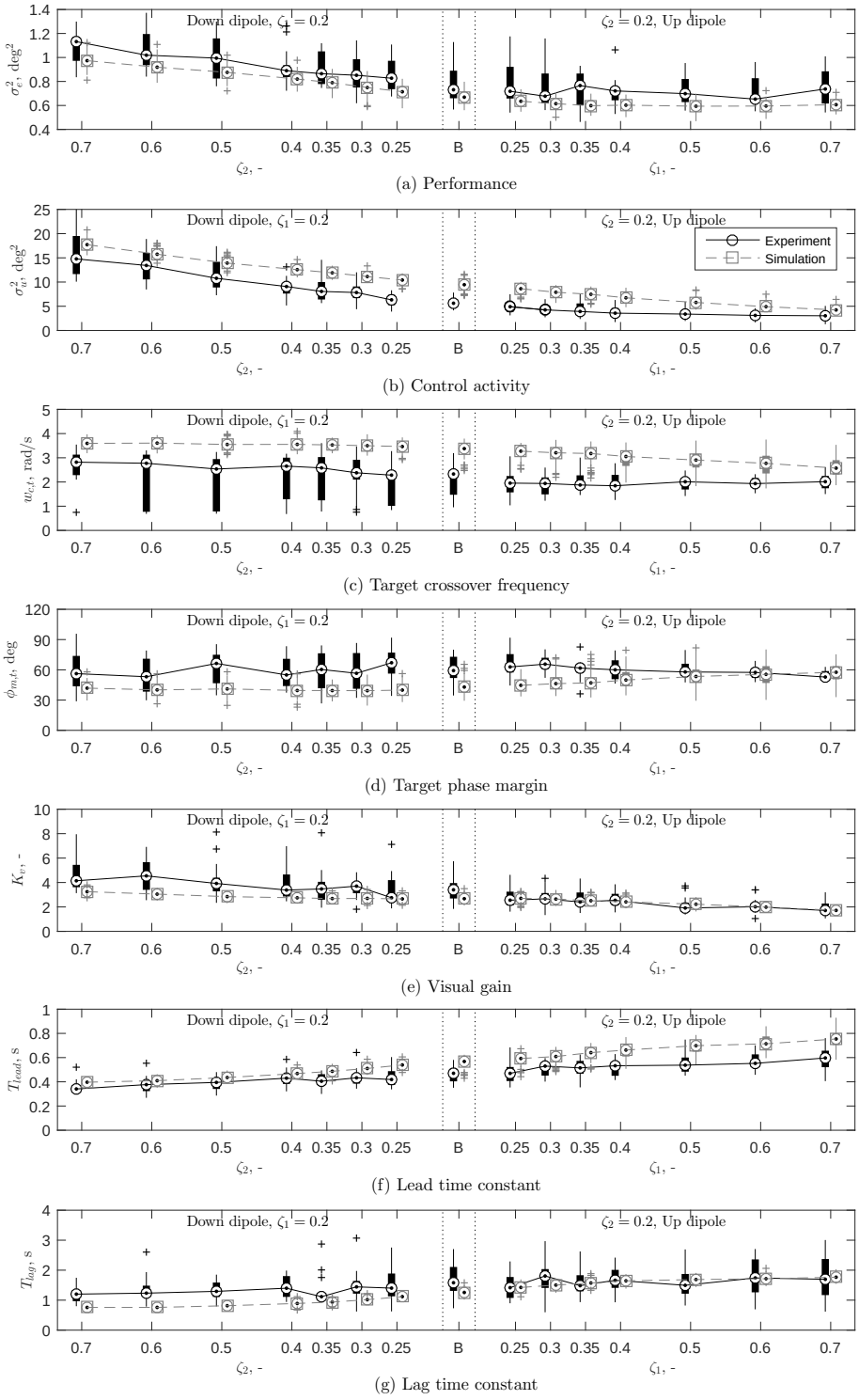

Figure 6.9: Comparison between experiment and simulation results.

In Figures 6.9e, 6.9f and 6.9g, it can be seen that there are offsets between the simulation and experiment results on visual gain, lead time constant and lag time constant over different conditions, respectively. For example, for both visual gain and lag time constant, the simulation results are closer with the experiment results for the up dipole dynamics than the down dipole dynamics. However, for lead time constant, the simulation results are closer with the experiment results for the down dipole dynamics. In general, the changing trends of these human operator model parameters over conditions are very similar to those of the experiment.

Figure 6.10 shows the comparison between the experiment and simulation results for the ratio of the visual gain and lag time constant. It can be seen that the simulation well predicts the changing trend of the experiment results, and the agreement between the simulation and experiment data is better for the up dipole dynamics than for the down dipole dynamics.

In Table 6.6 the correlations between the medians of the simulation and the experiment results are shown for performance, control activity, target crossover frequency, target phase margin, visual gain, lag time constant, ratio of the visual gain and lag time constant and lead time constant, respectively. The R value should be close to 1 if the correlation is significant. It can be seen that, except for the target phase margin, all variables have significantly high correlations between the simulation and experiment results. The low correlation of the target phase margin can also be seen in Figure 6.9d.

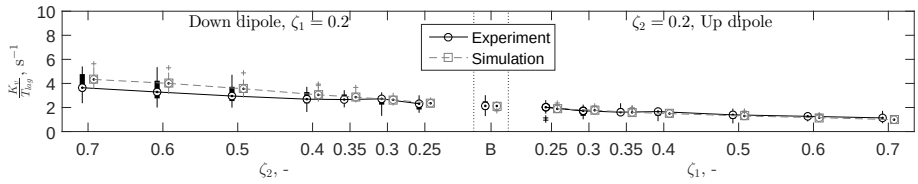

Figure 6.10: Comparison between experiment and simulation K_v / T_{lag}.

Table 6.6: Correlation coefficients for experiment and simulation data, where * indicates that the correlation is significant ($p < 0.05$), - is not significant ($p \geq 0.05$).

	σ_e^2	σ_u^2	$\omega_{c,t}$	$\phi_{m,t}$	K_v	T_{lag}	K_v / T_{lag}	T_{lead}
R	0.97	0.98	0.79	-0.23	0.88	0.82	0.97	0.97
Sig.	*	*	*	-	*	*	*	*

6.3.3. MANUAL CONTROL ADAPTATION BOUNDARIES VERIFICATION

RELATIVE CHANGES OF THE MCAB VARIABLES

In Figure 6.11, the relative changes of performance, control activity, ratio of the visual gain and lag time constant, and the lead time constant with respect to those of the baseline dynamics are shown (for experiment and simulation results, respectively). These dependent measures are the ones quantifying the MCAB (see Chapter 5). In Figure 6.11a, for example, the baseline condition (B) is in the middle. The down dipole dynamics conditions are shown on the left-hand side of the baseline condition, with $\zeta_1 = 0.2$ and ζ_2 changing from 0.25 (C8) to 0.7 (C14). The up dipole dynamics conditions are shown on the right-hand side of the

baseline condition, with $\zeta_2 = 0.2$ and ζ_1 changing from 0.25 (C1) to 0.7 (C7). The VAF values are shown to indicate the fittings of the simulation data to the experiment results for the up and down dipoles, respectively.

In Figures 6.11a and 6.11d, it can be seen that the relative changes of the performance and lead time constant are very similar for the experiment and simulation results, indicating that in Chapter 5 the MCAB for performance and lead time constant at 1 rad/s were indeed well predicted and need no further modification. The low VAF value for the up dipoles in Figures 6.11a is due to the relatively low values of the experiment data and their inconsistencies for different conditions. Since the maximum mismatch is only around 20% for C3 ($\zeta_1 = 0.35$, $\zeta_2 = 0.2$), the relative changes between the simulation and experiment data are still very close.

In Figure 6.11b, the relative changes of the control activity for the up dipole dynamics are also in very good agreement between the experiment and simulation results. However, for the down dipole dynamics the relative change of the simulation control activity is clearly underestimated when compared with the experiment results. The maximum mismatch is around 80% at C14 ($\zeta_1 = 0.2$, $\zeta_2 = 0.7$), and the VAF value 76.53% is relatively low, indicating that in Chapter 5 the MCAB for control activity at 1 rad/s may be overestimated and would be narrower (less qualified added dipole dynamics for fixed amount of relative change of control activity).

Similarly, in Figure 6.11c, the simulation data for $\Delta K_v / T_{lag}$ match well with the experiment results for the up dipole dynamics. However, for the down dipole dynamics the relative change of the simulated K_v / T_{lag} is strongly overestimated, with a mismatch that increases to around 30% at C14 ($\zeta_1 = 0.2$, $\zeta_2 = 0.7$), and the VAF value 69.94% is also relatively low. This suggests that the MCAB for $\Delta K_v / T_{lag}$ at 1 rad/s from Chapter 5 may be too conservative and shall actually be wider.

In Table 6.7, piecewise correlations for the medians of the simulation and the experiment results are shown for all the dependent measures in Figure 6.11. In Table 6.7, it can be seen that the R values are all very close to 1, meaning that the correlations are significant for all dependent measures. In summary, Figure 6.11 indicates that for the up dipole dynamics, the MCAB and the IMCAB at 1 rad/s (see Chapter 5) match the experiment data very well and do not need any further modification. For the down dipoles in Figure 6.11, due to the observed discrepancies in the relative changes in control activity and the ratio of the visual gain and lag time constant, further tuning and modification of the MCAB and the IMCAB would be necessary. These updates are presented and discussed in the following sections.

UPDATED SIMULATION-BASED MCAB

In Chapter 5, the parameter intervals of the dipole damping ratios of both ζ_1 and ζ_2 were set at 0.1, and in total 36 down dipoles were simulated at 1 rad/s. This resolution of the simulation down dipoles could be too low for correcting the MCAB. For example, in Chapter 5, there were 8 out of 36 down dipoles of which the relative changes of control activity were within 20%, and these eight "qualified" down dipoles were all within the MCAB lower magnitude at 1 rad/s.

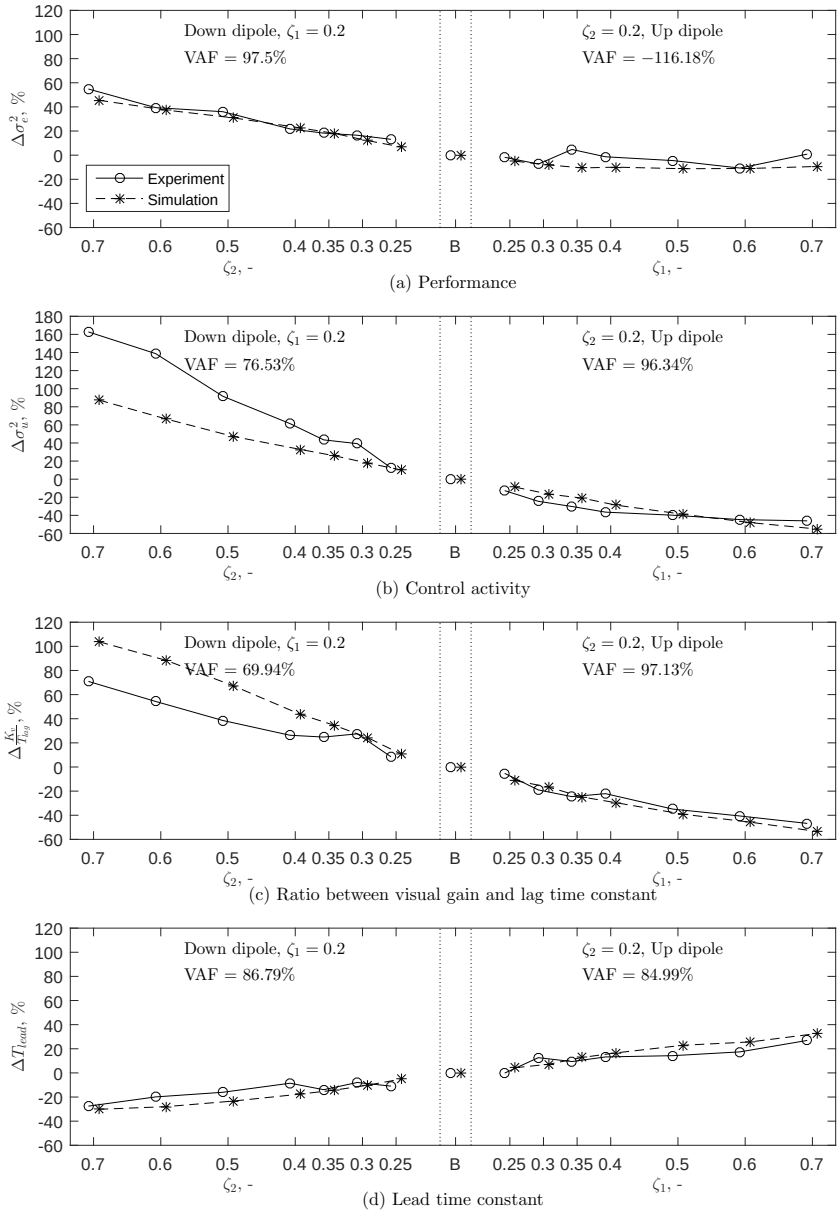

Figure 6.11: Comparison of the relative changes of the medians with respect to the baseline between the experiment and simulation results. The VAF values are shown to indicate the fittings of the simulation data to the experiment results for the up and down dipoles, respectively.

Table 6.7: Correlation coefficients for experiment and simulation data for the MCAB dependent measures, where * indicates that the correlation is significant ($p < 0.05$).

	$\Delta\sigma_e^2$	$\Delta\sigma_u^2$	$\Delta K_v / T_{lag}$	ΔT_{lead}
R	0.97	0.98	0.99	0.97
Sig.	*	*	*	*

According to Figure 6.11, the actual relative changes of control activity for down dipoles are higher than those of the simulation data. If the simulation control activity data for the 36 down dipoles obtained in Chapter 5 were enlarged, there could be no more "qualified" down dipoles of which the relative changes of control activity are within 20%. This could result in, for example, an updated MCAB lower magnitude at the 0 dB line (at 1 rad/s) even for a 20% relative change level, which does not make much sense. To avoid such problems, the simulation data in Chapter 5 were extended, and the total number of the down dipoles at 1 rad/s was increased in this chapter. The ranges of both ζ_1 and ζ_2 were still between 0.1 and 0.9 as used in Chapter 5. From 0.1 to 0.3, the parameter interval decreased to 0.02, and from 0.3 to 0.9, the parameter interval was kept at 0.1 as used in Chapter 5.

As a result of this increased number of down dipoles at 1 rad/s in the simulation, the MCAB for the individual dependent measures developed in Chapter 5 changed somewhat at 1 rad/s for the down dipole dynamics, which can be seen in Figure 6.12. In Figure 6.12c, the 20% MCAB lower magnitude boundary at 1 rad/s moved from -2 dB to -4 dB at the same frequency; the 40% MCAB lower magnitude boundary at 1 rad/s moved from -6 dB to around -7 dB. Similarly, in Figure 6.12d, the 20% MCAB lower magnitude boundary at 1 rad/s moves from -6 dB to -9 dB at the same frequency.

In Figure 6.13, the updated simulation-based IMCAB were generated based on the intersection part of all the sub-figures of Figure 6.12 for the magnitude and phase, respectively. Compared with the original IMCAB developed in Chapter 5, the 20% IMCAB lower magnitude boundary at 1 rad/s moved from -2 dB to -4 dB at the same frequency; the 40% IMCAB lower magnitude boundary moved from -6 dB to around -7 dB at 1 rad/s.

For the phases of both MCAB (Figures 6.12e, 6.12f, 6.12g, and 6.12h) and IMCAB (Figure 6.13b), there was no change for the updated boundaries compared with those in Chapter 5. This is due to the fact that the phase boundaries were formed based on all the up and down dipoles between 1 and 7 rad/s in the simulation. The newly added down dipoles did not change the phase boundaries at either 1 rad/s or at other frequencies.

MODIFICATIONS OF MCAB WITH EXPERIMENT DATA

Modifications on the simulation control activity and ratio of the visual gain and lag time constant obtained in Chapter 5 and the newly added down dipoles at 1 rad/s were made, based on the observed discrepancies between the simulation and experiment data in Figure 6.11. To correct the relative changes in the simulation data, for example, a scaling coefficient $c_{u(C*)}$ for control activity is calculated, to match $\Delta\sigma_u^2$ of the simulation the same with the experiment value, for each tested down dipole dynamics in the experiment:

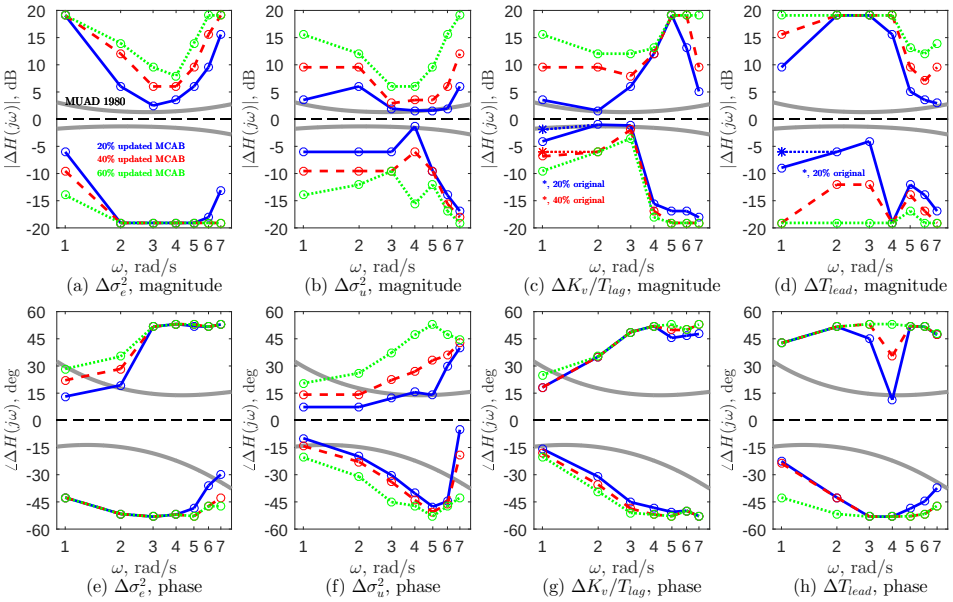

Figure 6.12: The updated simulation-based MCAB with various amounts of relative changes on the performance, control activity, ratio of the visual gain and lag time constant and lead time constant (blue: $|\Delta| \leq 20\%$, red: $|\Delta| \leq 40\%$, green: $|\Delta| \leq 60\%$) compared with the original MUAD envelopes [2] (grey). Figure 6.12c and 6.12d also show the changes compared with the original simulation-based MCAB developed in Chapter 5.

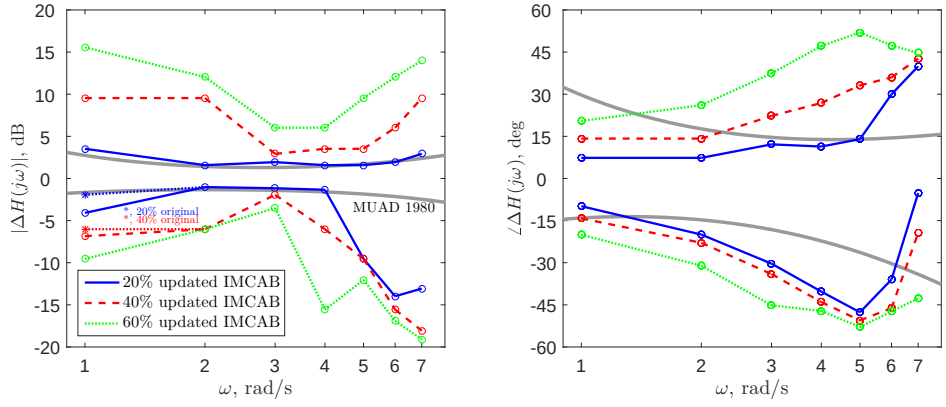

Figure 6.13: The updated simulation-based IMCAB based on the intersection part of all sub-figures of Figure 6.12 for magnitude and phase, respectively. Figure 6.13a also shows the changes compared with the original simulation-based IMCAB developed in Chapter 5.

$$c_{u(C*)} = \frac{\sigma^2_{u(C*),exp}}{\sigma^2_{u(C*),sim}} \cdot \frac{\sigma^2_{u(B),sim}}{\sigma^2_{u(B),exp}}, \tag{6.3}$$

where $\sigma^2_{u(C*),exp}$ is the median of the measured control activity of a certain down dipole (condition) tested in the experiment, $\sigma^2_{u(C*),sim}$ is the median of the simulation control activity of the same down dipole (condition), $\sigma^2_{u(B),sim}$ is the median of the simulation baseline control activity and $\sigma^2_{u(B),exp}$ is the median of the measured baseline control activity in the experiment. Coefficient $c_u(C*)$ was calculated for all the down dipole conditions (C8-C14) for the control activity, resulting in an average coefficient value of 1.24. To formulate a new set of modified MCAB of 20%, 40% and 60% based on the experiment results, the simulation control activity (for both of the data obtained in Chapter 5 and the newly added down dipoles at 1 rad/s) was then scaled with this average coefficient. Similarly, Eq. (6.3) was also applied to K_v/T_{lag} for all the down dipole conditions (C8-C14) and an average correction coefficient of 0.9 was obtained, which was then applied to the simulation K_v/T_{lag} data.

Figure 6.15 shows the modified MCAB for $\Delta\sigma^2_u$ and $\Delta K_v/T_{lag}$ with experiment data. For the ease of comparison, the updated simulation-based MCAB for $\Delta\sigma^2_u$ and $\Delta K_v/T_{lag}$ are shown in Figure 6.14 (copied from Figure 6.12). It can be seen that the modified MCAB magnitude for $\Delta\sigma^2_u$ (Figure 6.15a) is narrower than the one in Figure 6.14a at 1 rad/s, which corresponds with the observations in Figure 6.11b. The modified MCAB magnitude for $\Delta K_v/T_{lag}$ (Figure 6.15b) is wider than the one in Figure 6.14b at 1 rad/s, which corresponds with the observations in Figure 6.11c. The phases of the MCAB are not influenced by the modifications, since the phase boundaries at 1 rad/s are formed by added dipoles at other frequencies rather than the ones at 1 rad/s.

The resulting modified IMCAB can be seen in Figure 6.16, in which the added dipole dynamics of C1 and C8, for which the tracking performance, control activity, ratio of the visual gain and lag time constant and the lead time constant were all not significantly different from those of the baseline, are drawn for reference. In Figure 6.16a, it can be seen that the modified IMCAB lower magnitude boundary at 1 rad/s is just inside of the peak of C8. However, in general, the added dipole dynamics that are not significantly different from the baseline are still very close to the 20% boundaries in Figures 6.16a and 6.16b.

VERIFICATION OF THE MANUAL CONTROL ADAPTATION BOUNDARIES

The final MCAB for individual dependent measures include: Figures 6.12a and 6.12e for $\Delta\sigma^2_e$, Figures 6.12d and 6.12h for ΔT_{lead}, Figures 6.15a and 6.15c for $\Delta\sigma^2_u$, and Figures 6.15b and 6.15d for $\Delta K_v/T_{lag}$. The MCAB for $\Delta\sigma^2_e$ and ΔT_{lead} were not modified on the basis of experiment data, since in Figures 6.11a and 6.11d these two dependent measures match well between the simulation and experiment data, respectively.

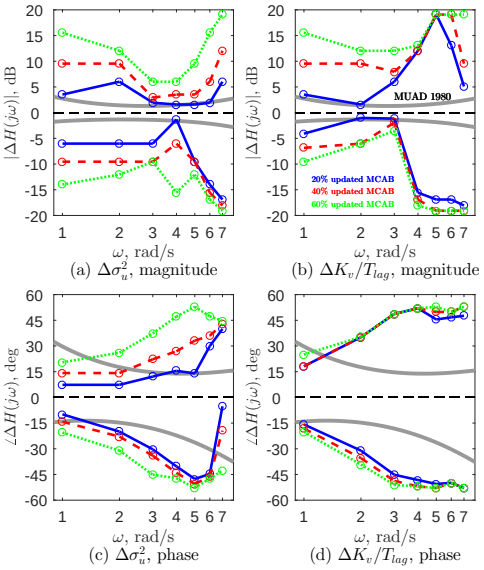

Figure 6.14: The updated MCAB for $\Delta\sigma_u^2$ and $\Delta K_v/T_{lag}$.

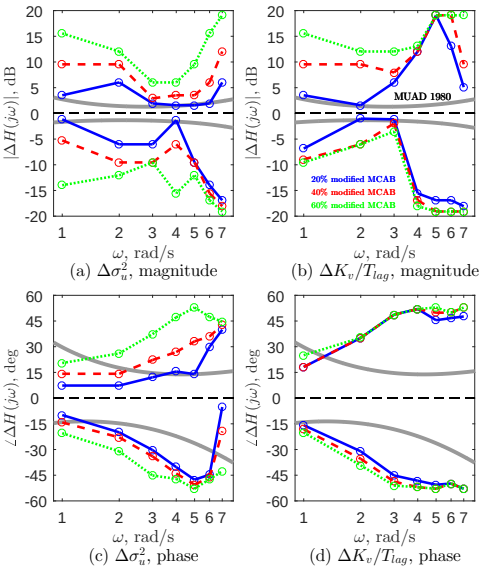

Figure 6.15: The modified MCAB for $\Delta\sigma_u^2$ and $\Delta K_v/T_{lag}$ with experiment data corrections.

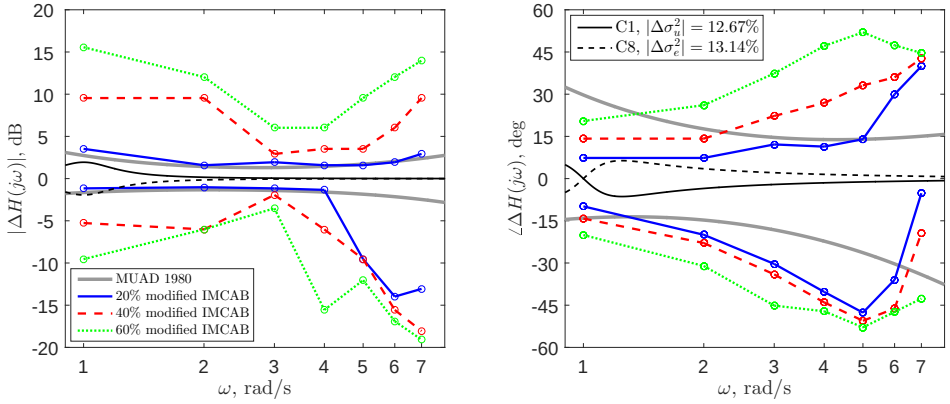

Figure 6.16: The modified IMCAB based on the intersection part of sub-figures in Figures 6.12a, 6.12d, 6.12e, 6.12h and Figure 6.15 for magnitude and phase, respectively. The added dipole dynamics of C1 and C8 (which are not significantly different from the baseline for the tracking performance, control activity, ratio of the visual gain and lag time constant and the lead time constant) are drawn for reference.

The MCAB for $\Delta\sigma_u^2$ and $\Delta K_v/T_{lag}$ were modified based on the experiment data, due to the clear discrepancies observed in Figures 6.11b and 6.11c for the down dipoles. To verify these MCAB, all added dipoles tested in the experiment (see Figure 6.2) are going to be drawn with the MCAB for individual dependent measures. Based on the MCAB formula-

tion approach in Chapter 5, the relative changes in $\Delta\sigma_e^2$, $\Delta\sigma_u^2$, $\Delta K_v/T_{lag}$ and ΔT_{lead} with each added dipole measured in the experiment (see Figure 6.11) will be used as indicators to judge whether the MCAB are accurate or not.

As an example, Figure 6.17 demonstrates the approach to verify the 20% MCAB for $\Delta\sigma_u^2$ using random added dipoles at 1 rad/s. In Figure 6.17a, H_{added1} is outside and H_{added2} is within the MCAB (comparing the dipole peak with the upper magnitude boundary point A0). According to Chapter 5, point A0 in Figure 6.17a is not affected by H_{added2}, no matter whether its $|\Delta\sigma_u^2| \leq 20\%$ or $|\Delta\sigma_u^2| > 20\%$ ($\Delta\sigma_u^2$ is not consistently constrained by the boundaries). For H_{added1}, if its $|\Delta\sigma_u^2| > 20\%$, point A0 is not affected; if its $|\Delta\sigma_u^2| \leq 20\%$, according to Chapter 5, point A0 should move upward to point A1, thus the upper magnitude boundary of the 20% MCAB for $\Delta\sigma_u^2$ is underestimated. In Figure 6.17b, H_{added3} is outside and H_{added4} is within the MCAB. Similar to H_{added2} in Figure 6.17a, the phase of MCAB in Figure 6.17b is not affected by H_{added4}. For H_{added3}, the added dynamics at 1, 4, 5, 6 and 7 rad/s do not affect MCAB since these parts are within the MCAB. At 2 and 3 rad/s, the added dynamics are outside the MCAB. According to Chapter 5, points B0 and C0 are not affected if H_{added3}'s $|\Delta\sigma_u^2| > 20\%$. While points B0 and C0 should move upward to points B3 and C3 if H_{added3}'s $|\Delta\sigma_u^2| \leq 20\%$, meaning that the upper phase boundary of the 20% MCAB for $\Delta\sigma_u^2$ is underestimated.

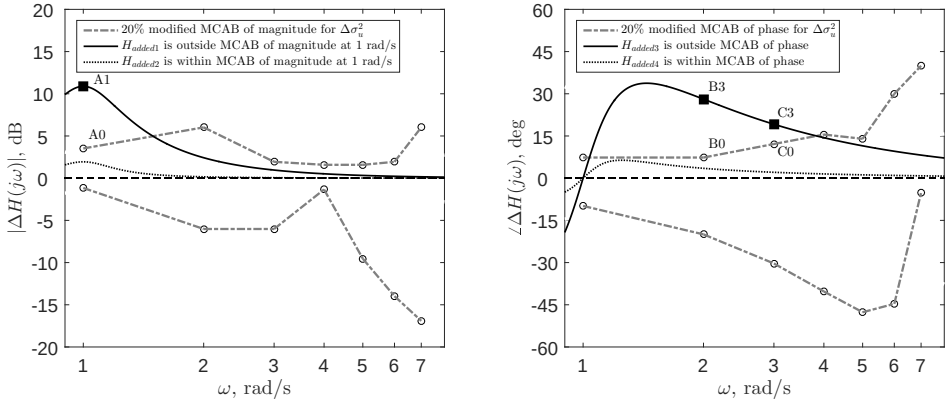

(a) Magnitude (b) Phase

Figure 6.17: A demonstration showing the approach to verify the MCAB for $\Delta\sigma_u^2$.

Figure 6.18 shows the MCAB for $\Delta\sigma_e^2$, $\Delta\sigma_u^2$, $\Delta K_v/T_{lag}$ and ΔT_{lead} with all the tested added dynamics, of which the relative changes in the dependent measures obtained from experiment (see Figures 6.11) are also shown for reference.

In Figure 6.18a, the upper magnitude MCAB of 20%, 40% and 60% at 1 rad/s are not affected, since all the up dipoles are within the MCAB at 1 rad/s. For the 20% lower magnitude MCAB at 1 rad/s, the down dipoles of C12-C14 are outside, all with $|\Delta\sigma_e^2| > 20\%$. For the 40% lower magnitude MCAB at 1 rad/s, the down dipole of C14 is outside the boundary, with $|\Delta\sigma_e^2| = 54.84\% > 40\%$. The 60% lower magnitude MCAB at 1 rad/s is not affected, since no down dipole is outside the boundary. In Figure 6.18b, for the 20% upper

phase MCAB, only at 2 rad/s the down dipoles of C13 and C14 are outside the boundary, all with $|\Delta\sigma_e^2| > 20\%$. The 40% and 60% upper phase MCAB and all the lower phase MCAB are not affected, since no dipole is outside these boundaries at 1, 2, 3, 4, 5, 6 and 7 rad/s. In general, the MCAB for $\Delta\sigma_e^2$ are accurate for all the tested dipoles.

In Figure 6.18c, for the 20% upper magnitude MCAB at 1 rad/s, the up dipoles of C3-C7 are outside the boundary, all with $|\Delta\sigma_u^2| > 20\%$. For the 40% upper magnitude MCAB at 1 rad/s, the up dipole of C7 is outside the boundary, with $|\Delta\sigma_u^2| = 46.07\% > 40\%$. The 60% upper magnitude MCAB at 1 rad/s is not affected, since no up dipole is outside its boundary. For the 20% lower magnitude MCAB at 1 rad/s, all down dipoles are outside the boundary, with $|\Delta\sigma_u^2| = 12.49\% < 20\%$ for C8 and $|\Delta\sigma_u^2| > 20\%$ for all other down dipoles. This suggests that the 20% lower magnitude MCAB at 1 rad/s should move slightly downward to the peak of the down dipole of C8. For the 40% lower magnitude MCAB at 1 rad/s, the down dipoles of C11-C14 are outside the boundary, all with $|\Delta\sigma_u^2| > 40\%$. The 60% lower magnitude MCAB at 1 rad/s is not affected, since no down dipole is outside the boundary. In Figure 6.18d, for the 20% upper phase MCAB, only at 2 and 3 rad/s there are down dipoles outside the boundary. At 2 rad/s, the down dipoles of C10-C14 are outside the boundary, all with $|\Delta\sigma_u^2| > 20\%$. At 3 rad/s, the down dipoles of C13 and C14 are outside the boundary, all with $|\Delta\sigma_u^2| > 20\%$. For the 40% upper phase MCAB, only at 2 rad/s there are down dipoles of C12-C14 outside the boundary, all with $|\Delta\sigma_u^2| > 40\%$. For the 60% upper phase MCAB, only at 2 rad/s there is down dipole of C14 outside the boundary, with $|\Delta\sigma_u^2| > 60\%$. For the 20% lower phase MCAB, only at 2 and 7 rad/s there are up dipoles of C6 and C7 outside the boundary, all with $|\Delta\sigma_u^2| > 20\%$. For the 40% lower phase MCAB, only at 2 rad/s there are up dipoles of C6 and C7 outside the boundary, all with $|\Delta\sigma_u^2| > 40\%$. The 60% lower phase MCAB is not affected since no dipole is outside the boundary. In general, the MCAB for $\Delta\sigma_u^2$ are accurate for all the tested dipoles, except for the 20% lower magnitude MCAB at 1 rad/s, which may move slightly downwards.

Using similar approach, the MCAB for $\Delta K_v/T_{lag}$ and ΔT_{lead} can be verified. In general, in Figures 6.18e, 6.18f, 6.18h, the MCAB for $\Delta K_v/T_{lag}$ and ΔT_{lead} correspond very well with the tested added dipoles. Except in Figure 6.18g, for the 20% lower magnitude MCAB at 1 rad/s, the down dipoles of C13 and C14 are outside the boundary, with $|\Delta T_{lead}| = 19.9\% < 20\%$ for C13 and $|\Delta T_{lead}| = 27.54\% > 20\%$ for C14. This suggests that the 20% lower magnitude MCAB at 1 rad/s should move slightly downward to the peak of the down dipole of C13.

In summary, the updated and modified MCAB match very well with the tested added dynamics in the experiment. This suggests that these boundaries can indeed be used to predict the relative changes in tracking performance, control activity and human operator control behavior with respect to those of the baseline dynamics.

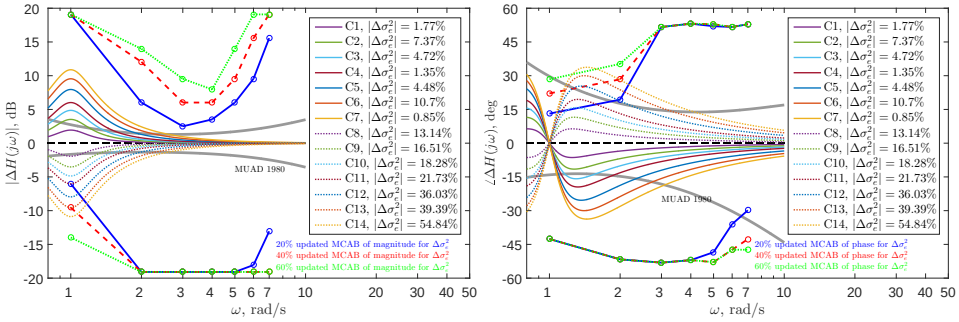

(a) Magnitude, $\Delta\sigma_e^2$

(b) Phase, $\Delta\sigma_e^2$

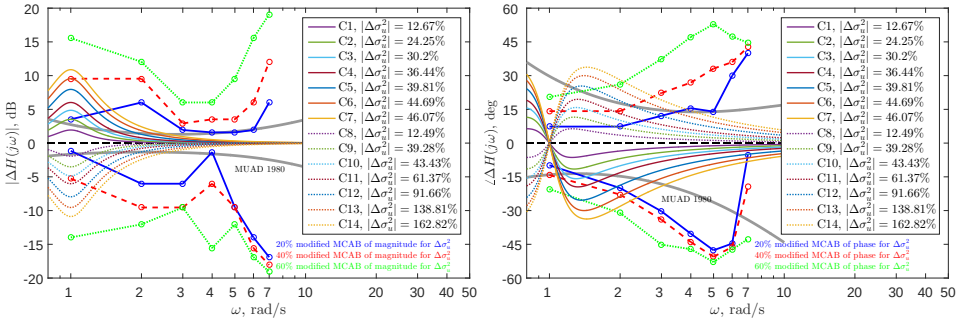

(c) Magnitude, $\Delta\sigma_u^2$

(d) Phase, $\Delta\sigma_u^2$

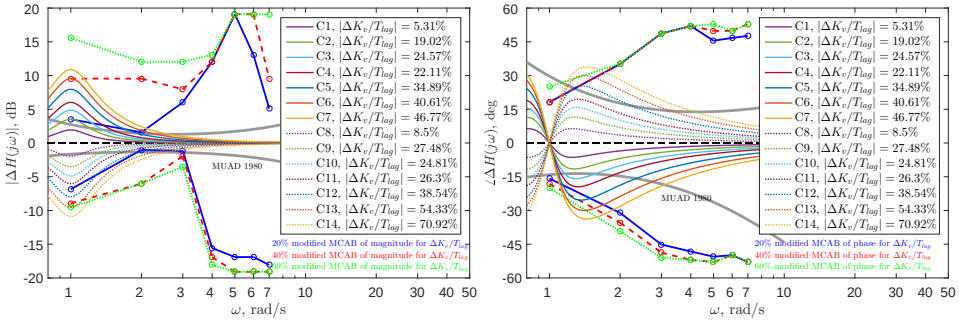

(e) Magnitude, $\Delta K_v/T_{lag}$

(f) Phase, $\Delta K_v/T_{lag}$

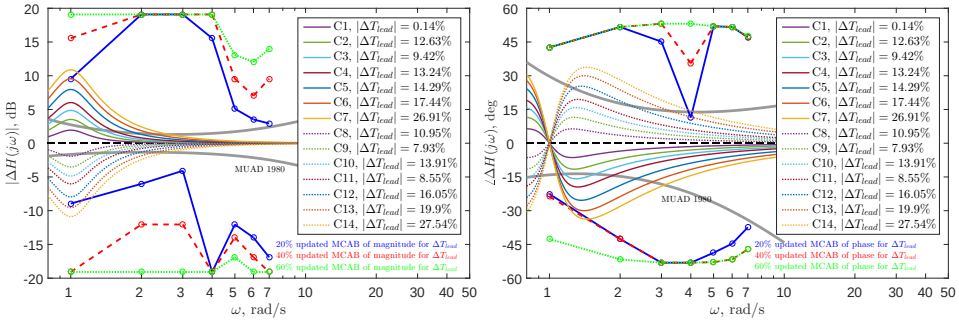

(g) Magnitude, ΔT_{lead}

(h) Phase, ΔT_{lead}

Figure 6.18: Verification of the MCAB. MCAB of $\Delta\sigma_u^2$ and $\Delta K_v/T_{lag}$ are modified based on experiment data.

6.4. DISCUSSION

In order to verify the MCAB developed in Chapter 5, an aircraft pitch attitude compensatory tracking task (also used in Chapter 4 and Chapter 5) with different added dipole dynamics was performed. In total 15 conditions were tested, with "down" and "up" dipole dynamics at 1 rad/s cascaded with the baseline aircraft pitch dynamics, as well as a reference baseline aircraft dynamics case. In addition, an offline computer simulation-based on optimal performance predictions with a human operator model – using a constrained nonlinear optimization algorithm – developed in Chapters 4 and 5 was used to predict performance, control activity, crossover frequency, phase margin and control behavioral parameters for the same test conditions. The simulation results were directly compared and correlated with the experiment data to verify the extent to which the observed human operator adaptations could be predicted. Moreover, the simulation and experiment results were compared for the relative changes of performance, control activity, ratio of the visual gain and lag time constant and lead time constant with respect to those of the baseline (which are the dependent measures quantifying the MCAB, see Chapter 5). Based on these comparison results, the MCAB and IMCAB developed in Chapter 5 were modified to better match the experiment results.

For the experiment and the considered variation in added dipole dynamics, two hypotheses were formulated. For *Hypothesis 1*, it was expected that the added dipole dynamics that are nearly within the subjective MUAD envelopes (C1&C2 and C8&C9) would have no effect on performance, control activity, target crossover frequency, target phase margin and human operator control behavior. It was also expected that the added dipole dynamics of C3-C7 and C10-C14 would have significant effects on either visual gain, lead time constant or lag time constant. Based on the experiment data, this hypothesis has to be rejected. The experiment results show that in C1&C2 and C8&C9, with the exception of the control activity, all other dependent measures are close to those of the baseline. The control activities of C2 ($\zeta_1 = 0.3$, $\zeta_2 = 0.2$) and C9 ($\zeta_1 = 0.2$, $\zeta_2 = 0.3$) are significantly different from that of the baseline, which indicates that the control activity is more sensitive to the added dipole dynamics than other dependent measures. The experiment results show that the visual gain is significantly lower than that of the baseline for C3-C7 and significantly higher than that of the baseline for C13-C14, the lead time constant of C5-C7 is significantly higher than that of the baseline and lower than that of the baseline for C12-C14, and the lag time constant of C14 is significantly lower than that of the baseline.

The second hypothesis (*Hypothesis 2*) stated that exact opposite effects of up and down dipole dynamics on performance and control activity were not expected. Considering the observed variations in the performance and control activity, this hypothesis is not rejected. The experiment results show that the performance of all up dipole dynamics is very similar to that of the baseline. The performance with the down dipole dynamics of C10-C14 is significantly worse than that of the baseline. The control activities of C1 and C8 are very similar with that of the baseline, and the control activities of C2-C7 and C9-C14 are all significantly different from that of the baseline. However, the relative changes of the control activities with the down dipole dynamics with respect to the baseline are much higher than those with the up dipole dynamics. For the human operator model parameters, only for the lead time constant the up and down dipole dynamics have opposite effects, where the lead time constant is significantly different from that of the baseline for C5-C7 with the up

dipole dynamics and for C12-C14 with the down dipole dynamics. The target crossover frequency, target phase margin, visual time delay, neuromuscular damping ratio and natural frequency of the tested conditions are all similar to those of the baseline.

Simulation results for conditions C1, C3, C8 and C10 were obtained using the simulation developed and validated in Chapter 4 (the initial guesses for the optimization variables were the same as the ones used in Chapter 5), and simulation results of other conditions in this chapter were directly obtained from Chapter 5. All dependent measures except for the target phase margin have significant correlation between the simulation and experiment results. This may be due to the fact that, for example, the up dipole dynamics increases the phase for $\omega < \omega_{dp}$ then decreases the phase for $\omega > \omega_{dp}$ of the controlled dynamics, which may lead to very sensitive and different phase margins depending on the control strategies of the human operators during the experiment.

High correlations were observed between the simulation and experiment results for the relative changes of performance, control activity, ratio of the visual gain and lag time constant and lead time constant with respect to those of the baseline dynamics. For both of the relative changes of the performance and lead time constant, the maximum mismatch between the simulation and experiments was within 17%, for all testing conditions. Obvious mismatches between the simulation and experiment results were observed for the control activity and the ratio of the visual gain and lag time constant for the down dipole dynamics, here the maximum mismatch for control activity is around 80% and for the ratio of the visual gain and lag time constant is around 30%. In general, for the tested up dipoles, the high match between the simulation and experiment (for the relative changes in tracking performance, control activity and control behavior) suggests that both the MCAB and the corresponding IMCAB developed in Chapter 5 are accurate.

For the down dipoles, three steps were carried out to correct the MCAB for the control activity and the ratio of the visual gain and lag time constant based on the experiment data. First, simulation data were expanded by also performing the simulation for conditions with extra down dipoles at 1 rad/s, and the updated simulation MCAB and IMCAB were developed. Second, a coefficient was introduced to explain for a consistent difference between the simulation and experiment, and this coefficient was multiplied with the simulation control activity for all down dipoles at $\omega_{dp} = 1$ rad/s (down dipoles from Chapter 5 and the extra down dipoles from this chapter). This coefficient is the average value needed to match the simulation relative changes of the control activity over tested down dipole conditions with those of the experiment. The same procedure was applied to the ratio of the visual gain and lag time constant. After the corrections, the modified MCAB of magnitude for control activity is narrower, and the modified MCAB of magnitude for the ratio of the visual gain and lag time constant is wider than the updated boundaries at 1 rad/s, respectively. Overall, the modified IMCAB of magnitude becomes narrower at 1 rad/s. Third, the modified MCAB were verified by investigating the tested added dynamics and their corresponding relative changes in control activity and ratio of the visual gain and lag time constant. It was found that, according to the MCAB formulation approach in Chapter 5, there is no need to further correct the modified MCAB and IMCAB based on the experiment results.

The modifications on the MCAB are provisional: first, the coefficients for different testing conditions are different and an average value representing the general level of mismatch between the simulation and experiment results would be rough; second, only 7 added down

dipole dynamics were tested in the experiment, whether the observed mismatches for the limited testing conditions still apply to the untested dynamics remains unknown. Moreover, the MCAB for $\omega = 2, 3, 4, 5, 6$ and 7 rad/s are not yet verified, it is unknown whether and how much the boundaries would change if experiment data of those frequencies were available.

For the tested added dipole dynamics, only conditions C1 and C8 are not significantly different from the baseline dynamics for tracking performance, control activity, ratio of the visual gain and lag time constant and lead time constant (these are the variables quantifying the MCAB, see Chapter 5). Moreover, it was found that the added dynamics of C1 and C8 are not only within the original MUAD envelopes of 1980 [2], but also match well with the modified IMCAB of 20% relative change. This indicates that for the unnoticeable added dynamics, for example the ones of C1 and C8, the corresponding objective relative change in tracking performance, control activity or control behavior is constrained within 20% (according to the experiment data, the maximum relative changes for both C1 (control activity) and C8 (performance) are around 13%). However, whether this applies to any other added dipole dynamics within the original MUAD envelopes of 1980 [2] is unknown. This question would be answered by the simulation developed in Chapter 4 and the approach of formulating the MCAB proposed in Chapter 5, however with a much finer resolution of added dynamics.

6.5. CONCLUSIONS

This chapter correlated and verified the MCAB developed in Chapter 5, with experimental measurements of performance, control activity and human operator control behavior. For this, a compensatory pitch attitude tracking experiment was performed, where subjects were asked to control the baseline aircraft pitch dynamics, as well as different "up" and "down" dipole dynamics centered on frequency of 1 rad/s – added to this baseline system. Experiment results show that the added dipole dynamics which located close to the original MUAD envelopes of 1980 still induce significant changes in control activity. Moreover, the effects of the up and down dipole dynamics are not opposite for the performance and control activity. The correlations between the simulation and experiment results are high for performance, control activity, target crossover frequency and all human operator model parameters. Between the simulation and experiment data, the trends of the relative changes in performance, control activity, ratio of the visual gain and lag time constant, and the lead time constant with respect to those of the baseline (dependent measures quantifying the MCAB) match very well. For the tested down dipoles, discrepancies were still observed for the control activity and the ratio of the visual gain and lag time constant. To guarantee enough "qualified" dipoles for the MCAB after modifications with experiment data, first, simulation data with extra down dipoles at 1 rad/s were added to those obtained in Chapter 5, to form the updated MCAB. Second, all these simulation data at 1 rad/s were scaled, in order to match the relative changes in the control activity and the ratio of the visual gain and lag time constant for the tested down dipoles between the simulation and experiment. Compared with the updated MCAB, the modified MCAB for the relative change of control activity became narrower, and the modified MCAB for the relative change of ratio of the visual gain and lag time constant became wider at 1 rad/s, respectively. Meanwhile, the modified IMCAB became narrower at 1 rad/s, compared with the updated IMCAB. According to the MCAB formulation approach in Chapter 5, the modified MCAB match

very well with the tested added dynamics. For the considered variations in the baseline and added dynamics, the MCAB are accurate in describing the relative changes in tracking performance, control activity and human operator control behavior when dipoles are added to the baseline dynamics at 1 rad/s. For the tested added dipoles which are not significantly different from the baseline for the tracking performance, control activity, ratio of the visual gain and lag time constant and the lead time constant, their dependent measures for the MCAB are all within 20% in the experiment. Moreover, these added dipoles are all very close to the 20% modified IMCAB, indicating that the 20% boundaries seem to be an appropriate objective limit for added dipoles, of which the tracking performance, control activity and human operator control behavior are similar to those of the baseline dynamics.

REFERENCES

[1] D. T. McRuer, D. Graham, E. S. Krendel, and W. J. Reisener, *Human Pilot Dynamics in Compensatory Systems, Theory Models and Experiments with Controlled Element and Forcing Function Variations*, Tech. Rep. AFFDL-TR-65-15 (Air Force Flight Dynamics Laboratory, Wright-Patterson Air Force Base (OH), 1965).

[2] J. R. Wood and J. Hodgkinson, *Definition of Acceptable Levels of Mismatch for Equivalent Systems of Augmented CTOL Aircraft*, Tech. Rep. MDC A6792 (McDonnell Aircraft Company, St. Louis (MO), 1980).

[3] M. M. van Paassen, *Biophysics in Aircraft Control, A Model of the Neuromuscular System of the Pilot's Arm*, Ph.D. thesis, Delft University of Technology, Faculty of Aerospace Engineering (1994).

[4] P. M. T. Zaal, D. M. Pool, Q. P. Chu, M. M. van Paassen, M. Mulder, and J. A. Mulder, *Modeling Human Multimodal Perception and Control Using Genetic Maximum Likelihood Estimation,* Journal of Guidance, Control, and Dynamics **32**, 1089 (2009).

[5] F. M. Nieuwenhuizen, P. M. T. Zaal, M. Mulder, M. M. van Paassen, and J. A. Mulder, *Modeling Human Multichannel Perception and Control Using Linear Time-Invariant Models,* Journal of Guidance, Control, and Dynamics **31**, 999 (2008).

[6] J. D. Gibbons and C. Subhabrata, *Nonparametric Statistical Inference, Fifth Edition* (Chapman and Hall/CRC, 2011).

7

CONCLUSIONS AND RECOMMENDATIONS

7.1. CONCLUSIONS

The goal of this thesis was set out to be:

> To develop the *Manual Control Adaptation Boundaries* (MCAB), which can objectively quantify to what an extent the task performance, control activity and human control behavior will change for the modified controlled dynamics, compared with the baseline system.

The *cybernetic approach* [1–4] was used throughout this thesis, to identify human control behavior with different (types of) controlled dynamics, both with and without simulator motion feedback. The mismatch between the modified controlled system and the baseline dynamics were represented by the *added dynamics* [5, 6], which were the main factor used to induce human control adaptation. These formed the basis of the work and were discussed in Part I of the thesis. Based on these initial studies, three objectives were formulated to meet the thesis goal in three steps:

1. To develop and validate a computer offline simulation, where task performance, control activity and human operator control behavior can be accurately predicted.

2. Gathering objective task performance, control activity and control behavior data based on the validated offline simulation, and generating simulation-based MCAB.

3. Modifying and verifying the simulation-based MCAB using new experiment data.

Objectives 1 and 2 were addressed in Part II and Objective 3 was tackled in Part III of the thesis. This chapter provides an overview, discussion and conclusions of previous chapters. Finally, recommendations for future studies are made.

7.1.1. GENERAL METHODS

THE CYBERNETIC APPROACH

The cybernetic approach and the *quasi-linear control-theoretical models* were used to quantify the human control behavior throughout this thesis. The goal of **Chapter 2** was to investigate whether these quasi-linear human operator models can be successfully applied to a wide variety of controlled dynamics. In this chapter, a human-in-the-loop yaw attitude compensatory tracking experiment was performed, with gain, single integrator and double integrator controlled dynamics both with and without simulator motion feedback.

The experiment results for the double integrator controlled dynamics were highly consistent with previous investigations [7–12], in which human operators made clear use of motion feedback to improve tracking performance, reduce control activity, decrease visual lead time constant and increase visual time delay. For the gain and single integrator controlled dynamics, both tracking performance and control activity were similar between the motion and no-motion cases. The identified human operator control behavior (based on the multi-channel model) indicated that the motion channel was much less utilized, compared with the double integrator case, and its contribution to the human control output was negligible compared with the visual channel. Moreover, it was found that the human operator control behavior for both gain and single integrator controlled dynamics was described very well by the single visual channel model. For the gain controlled dynamics, this result is explained by the fact that the controlled dynamics are so stable that the extra lead generated by the motion channel is not helpful in further improving tracking performance. For the single integrator controlled dynamics, small changes in the disturbance crossover frequency were observed between the no-motion and motion cases, which suggest that motion feedback may still have a minor effect on the human control behavior in disturbance rejection. The difficulties in detecting and quantifying the limited utilization of the motion feedback in the single integrator tracking tasks could be the reason for the inconsistent results previously reported in literature [7, 13, 14].

In general, Chapter 2 showed that the cybernetic approach can indeed be used to model and analyze human operator manual behavior, not only over a wide range of controlled dynamics, but also for cases both with and without motion feedback. Furthermore, for higher order controlled dynamics, motion feedback can make a significant difference in tracking performance, control activity and human operator control behavior. In the chapters of developing and verifying the MCAB, aircraft longitudinal pitch dynamics [15, 16] were used as the baseline dynamics. Since these dynamics approximate a double integrator at higher frequencies, motion feedback could be an important factor to be considered in developing the MCAB, and was thus included in later experiments in this thesis.

THE ADDED DYNAMICS EFFECTS

The first objective of **Chapter 3** was to examine the effects of added dynamics and the bandwidth of the baseline dynamics on human operator control behavior [17]. The second objective was to investigate whether the objective limits of tracking performance, control activity and human operator control behavior corresponded with the Maximum Unnoticeable Added Dynamics (MUAD) envelopes known from literature [5]. To this end, a human-in-the-loop pitch tracking experiment was performed, in which both low and high-bandwidth aircraft representative dynamics (to tie in with [17]) were perturbed by added

dipole dynamics, at a single tested frequency of 3 rad/s.

The results showed that, for the high-bandwidth baseline, the tracking performance was better, control activity was lower and the human operator lead time constant was lower. These findings were expected, since the high-bandwidth baseline dynamics have reduced phase lag compared with the low-bandwidth baseline, which makes the high-bandwidth system more responsive. For either low or high-bandwidth baseline, with increasing perturbations of the added dipole dynamics, tracking performance worsened, control activity decreased and the human operator visual gain decreased, while the lead time constant remained relatively constant. The dipole dynamics were found to not only influence the gain, but also the phase of the controlled system. For example, an "up" dipole increases the phase of the controlled dynamics just below the dipole natural frequency and decreases the phase of the controlled dynamics above the dipole natural frequency. Thus depending on the dipole natural frequency, by either increasing or decreasing the phase lead or lag of the controlled system, the added dipole dynamics would indeed induce the necessary change in the lead time constant, which is usually adapted by human operators for appropriate lead equalization [1]. However, for the tested dipoles in this chapter, the effects of the induced phase changes on system's stability were quite small, and it was found that the lead time constant was not influenced by the added dynamics.

In general, for the considered variations in the baseline and added dynamics, the experiment results showed that the potential range of the objective limits of tracking performance, control activity and human operator control behavior corresponded well with the original MUAD envelopes [5]. Overall, the effects of the added dipole dynamics on tracking performance, control activity and human operator control behavior were very similar between the low and high-bandwidth baseline systems. This indicates that for the tested baseline and added dynamics, the bandwidth of the baseline only has a negligible effect on the relative changes in these dependent measures with respect to the baseline. This also means that the MCAB would also be independent of the baseline bandwidth. However, the findings in this chapter are not intended to deny any potential bandwidth-dependent characteristics of the original MUAD envelopes [17]. The MUAD [5, 6] and AE envelopes [17] were developed based on subjective ratings and had not been correlated with any objective measures. Moreover, the control task, forcing functions and baseline dynamics used in [5, 6, 17] were not the same as the ones used in Chapter 3.

In summary, Chapter 3 demonstrated the feasibility of a general method to study human control behavior adaptation to added dynamics, and this approach would be used in the rest of the thesis to further form the MCAB. Moreover, since the bandwidth of the baseline dynamics was found to have minor effects on the changing trends of human operator control behavior for different added dynamics, in the rest of this thesis, only one set of baseline dynamics would be used to further develop the MCAB.

7.1.2. SIMULATION-BASED (I)MCAB

OFFLINE SIMULATION DEVELOPMENT

The goal of **Chapter 4** was to develop and validate a computer offline simulation to predict task performance, control activity and human operator control behavior, which would be strongly relied on to develop the MCAB and the *Integrated Manual Control Adaptation Boundaries* (IMCAB) in the later chapters of the thesis. In this chapter, a human-in-the-

loop pitch attitude tracking experiment was performed, in which aircraft baseline dynamics [15, 16] were perturbed by an added up or down dipole at 1, 3 and 7 rad/s, respectively.

Subjective ratings and comments on the noticeability of the added dynamics were collected from all seven subjects who performed the experiment. It was found that the ratings were inconsistent among subjects. Moreover, the ratings for the baseline condition did not always show that there was no difference between the tested baseline dynamics and the baseline that was compared with. This strongly suggested that the subjective ratings obtained in this experiment were not accurate and cannot truly reflect the level of differences in the controlled dynamics. Due to these inconsistencies and inaccuracies, collection of subjective rating data was abandoned in all later experiments, and no explicit effort to correlate the subjective ratings and objective measures was made in this thesis.

In Chapter 4, to develop an offline simulation tool for the further development of the MCAB, the same compensatory tracking tasks as tested experimentally were simulated with the same forcing functions, baseline dynamics and added dynamics as used in the experiment. The same human operator model used for identifying the human operator control behavior in the experiment was used in the simulation, and its parameters were predicted by using constrained nonlinear optimization techniques [18]. This simulation was validated by correlating the simulation results with the experiment data for tracking performance, control activity, target crossover frequency, target phase margin and human operator parameters (visual gain, lead time constant and lag time constant). In the simulation, human operator visual time delay, neuromuscular damping ratio and natural frequency were kept constant, since they represent human operator's limitations and the variations within each of these three parameters are relatively small. The value of the remnant-to-control variance ratio in the simulation was tuned to obtain the highest correlation between the simulation and experiment data, and this value was fixed for the simulations in Chapters 5 and 6.

The offline simulation was found to predict the trends of tracking performance, control activity and human operator parameters over the tested conditions very well. However, a sufficient match of the absolute values of these dependent measures with the experiment data was not achieved. In the experiment, even though subjects were instructed to minimize the error signal as best as they could, the control effort is also known to be considered by subjects to avoid getting exhausted in controlling. So in reality, a trade-off between task performance and control effort is generally made. Considering this, the objective function in the simulation usually contains both the variance of the error signal and the weighted variance of the control signal [15]. However, in the simulation of Chapter 4, to find a common value of the control activity weighing factor for the multiple tested added dynamics proved challenging, indicating that human operators may apply different levels of trade-off between task performance and control effort for different controlled dynamics. Moreover, considering that many more added dynamics would be simulated to form the MCAB in a later large scale simulation in Chapter 5, it was very likely that for different controlled dynamics, the trade-off between task performance and control activity would be different, which is difficult to know in advance. In the end, the weighing factor for the control activity in the simulation was kept at zero throughout the thesis. Another potential cause for the discrepancies is the unknown remnant spectrum, which is impossible to know in advance without performing an experiment.

In summary, considering repeatability, the simulation was kept as simple as possible.

A high correlation between the simulation and experiment results can be obtained by tuning the remnant-to-control variance ratio. Even though offsets between the simulations and experiment still existed for some dependent measures, the trends over different added dynamics between simulation and experiment were highly similar. It was concluded that the validated offline simulation was sufficient to be used to further develop the MCAB, since the MCAB are only based on the relative changes (i.e., trends) in tracking performance, control activity and human operator control behavior with respect to those of the baseline.

SIMULATION-BASED (I)MCAB

The goal of **Chapter 5** was to develop the simulation-based (I)MCAB by using the offline simulation developed in Chapter 4. In this chapter, aircraft pitch attitude tracking tasks were simulated, in which the forcing functions and baseline dynamics were the same as those used in Chapter 4. The added dipole natural frequency was varied between 1 and 7 rad/s, with steps of 1 rad/s. Furthermore, a full factorial combination of the two dipole damping ratios, where each varied between 0.1 and 0.9, with steps of 0.1, were considered. At each dipole natural frequency, thus in total 36 up and 36 down dipoles were simulated.

It was found that for dipoles added at 1 rad/s, the tracking performance of the down dipoles was in general worse than that of the baseline and the tracking performance of the up dipoles was similar to that of the baseline. However, for dipoles added at other frequencies, the patterns in tracking performance between the down and up dipoles inverted compared to those at 1 rad/s. Through both open-loop and closed-loop analyses, it was found that tracking performance with down dipoles at 1 rad/s, for example, cannot be further improved by varying human operator's visual gain, since the system would become unstable. For the control activity, the patterns between the down and up dipoles were consistent for all simulation dipole frequencies, in which the control activity of the down dipoles was generally higher than that of the baseline, and the control activity of the up dipoles was lower than that of the baseline. This was expected because the down dipoles reduce the overall gain of the controlled system, thus human operators need to have a higher control gain to compensate (vice versa for the up dipoles). The expected matching variations in the visual gain were also observed. The lead time constant, which is usually generated by the human operator to counter the phase lag of the controlled system, varied depending on the dipole natural frequency and damping ratios.

Based on the simulation data, the relative changes of tracking performance, control activity, ratio of the visual gain and lag time constant and the lead time constant with respect to those of the baseline were selected as the four dependent measures quantifying the MCAB. Tracking performance and control activity were selected, since human operator may first notice the changes in task performance and control output when the controlled dynamics change. These two variables can be directly measured in the experiment, which is useful for verifying the simulation-based MCAB. In addition, the ratio of the visual gain and lag time constant and the lead time constant were also selected as the key MCAB dependent measures, since the visual gain, lag time constant and the lead time constant are the human operator model equalization parameters, which explicitly quantify human control behavior's optimization to different controlled dynamics. However, because of the low accuracy of estimating the lag time constant in the experiment, which in turn would affect the accuracy of the estimated visual gain, these two parameters were not individually considered as dependent measures due to their strong correlation. The crossover frequency and phase

margin were not used to quantify the MCAB, since these two variables can be derived from the human operator dynamics and the controlled dynamics, and would be redundant if used together with tracking performance and control activity.

For example, to form the MCAB for the control activity, first all the simulation dipoles of which the relative changes in the control activity within a definite amount, e.g., a tested value of 20%, were found and their frequency responses were plotted in magnitude and phase, respectively. Then the 20% MCAB were formulated by connecting the "outermost" dipoles, which were the ones most deviated from the 0 dB (or 0 deg) line in magnitude (or phase) at 1, 2, 3, 4, 5, 6 and 7 rad/s. The same approach was used to form the MCAB for performance, ratio of the visual gain and lag time constant, and the lead time constant. The shapes of the MCAB for these individual dependent measures were found to be distinctly different from each other, which suggests that human control behavior adaptation may be dominated by different variables.

In this chapter, as an example, the MCAB were developed for 20%, 40% and 60% allowed relative changes in the dependent measures. Using the same approach, the MCAB corresponding with other different levels of relative change can be easily derived as well. By seeking the *intersections* of all four MCAB in magnitude and phase at 1, 2, 3, 4, 5, 6 and 7 rad/s, respectively, the *I*MCAB were generated, which represent the "tightest" objective boundaries for all the MCAB dependent measures. For example, if any added dipole dynamics are within the 20% IMCAB, the corresponding relative changes in tracking performance, control activity and human operator control behavior with respect to those of the baseline could be constrained within 20%. It was also found that in terms of system magnitude, the 20% IMCAB corresponded very well with the MUAD magnitude envelope [5]. This implied (but not yet proved) that for added dynamics which were hypothesized to be subjectively unnoticeable, the objective relative changes in tracking performance, control activity and human operator control behavior would be within 20%. Similar to the MUAD envelopes, the magnitude IMCAB is "hourglass-shaped" and narrowest at 3 rad/s. This corresponds well with manual control theory, which states that task performance and human operator control behavior are most sensitive in the crossover frequency region [1].

In Chapter 5, the tested added dipoles fully within the MUAD envelopes [5] in both magnitude and phase were identified, and these dipoles were hypothesized to be subjectively unnoticeable according to [5]. It was thought to be of interest to investigate to what an extent the tracking performance, control activity and human operator control behavior change compared with those of the baseline for these added dynamics. It was found that, for the dipoles between 1 rad/s and 7 rad/s, on average the control activity changed the most (24%), compared with the tracking performance (6%), target crossover frequency (5%), target phase margin (11%), visual gain (13%), lead time constant (11%), and lag time constant (6%). This corresponds well with the 20% IMCAB of magnitude. All these indicate that 20% may be the objective tolerance range for subjectively unnoticeable added dynamics. However, it was found that the (I)MCAB did not guarantee that for any added (dipole) dynamics within the boundaries, the relative change of performance, control activity or human operator control behavior would always be consistently constrained by the boundaries. For example, a dipole within the 20% IMCAB could induce a relative change in the control activity above 20%. These inconsistencies may be caused by the specific phase characteristic of the added dipoles, which nonlinearly changes the system's stability. Thus tracking

performance, control activity and human operator control behavior could also change inconsistently, when the perturbation of the added dipoles gradually increases.

In summary, Chapter 5 developed the simulation-based (I)MCAB for the relative changes of tracking performance, control activity, ratio of the visual gain and lag time constant and the lead time constant. The distinctly different shapes of MCAB for these dependent measures indicate that to study human control adaptation, different dependent measures need to be considered. The next step in this thesis is thus to experimentally verify these objective boundaries.

7.1.3. EXPERIMENTAL VERIFICATION OF THE MCAB

In Chapter 2, it was found that motion feedback can significantly affect tracking performance, control activity and human operator control behavior with high order dynamics, which could make a difference in the (I)MCAB if motion feedback was considered. As described in Appendix D, to verify this, first an aircraft pitch attitude tracking experiment similar to the one in Chapter 4 was conducted both without and with simulator motion feedback. In total fifteen added dipoles were tested at the frequencies of 1, 2 and 3 rad/s. In general, it was found that for conditions with and without motion, the trends in the relative changes in tracking performance, control activity, ratio of the visual gain and lag time constant, and the lead time constant over different added dynamics were essentially equivalent. Moreover, even though some discrepancies for the MCAB dependent measures between motion and no-motion cases were observed, these differences were in general very small, which may be due to the fact that motion feedback has very limited improvement for tracking performance with the specific baseline aircraft dynamics used in this experiment. Thus, it was concluded that in this thesis the (I)MCAB would be developed and verified without further considering motion feedback.

The main goal of **Chapter 6** was to verify the simulation-based MCAB developed in Chapter 5. Obviously, it was impossible to verify all added dynamics which were used to formulate the MCAB. Only a limited number of added dipoles (with gradually increasing perturbations on the baseline) with the dipole natural frequency at 1 rad/s were tested, because of the unique pattern of the tracking performance between the up and down dipoles, which was different from the dipoles added at other frequencies, observed from the simulation data in Chapter 5. Using the offline simulation developed in Chapter 4, the tracking performance, control activity and human operator control behavior were also predicted for the same tested conditions. It was found that for the tested up dipoles, the match between the simulation and experiment data for the relative changes of tracking performance, control activity, ratio of the visual gain and lag time constant, and the lead time constant was very good. For the down dipoles, the simulation and experiment data for the relative changes of tracking performance and lead time constant were found to be highly similar. For the relative changes of control activity and ratio of the visual gain and lag time constant, the trends over different conditions between simulation and experiment data were still similar, but with clear mismatches in magnitude. This implies that for the down dipoles, the simulation-based MCAB developed in Chapter 5 for control activity and ratio of the visual gain and lag time constant were not sufficiently accurate.

It was found that, if the simulation control activity data in Chapter 5 were modified based on the experiment data in this chapter, the lower magnitude of the new 20% MCAB

for the control activity would become 0 dB at 1 rad/s, which does not make much sense. To avoid this problem, the collection of simulation data of Chapter 5 was expanded by simulating more down dipoles at 1 rad/s. These newly added down dipoles had finer resolutions in the changes of the damping ratios, compared with those used in Chapter 5. Based on the new simulation data, the *updated* simulation-based (I)MCAB were generated using the same approach proposed in Chapter 5.

To better match the simulation relative changes of control activity and ratio of the visual gain and lag time constant with experiment data, for the tested down dipoles in the experiment, two coefficients were estimated to quantify the average mismatches between the simulation and experiment data. These coefficients were multiplied with the updated simulation data to derive the *modified* (I)MCAB. Because the correction coefficients were all very close to 1 (1.24 for the control activity and 0.9 for the ratio of the visual gain and lag time constant), the modified (I)MCAB were found to still be very similar to the (updated) simulation-based (I)MCAB. The modified MCAB were further verified by comparing with the tested added up and down dipoles with their relative changes in tracking performance, control activity, ratio of the visual gain and lag time constant, and lead time constant. According to the MCAB formulation approach in Chapter 5, for all the tested added dynamics in this experiment, in general the modified MCAB can accurately quantify these dependent measures at 1 rad/s.

In Chapter 6, it was also found that the added dipoles that were not significantly different from the baseline for tracking performance, control activity, ratio of the visual gain and lag time constant and lead time constant were in general within the 20% modified IMCAB, indicating that the 20% boundaries seem to be an appropriate objective limit for these added dipoles.

In summary, the verified (I)MCAB in Chapter 6 are the final results of this thesis. By using the (I)MCAB, the relative changes in tracking performance, control activity and objective human control behavior adaptation to the changes in the controlled system can be estimated without performing an experiment. The proposed simulation-experiment combined approach to formulate the (I)MCAB would be also applied to, for example, other forcing functions, baseline aircraft (or vehicles) and added dynamics. Together with the original subjective MUAD envelopes, for example, these objective (I)MCAB can serve as an alternative tool in evaluating the effects of the mismatches between two different controlled systems on human control adaptation.

7.1.4. LIMITATIONS AND INTERPRETATIONS OF (I)MCAB

Despite all the efforts in this thesis to develop the (I)MCAB, there are still limitations on the current modified and verified (I)MCAB in Chapter 6. As a result, when using these boundaries in any research for evaluating the changes in tracking performance, control activity and human operator control behavior to the added dynamics, careful interpretation of the results is necessary.

The first limitation originates from the fact that the current (I)MCAB are developed only based on the specific target and disturbance forcing functions, baseline aircraft, and added dipole dynamics tested. It cannot be guaranteed that using other forcing functions, baseline or added dynamics would result in equivalent (I)MCAB. Second, the current (I)MCAB were only experimentally verified at 1 rad/s. For the dipole dynamics added at other fre-

quencies, the accuracy of the boundaries is yet unknown, but can be verified with the approach followed in Chapter 6.

For the interpretations of the MCAB for one dependent measure (for example, 20% MCAB for the control activity), first it should be noted that, if an added dipole is outside either the magnitude or phase of the MCAB, the relative change in control activity is hypothesized to be above 20%. Second, if any added dipole is within the MCAB in both magnitude and phase, it is not guaranteed that the relative change in control activity is within 20%. This was confirmed based on the offline simulation results obtained in Chapter 5. Thus to verify the MCAB, as long as the added dynamics are within the MCAB, no matter whether the dependent measures are below or above 20%, the MCAB are always valid. Only when the added dynamics are outside the MCAB *and* the relative change in the dependent measure is below 20%, the MCAB are then assumed to be "underestimated" and narrower than it should be (see Chapter 6).

For the IMCAB (for example, the 20% IMCAB): first, the IMCAB represent the "common" boundaries of the relative changes in tracking performance, control activity, ratio of the visual gain and lag time constant, and the lead time constant, which are all constrained within 20%. If a dipole is within the IMCAB, mostly its relative changes in all dependent measures will be within 20%. However, this is not guaranteed (see Chapter 5). Second, if any added dipole is outside either the IMCAB magnitude or phase boundary, it is known that this added dipole is outside certain MCAB, which are the most critical ones at the considered dipole natural frequency. However, since the IMCAB are the lumped results of the four individual MCAB, it is difficult to know exactly which dependent measure changes, due to the multidimensional characteristic of the human control adaptation. Rather than using the IMCAB alone, it is more useful to compare the added dynamics with the individual MCAB of dependent measures, as this provides direct insights into the relative changes in tracking performance, control activity and human operator control behavior, respectively.

7.2. RECOMMENDATIONS

7.2.1. DIFFERENT BASELINE AND ADDED DYNAMICS

In this thesis, when developing the (I)MCAB, only the linearized Cessna Citation I's aircraft pitch dynamics [15, 16] were used as the baseline dynamics and a specific type of dipoles were applied as the added dynamics. In earlier projects developing the MUAD envelopes [5, 6, 19–21], different types of added dynamics with both longitudinal and lateral/directional aircraft dynamics were used. The shapes of the CTOL [5] and the V/STOL [6] MUAD envelopes are similar in the crossover frequency region, but notably different below 1 rad/s. Apart from the variation caused by different pilots and the use of subjective ratings for developing the MUAD, other potential factors leading to the different shapes in these two envelopes include, but are not limited to: the differences in the control tasks, the baseline aircraft dynamics and the added dynamics. As has been stated in [1], any changes in any of the *task variables* can strongly affect human operator control behavior. Thus, it is also likely, though not yet proved in this thesis, that the shape of the (I)MCAB would also change when different baseline or added dynamics are considered.

In this thesis, it was found that the bandwidth of the baseline dynamics has no effect on the trends of tracking performance, control activity, or human operator control behavior

over different added dynamics. Thus it was expected that the (I)MCAB would have no obvious difference for the low and high-bandwidth baseline dynamics. However, in Chapter 3, the relative changes in tracking performance, control activity and human operator control behavior with respect to those of the baseline were not calculated for the experiment data. It is thus not yet known how large (or small) these potential differences are, if the (I)MCAB are developed based on baseline dynamics with different bandwidth. In future studies, it is of interest to investigate this problem by first conducting offline simulations with a much wider range of baseline bandwidth settings, using the validated simulation toolbox developed in this thesis.

Up to now, most of the work related with the MUAD envelopes [5, 6, 19–23], AE envelopes [17] and the (I)MCAB developed in this thesis uses added dynamics to induce mismatches between the modified and the baseline dynamics. Few studies have investigated the effects of the mismatches brought by the differences in the aircraft dynamics themselves, for example, by varying the baseline model's parameters. Rather than adding extra dynamics to the baseline system, varying the parameters of the baseline dynamics can be more valuable, for example, for studying the effects of *aircraft model fidelity* on human operator control behavior. It is of interest to investigate, for example, how baseline aircraft dynamics with different handling qualities [24] would affect the (I)MCAB [25]. Again, the offline simulation developed in this thesis can be first used to gain some insights into this problem even without performing a human-in-the-loop experiment.

When formulating the MCAB, the lead time constant was selected as one of the dependent measures quantifying the adaptation of human operator control behavior to the changes in the controlled dynamics. Based on the experiment results in Chapter 4 and the simulation results in Chapter 5, it is known that the pattern of the lead time constant for the up and down dipoles changes when the dipole natural frequency moves from 1 rad/s to 7 rad/s. This is caused by the unique characteristic of the dipoles used in this thesis: for an up dipole, the phase of the controlled dynamics at frequencies below the dipole natural frequency is increased, while it is decreased at frequencies above the dipole natural frequency. It is likely (though not yet proved) that if different added dynamics (for example, a first-order lag, which only induces phase lag) are used, the MCAB of the lead time constant would be different from the current ones. Future studies need to investigate how different types of added dynamics affect the (I)MCAB.

7.2.2. CORRELATING OBJECTIVE AND SUBJECTIVE DATA

In Chapter 4, subjective ratings and comments were collected for different controlled dynamics during the experiment. However, these subjective ratings were found to be very inconsistent among the subjects and also inaccurate, which may have been caused by several factors. First, due to the potential differences in motivation, skill and experience, the tracking performance, control activity and subjective noticeability of added dynamics vary strongly among different subjects. Also, for any subject, if his/her control behavior is not consistent for two testing runs even with the same controlled dynamics, the ratings could be different. For example, subjects regularly claimed that two consecutively tested baseline dynamics were different from each other. Second, in the experiment of Chapter 4, the subjective rating phase was conducted after the 95 s testing run. The reason for this long run time was mainly for the human operator model identification. However, it is possible

that participants already "forgot" how the controlled dynamics that they needed to compare with felt like, which leads to inaccurate ratings. Thus in the rest of this thesis, there was no further analysis on, for example, how the objective (I)MCAB correlate with subjective ratings or noticeability of the added dynamics.

However, in future studies, it is still interesting to reflect on the relationship between the subjective data and objective metrics. The main reason is that the subjective approach and the original MUAD envelopes have already been widely used to, for example, evaluate aircraft handling qualities [26], aircraft model fidelity [27–33], and help design flight control systems [29, 34, 35]. The (I)MCAB would be much more valuable to be used in parallel with these existing subjective criteria, if we know, for example, which dependent measures relate the most with subjective data [19, 20, 22], how much relative changes in these dependent measures corresponds with different levels of subjective ratings, and whether unnoticeable added dynamics would always correspond with the 20% IMCAB. If these questions can be answered, the (I)MCAB developed in this thesis then could also be used to predict subjective ratings.

Several suggestions are proposed here for future investigations. First, it is recommended to use a more homogeneous subject pool, e.g., all pilots, from whom more consistent rating data would be expected. Second, formal calibrated aircraft handling qualities rating criteria are needed [26], which in turn needs pilots rather than non-pilots to conduct experiments. Third, it is recommended to add another "subjective rating session" to the current experiments performed in this thesis. In this new session, subjective ratings for systems with added dynamics can be collected based on pairwise comparisons with the baseline dynamics. The measured data in this session are not needed for human model identification, thus the testing run time can be much shorter, to prevent subjects from forgetting the controlled dynamics which are compared with. Moreover, the unnoticeable added dynamics could be found through the adaptive staircase algorithm [36], as used for measuring motion perception coherence zones [37], and detecting humans' just noticeable difference (JND) in the haptic perception of manipulator stiffness [38].

7.2.3. OFFLINE SIMULATION EXTENSION

The offline simulation developed in this thesis played a critical role in formulating the (I)MCAB. With the high accuracy of predicting performance, control activity and human operator control behavior, the simulation-based MCAB needed only minor modifications according to the experiment data in Chapter 6. However, there are several limitations on the current offline simulation, which can be further improved.

First, in the current offline simulation implementation, the visual time delay is kept as a constant, representing one of the inherent limitations in humans. Another reason to fix the visual time delay as a constant is that, the objective function in the optimization is only based on tracking performance. If the visual time delay is considered as a free decision variable in optimization, it is expected that the optimal visual time delay will be at its defined lower boundary, which makes it meaningless to optimize this variable. However, in Chapter 2 it was found from experiment data that the visual time delay can still change significantly for different types of controlled dynamics, and also with the presence of motion feedback. Thus humans' adaptation in terms of the change in the visual time delay cannot be predicted by the current offline simulation.

Second, currently only the visual channel of the human operator model is considered. To be able to predict humans' adaptation to the presence of motion feedback, the multi-channel human operator model including both visual and motion channels as used in Chapter 2 is needed. However, the multi-channel model will induce two more variables (motion gain and motion time delay) into the simulation. It is also known that the motion channel is used by human operators as an extra lead for stabilizing the controlled system and helping improve task performance, meaning that the motion gain and the visual lead time constant are coupled with each other. Using the current local optimum algorithm, it is very difficult to consistently distinguish the separate contributions of the visual and motion channels to human operator's control. Moreover, since the motion time delay is usually lower than the visual time delay, this relationship has to be taken as an extra constraint, which further complicates the optimization.

In future investigations, to be able to study humans' adaptation to the visual time delay and the presence of motion feedback, it is recommended to include weighted control activity into the objective function in optimization, which could prevent the visual and motion time delays from reaching their defined lower boundaries. Moreover, global optimization techniques such as interval analysis [39] are recommended to consistently predict the separate utilizations of the visual and motion channels.

7.2.4. POTENTIAL APPLICATIONS AND FUTURE DEVELOPMENT

Based on the high accuracy of the offline simulation developed in this thesis, the (I)MCAB can serve as an alternative objective approach to evaluate, for example, aircraft model fidelity [27–33] and help develop flight control systems [29, 34, 35], as was previously done only using the original subjective MUAD envelopes [5, 6] and no quantitative measures were available. For example, by comparing the frequency response of a flight control system to the (I)MCAB, the relative changes in performance, control activity and human operator control behavior can be estimated.

Some may argue that the compensatory tracking tasks used to develop the (I)MCAB only poorly represent real manual control tasks, thus the (I)MCAB are not valid for more realistic control tasks such as pursuit or preview tracking. As has been stated in Chapter 1, human control adaptation may happen when any of the task variables change (including control task), thus it is possible that the (I)MCAB corresponding with pursuit and preview tracking tasks would be different from the ones for compensatory tracking tasks. However, these do not prevent us from applying the simulation-experiment combined approach developed in this thesis to formulate (I)MCAB for pursuit and preview tracking tasks. In recent years, extensive efforts have been made in modeling human operator control behavior in these control tasks, which already helped us gain much more insights into how humans carry out these more realistic and complicated tasks [40–42]. It is thus perhaps possible to apply the (I)MCAB concept to the state-of-the-art pursuit and preview human control models [40–42] to develop the corresponding adaptation boundaries. This work could be even more valuable if these models can describe the measured control output and human control behavior with higher accuracies, to the levels of the compensatory human control models used in this thesis.

As has been pointed out in [42], many existing human manual control models for compensatory, pursuit and preview tracking tasks are linear and time-invariant (LTI). These

models can only represent "fully proficient and well trained" human operators in these tasks, and the quantified *adaptation* and *optimization* of human operator control behavior to the changes of the controlled dynamics are stationary [42]. Similarly, for the offline simulation developed in Chapter 4, the optimal human operator control behavior with different added dynamics is also stationary (and locally optimal).

Thus, through the current (I)MCAB, which can only represent human control adaptation in a lumped and stationary way, it is not possible to know how human operator control behavior continuously changes from one optimal state to another, which is crucially important to gain insights into the *time-varying* nature of human manual control [43, 44], for example, in "changing in the controlled dynamics, modified task constraints, loss-of-control and automatic-to-manual control transitions" [42]. It can be imagined that, during an experiment testing run, tracking performance, control activity and human operator control behavior would change with the changes in the controlled dynamics. If the testing run time is sufficiently long, then these dependent measures could eventually converge to their optimal states, which are the stationary values both identified in the experiment and predicted using the offline simulation in this thesis. If this is the case, the shape(s) of the (I)MCAB would not change for these time-varying experiments. However, when the testing run time is not long enough, the dependent measures may not converge to their optimal states. Moreover, depending on the added dynamics, the changes in the dependent measures could be either very smooth or very sudden (e.g., overshoot). In this case, at what time instant these dependent measures should be sampled to quantify human control adaptation is not clear, thus a proper definition of the "time-varying" (I)MCAB need further discussion. No matter whether these new boundaries can be eventually derived in the future, accurate time-varying human operator model identification techniques [43, 45–50] are first needed, which can lead us into a whole new era in the human-machine interaction domain.

REFERENCES

[1] D. T. McRuer and H. R. Jex, *A Review of Quasi-Linear Pilot Models,* IEEE Transactions on Human Factors in Electronics **HFE-8**, 231 (1967).

[2] R. L. Stapleford, D. T. McRuer, and R. E. Magdaleno, *Pilot Describing Function Measurements in a Multiloop Task,* IEEE Transactions on Human Factors in Electronics **8**, 113 (1967).

[3] M. M. van Paassen and M. Mulder, *Identification of Human Operator Control Behaviour in Multiple-Loop Tracking Tasks,* in *Proceedings of the Seventh IFAC/IFIP/IFORS/IEA Symposium on Analysis, Design and Evaluation of Man-Machine Systems, Kyoto Japan* (Pergamon, 1998) pp. 515–520.

[4] P. M. T. Zaal, D. M. Pool, Q. P. Chu, M. M. van Paassen, M. Mulder, and J. A. Mulder, *Modeling Human Multimodal Perception and Control Using Genetic Maximum Likelihood Estimation,* Journal of Guidance, Control, and Dynamics **32**, 1089 (2009).

[5] J. R. Wood and J. Hodgkinson, *Definition of Acceptable Levels of Mismatch for Equivalent Systems of Augmented CTOL Aircraft*, Tech. Rep. MDC A6792 (McDonnell Aircraft Company, St. Louis (MO), 1980).

[6] C. G. Carpenter and J. Hodgkinson, *V/STOL Equivalent Systems Analysis*, Tech. Rep. NADC-79141-60 (McDonnell Aircraft Company, St. Louis (MO), 1980).

[7] R. S. Shirley and L. R. Young, *Motion Cues in Man-Vehicle Control – Effects of Roll-Motion Cues on Human Operator's Behavior in Compensatory Systems with Disturbance Inputs,* IEEE Transactions on Man-Machine Systems **9**, 121 (1968).

[8] R. L. Stapleford, R. A. Peters, and F. R. Alex, *Experiments and a Model for Pilot Dynamics with Visual and Motion Inputs*, Tech. Rep. NASA CR-1325 (Systems Technology, Inc., Hawthorne (CA), 1969).

[9] R. F. Ringland and R. L. Stapleford, *Motion Cue Effects on Pilot Tracking,* in *Seventh Annual Conference on Manual Control* (1971) pp. 327–338.

[10] J. C. van der Vaart, *Modelling of Perception and Action in Compensatory Manual Control Tasks*, Ph.D. thesis, Delft University of Technology, Faculty of Aerospace Engineering (1992).

[11] R. J. A. W. Hosman, *Pilot's Perception and Control of Aircraft Motions*, Ph.D. thesis, Delft University of Technology, Faculty of Aerospace Engineering (1996).

[12] T. L. Dehouck, M. Mulder, and M. M. van Paassen, *The Effects of Simulator Motion Filter Settings on Pilot Manual Control Behaviour,* in *Proceedings of the AIAA Modeling and Simulation Technologies Conference and Exhibit, Keystone (CO)*, AIAA-2006-6250 (2006).

[13] H. P. Bergeron, *Investigation of Motion Requirements in Compensatory Control Tasks,* IEEE Transactions on Man-Machine Systems **MMS-11**, 123 (1970).

[14] A. M. Junker and C. R. Replogle, *Motion Effects on the Human Operator in a Roll Axis Tracking Task,* Aviation, Space, and Environmental Medicine **46**, 819 (1975).

[15] P. M. T. Zaal, D. M. Pool, J. de Bruin, M. Mulder, and M. M. van Paassen, *Use of Pitch and Heave Motion Cues in a Pitch Control Task,* Journal of Guidance, Control, and Dynamics **32**, 366 (2009).

[16] D. M. Pool, *Objective Evaluation of Flight Simulator Motion Cueing Fidelity Through a Cybernetic Approach*, Ph.D. thesis, Delft University of Technology, Faculty of Aerospace Engineering (2012).

[17] D. G. Mitchell, R. H. Hoh, C. He, and K. Strope, *Determination of Maximum Unnoticeable Added Dynamics,* in *Proceedings of the AIAA Atmospheric Flight Mechanics Conference and Exhibit, Keystone (CO)*, AIAA-2006-6492 (2006).

[18] S. J. Wright and J. Nocedal, *Numerical Optimization* (Springer Science, 2006).

[19] T. P. Neal and R. E. Smith, *An In-flight Investigation to Develop Control System Design Criteria for Fighter Airplanes*, Tech. Rep. AFFDL-TR-70-74, Volume 1 (Air Force Flight Dynamics Laboratory, 1970).

[20] T. P. Neal and R. E. Smith, *An In-flight Investigation to Develop Control System Design Criteria for Fighter Airplanes*, Tech. Rep. AFFDL-TR-70-74, Volume 2 (Air Force Flight Dynamics Laboratory, 1970).

[21] R. E. Smith, *Effects of Control System Dynamics on Fighter Approach and Landing Longitudinal Flying Qualities*, Tech. Rep. AFFDL-TR-78-122, Volume 1 (CALSPAN ADVANCED TECHNOLOGY CENTER BUFFALO NY, 1978).

[22] R. A. Hess, *Analytical Assessment of Performance, Handling Qualities, and Added Dynamics in Rotorcraft Flight Control,* IEEE Transactions on Systems, Man, and Cybernetics — Part A: Systems and Humans **39**, 262 (2009).

[23] M. Li, *Effects of Helicopter Degree of Freedom and Motion Cues On Allowable Error Envelopes*, Master's thesis, Delft University of Technology (2016).

[24] M. Cook, *Flight Dynamics Principles: A Linear Systems Approach to Aircraft Stability and Control* (Butterworth-Heinemann, 2012).

[25] S. Fasiello, *A Cybernetic Analysis of the Noticeability of Different Controlled Aircraft Pitch Dynamics Parameter Settings*, Master's thesis, Delft University of Technology (2016).

[26] G. E. Cooper and R. P. Harper, Jr., *The Use of Pilot Rating in the Evaluation of Aircraft Handling Qualities*, Tech. Rep. NASA TN D-5153 (National Aeronautics and Space Administration, 1969).

[27] J. T. Bosworth and P. S. Williams-Hayes, *Flight Test Results from the NF-15B Intelligent Flight Control System (IFCS) Project with Adaptation to a Simulated Stabilator Failure,* in *Proceedings of the AIAA Infotech at Aerospace 2007 Conference and Exhibit, Rohnert Park (CA)*, AIAA-2007-2818 (2007).

[28] S. Geluardi, F. M. Nieuwenhuizen, L. Pollini, and H. H. Bülthoff, *Frequency Domain Identification of a Light Helicopter in Hover,* in *Proceedings of the AHS 70th Annual Forum, Montreal, Canada* (2014).

[29] M. B. Tischler, *System Identification Methods for Aircraft Flight Control Development and Validation*, NASA Technical Memorandum 110369 (NASA Ames Research Center, Moffett Field (CA), 1995).

[30] P. G. Hamel and K. Jürgen, *Advances in Rotorcraft System Identification,* Progress in Aerospace Sciences **33**, 259 (1997).

[31] Cicolani and Luigi, *Flight Test Identification and Simulation of a UH-60A Helicopter and Slung Load*, Tech. Rep. NASA/TM-2001-209619 (NASA, Ames Research Center Moffett Field, California, 2001).

[32] P. G. Hamel and R. V. Jategaonkar, *Evolution of flight vehicle system identification,* Journal of aircraft **33**, 9 (1996).

[33] P. G. Hamel, *In-Flight Simulators and Fly-by-Wire/Light Demonstrators: A Historical Account of International Aeronautical Research* (Springer, 2017).

[34] C. J Miller, *Nonlinear Dynamic Inversion Baseline Control Law: Flight-Test Results for the Full-scale Advanced Systems Testbed F/A-18 Airplane,* (AIAA Guidance, Navigation, and Control Conference, 2011) pp. 1–25.

[35] M. R. Anderson, *Robustness evaluation of a flexible aircraft control system,* Journal of guidance, control, and dynamics **16**, 564 (1993).

[36] H. Levitt, *Transformed Up-Down Methods in Psychoacoustics,* Journal of the Acoustical Society of America **49**, 467 (1971).

[37] A. R. Valente Pais, *Perception Coherence Zones in Vehicle Simulation*, Ph.D. thesis, Delft University of Technology, Faculty of Aerospace Engineering (2013).

[38] W. Fu, M. M. van Paassen, and M. Mulder, *The Influence of Discrimination Strategy on the JND in Human Haptic Perception of Manipulator Stiffness,* in *AIAA Modeling and Simulation Technologies Conference* (2017) p. 3668.

[39] E. van Kampen, *Global Optimization using Interval Analysis. Interval optimization for aerospace applications.*, Ph.D. thesis, Delft University of Technology (2010).

[40] F. M. Drop, *Control-Theoretic Models of Feedforward in Manual Control*, Ph.D. thesis, Delft University of Technology, Faculty of Aerospace Engineering (2016).

[41] K. van der El, D. M. Pool, M. M. van Paassen, and M. Mulder, *Effects of Linear Perspective on Human Use of Preview in Manual Control,* IEEE Transactions on Human-Machine Systems (2017), 10.1109/THMS.2017.2736882.

[42] M. Mulder, D. M. Pool, D. A. Abbink, E. R. Boer, P. M. T. Zaal, F. M. Drop, K. van der El, and M. M. van Paassen, *Manual Control Cybernetics: State-of-the-Art and Current Trends,* IEEE Transactions on Human-Machine Systems (2017), 10.1109/THMS.2017.2761342.

[43] R. A. Hess, *Modeling Pilot Detection of Time-Varying Aircraft Dynamics,* Journal of Aircraft **49**, 2100 (2012).

[44] P. M. T. Zaal, *Manual Control Adaptation to Changing Vehicle Dynamics in Roll–Pitch Control Tasks,* Journal of Guidance, Control, and Dynamics **39**, 1046 (2016).

[45] P. M. Thompson, D. H. Klyde, and M. J. Brenner, *Wavelet-Based Time-Varying Human Operator Models,* in *Proceedings of the AIAA Atmospheric Flight Mechanics Conference and Exhibit, Montreal (CA)*, AIAA-2001-4009 (2001).

[46] T. Verspecht, *Identification of Time Variant Neuromuscular Admittance using Wavelets*, Master's thesis, Delft University of Technology, Faculty of Aerospace Engineering (2011).

[47] P. M. T. Zaal and B. T. Sweet, *Identification of Time-Varying Pilot Control Behavior in Multi-Axis Control Tasks,* in *Proceedings of the AIAA Modeling and Simulation Technologies Conference 2012, Minneapolis (MN)*, AIAA-2012-4793 (2012).

[48] M. Olivari, F. M. Nieuwenhuizen, H. H. Bülthoff, and L. Pollini, *Identifying Time-Varying Neuromuscular System with a Recursive Least-Squares Algorithm: a Monte-Carlo Simulation Study,* in *Proceedings of the 2014 IEEE International Conference on Systems, Man, and Cybernetics, San Diego (CA)* (2014) pp. 3573–3578.

[49] A. J. Pronker, D. A. Abbink, M. M. van Paassen, and M. Mulder, *Estimating driver time-varying neuromuscular admittance through LPV model and grip force,* in *Proceedings of the the 20th IFAC World Congress, Toulouse, France* (2017) pp. 15481–15486.

[50] A. Popovici, P. M. T. Zaal, and D. M. Pool, *Dual Extended Kalman Filter for the Identification of Time-Varying Human Manual Control Behavior,* in *Proceedings of the AIAA Modeling and Simulation Technologies Conference, Denver (CO)*, AIAA-2017-3666 (2017).

A

SIMULATION RESULTS WITH VARIOUS REMNANT RATIOS

This appendix shows the comparison of the experiment results of Chapter 4 and corresponding simulation results with 5 different remnant-to-control variance ratios. Eventually the remnant-to-control variance ratio 0.25 *was selected as the final value for the computer offline simulations carried out in Chapter 5 and Chapter 6, because it led to the best correspondence to the results from the experiment and simulation reported in Chapter 4.*

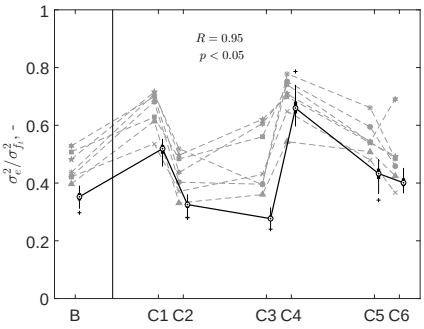

(a) Performance

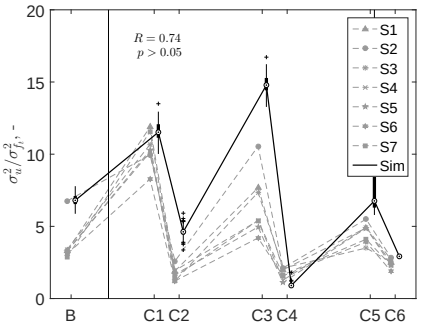

(b) Control activity

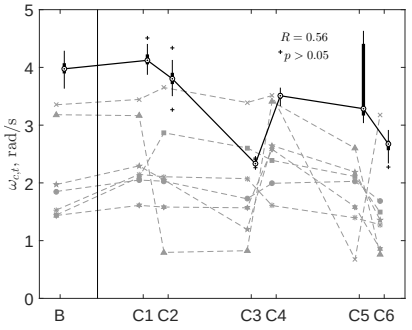

(c) Target crossover frequency

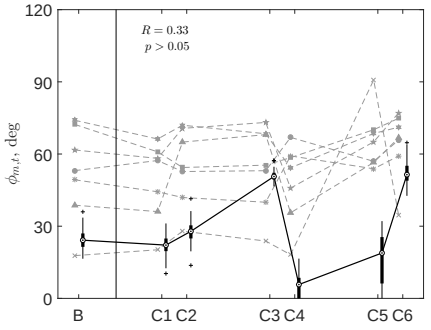

(d) Target phase margin

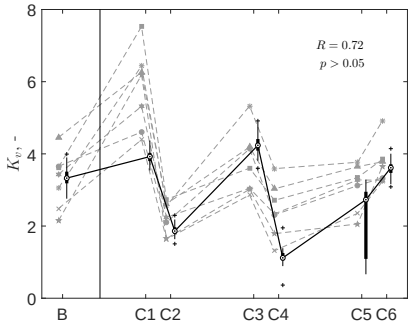

(e) Visual gain

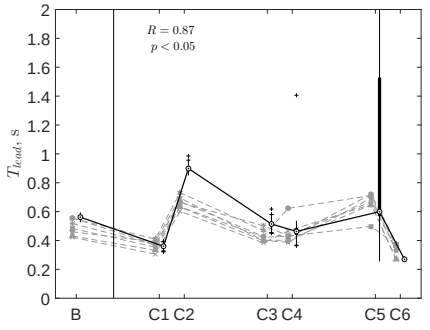

(f) Lead time constant

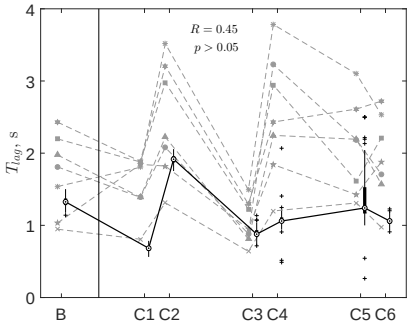

(g) Lag time constant

Figure A.1: Comparison between experiment and simulation results (in simulation $\sigma_n^2/\sigma_u^2 = 0.1$).

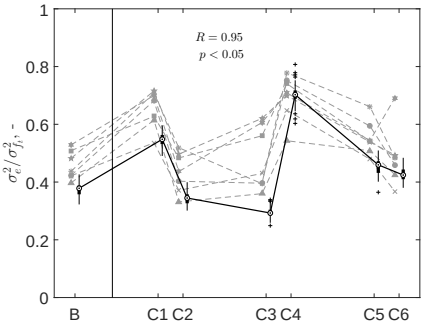

(a) Performance

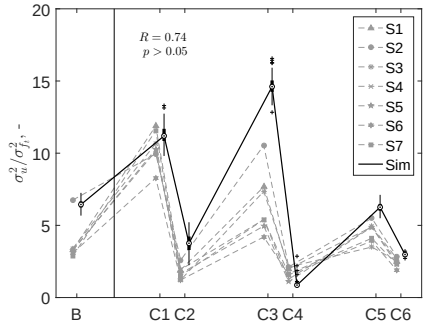

(b) Control activity

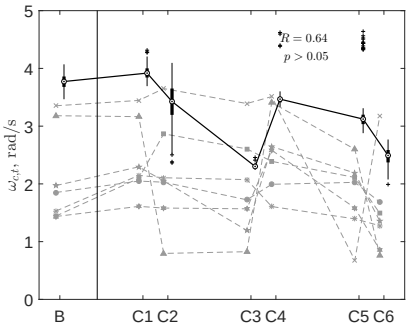

(c) Target crossover frequency

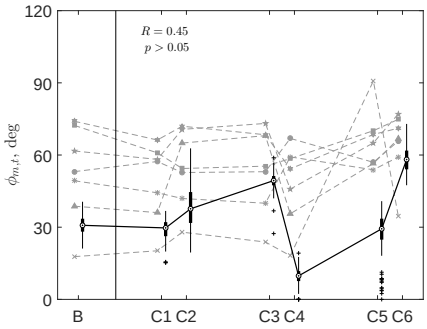

(d) Target phase margin

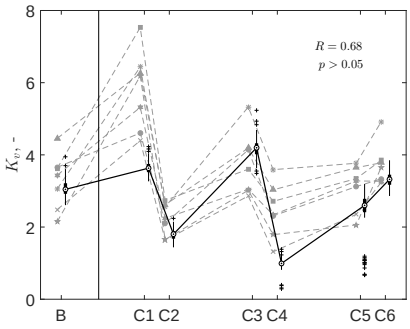

(e) Visual gain

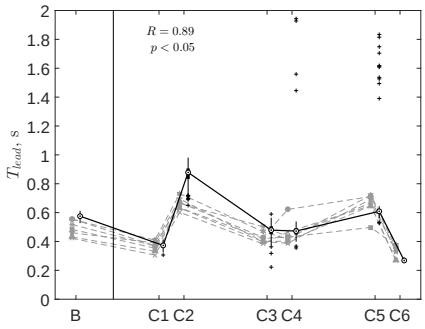

(f) Lead time constant

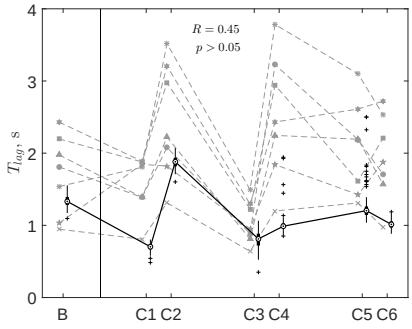

(g) Lag time constant

Figure A.2: Comparison between experiment and simulation results (in simulation $\sigma_n^2/\sigma_u^2 = 0.15$).

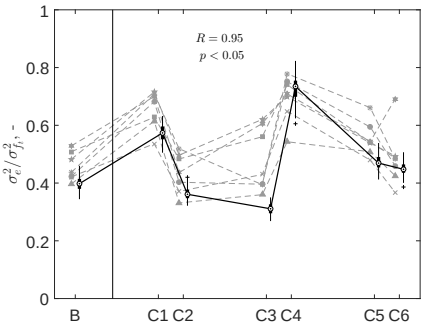

(a) Performance

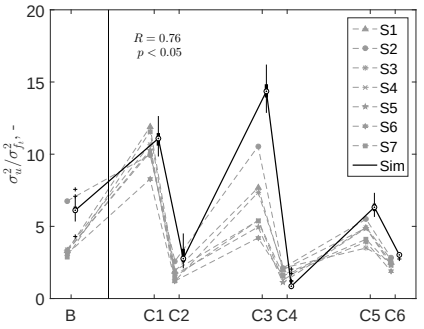

(b) Control activity

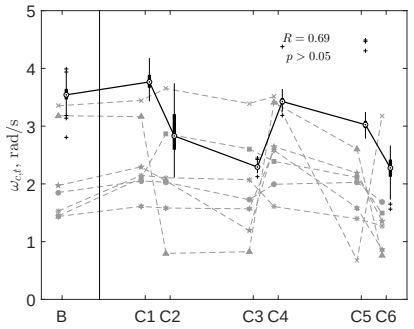

(c) Target crossover frequency

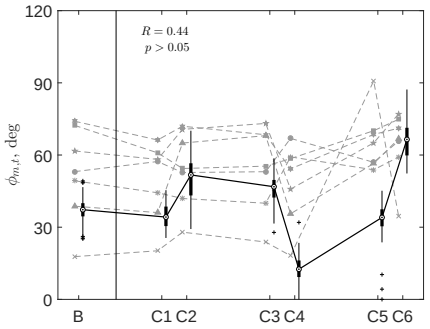

(d) Target phase margin

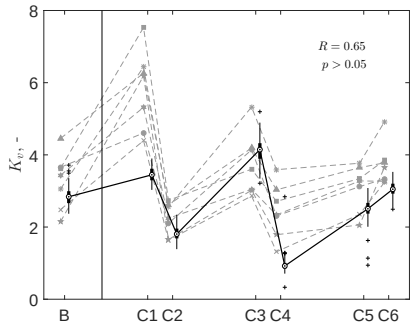

(e) Visual gain

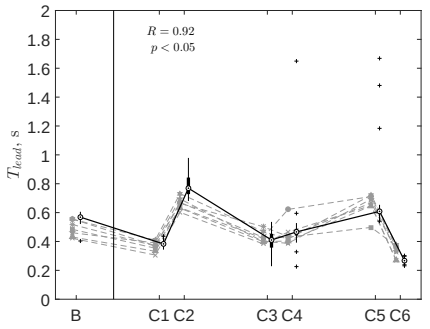

(f) Lead time constant

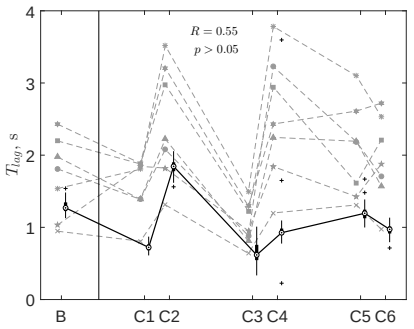

(g) Lag time constant

Figure A.3: Comparison between experiment and simulation results (in simulation $\sigma_n^2/\sigma_u^2 = 0.2$).

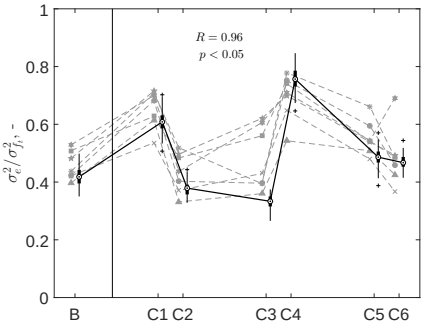

(a) Performance

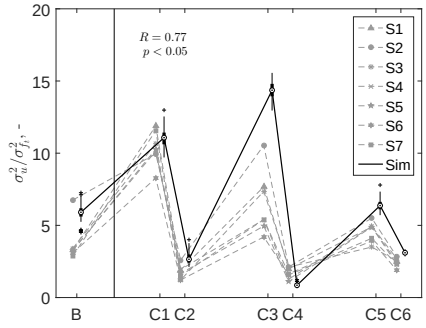

(b) Control activity

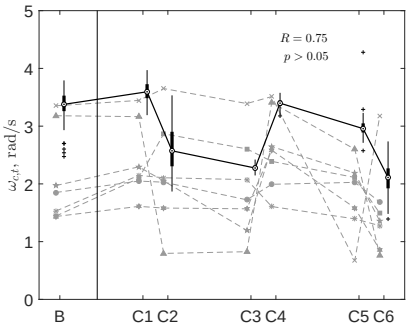

(c) Target crossover frequency

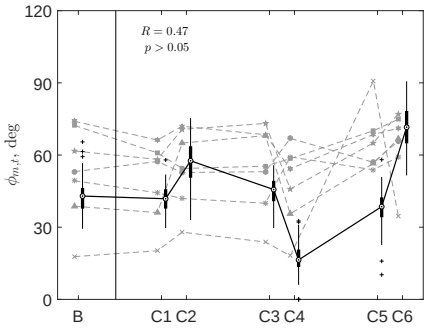

(d) Target phase margin

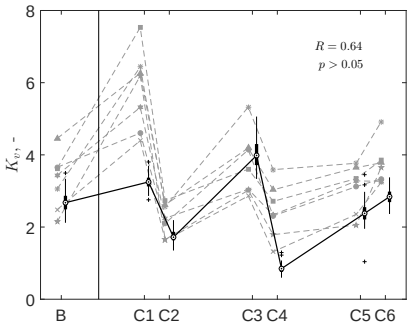

(e) Visual gain

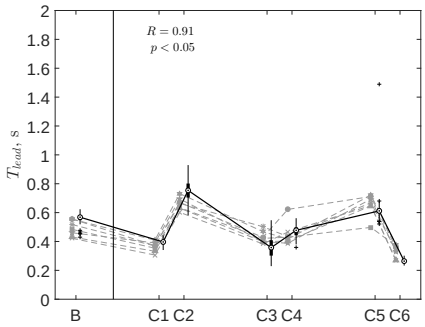

(f) Lead time constant

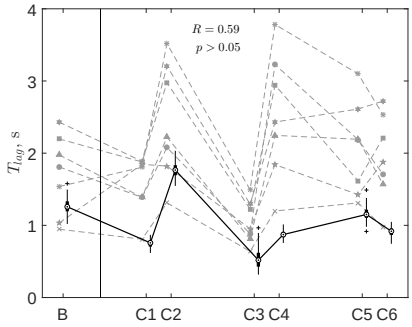

(g) Lag time constant

Figure A.4: Comparison between experiment and simulation results (in simulation $\sigma_n^2/\sigma_u^2 = 0.25$).

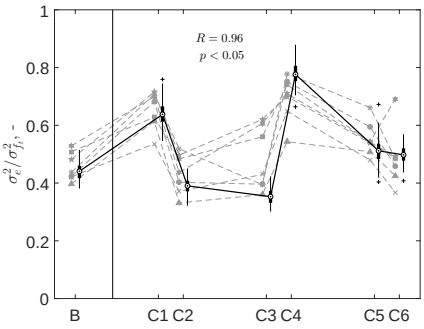

(a) Performance

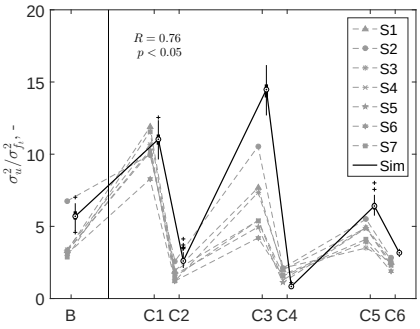

(b) Control activity

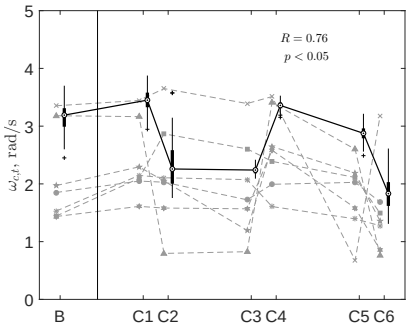

(c) Target crossover frequency

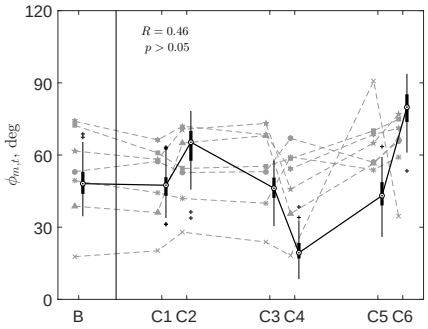

(d) Target phase margin

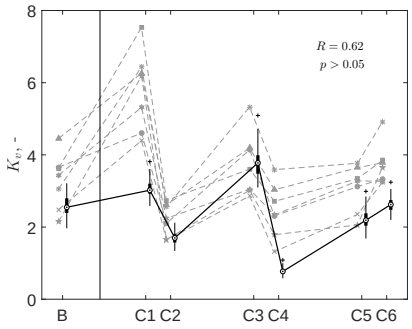

(e) Visual gain

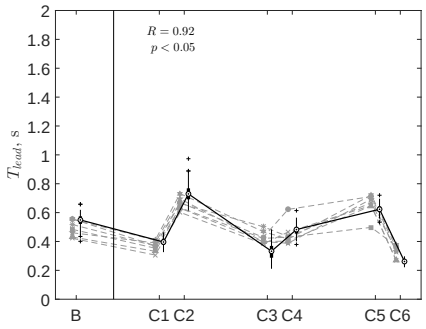

(f) Lead time constant

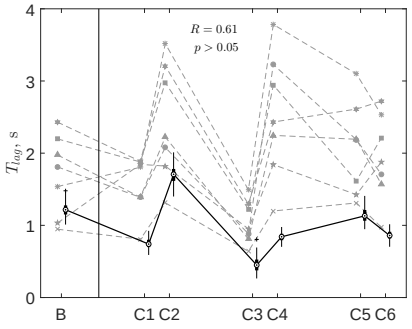

(g) Lag time constant

Figure A.5: Comparison between experiment and simulation results (in simulation $\sigma_n^2/\sigma_u^2 = 0.3$).

B

SUBJECTIVE RATINGS

This appendix presents the subjective ratings and comments of the seven subjects obtained during the experiment in Chapter 4. The subjective ratings are also analyzed and discussed in Chapter 4. In summary, these subjective ratings were found to be very inconsistent among the subjects and also inaccurate. Thus in the remainder of the thesis, no further subjective rating phase was conducted, and no correlations were made between any subjective and objective data.

B

Condition	C1			C2			C3		
Run number	R2 VS R1	R3 VS R2	R4 VS R3	R2 VS R1	R3 VS R2	R4 VS R3	R2 VS R1	R3 VS R2	R4 VS R3
Score	1	1	2	2	1	0	1	1	1
Performance better									×
Performance worse								×	
Control more	×		×		×			×	
Control less									×
Dynamics faster		×		×			×		
Dynamics slower								×	×

Condition	C4			C5			C6		
Run number	R2 VS R1	R3 VS R2	R4 VS R3	R2 VS R1	R3 VS R2	R4 VS R3	R2 VS R1	R3 VS R2	R4 VS R3
Score	1	0	1	0	1	1	1	1	1
Performance better	×								
Performance worse					×				
Control more							×		
Control less	×								×
Dynamics faster					×			×	
Dynamics slower			×						

Condition	C7 (B)		
Run number	R2 VS R1	R3 VS R2	R4 VS R3
Score	1	1	2
Performance better		×	×
Performance worse			
Control more	×		
Control less			×
Dynamics faster			
Dynamics slower		×	×

Subjective evaluation stage			
R1	R2	R3	R4
C3	B	C3	C3
C1	C1	B	C1
B	C5	C5	C5
C4	C4	C4	B
(C7) B			
B	C2	C2	C2
C6	B	C6	C6

Score meaning
0: no difference
1: slightly different
2: notably different
3: very different

Figure B.1: Subjective evaluation stage ratings of Subject 1.

Condition	C1			C2			C3		
Run number	R2 VS R1	R3 VS R2	R4 VS R3	R2 VS R1	R3 VS R2	R4 VS R3	R2 VS R1	R3 VS R2	R4 VS R3
Score	1	1	0	1	2	0	1	1	1
Performance better					×		×		
Performance worse		×							×
Control more									
Control less	×				×		×	×	×
Dynamics faster					×			×	
Dynamics slower	×	×		×			×		

Condition	C4			C5			C6		
Run number	R2 VS R1	R3 VS R2	R4 VS R3	R2 VS R1	R3 VS R2	R4 VS R3	R2 VS R1	R3 VS R2	R4 VS R3
Score	0	2	2	0	1	1	1	2	2
Performance better		×			×		×		×
Performance worse			×			×		×	
Control more		×	×		×			×	
Control less						×	×		
Dynamics faster			×					×	
Dynamics slower		×				×	×		×

Condition	C7 (B)		
Run number	R2 VS R1	R3 VS R2	R4 VS R3
Score	1	0	2
Performance better	×		×
Performance worse			
Control more			×
Control less	×		
Dynamics faster			
Dynamics slower			×

Subjective evaluation stage			
R1	R2	R3	R4
B	C5	C5	C5
C3	C3	B	C3
C7 (B)			
C6	C6	C6	B
C2	B	C2	C2
C4	C4	B	C4
B	C1	C1	C1

Score meaning
0: no difference
1: slightly different
2: notably different
3: very different

Figure B.2: Subjective evaluation stage ratings of Subject 2.

Condition	C1			C2			C3		
Run number	R2 VS R1	R3 VS R2	R4 VS R3	R2 VS R1	R3 VS R2	R4 VS R3	R2 VS R1	R3 VS R2	R4 VS R3
Score	0	2	1	0	1	1	1	2	1
Performance better			×		×	×	×	×	
Performance worse		×							×
Control more			×			×	×		×
Control less		×						×	
Dynamics faster			×			×			×
Dynamics slower		×			×		×	×	

Condition	C4			C5			C6		
Run number	R2 VS R1	R3 VS R2	R4 VS R3	R2 VS R1	R3 VS R2	R4 VS R3	R2 VS R1	R3 VS R2	R4 VS R3
Score	2	1	1	1	1	2	2	1	2
Performance better	×			×	×		×	×	×
Performance worse		×	×			×			
Control more			×			×	×		
Control less	×	×		×				×	×
Dynamics faster		×				×	×	×	
Dynamics slower	×		×	×	×				×

Condition	C7 (B)		
Run number	R2 VS R1	R3 VS R2	R4 VS R3
Score	0	1	1
Performance better		×	
Performance worse			×
Control more			
Control less		×	×
Dynamics faster			
Dynamics slower		×	×

Subjective evaluation stage			
R1	R2	R3	R4
C4	B	C4	C4
C2	C2	C2	B
B	C6	C6	C6
C5	C5	B	C5
C1	B	C1	C1
C3	C3	C3	B
C7 (B)			

Score meaning
0: no difference
1: slightly different
2: notably different
3: very different

Figure B.3: Subjective evaluation stage ratings of Subject 3.

Condition	C1			C2			C3		
Run number	R2 VS R1	R3 VS R2	R4 VS R3	R2 VS R1	R3 VS R2	R4 VS R3	R2 VS R1	R3 VS R2	R4 VS R3
Score	0	1	0	1	0	1	2	2	2
Performance better		×		×		×		×	
Performance worse							×		×
Control more		×		×		×	×	×	×
Control less									
Dynamics faster						×		×	
Dynamics slower		×		×			×		×

Condition	C4			C5			C6		
Run number	R2 VS R1	R3 VS R2	R4 VS R3	R2 VS R1	R3 VS R2	R4 VS R3	R2 VS R1	R3 VS R2	R4 VS R3
Score	1	2	1	0	1	1	2	1	0
Performance better	×	×	×			×		×	
Performance worse					×		×		
Control more		×			×		×		
Control less	×		×			×		×	
Dynamics faster		×				×	×		
Dynamics slower	×		×		×			×	

Condition	C7 (B)		
Run number	R2 VS R1	R3 VS R2	R4 VS R3
Score	1	0	1
Performance better	×		×
Performance worse			
Control more	×		
Control less			×
Dynamics faster	×		×
Dynamics slower			

Subjective evaluation stage			
R1	R2	R3	R4
B	C6	C6	C6
C4	C4	C4	B
C1	B	C1	C1
C7 (B)			
C3	C3	B	C3
C5	C5	C5	B
B	C2	C2	C2

Score meaning
0: no difference
1: slightly different
2: notably different
3: very different

Figure B.4: Subjective evaluation stage ratings of Subject 4.

Condition	C1			C2			C3		
Run number	R2 VS R1	R3 VS R2	R4 VS R3	R2 VS R1	R3 VS R2	R4 VS R3	R2 VS R1	R3 VS R2	R4 VS R3
Score	1	3	2	2	1	0	2	3	1
Performance better		×						×	
Performance worse			×	×					
Control more			×				×		
Control less	×	×			×				×
Dynamics faster		×			×			×	×
Dynamics slower				×			×		

Condition	C4			C5			C6		
Run number	R2 VS R1	R3 VS R2	R4 VS R3	R2 VS R1	R3 VS R2	R4 VS R3	R2 VS R1	R3 VS R2	R4 VS R3
Score	2	1	1	1	2	2	1	1	1
Performance better									
Performance worse	×		×	×		×			
Control more	×			×		×	×		
Control less					×			×	×
Dynamics faster	×		×		×				
Dynamics slower		×							

Condition	C7 (B)		
Run number	R2 VS R1	R3 VS R2	R4 VS R3
Score	1	0	0
Performance better			
Performance worse			
Control more			
Control less			
Dynamics faster			
Dynamics slower	×		

Subjective evaluation stage			
R1	R2	R3	R4
C1	C1	B	C1
B	C6	C6	C6
C3	C3	C3	B
C2	B	C2	C2
C5	C5	B	C5
C7 (B)			
B	C4	C4	C4

Score meaning
0: no difference
1: slightly different
2: notably different
3: very different

Figure B.5: Subjective evaluation stage ratings of Subject 5.

Condition	C1			C2			C3		
Run number	R2 VS R1	R3 VS R2	R4 VS R3	R2 VS R1	R3 VS R2	R4 VS R3	R2 VS R1	R3 VS R2	R4 VS R3
Score	2	1	1	1	0	1	1	1	2
Performance better	×	×					×	×	
Performance worse			×			×			×
Control more	×						×	×	
Control less			×						
Dynamics faster				×					
Dynamics slower		×						×	

Condition	C4			C5			C6		
Run number	R2 VS R1	R3 VS R2	R4 VS R3	R2 VS R1	R3 VS R2	R4 VS R3	R2 VS R1	R3 VS R2	R4 VS R3
Score	1	2	0	2	1	1	1	1	1
Performance better	×	×		×		×		×	×
Performance worse					×		×		
Control more		×				×			×
Control less				×			×		
Dynamics faster					×				
Dynamics slower		×		×					

Condition	C7 (B)		
Run number	R2 VS R1	R3 VS R2	R4 VS R3
Score	1	2	1
Performance better	×		×
Performance worse		×	
Control more		×	
Control less	×		×
Dynamics faster		×	
Dynamics slower	×		×

Subjective evaluation stage			
R1	R2	R3	R4
C7 (B)			
B	C5	C5	C5
C2	B	C2	C2
C1	C1	B	C1
C4	C4	C4	B
C6	B	C6	C6
B	C3	C3	C3

Score meaning
0: no difference
1: slightly different
2: notably different
3: very different

Figure B.6: Subjective evaluation stage ratings of Subject 6.

Condition	C1			C2			C3		
Run number	R2 VS R1	R3 VS R2	R4 VS R3	R2 VS R1	R3 VS R2	R4 VS R3	R2 VS R1	R3 VS R2	R4 VS R3
Score	1	0	1	1	0	2	2	2	1
Performance better			×	×			×	×	
Performance worse	×					×			
Control more	×					×	×		×
Control less			×	×					
Dynamics faster						×			
Dynamics slower								×	

Condition	C4			C5			C6		
Run number	R2 VS R1	R3 VS R2	R4 VS R3	R2 VS R1	R3 VS R2	R4 VS R3	R2 VS R1	R3 VS R2	R4 VS R3
Score	3	0	1	0	1	2	0	1	0
Performance better					×	×		×	
Performance worse	×								
Control more	×								
Control less			×					×	
Dynamics faster	×								
Dynamics slower					×	×			

Condition	C7 (B)		
Run number	R2 VS R1	R3 VS R2	R4 VS R3
Score	1	1	0
Performance better		×	
Performance worse			
Control more			
Control less			
Dynamics faster			
Dynamics slower	×		

Subjective evaluation stage			
R1	R2	R3	R4
C2	C2	C2	B
C7 (B)			
B	C4	C4	C4
C3	C3	B	C3
C6	B	C6	C6
B	C1	C1	C1
C5	C5	C5	B

Score meaning
0: no difference
1: slightly different
2: notably different
3: very different

Figure B.7: Subjective evaluation stage ratings of Subject 7.

C

MCAB Simulation Data Base

This appendix presents the simulation results of Chapter 5 for the $\omega_{dp} = 4, 5, 6$ *and* 7 rad/s *dipoles. Using the constrained nonlinear optimization based simulation developed in Chapter 4, the tracking performance, control activity and human operator adaptations to the extra added dipole cascaded to the baseline aircraft dynamics were studied. Together with the simulation results shown in Chapter 5, the data shown in this appendix form the MCAB in Chapter 5.*

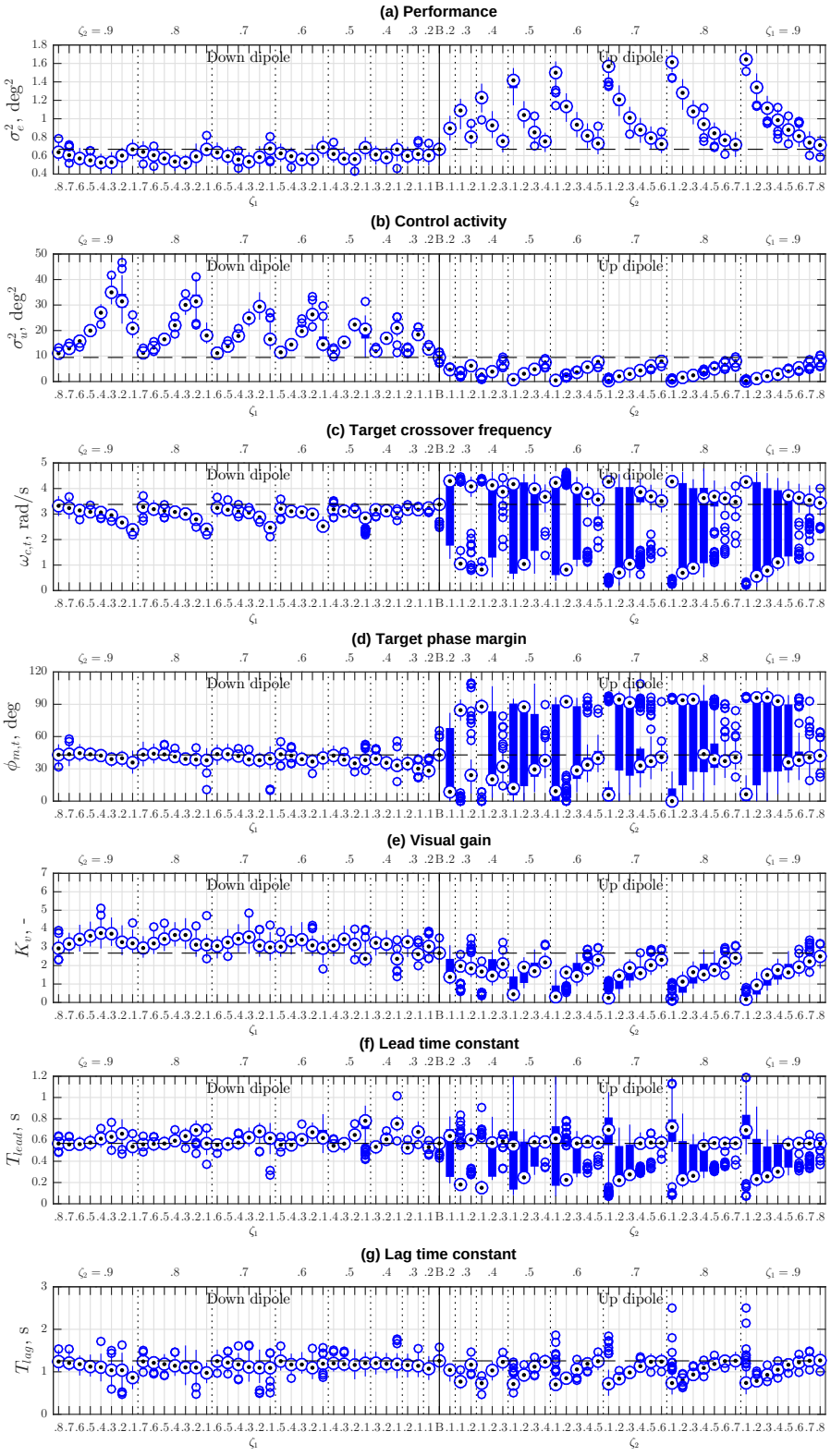

Figure C.1: All simulation results at $\omega_{dp} = 4$ rad/s.

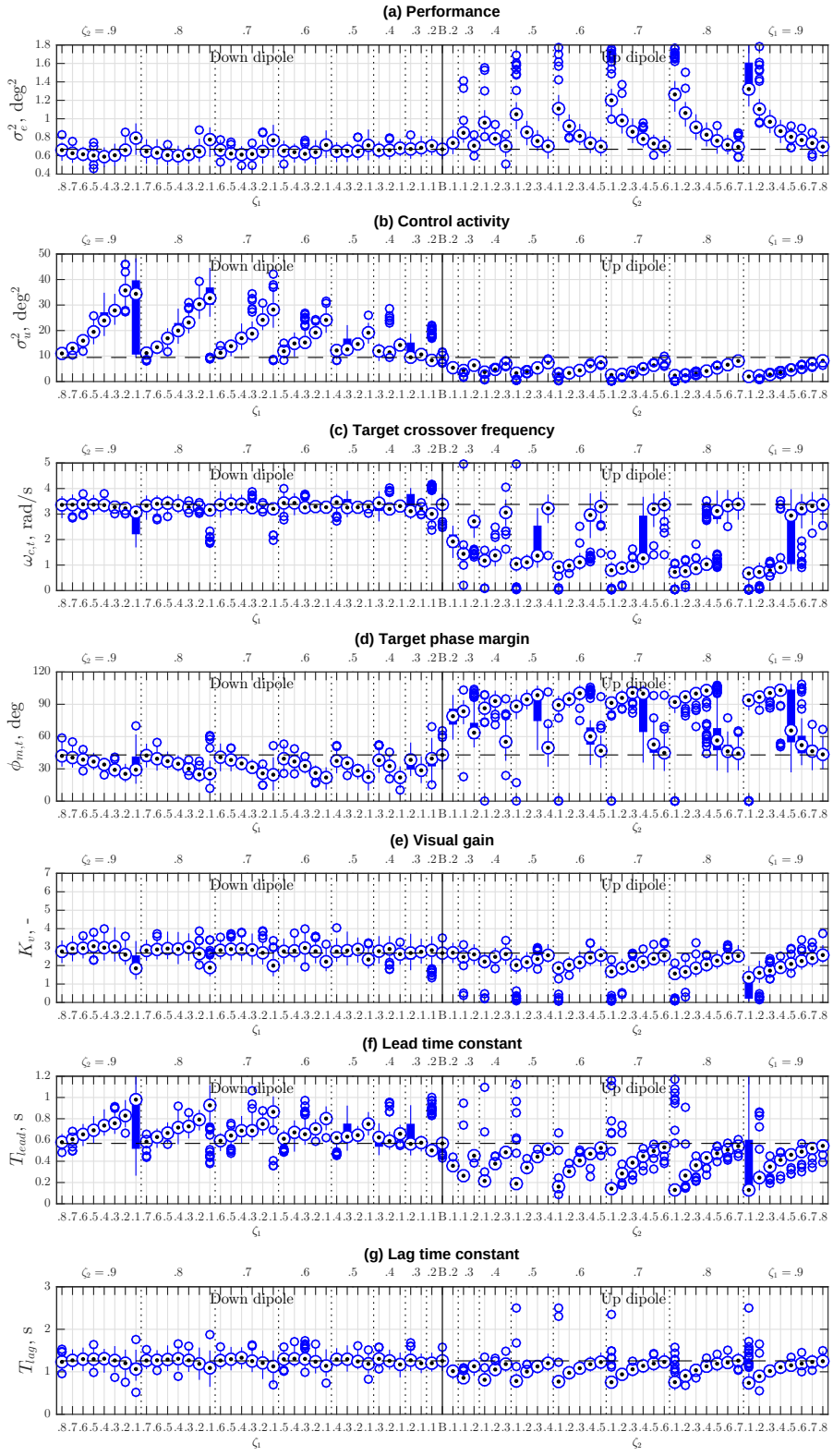

Figure C.2: All simulation results at $\omega_{dp} = 5$ rad/s.

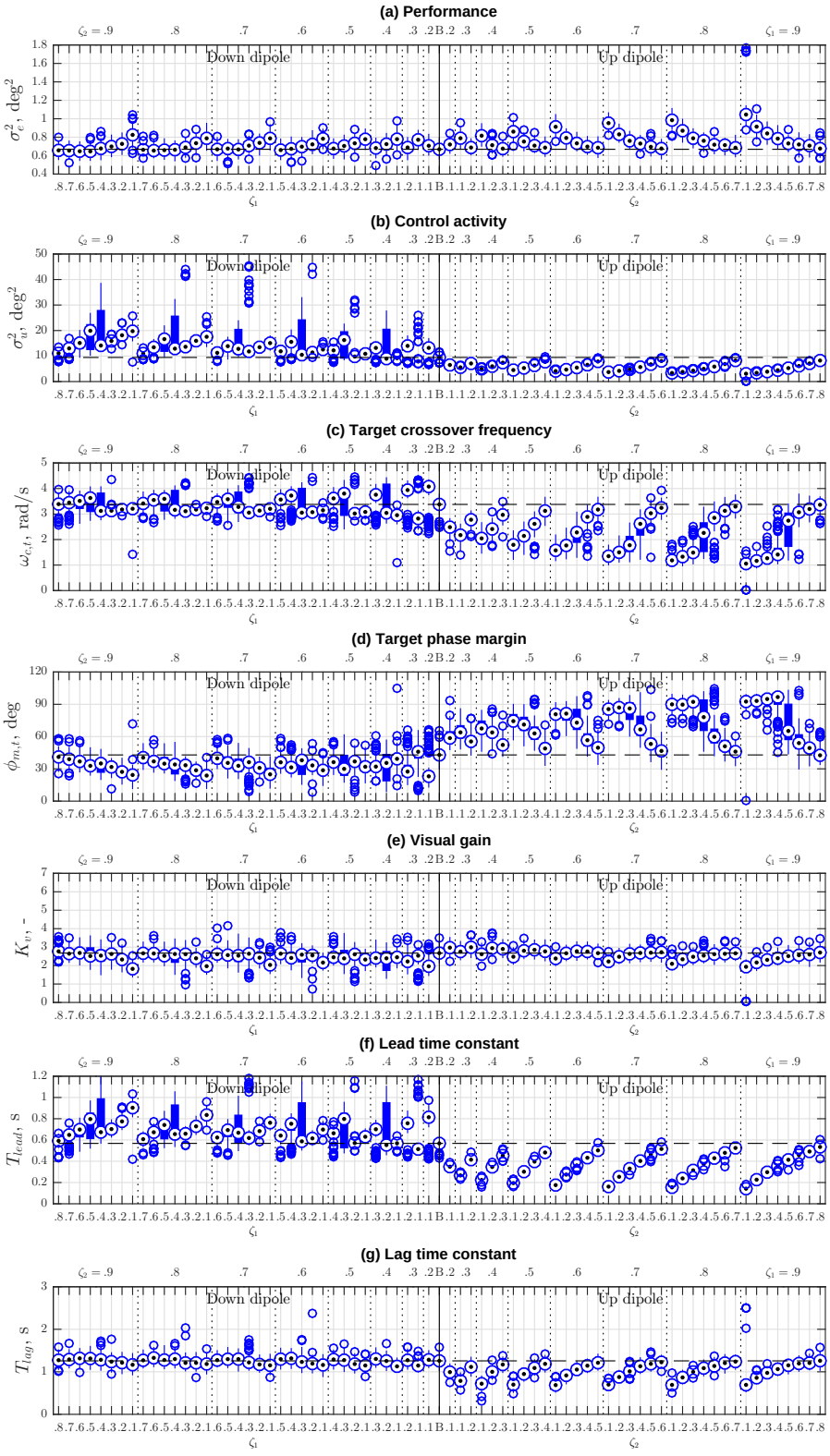

Figure C.3: All simulation results at $\omega_{dp} = 6$ rad/s.

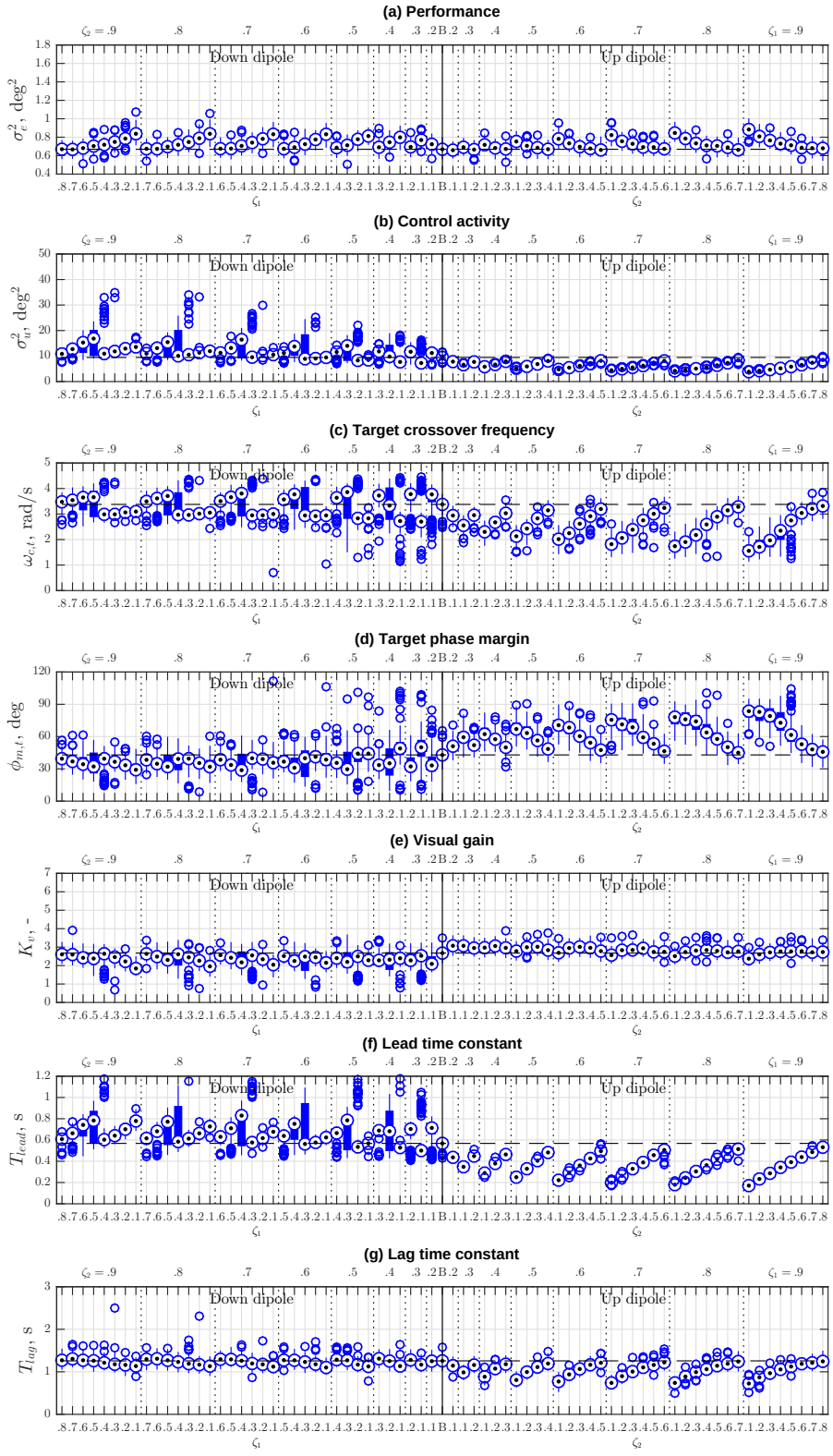

Figure C.4: All simulation results at $\omega_{dp} = 7$ rad/s.

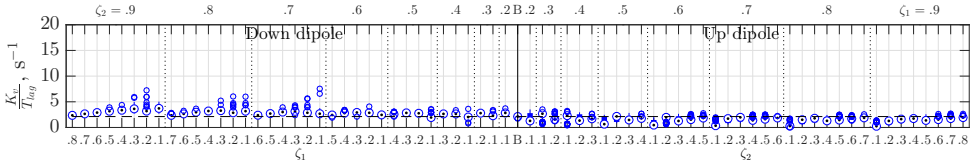

(a) ω_{dp} = 4 rad/s

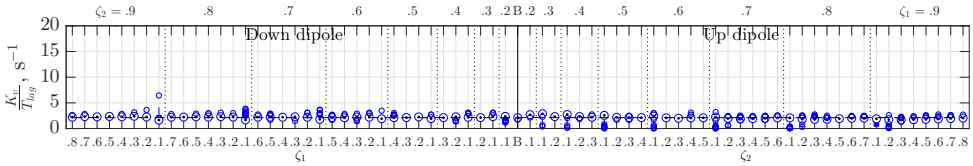

(b) ω_{dp} = 5 rad/s

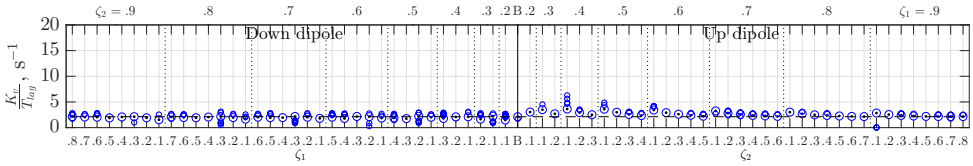

(c) ω_{dp} = 6 rad/s

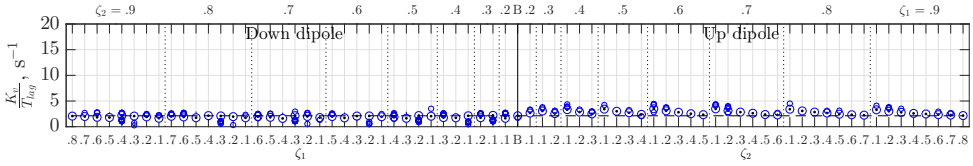

(d) ω_{dp} = 7 rad/s

Figure C.5: Ratio between visual gain and lag time constant at different ω_{dp}.

D

EFFECTS OF ADDED DYNAMICS AND MOTION FEEDBACK ON MANUAL CONTROL BEHAVIOR

This appendix presents the results of a preliminary experiment as an extension to Chapter 6 to investigate whether the (simulator) motion feedback could affect the human operator control behavior corresponding with different added dynamics cascaded to the baseline aircraft dynamics in a target tracking task, which could further affect the developed MCAB in Chapters 5 and 6. Added dipole dynamics with slightly different natural frequencies and damping ratios than those used in Chapter 6 were used in this experiment. Data were collected from three subjects for conditions both with and without motion feedback. Experiment results show that the interaction between the added dynamics and motion feedback has no effect on the relative changes of tracking performance, control activity or human operator control behavior. The experiment data might be used as a reference to indicate how the MCAB with motion would be different from those developed in Chapters 5 and 6. However, given the limited differences in the MCAB dependent measures between the motion and no-motion cases, it was decided not to study the MCAB with motion in this thesis.

D.1. INTRODUCTION

In order to know whether the motion feedback of the flight simulator would make a difference in human operator adaptations to the changes of controlled dynamics, which could further influence formulating the MCAB (Chapter 5), an aircraft pitch attitude tracking task with both motion on and off cases was carried out as an extension to the experiment of Chapter 6.

D.2. METHODS

D.2.1. CONTROL TASK

A schematic representation of the tracking task is shown in Figure D.1. The total controlled aircraft dynamics consist of the baseline dynamics $H_{baseline}$, cascaded with the added dynamics H_{added}. The human operator (modeled by a linear transfer function H_p representing the visual channel, a linear transfer function H_m representing the motion channel consistent with the ones in 2 and the remnant n) controls the pitch angle θ of the total aircraft dynamics ($H_{baseline}H_{added}$) by tracking the target signal f_t to minimize the error signal e, which is the difference between the target signal f_t and the aircraft pitch angle θ. In Figure D.1, u is the human operator control signal, K_s is the stick gain, u_s is the control signal from the stick, u_a is the signal out from the added dynamics, and δ_e is the signal directly feeding into the baseline aircraft dynamics. Besides the target forcing function f_t, a disturbance signal f_d is also added into the loop to facilitate identifying both H_p and H_m responses [1–3]. The forcing functions f_t and f_d, stick gain K_s, baseline aircraft dynamics $H_{baseline}$ and types of added dipole dynamics H_{added} are the same with those tested in Chapter 6. The visual channel of the human operator H_p is modeled as in Chapter 6, while for the motion channel of the human operator H_m is the same as used in Chapter 2.

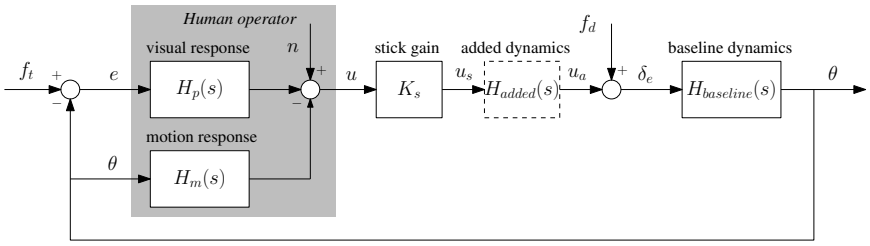

Figure D.1: A schematic representation of the aircraft pitch attitude tracking task with motion feedback.

In Chapter 5, it was found that the tracking performance pattern (between up and down dipoles) of dipole natural frequency $\omega_{dp} = 1$ rad/s is unique and different from ω_{dp} of other frequencies. Thus in this appendix, it was of interest to investigate, for example, the changes in tracking performance, control activity and human operator control behavior when ω_{dp} was varied from 1 rad/s to 3 rad/s. The difference between the damping ratios ($\zeta_2 - \zeta_1$) was kept at 0.1 over different ζ_1 and ζ_2 settings, since simulation results in Chapter 5 showed that such a small difference could make a difference in human operator control behavior. Moreover, in Chapter 3, since up dipole dynamics had already been investigated, it would be of more interest in this appendix to focus on the down dipoles. The parameters of the

tested added dipole dynamics are listed in Table D.1. The frequency responses of the tested dipole dynamics are shown in Figure D.2, where the subjective MUAD envelopes [4] are drawn for reference. For all the dynamics in Table D.1, both motion and no-motion cases were tested in the experiment.

Table D.1: Experiment conditions (all conditions were tested both with and without motion in the experiment)

Conditions	ω_{dp}, rad/s	ζ_1,-	ζ_2,-
C1	1	0.8	0.9
C2	1	0.7	0.8
C3	1	0.6	0.7
C4	1	0.4	0.5
C5	1	0.3	0.4
C6	1	0.2	0.3
C7	1	0.1	0.2
C8	2	0.8	0.9
C9	2	0.7	0.8
C10	2	0.6	0.7
C11	2	0.4	0.5
C12	2	0.3	0.4
C13	3	0.8	0.9
C14	3	0.7	0.8
C15	3	0.6	0.7
Baseline (B)	-	-	-

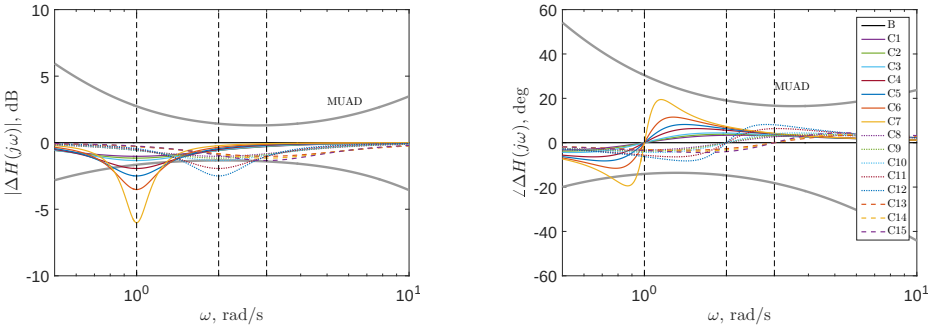

(a) Magnitude

(b) Phase

Figure D.2: The MUAD envelopes [4] and all added dynamics. The vertical dashed lines indicate the natural frequencies of the added dynamics (see Table D.1).

D.2.2. EXPERIMENT

The experiment was performed in the SIMONA Research Simulator (SRS) of Delft University of Technology (see Figure D.3a). During the experiment, subjects were seated in the right cockpit seat and a right-handed sidestick was used for giving inputs to the controlled dynamics. Only the pitch axis of the sidestick was active during the experiment; the roll axis of the sidestick was fixed at the neutral position. The tracking error e in Figure D.1 was presented to the subject through the primary flight display (PFD) directly in front of the

right seat, as shown in Figure D.3(b). The display shows the pitch attitude tracking error e as the distance between the center fixed aircraft symbol and the moving target line. The aircraft symbol was static, and the target line moved to indicate the current tracking error e. No other visual cues were presented during the experiment, that is, the secondary flight displays and the outside visual system were switched off. During the test with motion feedback, one-to-one pitch motion cues (without washout) were provided through the motion system for all conditions in Table D.1. Before the test run of each condition (including the no-motion conditions), the SRS was moved to the trim pitch attitude, which is the position relative to the subject head position as it was measured in real flight for the same baseline aircraft dynamics [5].

To make sure that the subjects only utilized and responded to the visual information and the motion feedback provided by the motion system, a noise-canceling headset was used to prevent subjects from hearing any noise produced by the motion system's actuators. Additionally, aircraft engine noise was played over the headset to further keep the subjects from hearing the actuator sliding noise. The subjects wore the headset for all the testing dynamics in Table D.1, for both motion and no-motion test cases.

(a) The SIMONA Research Simulator (SRS).

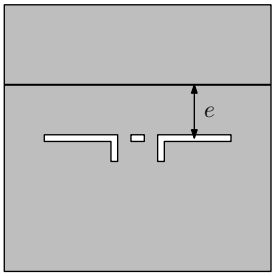

(b) Compensatory pitch tracking display.

Figure D.3: The SIMONA Research Simulator (SRS) and compensatory pitch tracking display.

Three subjects participated in this experiment, all students or staff at Aerospace Engineering at Delft University of Technology. All subjects had experience with similar manual control tasks from previous human-in-the-loop experiments. Each subject received an experimental briefing on the overview and objective of the experiment. The subjects were informed the nature of the different experimental conditions (Table D.1) without providing the details of the dynamics of the controlled elements. The subjects were instructed to minimize the pitch attitude tracking error e presented on the PFD as best as possible. Finally, all the subjects gave written informed consent before the start of the experiment.

The order of the testing was determined for each subject by a Latin square. Considering the large amount of conditions and testing runs, the experiment for each subject was divided into two sessions on two different days: one day without motion for all tested added dynamics; and one day for all motion conditions). For each subject, the experiment started with an initial familiarization. During this phase, subjects were allowed to familiarize themselves with the baseline aircraft dynamics (condition B) for a total of 4 tracking

runs. Following this initial familiarization, the measurement runs for all experiment conditions were performed. The root mean square (RMS) of the error signal e was recorded by the experimenter and reported to the subject after each run. For each subject 4 repetitions were collected, then the testing of this condition was completed.

Each testing run lasted 95 s. In order to obtain stable control output from the subject, the first 13.08 s data were cut off for data analysis. Thus 81.92 s data were used for the data analysis. The sampling frequency of the experiment data was 100 Hz.

D.3. RESULTS

D.3.1. PERFORMANCE AND CONTROL ACTIVITY

Figure D.4 shows the performance and control activity, in terms of measured error and control signal variances, measured for the three subjects for all tested conditions. In Figure D.4a, for example, the solid line connects the medians of performance for conditions without motion feedback, and the dashed line connects the medians of performance for conditions with motion feedback. The vertical dashed lines separate the conditions into three parts, of which the added dipole dynamics' natural frequency is 1, 2 and 3 rad/s, respectively.

In Figure D.4a, it can be seen that the performance with the baseline dynamics (B) is equivalent between no-motion and motion cases. For some conditions, such as C3, C8 and C15, small performance degradations are found for the motion cases. In general, however, the motion feedback does not induce an obvious difference in performance over different conditions. Moreover, the changing trends from C1 to C15 are equivalent between no-motion and motion cases, indicating that the interaction between the added dynamics and motion feedback has no effect on performance.

In Figure D.4b, it can be seen that the difference of the control activity for the baseline (B) between no-motion and motion cases is also small. This may be due to the fact that the baseline aircraft dynamics are already quite stable (motion feedback has only a limited contribution of increasing the stability of the system), thus the human operators may achieve similar performance by using similar control activity. For other conditions with added dynamics, in general, the control activity with motion is seen to be lower than without motion. The lower control activity with the presence of motion feedback in target tracking tasks was also found in Chapter 2 and [6]. Moreover, the very similar changing trends from C1 to C15 between no-motion and motion cases indicate that the interaction between the added dynamics and motion feedback has no effect on control activity.

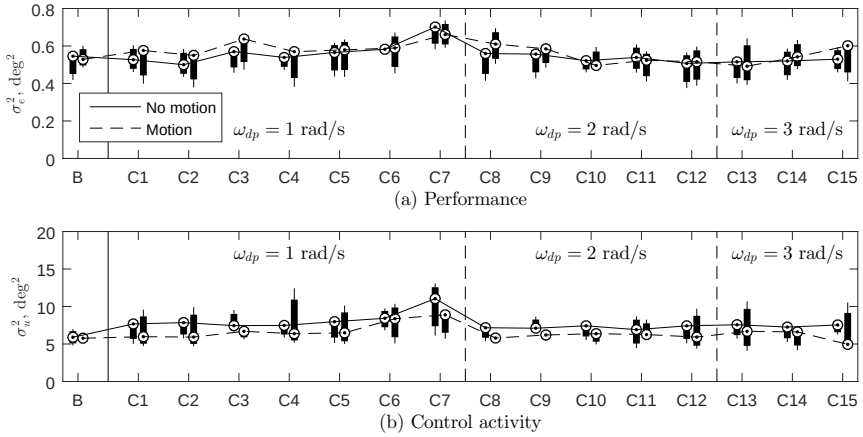

(a) Performance

(b) Control activity

Figure D.4: Comparison of the performance and control activity between no-motion and motion cases.

D.3.2. CROSSOVER FREQUENCIES AND PHASE MARGINS

In Figure D.5, the measured target crossover frequencies and target phase margins of three subjects for all conditions are shown. Again, the solid line connects the medians of the conditions without motion feedback, and the dashed line connects the medians of the data from conditions with motion feedback.

In Figure D.5a it can be seen that the crossover frequencies with motion are in general lower than those of without motion. In Figure D.5b it can be seen that the target phase margins of motion are in general higher than those of no-motion. Again, these are consistent with earlier findings such as in Chapter 2 and [6] for target tracking tasks in the presence of motion feedback. Moreover, the similar changing trends from C1 to C15 between no-motion and motion cases indicate that the interaction between the added dynamics and motion feedback has no effect on either target crossover frequency or phase margin.

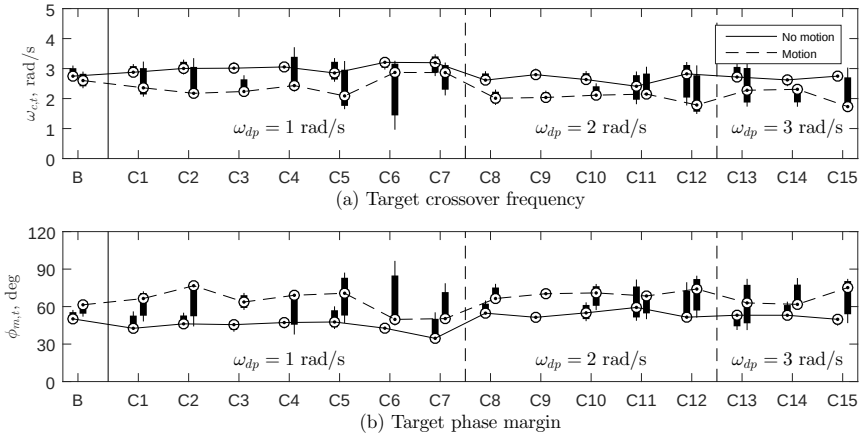

(a) Target crossover frequency

(b) Target phase margin

Figure D.5: Comparison of the target crossover frequencies and target phase margins between no-motion and motion cases.

D.3.3. HUMAN OPERATOR MODEL PARAMETERS

Figure D.6 shows the estimated human operator model parameters: the visual gain K_v, the lead time constant T_{lead}, the lag time constant T_{lag}, the visual time delay τ_v, the neuromuscular damping ratio ζ_{nm} and the natural frequency ω_{nm}, respectively. The motion gain K_m and motion time delay τ_m of the motion channel are not shown since it was found that, similar to the gain and single integrator cases in Chapter 2, motion channel had much less contribution to the control activity compared with the visual channel in target tracking tasks, thus the identification of the motion channel parameters could be less accurate.

In Figures D.6a and D.6c, it can be seen that both visual gain and lag time constant with motion are lower than those for the no-motion conditions. Figure D.6c shows a small drop in the lead time constant for all motion conditions. This shows the expected fact that the motion feedback increases the stability of the system thus the human operators do not need to generate much lead to stabilize the system. Correspondingly, in Figure D.6d, the visual time delay increases slightly when motion feedback is present. In Figure D.6e and Figure D.6f, both the neuromuscular damping ratio and natural frequency have small changes when there is motion feedback. Moreover, for all parameters in Figure D.6, the changing trends from C1 to C15 between no-motion and motion cases are generally equivalent (with only small trend differences between some conditions such as C14 and C15 of K_v and T_{lag}), which indicate that the interaction between the added dynamics and motion feedback has no obvious effect on human operator control behavior.

D.3.4. THE MCAB DEPENDENT MEASURES

Figure D.7 shows the relative changes on performance $\Delta\sigma_e^2$, control activity $\Delta\sigma_u^2$, ratio of the visual gain and lag time constant K_v/T_{lag}, and lead time constant T_{lead} with respect to those with the baseline dynamics, respectively. These four dependent measures in Figure D.7 were used in Chapter 6 to quantify the proposed MCAB.

In Figures D.7a and D.7d, it can be seen that the differences between no-motion and motion cases for the relative changes in tracking performance and lead time constant are only modest over the different conditions, with average differences of 7.8% and 12.3% respectively for all added dynamics conditions. In Figures D.7b and D.7c, the differences between no-motion and motion cases for the relative changes in control activity and ratio of the visual gain and lag time constant are higher, with average differences of 19% and 28.6% respectively for all added dynamics conditions. However, for these four parameters, the changing trends from C1 to C15 between no-motion and motion cases are similar (though there is a bit more difference for $\Delta K_v/T_{lag}$), indicating that the interaction between the added dynamics and motion feedback has little effect on the relative changes of tracking performance, control activity and human operator control behavior.

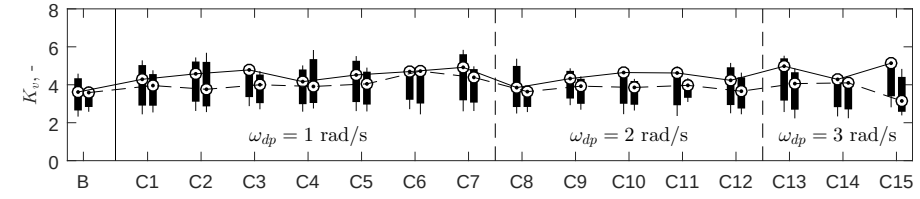

(a) Visual gain

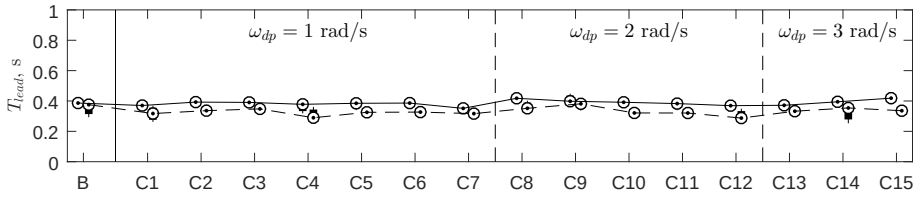

(b) Lead time constant

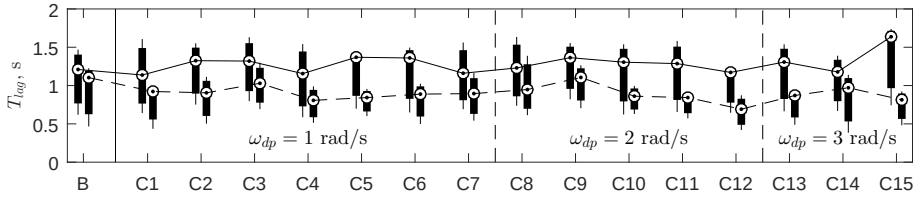

(c) Lag time constant

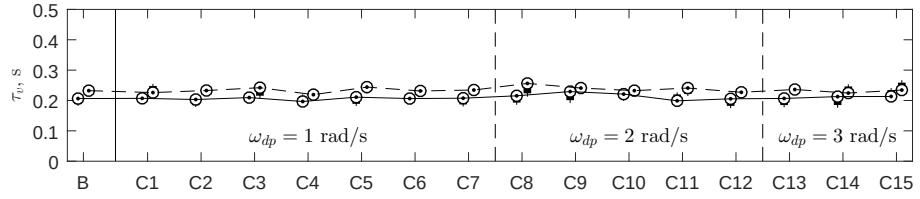

(d) Visual time delay

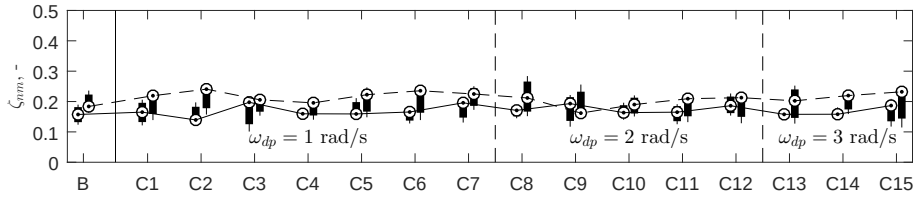

(e) Neuromuscular damping ratio

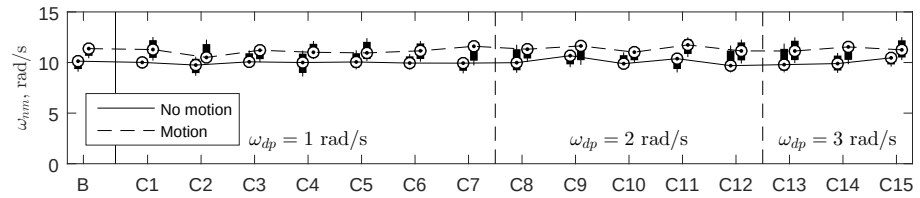

(f) Neuromuscular natural frequency

Figure D.6: Comparison of the human operator model parameters between no-motion and motion cases.

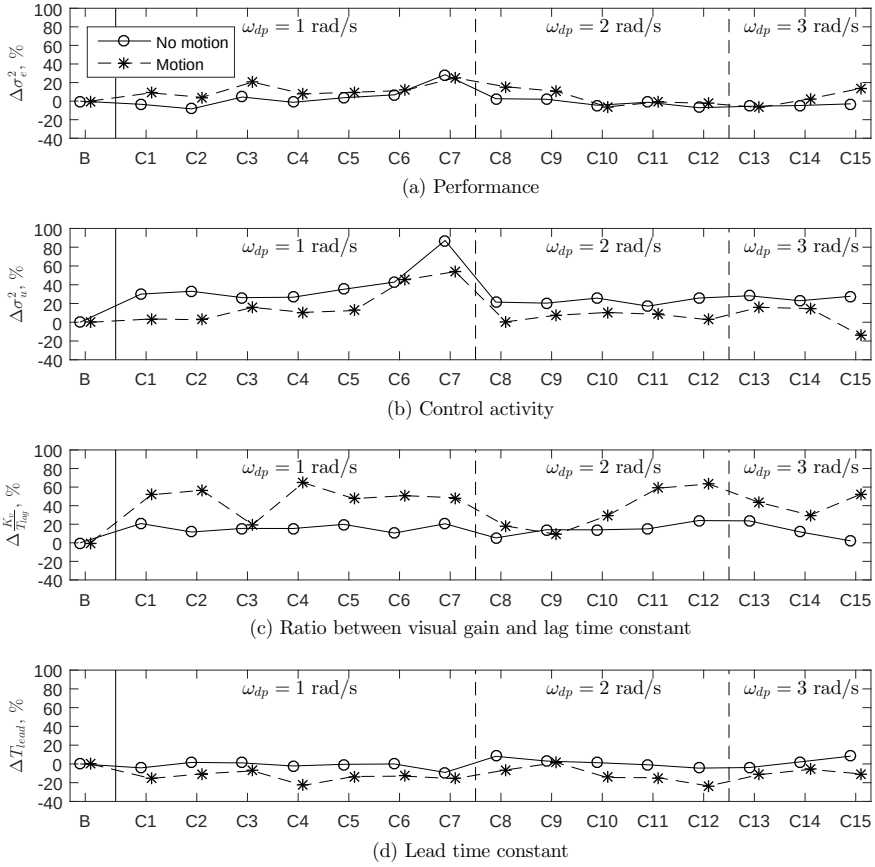

(a) Performance

(b) Control activity

(c) Ratio between visual gain and lag time constant

(d) Lead time constant

Figure D.7: Comparison of the dependent measures quantifying the MCAB between no-motion and motion cases.

D.4. SUMMARY

In order to know whether the flight simulator motion feedback could make any difference on the performance, control activity and human operator control behavior to changes in controlled dynamics, and thus the MCAB developed in this thesis (Chapter 5), an aircraft pitch attitude tracking experiment with different added dipole dynamics was performed in the SIMONA Research Simulator of Delft University of Technology. In total sixteen dynamics (each dynamics with both motion on and off) were tested, with "down" dipole dynamics at $1, 2, 3$ rad/s cascaded with the baseline aircraft pitch dynamics, as well as a reference baseline aircraft dynamics case. Trends in tracking performance, control activity, target crossover frequency, target phase margin and human operator model parameters due to the added dipole dynamics were compared between the no-motion and motion cases, respectively.

The effect of the presence of motion feedback on performance was found to be small, since no clear change on the performance was observed when motion is added. In general the control activity for all added dynamics was lower with motion feedback than without,

this may be due to the fact that motion feedback increases the stability of the system thus human operators could use less control activity to achieve similar performance of no-motion case, a result consistent with earlier findings in Chapter 2 and [6]. Clear differences on the target crossover frequencies and target phase margins were observed between motion and no-motion cases. These may be also due to the fact that motion feedback helps stabilize the system, as target phase margins with motion were higher than those without motion feedback. For the human operator model parameters, both visual gain and lag time constant decrease with the presence of motion. The lead time constant decreases and the visual time delay increases when there is motion, which are clear evidences that motion feedback increases the stability of the system. Moreover, the effects of the motion feedback on the baseline dynamics are not as obvious as those of other conditions with added dynamics, especially for the performance, control activity, target crossover frequency, visual gain and lead time constant. In general, for all the human operator parameters, the similar trends from C1 to C15 between no-motion and motion cases indicate that the interaction between the added dynamics and motion feedback has no effect on human operator control behavior.

According to the dependent measures quantifying the MCAB proposed in Chapter 5, the relative changes in the performance, control activity, ratio of the visual gain and lag time constant, and the lead time constant with respect to those with the baseline were studied for both the no-motion and motion cases. It was found that the differences of the relative changes in the performance and lead time constant between no-motion and motion cases are relatively small, compared with more obvious changes for the control activity and ratio of the visual gain and lag time constant. If the simulation-based MCAB developed in Chapter 5 are accurate (verified in Chapter 6), and if the MCAB with motion feedback are necessary, based on the experiment data, the modifications on the MCAB for the relative changes of tracking performance and lead time constant can be relatively small; and modifications on the MCAB for the relative changes in the control activity and the ratio of the visual gain and lag time constant may be higher. Considering these observed differences between no-motion and motion cases, direct application of the MCAB developed in Chapter 5 to motion case in not recommended. The experiment results in this appendix might be used as a reference to modify the simulation data in Chapter 5 to come up with the MCAB with motion feedback. However, this is not performed in this thesis, since the differences between the no-motion and motion cases for the dependent measures are not so large. Moreover, due to extra parameters in the motion channel, an offline simulation with multimodal human operator model could be much less accurate in predicting human operator control behavior than the simulation with only visual channel (Chapter 5). The development of the (I)MCAB with motion is of interest for future studies.

In this experiment, the tracking performance between no-motion and motion conditions were found very similar. Unlike the double integrator controlled dynamics used in Chapter 2, the baseline aircraft dynamics used in this experiment are more stable, thus motion feedback may contribute less in improving tracking performance by increasing the stability of the system. In future studies, larger differences between the dipole damping ratios ($\zeta_1 - \zeta_2$) are recommended to be tested, since the system stability would be more affected by added dynamics with larger perturbations on the baseline system. Thus more clear differences in tracking performance and human operator control behavior could be observed.

REFERENCES

[1] R. L. Stapleford, D. T. McRuer, and R. E. Magdaleno, *Pilot Describing Function Measurements in a Multiloop Task,* IEEE Transactions on Human Factors in Electronics **8**, 113 (1967).

[2] M. M. van Paassen and M. Mulder, *Identification of Human Operator Control Behaviour in Multiple-Loop Tracking Tasks,* in *Proceedings of the Seventh IFAC/IFIP/IFORS/IEA Symposium on Analysis, Design and Evaluation of Man-Machine Systems, Kyoto Japan* (Pergamon, 1998) pp. 515–520.

[3] P. M. T. Zaal, D. M. Pool, Q. P. Chu, M. M. van Paassen, M. Mulder, and J. A. Mulder, *Modeling Human Multimodal Perception and Control Using Genetic Maximum Likelihood Estimation,* Journal of Guidance, Control, and Dynamics **32**, 1089 (2009).

[4] J. R. Wood and J. Hodgkinson, *Definition of Acceptable Levels of Mismatch for Equivalent Systems of Augmented CTOL Aircraft*, Tech. Rep. MDC A6792 (McDonnell Aircraft Company, St. Louis (MO), 1980).

[5] P. M. T. Zaal, D. M. Pool, M. M. van Paassen, and M. Mulder, *Comparing Multimodal Pilot Pitch Control Behavior Between Simulated and Real Flight,* Journal of Guidance, Control, and Dynamics **35**, 1456 (2012).

[6] D. M. Pool, M. Mulder, M. M. van Paassen, and J. C. van der Vaart, *Effects of Peripheral Visual and Physical Motion Cues in Roll-Axis Tracking Tasks,* Journal of Guidance, Control, and Dynamics **31**, 1608 (2008).

E

CROSSOVER FREQUENCY CALCULATION

This appendix describes the approach to calculate the open-loop target (or disturbance) crossover frequency and corresponding phase margin for any subject and any testing condition throughout this thesis. From Chapter 3 to Chapter 6 the controlled system is the combination of baseline aircraft dynamics and added dipole dynamics, which makes the crossover frequency and corresponding phase margin very sensitive to the visual gain of the human operator. In this appendix, the open-loop frequency responses of Subject 2 and Subject 4 of the same testing condition C13 (added down dipole dynamics at 1 rad/s) in Chapter 6 are shown as an example of how the crossover frequency and phase margin were determined in this thesis.

Figure E.1 shows the target open-loop described by both frequency response functions (FRF) and identified human operator model for Subject 2 and Subject 4 of condition C13 in Chapter 6, respectively. The frequency responses of the baseline, added and total dynamics are drawn for reference. In Figure E.1a, for example, a vertical dashed line is drawn to indicate the target crossover frequency and a horizontal line is drawn at unit 1 for reference; in Figure E.1c, a horizontal line is drawn at −180 deg to indicate the stability of the system.

In Figure E.1a, it can be seen an obvious valley caused by the added down dipole at 1 rad/s. Since there is only one crossover frequency, it is naturally selected as the crossover frequency for Subject 2 in condition C13.

In Figure E.1b, due to the fact that Subject 4 has higher visual gain than for Subject 2, five potential crossover frequencies exist. In Figure E.1b, the last two crossover frequencies at around 8 rad/s are caused by the human operator neuromuscular dynamics. However, in Figure E.1d their corresponding phases are below −180 deg. Finally $\omega = 3.3$ rad/s is chosen as the real crossover frequency due to its highest value and corresponding phase above −180 deg.

Throughout this thesis, the selected target (or disturbance) crossover frequency is always the one with the highest frequency with corresponding positive phase margin.

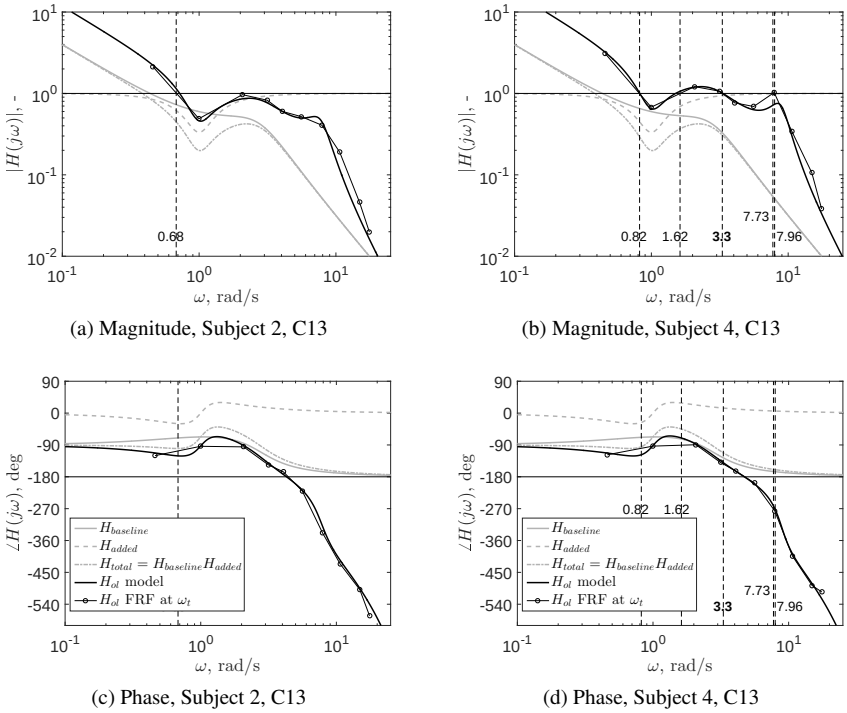

(a) Magnitude, Subject 2, C13

(b) Magnitude, Subject 4, C13

(c) Phase, Subject 2, C13

(d) Phase, Subject 4, C13

Figure E.1: Open-loop frequency responses of Subject 2 and Subject 4 in condition C13 (Chapter 6).

CURRICULUM VITÆ

Tao Lu was born in Chengdu. He started as a Ph.D. student at the Control and Simulation Division of the Faculty of Aerospace Engineering at Delft University of Technology in 2013. His research as de-scribed in this thesis, mainly focused on objective evaluation of the adaptation of human manual control behavior to the changes in the dynamics of controlled systems.

LIST OF PUBLICATIONS

6. T. Lu, D. M. Pool, M. M. van Paassen, and M. Mulder, *Experimental Verification of Objective Manual Control Adaptation Boundaries in Aircraft Pitch Tracking Tasks*, Journal of Guidance, Control, and Dynamics, to be submitted.

5. T. Lu, D. M. Pool, M. M. van Paassen, and M. Mulder, *Simulation Prediction of Objective Manual Control Adaptation Boundaries in Aircraft Pitch Tracking Tasks*, Journal of Guidance, Control, and Dynamics, to be submitted.

4. S. Fasiello, T. Lu, D. M. Pool, M. M. van Paassen, *A Cybernetic Analysis of the Noticeability of Different Controlled Aircraft Pitch Dynamics Parameter Settings*, in Proceedings of the AIAA Modeling and Simulation Technologies Conference, San Diego (CA), (2019), to be submitted.

3. T. Lu, D. M. Pool, M. M. van Paassen, and M. Mulder, *Quantifying the Effects of Added Dynamics with Human Operator Control Behavior Measurements and Simulations*, in Proceedings of the AIAA Modeling and Simulation Technologies Conference, Denver (CO), AIAA-2017-3667 (2017).

2. I. Matamoros, T. Lu, M. M. van Paassen, D. M. Pool, *A Cybernetic Analysis of Maximum Unnoticeable Added Dynamics for Different Baseline Controlled Systems*, in Proceedings of the 20th IFAC World Congress, Toulouse, France, 16417-16422 (2017).

1. T. Lu, D. M. Pool, M. M. van Paassen, and M. Mulder, *Use of Simulator Motion Feedback for Different Classes of Vehicle Dynamics in Manual Control Tasks*, in Proceedings of the 5th CEAS Air & Space Conference, Delft, The Netherlands, 2015.